

Slope Stability Analysis of Open Pit Mines under Geomechanical Uncertainty

By

Christian Andres Obregon Mitma

A thesis submitted to the Faculty of Graduate and Postdoctoral Studies

In conformity with the requirements for
the degree of Master of Engineering



Department of Mining and Material Engineering

McGill University, Montreal, Canada

June 2020

© Christian Obregon, 2020

Abstract

In open pit mining, a major geotechnical challenge involves the excavation of the steepest possible slope angle to achieve the lowest stripping ratio while ensuring maximum ore recovery. This generally means a good overall profitability since waste rock removal is kept to a minimum. However, steepening pit slopes may induce failures, which may disprove the economic benefits that were initially aimed at and which may also result in loss of life, damage to equipment and environment. As a result, the selection of slope angle is a critical decision that can have far-reaching effects on the economics and operation of the mining project

Traditionally, slope stability assessments for pit slopes are carried out by means of a 2D deterministic analysis. However, there are two major drawbacks with this approach. First, a deterministic approach is unable to account for the variability and uncertainty in the rock mass strength properties. Second, a two-dimensional analysis cannot capture the complex open pit geology and varying geometry which is inherently 3D in character.

This work deals with the geotechnical slope design of three open pit case studies by means of a probabilistic-based approach in order account for the variability and uncertainty in the properties corresponding to both the intact rock and geological discontinuities. Rock slope stability assessments are carried out at three different scales: bench, inter-ramp and global pit slope by means of analytical and numerical tools.

Both kinematic and kinetic analysis for structurally controlled failure mechanisms were carried out at the bench scale by means of classical Limit Equilibrium Analysis (LEA). Also, a novel Discrete Fracture Network (DFN) modelling technique was used for the stochastic representation of discrete rock blocks. Slope stability analysis at the inter-ramp slope was performed through a deterministic approach of major large-scale discontinuities mapped during field geological characterization. The global pit slope stability analysis focused on investigating the uncertainty in intact rock and rock mass Hoek-Brown shear strength envelopes and was conducted using 2D/3D Limit Equilibrium Analysis (LEA) vs Finite Element Analysis (FEA). Finally, deterministic vs probabilistic, LEA vs FEA and 2D vs 3D slope stability analysis tools are compared, and their results are discussed.

Résumé

Dans l'exploitation minière à ciel ouvert, un défi géotechnique majeur consiste à l'excavation de l'angle de pente le plus raide possible pour le ratio de décapage le plus bas tout en assurant une récupération maximale du minerai. Cela signifie une bonne rentabilité globale puisque l'enlèvement des stériles est réduit au minimum. Toutefois, le raidissement des pentes des fosses peut entraîner des défaillances, ce qui peut réfuter les avantages économiques qui étaient initialement visés et qui peuvent aussi entraîner des pertes de vie, des dommages à l'équipement et à l'environnement. Par conséquent, le choix de l'angle de pente est une décision cruciale qui peut avoir des effets de grande envergure sur l'économie et l'exploitation du projet minier.

Traditionnellement, les évaluations de la stabilité des pentes pour les pentes des fosses sont effectuées au moyen d'une analyse déterministe 2D. Cependant, il y a deux inconvénients majeurs avec cette approche. Tout d'abord, une approche déterministe est incapable de tenir compte de la variabilité et de l'incertitude dans les propriétés de résistance de masse rocheuse. Deuxièmement, une analyse bidimensionnelle ne peut pas capturer la géologie complexe à ciel ouvert et la géométrie variable qui est intrinsèquement de caractère 3D.

Ces travaux portent sur la conception de la pente géotechnique de trois études de cas à ciel ouvert au moyen d'une approche probabiliste afin de tenir compte de la variabilité et de l'incertitude dans les propriétés correspondant à la fois à la roche intacte et aux discontinuités géologiques. Les évaluations de la stabilité des pentes rocheuses sont effectuées à trois échelles différentes : banc, inter-rampe et pente des fosses mondiales.

L'analyse cinématique et cinétique des mécanismes de défaillance structurellement contrôlés a été réalisée à l'échelle du banc au moyen de l'analyse classique d'équilibre limite (LEA). De plus, une nouvelle technique de modélisation du réseau de fracture discrète (DFN) a été utilisée pour la représentation stochastique de blocs de roche discrets. L'analyse de la stabilité des pentes à la pente inter-rampes a été réalisée par une approche déterministe des principales discontinuités à grande échelle cartographiées lors de la caractérisation géologique sur le terrain. L'analyse globale de la stabilité de la pente de la fosse s'est concentrée sur l'étude de l'incertitude dans les enveloppes de résistance au cisaillement Hoek-Brown de la roche intacte et de la masse rocheuse et a été réalisée en utilisant une analyse d'équilibre limite 2D / 3D (LEA) vs une analyse par éléments finis (FEA). Enfin, les outils d'analyse de stabilité déterministe vs probabiliste, LEA vs FEA et 2D vs 3D sont comparés et leurs résultats sont discutés.

Acknowledgements

I would like to express my gratitude to those who have supported me while this work was being done.

First and foremost, to my family - Mom, Dad, Jaime, Nana, Lupe - for their unconditional love and continuous support throughout all this time away from home. You are all my cornerstone and my deepest source of strength, encouragement and inspiration.

Secondly, but just as importantly, I would like to thank my supervisor, Prof. Hani Mitri, for his constant support, invaluable guidance and constructive comments throughout my master's studies. Many thanks as well for all the Christmas lunches and Group Summer BBQ's. I will keep fond memories of all of them, specially the card games that I will always lose!

I would also like to express my deep gratitude to the Peruvian Institute of Mining Engineers (IIMP) for fully funding my graduate studies at McGill through the 'Beca IIMP' scholarship program. My sincere gratefulness is extended to the past and current IIMP President Ing. Luis Rivera and Ing. Victor Gobitz, respectively.

To my friends in the Mine Design Lab at McGill University – Issac Vennes, Kelly Habib, Jorge Alvarez, Tuo Cheng and Yizhuo Li. Thanks for your friendship, your support and for making my stay in Canada a cozy experience. Special thanks to Dr. Shahe Shnorhokian, for his friendship and long discussions while having Peruvian food near Jean Talon metro. His love for Rock Mechanics is contagious and I am so lucky that we both share the same rock mechanics 'addictions'. I will be looking forward to your next visit in Peru. This time, we are going to make it to the Sun Gate in MacchuPicchu!

To the Rocscience technical team at Toronto office: Heather Trommels, Robert Bradford and Daniel Wai. Many thanks for your patience and help with all the questions I sent you regarding the use of Slide3D and RS3 software. I know I have been bombarding you with a lot of questions during the past months and I do appreciate the time you took to respond all my queries.

I am also very grateful to Drs. Mark Cottrell and Steve Rogers (Golder Associates) for providing me with an academic license of the Fracman software and for their useful insights and suggestions in my first contact with Discrete Fracture Network (DFN) modelling.

To Dr. Julian Watson (Mining One), Dr. Abouzar Vakili (Cavroc), Dr. Omid Mahabadi (Geomechanica), Dr. Evan Jones (BHP-Australia) for all the stimulating discussions, immense help and advice on my pursue of a deeper understanding of modelling techniques for mining rock mechanics applications. Thanks a lot for your prompt response to my endless e-mail questions.

To my old Peruvian friends: Sammy Lucano and Guillermo Condori, for the long discussions at night through skype calls on a topic that we all love and feel passionate about i.e. Rock Mechanics.

To my new Canadian friends: Gabriel Vaillancourt and Camilie Chabot for all the breakfasts spent at Cora and the fun times at LaRonde. Taking the Goliath ride together with its 170 feet drop at a 70-degree angle was an amazing experience. But I am not willing to do it again, and you won't convince me this time!

Finally, I would like to dedicate this thesis to my beloved parents, Lino and Digna, who taught me the meaning of hard work and perseverance. Hope this thesis makes you proud.

Contributions of the Author

The author hereby certify that all the work described within this thesis was carried out by himself and corrections made by his supervisor. This thesis led to the publication of one journal article entitled “Probabilistic approach for open pit bench slope stability analysis–A mine case study”. This was published in the International Journal of Mining Science and Technology – June 2019 Edition (<https://doi.org/10.1016/j.ijmst.2019.06.017>). The literature review, numerical modelling, and analysis of results presented in this publication was conducted by the candidate and co-authored by Prof. Hani Mitri in his capacity as thesis supervisor.

Research contributions are given in the form of several case studies presented in this thesis for real mining projects and/or operations for which the author has directly or indirectly worked in the last six years of his industry experience. The data processing and interpretation as well as the stability analysis and numerical modelling are wholly authored by the candidate.

Table of Contents

Abstract.....	1
Résumé.....	2
Acknowledgements	3
Contributions of the Author	5
Table of Contents	6
List of Figures.....	10
List of Tables	17
1 Introduction.....	18
1.1 Problem Definition.....	18
1.1.1 Uncertainty and Variability in Rock Properties	18
1.1.2 Conventional Two-Dimensional (2D) Stability Assessment	19
1.2 Scope of Work	19
1.3 Research Objectives.....	19
1.4 Thesis Structure	20
2 Literature Review	22
2.1 Uncertainty in Rock Engineering Systems	22
2.1.1 Components of Total Uncertainty.....	24
2.1.2 Epistemic or Knowledge Uncertainty	25
2.1.3 Aleatory or Natural Variability	25
2.2 Open Pit Slope Stability Assessment.....	26
2.2.1 Impact of Slope Instability in Mining	27
2.2.2 Open Pit Slope Design Procedure.....	30
2.3 Typical Modes of Failure in Open Pit Slopes	35
2.3.1 Structurally Controlled Failure Mechanisms	37
2.3.2 Non-Structurally Controlled Failure Modes	41
2.4 Geotechnical Design Methods for Pit Slopes.....	43
2.4.1 Empirical Methods.....	44
2.4.2 Analytical Methods.....	44
2.4.3 Numerical Methods.....	45
2.4.4 Observational Method.....	46
2.5 Approaches in Slope Stability Analysis.....	47

2.5.1	Deterministic Analysis	48
2.5.2	Probabilistic Analysis	48
2.6	Acceptance Criteria for Open Pit Design.....	48
2.6.1	The Concept of Slope Failure	48
2.6.2	Factor of Safety (FoS).....	49
2.6.3	Margin of Safety (MoS).....	51
2.6.4	Probability of Failure (PoF)	52
2.6.5	Suggested Design Criteria.....	53
2.7	Chapter Summary	54
3	Analysis of Structural Geological Data.....	55
3.1	Methods of Field Data Collection	55
3.1.1	Surface Structural Mapping	56
3.1.2	Geomechanical Core Logging	62
3.1.3	Other Non-Traditional Methods.....	63
3.2	Assessing the Geometrical Properties of Rock Joints.....	66
3.2.1	Joint Orientation.....	67
3.2.2	Joint Spacing	73
3.2.3	Joint Persistence.....	78
3.3	Characterizing the Shear Strength of Geological Discontinuities.....	80
3.3.1	The Mohr-Coulomb Linear Model.....	81
3.3.2	The Barton-Bandis Non-Linear Model	82
3.3.3	The General Power Curve Model	89
3.4	Chapter Summary	91
4	Bench-Slope Scale	92
4.1	Analysis of Structurally Controlled Failure Mechanisms	92
4.1.1	Kinematic Analysis of Rock Blocks	93
4.1.2	Kinetic Analysis of Rock Blocks	94
4.1.3	Discrete Fracture Network (DFN) Modelling.....	96
4.2	Case Studies	98
4.2.1	Case Study #1	98
4.2.2	Case Study #2	114
4.2.3	Case Study #3	123
4.3	Chapter Summary	134

5	Inter-Ramp Slope Scale.....	136
5.1	Structural Stability Analysis of Major Discontinuities	136
5.2	Case Studies	136
5.2.1	Case Study #1	137
5.2.2	Case Study #2.	144
5.2.3	Case Study #3	151
5.3	Chapter Summary	161
6	Global Pit Slope.....	162
6.1	Assessment of Rock Mass Properties	162
6.2	Intact Rock Strength	163
6.2.1	Uniaxial Compressive Strength (UCS)	163
6.2.2	Triaxial Compressive Strength (TX).....	164
6.2.1	Brazilian Tensile Strength (BTS).....	165
6.2.2	Uncertainty in Intact Rock Strength Parameters	166
6.3	Rock Mass Strength	168
6.3.1	Rock Mass Classification Schemes.....	169
6.3.2	Rock Mass Shear Strength Models	173
6.3.3	Uncertainty in Rock Mass Strength Parameters.....	178
6.4	Case Studies	179
6.4.1	Case Study #1	179
6.4.2	Case Study #2	190
6.4.3	Case Study #3	205
6.5	Chapter Summary	214
7	Three-Dimensional Slope Stability Analysis.....	216
7.1	Geometrical Complexities in Open Pit Mines	216
7.2	Comparison of 2D vs. 3D Analyses Results	217
7.2.1	3D Effect of Length of Extrusion	218
7.2.2	3D Effect of Turning Corners	220
7.3	3D Slope Stability Analysis	223
7.3.1	Case Study #1	223
7.3.2	Case Study #2	226
7.3.3	Case Study #3	230
7.4	Chapter Summary	233

8	Summary and Conclusions.....	235
8.1	Conclusions.....	235
8.2	Future Work.....	238
	References.....	239
	Appendix.....	257
	Structural Data of Case Studies	257

List of Figures

Figure 2.1 Flowchart for the estimation of rock mass properties based on laboratory and field data.	23
Figure 2.2 RES interaction matrix example (Azadmehr et al., 2019).....	23
Figure 2.3 Total Uncertainty Transition from epistemic to aleatory uncertainty as a function of the degree of knowledge and/or available information (Contreras & Ruest, 2016).....	24
Figure 2.4 Impact a steeper slope angle on an open pit mining operation (Read and Stacey, 2009).....	26
Figure 2.5 Effect of change in overall pit slope angle on stripping volume: a) Stripping volume calculation; b) Economic impact due to slope instability. (Call, 1972).....	28
Figure 2.6 Typical open pit mine layout: a) Slope scale-based types and b) Bench, Inter-ramp and Global slopes geometry configuration	31
Figure 2.7 Inputs for the construction of an open pit geotechnical model (Guest and Read, 2009).....	32
Figure 2.8 Open pit slope design process (Read and Stacey, 2009).	33
Figure 2.9 Three typical types of failures in open it mines (Patton & Deere, 1970)	35
Figure 2.10 Main failure mechanisms in rock slopes: a) Planar, b) Wedge, c) Toppling and d) Circular.	37
Figure 2.11 Geometrical conditions for planar failure (Hoek and Bray, 1981)	38
Figure 2.12 Wedge failure: a) Geometry of a biplanar wedge and b) Wedge geometry with an upper face (Hoek and Bray 1981)	39
Figure 2.13 Common types of toppling: (a) block toppling, (b) flexural toppling and (c) block-flexural toppling (Wyllie & Mah, 2004; Goodman & Bray, 1976)	41
Figure 2.14 Rock mass fracture pattern at different slope scales: a) massive rock mass, b) competent rock mass with few discontinuities, c) and d) blocky rock masses, e) very blocky rock mass and f) highly fractured rock mass (Agharazi, 2013)	42
Figure 2.15 The four different basic methods to rock mechanics and rock engineering analysis and design (Jing & Hudson, 2002)	43
Figure 2.16 Approaches in slope stability analysis: a) Deterministic and b) Probabilistic.....	47
Figure 2.17 Different types of pit slope performance. a) Global circular failure, b) Inter-ramp scale failure, c) Bench slope local failure d) Stable open pit design	49
Figure 2.18 Variation of the Factor of Safety (FoS) at different stages of a mining project (Terbrugge et al., 2009 & Fillion, 2018).	50
Figure 2.19 Probability density functions for: a) Capacity and Demand, b) Margin of Safety and c) Factor of Safety (Savely, 1987).....	52
Figure 3.1 Jointed rock mass with three principal joint sets.	55
Figure 3.2 Recommended ISRM discontinuity properties to be described during structural field mapping (Harrison & Hudson, 1997).....	56
Figure 3.3 Principal rock discontinuity properties as suggested by the ISRM: 1) Joint Orientation; 2) Joint Spacing; 3) Joint Trace Length; 4) Joint Roughness; 5) Joint Wall Strength; 6) Joint Aperture; 7) Joint Infilling; 8) Water Condition 9) Joint Set Number and 10) Rock Block Size (Barton, 1978).....	58
Figure 3.4 Example of a structural window mapping with joint traces highlighted.	59

Figure 3.5 Example of a structural scanline mapping intersecting ten rock joints.	59
Figure 3.6 Number of observations required to estimate of the mean discontinuity spacing (Priest and Hudson, 1981)	61
Figure 3.7 Reflex ACT II orientation tools (Reflex Instruments, 2013).....	62
Figure 3.8 Angle conventions in oriented drill core (Holcombe et al., 2013)	63
Figure 3.9 Example of ATV and OTV images of a vertical borehole (Piffer & Rinaldi, Waterstones Srl).	64
Figure 3.10 Orientation of discontinuity in borehole: (a) elliptical intersection between discontinuity and core; (b) ‘unwrapped’ view of borehole wall with discontinuity (Colog Inc. 1995).....	65
Figure 3.11 Example of a mapping window from camera imaging overlain with the 3-D terrain model of a pit sector. One major discontinuity (in red) and several rock joints (in green) were mapped (Tuckey, 2012).	66
Figure 3.12 Sampling bias imposed by one-dimensional (linear) discontinuity sampling represented by a drill hole with a plunge of 45° to the west (Fowler, 2013).....	68
Figure 3.13 Terzagui correction factor for a) a scanline at an angle α with the normal to a fracture set and b) a rock slope whose normal F makes an angle β with the fracture normal n (Wang & Mauldon, 2006)	68
Figure 3.14 No bias-corrected contour plot corresponding to the three oriented boreholes.	70
Figure 3.15 Blind zones associated to three oriented boreholes: BH1, BH2 and BH3.....	70
Figure 3.16 Bias-corrected contour plot corresponding to the three oriented boreholes	71
Figure 3.17 Equal-area contour plot for boreholes BH1, BH2 and BH3 with three identified main joint sets J1, J2 and J3.....	71
Figure 3.18 Example of variability in joint orientation (dip angles) for outcrop 1 (highly variable) and outcrop 2 (tightly clustered).	72
Figure 3.19 Normal distribution fit for the trend ($R\beta$) and plunge ($R\alpha$) histograms (Wittke, 2014)	73
Figure 3.20 A jointed rock mass containing three main joint sets with their true spacing being indicated (Chang & Konietzky, 2018)	74
Figure 3.21 The true joint spacing (λ) calculation from apparent spacing (λ_s) for one joint set	75
Figure 3.22 The true joint spacing (λ) calculation from apparent spacing (λ_s) for two joint sets.	75
Figure 3.23 Fracture frequency counter plot for a rock mass with four joint sets.	76
Figure 3.24 Joint spacing counter plot for a rock mass with four joint sets.....	76
Figure 3.25 Statistical analysis of total joint spacing. a) Contour plot of corelogging data; b) Histogram of the total joint spacing; c) Spreadsheet for core logging data processing as an output of Dips software.	77
Figure 3.26 Mean joint trace length estimation based on the method developed by Pahl (1981)	78
Figure 3.27 Trace length histogram for a total of 581 measurements obtained through camera image of a bench slope of orientation 73/121.	80
Figure 3.28 Mohr-Coulomb relationship between shear strength and normal stress (Hoek and Bray, 1981)	82

Figure 3.29 B-B criterion for different JRC values, JCS = 50 MPa and $\phi_r=30$ deg. (Prasetyo et al., 2017)	83
Figure 3.30 Field tests for B-B input parameters: 1) Schmidt hammer, 2) Barton's comb, 3) Tilt test.....	84
Figure 3.31 JCS from Schmidt hammer test. (Deere & Miller, 1966).....	86
Figure 3.32 JRC from visual comparison with standard profiles (Barton & Choubey, 1977).....	87
Figure 3.33 JRC from measurements of surface roughness using Barton's comb (Barton,1982)	88
Figure 3.34 Examples of modified power regression curves for describing shear strength of a single test for two specimens. Adapted from Miller & Borgman (1984).	90
Figure 3.35 Power shear strength criteria showing variability for a specific normal load (Savelly,1987) ..	90
Figure 4.1 Input rock mass properties for rock engineering surveys (Chaminé et al., 2015)	92
Figure 4.2 a) Modes of different structurally controlled rock slope failures. Stereographic projections for both the a) Deterministic and c) Probabilistic kinematic analysis approaches are shown	95
Figure 4.3 Joint Pole Orientation. a) Fisher distribution as concentric circles. b) Three-dimensional view of dip and dip direction distribution on the sphere (Ron Crouse, 2008)	96
Figure 4.4 Variation in the degree of joint orientation clustering for varying Fisher 'constant values of 15, 30 and 60	96
Figure 4.5 Example showing the limitations of ISRM suggested methods (Elmo et al., 2015)	97
Figure 4.6 Comparison of limit equilibrium analysis and DFN modeling approach (Miyoshi, 2018)	98
Figure 4.7 Geological map of the open pit mine with zoning limits. The study area corresponds to zone 05	99
Figure 4.8 Perspective 3D view of the open pit mine. The study area corresponding to zone 05 is shown	100
Figure 4.9 Very blocky rock mass type in the open pit mine	101
Figure 4.10 Structural window mapping (WM) point locations within zone 05 of the open pit mine	102
Figure 4.11 Composite stereonet plots for the orientation of joint sets in zone 05 of the open pit mine. a) Unweighted contour plot. b) Weighted contour plot.....	103
Figure 4.12 Laboratory tests results for unit weight measurements	104
Figure 4.13 Mohr-Coulomb linear regression analysis for direct shear tests on joint samples.	105
Figure 4.14 Power Curve regression analysis for direct shear tests on joint samples.....	106
Figure 4.15 Random shear strength envelope model	106
Figure 4.16 Deterministic kinematic stereographic analyses plots.	108
Figure 4.17 Experimental histograms for dip and dip direction angles of joint sets J1, J2 and J3.	109
Figure 4.18 Scatter plot for dip and dip direction angles for Joint Set 3. One and two standard deviation ellipses are drawn centered at the mean values.	113
Figure 4.19 Total Probability of Failure (PoF) for each design sector of the pit.	113
Figure 4.20 Geological cross section of the mine project.	114
Figure 4.21 Outcrop of a limestone rock type.	115

Figure 4.22 Contour plot based on surface mapping data for the limestone.....	116
Figure 4.23 Contour plot based on core logging data for the limestone.	116
Figure 4.24 Contour plot based on core logging data for the skarn.	117
Figure 4.25 Contour plot based on core logging data for the ore body.....	117
Figure 4.26 Open pit sectorization for case study 2.....	119
Figure 4.27 Unit weight values	120
Figure 4.28 Joint shear strength envelopes	121
Figure 4.29 Total Probability of Failure (PoF) for planar failure	122
Figure 4.30 Total Probability of Failure (PoF) for wedge failure.....	122
Figure 4.31 Mapping a bench face in an hornfels rock type	123
Figure 4.32 Bench mapping sites distribution within the pit. The open pit design sectors are also shown	125
Figure 4.33 Composite contour plot for all minor discontinuities mapped in exposed benches	125
Figure 4.34 Bar graph of the persistence distribution of rock joints.....	126
Figure 4.35 Bar graph of the spacing distribution of rock joints.	126
Figure 4.36 Histogram of rock unit weight measurements	127
Figure 4.37 Distribution of basic friction angle as measured in tilt tests.....	128
Figure 4.38 Distribution of scaled values of JRC from Barton's comb measurements	128
Figure 4.39 Distribution of scaled values of JCS from Schmidt hammer measurements.....	129
Figure 4.40 North Bench slope DFN model with rock blocks of $FoS \leq 1$ highlighted.....	130
Figure 4.41 South-West Bench slope DFN model with rock blocks of $FoS \leq 1$ highlighted	130
Figure 4.42 South Bench slope DFN model with rock blocks of $FoS \leq 1$ highlighted.....	131
Figure 4.43 North-East Bench slope DFN model with rock blocks of $FoS \leq 1$ highlighted.	131
Figure 4.44 Summary of the PoF based on the DFN approach under static and pseudo-static conditions	134
Figure 5.1 Distribution of mapped faults within the open pit mine – case study #1.....	137
Figure 5.2 Equal area stereo plot of mapped faults within the open pit mine – case study #1	138
Figure 5.3 Inter-ramp slope configuration – case study #1.....	138
Figure 5.4 Radar plot of design sectors for the open pit mine – case study #1.....	139
Figure 6.5 Kinematic analysis results for planar failure of each pit designing sector – case study #1	141
Figure 6.6 Kinematic analysis results for wedge failure of each pit designing sector – case study #1.....	142
Figure 6.7 Kinematic analysis results for toppling failure of each pit designing sector – case study #1..	143
Figure 5.8 LE analysis results for wedge failure formed by F-15 & F-16 faults.....	144
Figure 5.9 Equal area stereo plot of mapped faults within the open pit mine – case study #2	145
Figure 5.10 Inter-ramp slope configuration – case study #2.....	145

Figure 5.11 Open pit design sectors – case study #2	146
Figure 5.12 Kinematic analysis results for planar failure for each sector – case study #2	147
Figure 5.13 Kinematic analysis results for wedge failure for each sector – case study #2.....	148
Figure 5.14 Kinematic analysis results for toppling failure for each sector – case study #2.....	149
Figure 5.15 LE analysis results for wedge failure formed by F-1 & F-2 faults – case study #2.....	150
Figure 5.16 Distribution of mapped faults within the open pit mine – case study #3.....	151
Figure 5.17 Equal area stereo plot of mapped faults within the open pit mine – case study #3	152
Figure 5.18 Inter-ramp slope configuration – case study #3.....	152
Figure 5.19 Radar plot of design sectors for the open pit mine – case study #3.....	153
Figure 5.20 Kinematic analysis results for planar failure for each sector – case study #3	154
Figure 5.21 Kinematic analysis results for wedge failure for each sector – case study #3.....	155
Figure 5.22 Kinematic analysis results for toppling failure for each sector – case study #3.....	156
Figure 5.23 LE analysis results for wedge failure formed by F-3 & F-30 faults – case study #3.....	158
Figure 5.24 LE analysis results for wedge failure formed by F-3 & F-39 faults – case study #3.....	159
Figure 5.25 LE analysis results for wedge failure formed by F-3 & F-48 faults – case study #3.....	159
Figure 5.26 LE analysis results for toppling failure formed by F-23 fault – case study #3.....	160
Figure 5.27 LE analysis results for toppling failure formed by F-76 fault – case study #3.....	160
Figure 6.1 Rock mass characterization framework.....	162
Figure 6.2 Stress–strain diagram showing the different stress levels of a rock subjected to uniaxial compression (Cai et al., 2004).....	163
Figure 6.3 Triaxial test for rock samples a) Hoek cell and b) loading machine.	165
Figure 6.4 Brazilian tensile testing for rock samples a) before, b) during and c) after.....	166
Figure 6.5 Intact rock strength envelopes. a) Combining DTS, UCS & TX tests and b) Intact rock strength variability (Langford & Diederichs, 2015).....	168
Figure 6.6 Rock Mass Rating (RMR ₈₉) System after Bieniawski (1989).....	170
Figure 6.7 Geological Strength Index (GSI) lookup chart for rock masses (Marinos & Hoek 2000).	172
Figure 6.8 Guidelines for estimating disturbance factor D due to stress relaxation and blasting damage (Hoek & Brown, 2019).....	174
Figure 6.9 Transition of the Hoek-Brown envelope for intact rock to that for rock mass (Eberhardt, 2012)	175
Figure 6.10 Mohr-Coulomb criterion in terms of a) Principal stresses and b) Normal and Shear stresses (Edelbro, 2003).....	176
Figure 6.11 Relationship between maximum/minimum principal stresses of Hoek-Brown criterion and equivalent values obtained using Mohr-Coulomb criterion (Panji et al., 2016).....	177
Figure 6.12 Monte Carlo simulation approach for estimation of Hoek-Brown rock mass parameters	179
Figure 6.13 Histogram of rock mass characterization parameters a) RMR and b) GSI – Case study #1 .	180

Figure 6.14 Box plots showing the Uniaxial Compressive Strength (UCS) of rock samples – case study #1	181
Figure 6.15 Intact rock properties a) UCS and b) m_i values – case study #1	182
Figure 6.16 Intact rock strength envelope – case study #1	183
Figure 6.17 Input parameters for estimation of the rock strength envelope – case study #1	184
Figure 6.18 Distribution of estimated rock mass parameters a) ‘mb’, b) ‘s’ and c) ‘a’ – case study #1...	185
Figure 6.19 Case study #1 Open pit mine – zone 05 a) 3D perspective view and b) Cross sections.....	186
Figure 6.20 LEM Slope stability results – Case study #1	189
Figure 6.21 Histogram of a) RMR and b) GSI for the Limestone – case study #2.....	191
Figure 6.22 Histogram of a) RMR and b) GSI for the Skarn – case study #2	192
Figure 6.23 Intact rock properties for limestone a) UCS, b) DTS and c) m_i values – case study #2	193
Figure 6.24 Intact rock properties for skarn a) UCS, b) DTS and c) m_i values – case study #2	194
Figure 6.25 Intact rock strength envelope for a) limestone and b) skarn – Case study #2	195
Figure 6.26 Distribution of estimated rock mass parameters for limestone a) ‘mb’, b) ‘s’ and c) ‘a’ – Case study #2	197
Figure 6.27 Distribution of estimated rock mass parameters for skarn a) ‘mb’, b) ‘s’ and c) ‘a’ – Case study #2	198
Figure 6.28 Case study #2 Open pit mine a) 3D perspective view and b) Cross sections	199
Figure 6.29 2D LEM Slope stability results – Case study #2	204
Figure 6.30 Histogram of rock mass characterization parameters a) RMR and b) GSI – case study #3..	205
Figure 6.31 Figure Intact rock properties - UCS values	206
Figure 6.32 Intact rock strength envelope for hornfels – Case study #3.....	207
Figure 6.33 Input parameters for estimation of the rock strength envelope – case study #3.....	208
Figure 6.34 Distribution of estimated rock mass parameters a) ‘mb’, b) ‘s’ and c) ‘a’ – case study #3...	209
Figure 6.35 Case study #3 open pit mine cross sections.....	210
Figure 6.36 2D LEM Slope stability results – Case study #3	213
Figure 7.1 3D model of an open pit mine of complex geology and geometry. a) Different cross sections and b) 2D section cutting through the tallest pit wall.....	216
Figure 7.2 Factors of safety from 3D analysis and various 2D sections.....	218
Figure 7.3 Comparison of 2D and 3D FoS for varying length of extrusion of a homogenous slope.....	219
Figure 7.4 Stress conditions acting on an open pit mine with concave and convex slope curvatures (Sjöberg, 1999).....	220
Figure 7.5 3D Effect of turning corners in pit slope stability: a) example of a real open pit mine and b) concave and convex slope curvatures.....	221
Figure 7.6 3D slope stability analysis using a) LEA and b) FEA	222
Figure 7.7 3D FEA results for the global open pit mine – case study #: a) Plan and b) Perspective view	225

Figure 7.8 3D LEA results for the global open pit mine – case study #: a) Plan and b) Perspective view	225
Figure 7.9 Histogram of the FoS from the 3D probabilistic LEA – case study #1	226
Figure 7.10 3D open pit model: a) Pit geology and b) Proposed open pit design.....	227
Figure 7.11 3D LEA for the pit mine – case study #2: a) Search of the critical failure surface and b) Calculation of the min, max and average FoS.....	229
Figure 7.12 Comparison of analysis methods: a) 3D LEA b) 3D FEA – case study #2.....	229
Figure 7.13 Histogram of the FoS from the 3D probabilistic LEA – case study #2	230
Figure 7.14 3D deterministic LEA isotropic rock mass – case study #3	231
Figure 7.15 Histogram of the FoS from the 3D probabilistic LEA isotropic – case study #3	231
Figure 7.16 3D deterministic LEA anisotropic rock mass – case study #3	232
Figure 7.17 Histogram of the FoS from the 3D probabilistic LEA anisotropic – case study #3	232

List of Tables

Table 2.1 Suggested acceptable criteria for open pit slope design	54
Table 4.1 Summary of mean joint sets orientation – case study 1	102
Table 4.2 Summary of statistical distribution for joint orientation – Case study 1	107
Table 4.3 Summary of joint shear strength envelope – Case study 1	107
Table 4.4 Summary of deterministic and probabilistic kinematic analysis.....	110
Table 4.5 Summary of deterministic and probabilistic kinetic analysis	111
Table 4.6 Total probability of failure.....	112
Table 4.7 Summary of joint orientation for limestone – Case study 2.....	118
Table 4.8 Summary of joint orientation for skarn - Case study 2	118
Table 4.9 Summary of joint orientation for ore body - Case study 2.....	118
Table 4.10 Summary of joint shear strength envelope – Case study 2	121
Table 4.11 Summary of mean joint sets orientation – Case study 3	126
Table 4.12 Summary input parameters for DFN model – Case study 3	129
Table 4.13 Summary of static kinetic and kinematic analysis DFN approach – Case study 3	132
Table 4.14 Summary of pseudo-static kinetic and kinematic analysis DFN approach – Case study 3	133
Table 5.1 Summary of kinematic analysis for the inter-ramp slope – case study #1	140
Table 5.2 Summary of LE analysis for the inter-ramp slope – case study #1.....	144
Table 5.3 Summary of kinematic analysis for the inter-ramp slope – case study #2.....	150
Table 5.4 Summary of LE analysis for the inter-ramp slope – case study #2.....	150
Table 5.5 Summary of kinematic analysis for inter-ramp slope – case study #3.....	157
Table 5.6 Summary of LE analysis for the inter-ramp slope – case study #3.....	157
Table 6.1 Rock mass classes based on the RMR system (Bieniawski, 1989).....	171
Table 6.2 Summary of the 2D LEM global slope stability analyses – Case study #1	190
Table 6.3 Summary of the 2D LEM global slope stability analyses – Case study #2	200
Table 6.4 Summary of the 2D LEM global slope stability analyses – Case study #3	211
Table 7.1 3D LEA and 3D FEA deterministic stability analysis results – case study #1	224
Table 7.2 3D LEA deterministic stability analysis results – case study #3	230

Chapter 1

Introduction

1.1 Problem Definition

One major challenge in open pit mining has to do with the stability of pit slopes. In simple terms, this involves finding a delicate balance between the safety and economics of the project. That is to say that we want to achieve the steepest possible pit slope angle while ensuring geotechnical stability. Traditionally, slope stability assessment is carried out by means of a 2D deterministic analysis. However, there are two major drawbacks with this approach. First, a deterministic approach is unable to account for the variability and uncertainty in rock strength properties. Second, a two-dimensional analysis cannot capture the complex open pit geology and varying geometry which is inherently 3D in character.

A possible solution for this is to consider a probabilistic approach as opposed to a deterministic analysis and to switch from 2D to 3D slope stability analysis tools.

1.1.1 Uncertainty and Variability in Rock Properties

Rock masses are rarely uniform or isotropic, they are in fact complex materials that exhibit different degrees of variability and uncertainty in their mechanical parameters. Whereas uncertainty represents a lack of knowledge mainly because of limited available information, variability represents the inherent randomness related to natural fluctuations of the rock mass properties. Our inability to fully predict the mechanical behavior of a rock mass precisely is then due to the combination of both epistemic uncertainty (lack of knowledge) and aleatory variability (randomness) for any given rock engineering system.

Traditional slope stability analysis follows a deterministic approach whereby the input is a set of parameters that are fixed quantities, usually taken as the mean values of the data obtained from site investigation or laboratory testing. Although, simple and straightforward, the deterministic analysis fails to account for the different degrees of variability and uncertainty often encountered in rock properties. Consequently, it is necessary to evaluate the stability of a rock slope through an approach that will enable us to overcome this shortcoming. In this respect, the application of probability theory provides rational means to treat the underlying uncertainties in a systematic manner. In recent years, the probabilistic approach along with the calculation of probability of failure (PoF) instead of a Factor of Safety (FoS) has become more common as a design criterium.

1.1.2 Conventional Two-Dimensional (2D) Stability Assessment

For slope stability assessment purposes, classical two-dimensional (2D) analysis have widely been used due to its relatively simple formulation. It is current industry practice to perform 2D slope stability analysis for open pit mining. However, 2D analyses rely on several assumptions that are seldom encountered in real open pit mines. Open pit geology and geometry is complex and inherently 3D in character which cannot be adequately captured into a 2D plane strain representation. Therefore, a 3D slope stability analyses is needed for a more accurate representation of the failure mechanisms. In this chapter, 3D slope stability analysis is introduced, and a comparison made between 2D and 3D slope stability results. The advantage of performing 3D Limit Equilibrium Analysis (LEA) and 3D Finite Element Analysis (FEA) to arrive at the direction and location of the critical failure surface for a given open pit slope is shown through different case studies.

1.2 Scope of Work

This work is mainly concerned with the stability of rock slopes in open pit mining. It focuses on field data collection, processing and interpretation using statistical tools to arrive at a suitable geotechnical model from which a slope stability analysis can begin. For this thesis, the geotechnical database of three Peruvian mine sites was used to conduct the analyses. In these mines, there were no major issues associated with the presence of water either because the site dry conditions were reported and/or implementation of horizontal drains and/or pumping wells were considered to depressurize the pit walls. Because of those considerations, a detailed description of hydrogeological conditions is beyond the scope of this thesis. Factor of Safety (FoS) and Probability of Failure (PoF) of rock slopes following a deterministic and probabilistic approach, respectively are calculated and then contrasted to assess whether the design criteria are met or not. The objectives of the thesis are relevant for other projects in the field of rock mechanics and engineering geology when similar settings and project scale are encountered. This thesis aims at showing how probabilistic methods can be used for the geotechnical assessment of rock slopes in surface mining and how we can greatly benefit from using this approach in terms of safety and economics.

1.3 Research Objectives

The objectives of this study are:

- To perform a geotechnical slope stability assessment for different open pit mine case studies by following a deterministic and probabilistic approach.
- To perform a geotechnical slope stability assessment for different open pit mine case studies by following a kinematic and kinetic type of analysis.

- To quantify the Factor of Safety (FoS) and Probability of Failure (PoF) of rock slopes at the bench, inter-ramp and global scale of analysis for the different mine case studies.
- To calculate the uncertainty and variability of the intact rock and rock mass shear strength envelopes and account for their impact on the stability of open pit slopes.
- To investigate the limitations of 2D slope stability analysis and the explore the advantages of 3D slope stability analyses tools.

1.4 Thesis Structure

This thesis consists of eight chapters which are outlined below.

Chapter 1 presents a brief discussion of the use of probabilistic-based design methods in rock slope engineering as a mean for accounting uncertainty and variability of rock mass properties. It also describes the scope and objectives of this study.

Chapter 2 provides is a literature review on the current geotechnical design practice used for rock slope stability analysis. It presents the methods for uncertainty characterization and quantification in rock slope engineering problems. It also describes the geotechnical design procedure and explains the different design approaches. It also summarizes the most common used acceptance criteria for open pit mine design.

Chapter 3 covers an extensive and comprehensive review of structural geological data collection, processing and interpretation for rock slope stability assessment purposes. The key elements described are the geometrical and shear strength properties of discontinuities.

Chapter 4 provides a brief review of kinematic and kinetic analysis for structurally controlled failure mechanisms in bench slopes. This is followed by an introduction to the novel Discrete Fracture Network (DFN) Modelling technique for rock slope engineering applications. All the concepts and theory are then illustrated with three case studies of real open pit mining operations and projects.

In Chapter 5, kinematic and kinetic analyses for structurally controlled failures at the inter-ramp slope scale are presented for three case studies. Slope stability analyses are performed through a deterministic approach of major -large-scale- discontinuities mapped during field geological characterization.

Chapter 6 covers the main rock laboratory tests and rock mass classification schemes. Emphasis is given to the assessment of uncertainty in intact rock and rock mass Hoek-Brown shear strength envelopes. Finally, global pit slope stability analysis is carried out for three case studies and Factors of Safety (FoS) as well as Probabilities of Failure (PoF) are calculated and contrasted with the design target criteria.

In Chapter 7, 3D slope stability analysis is introduced, and a comparison made between 2D and 3D slope stability results. This chapter provides some insight into the main assumptions and limitations of classical two-dimensional (2D) slope stability analyses for open pit mining. It highlights the advantages of performing 3D Limit Equilibrium Analysis (LEA) by means of three case studies.

Chapter 8 draws together the conclusions reached through this research and presents proposals for further research. Finally, the thesis is supported by references and various appendices.

Chapter 2

Literature Review

This chapter provides an overview of the current geotechnical design practice used for rock slope stability analysis and its impact on surface mining operations. It starts by presenting a review of uncertainty characterization and quantification in rock slope engineering problems. It then describes the geotechnical design procedure and explains the different design approaches highlighting, among others, the deterministic and probabilistic methods. Finally, it summarizes the most common used acceptance criteria for open pit mine design.

2.1 Uncertainty in Rock Engineering Systems

A rock mass is a three-dimensional discontinuous medium that can be thought of as an assembly of individual blocks (i.e. intact rock pieces) delimited by natural discontinuities (i.e. geological structures). Rock masses are rarely uniform or isotropic, they are in fact complex materials that exhibit different degrees of variability and uncertainty in their mechanical parameters (Park et al., 2012; Jimenez-Rodriguez et al., 2006). The characterization of rock properties is a critical stage in defining the input parameters for an engineering analysis. This process combines data obtained from site investigation and laboratory testing in order to estimate the rock mass properties by using an empirical approach such as a rock mass classification scheme (e.g. RMR, GSI, RMi, etc.). Figure 2.1 shows the main steps involved in the rock mass characterization procedure and the determination of scaled rock mass properties. Since estimates of rock properties are major input values in analysis and/or design of rock structures, they are subsequently influenced by the uncertainties associated with rock property characterization.

The concept of a Rock Engineering System (RES) was originally developed by Hudson (1992) as a tool that aims to reduce the level of uncertainty by considering the interactions of the main parameters thought to govern a particular phenomenon (e.g. slope failure). The RES methodology is an analytic approach that uses an interaction matrix an example of which is shown in Figure 2.2. In this matrix all major influencing parameters are arranged along the leading diagonal of the matrix and the influence of each parameter on the other parameters is accounted for the corresponding off-diagonal positions. A compressive review of RES applications is outside the scope of this thesis, but this can be found elsewhere (Mazzoccola and Hudson, 1996; Rozos et al., 2011, Faramarzi et al., 2013; Hudson, 2013). It should be noted that one characteristic of the RES approach is that it clearly differentiates between the uncertainty concerned with our lack of knowledge about a process or model, and the uncertainty concerned with the inherent randomness of a process or model. In this regard, it is important to understand these differences prior to

any uncertainty quantification analysis. In the following sections formal definitions of uncertainty and variability are presented as they are currently used in Rock Mechanics and Rock Engineering.

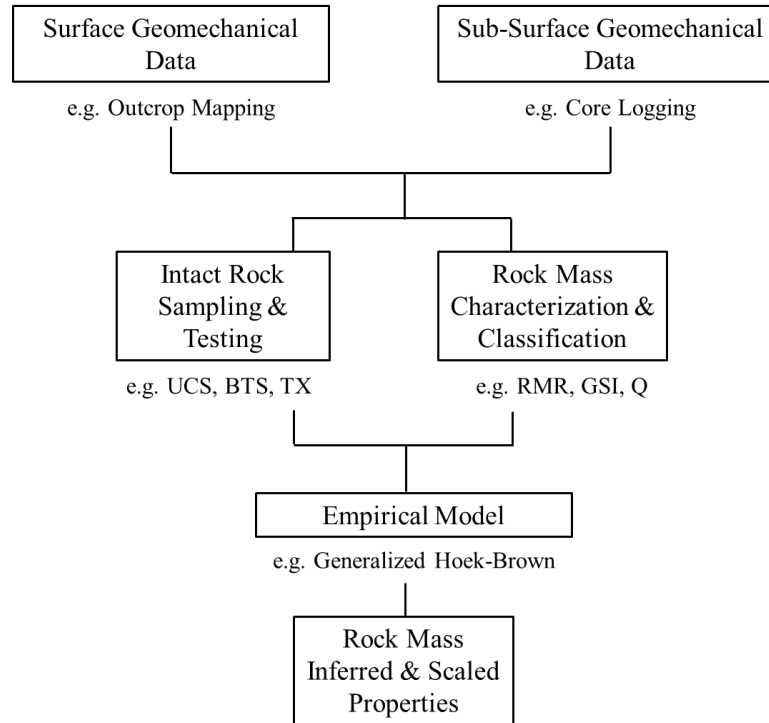


Figure 2.1 Flowchart for the estimation of rock mass properties based on laboratory and field data.

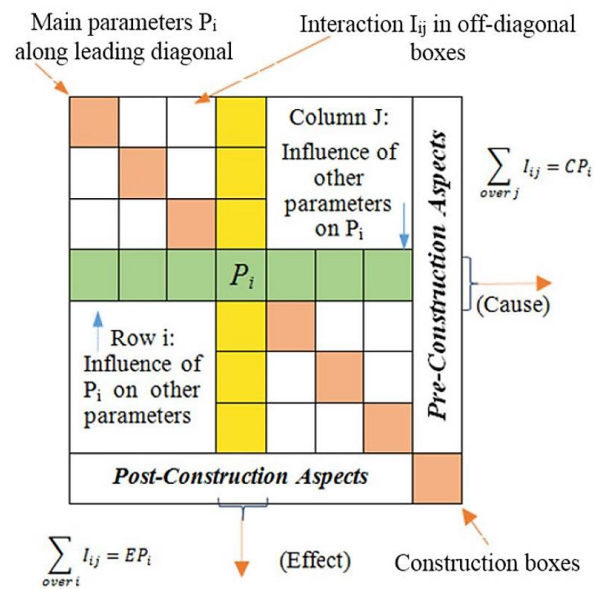


Figure 2.2 RES interaction matrix example (Azadmehr et al., 2019)

2.1.1 Components of Total Uncertainty

In the technical literature – and geotechnical engineering is not an exception – the terms variability and uncertainty are used interchangeably (Uzielli, 2008). Strictly speaking this is not correct. Although these two are components that contribute to the total unpredictability within a parameter or system, they are not the same. Uncertainty is often characterized as either epistemic or aleatory (Oberkampf et al., 2002; Baecher and Christian, 2003; Kiureghian, 2007). While epistemic uncertainty is due to imperfect knowledge, aleatory uncertainty arises from the inherent randomness in a system (Bedi, 2013).

Quantification of these two types of uncertainty requires the employment of varying models of uncertainty. In the case of aleatory uncertainties, quantification can be conducted using traditional probability-based methods such as the Monte Carlo, Rosenblueth point estimate, or first order and second moment (FOSM) methods (Harr, 1987), whereas epistemic uncertainties are treated using methods such as fuzzy logic or evidence theory (Mullarkey & Fenvesf, 1986; Adoko, & Wu, 2011; Cabalar et al., 2012).

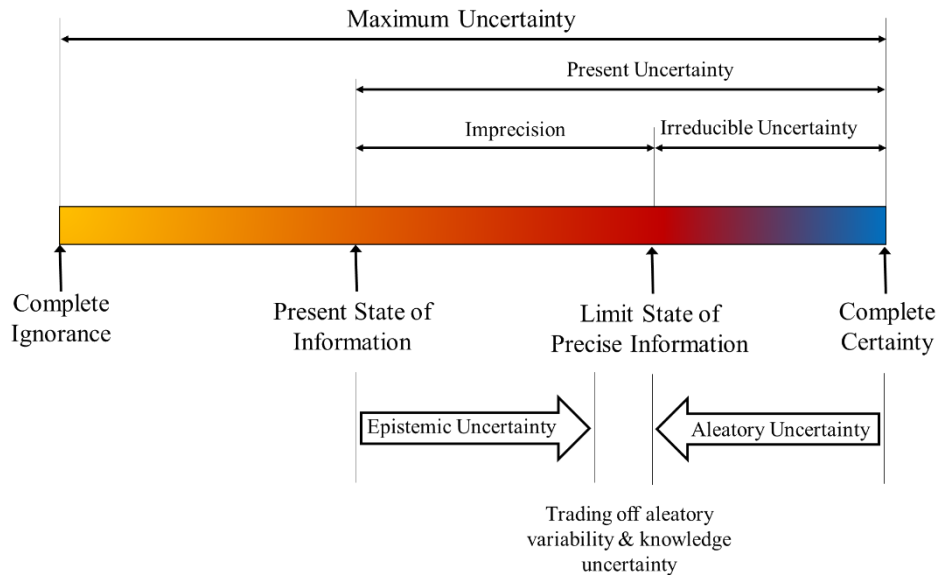


Figure 2.3 Total Uncertainty Transition from epistemic to aleatory uncertainty as a function of the degree of knowledge and/or available information (Contreras & Ruest, 2016)

Figure 2.3 shows the difference between epistemic and aleatory uncertainty as a function of the available information or degree of knowledge at a given time. This ranges from complete ignorance to complete knowledge as it gradually moves from the left towards the right end. This transition results from a better understanding of the process under study by acquiring more information and/or data. However, as shown in Figure 2.3 there is a limit state beyond which additional data do not change the level of uncertainty. This defines the point of irreducible or aleatory uncertainty (Bozorgzadeh, 2018). It has been suggested that the

separation between epistemic and aleatory uncertainty in a model is the result of a trade-off defined by the geotechnical engineer to treat the uncertainty (Baecher and Christian, 2003).

2.1.2 Epistemic or Knowledge Uncertainty

Epistemic uncertainty pertains to the modeler's state of knowledge as opposed to an underlying inherent randomness (Nadim, 2007). This is also referred to as subjective or systematic uncertainty, and it basically represents a lack of knowledge, and thus a deficiency in the available information, which may be qualitative or quantitative in nature (Der Kiureghian & Ditlevsen, 2009; Bedi, 2014). A key aspect of rock engineering design is, therefore, to increase the knowledge about the rock mass through further geotechnical investigations or other observations, thereby reducing the epistemic uncertainty (Spross et al., 2019).

In practice, however, information is never sufficient in quantity nor entirely accurate. Geomaterials are naturally variable and complex at all scales, ranging from the microstructure to the regional scale. As such, the initial design process will rather be based on limited information, possibly coming from the mapping of a few outcrops or logging of boreholes drilled at a widely spaced grid. The epistemic uncertainty will prevail until the rock mass is excavated and exposed; so that a detailed geotechnical investigation can be carried out. This effectively highlights that the epistemic uncertainty regarding the ground conditions being the main challenge before excavation.

Complete epistemic uncertainty elimination is, however, not possible; there is always going to be a remaining possibility of encountering different conditions than the ones expected. The involvement of an experienced engineering geologist is in many cases crucial. Some degree of subjective engineering judgement will therefore always be required in geotechnical design. The main uncertainty in the geotechnical slope design model is epistemic given that it can be reduced with collection of additional data at different stages of the project. As such, epistemic uncertainty is typically analyzed with probabilistic methods (Contreras & Ruest, 2016).

2.1.3 Aleatory or Natural Variability

This type of uncertainty is an innate property of geological systems. It is the result of different geological processes rock masses are subjected to (e.g. tectonism, magmatism, etc.) which leads to the variation of properties from one spatial location to another i.e. spatial variability, as well as variability of these properties at a single location over time i.e. temporal variability (Langford, 2013). Aleatory uncertainty is therefore related to the inherent random variation of one or more physical parameters or process (Bedi, 2013).

The natural variability of rock mass parameters is typically represented as a random process and is therefore considered to be aleatory. This natural variability, however, is one of the most important sources of uncertainty, especially when dealing with rock mass and discontinuity networks (Baecher & Christian, 2003). In rock masses, natural variability is a measure of the change of its characteristics over time and space (Joughin, 2018). This is also referred to as random or stochastic uncertainty and can be handled using stochastic methods (Aughenbaugh, 2006; Bozorgzadeh, 2018). This kind of uncertainty can be described with statistics and the probabilities related to it can be interpreted as a frequency of occurrence. As this variability is inherent in the material and therefore unpredictable, further laboratory testing or field measurements will not eliminate the uncertainty but will provide a more complete understanding of it (Shen, 2012; Bozorgzadeh, 2018).

2.2 Open Pit Slope Stability Assessment

In open pit mining, a major geotechnical challenge involves the excavation of the steepest possible slope angle to achieve the lowest stripping ratio while ensuring maximum ore recovery (Figure 2.4). This generally means a good overall profitability since waste rock removal is kept to a minimum. However, steepening rock slopes may induce failures, which may disprove the economic benefits that were initially aimed at and which may also result in loss of life and damage to equipment and environment. As a result, the selection of slope angle is critical; it can have far-reaching effects on the economics and operation of the mining project (Steffen et al., 2008; Hustrulid & Kuchta, 2013; Zevgolis et al., 2018).

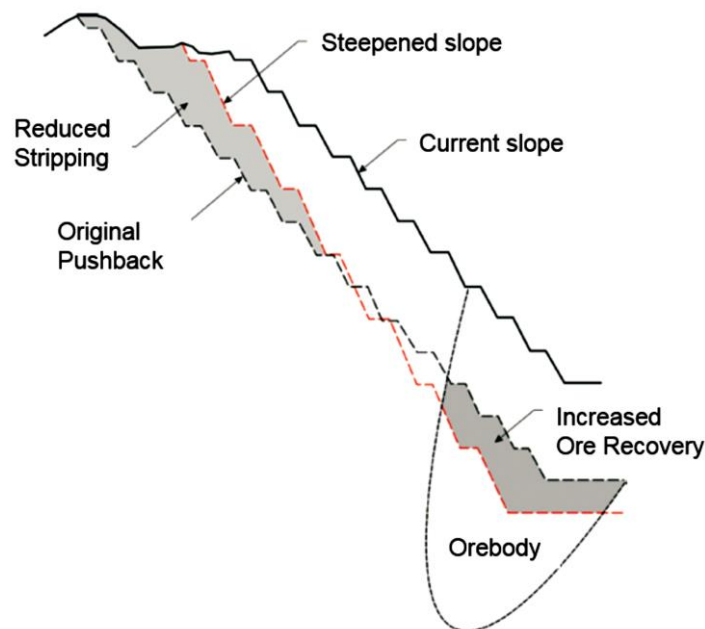


Figure 2.4 Impact of a steeper slope angle on an open pit mining operation (Read and Stacey, 2009).

2.2.1 Impact of Slope Instability in Mining

For an open pit mine, the design of the slopes is one of the major challenges at every stage of planning and operation (Read & Stacey, 2009). While managed instability subject to regulatory constraints and established acceptance criteria may be an integral part of the business strategy, unexpected or mismanaged instability can have a severe impact in several ways (Ortiz et al., 2015). The failure of slopes in open pit mining can have major impacts which can be broken down into three broad categories: safety and social factors, economic impact and environmental and regulatory impact (Read & Stacey, 2009).

2.2.1.1 Safety and Social Factors

Open pit slopes are generally cut in complex rock masses which are prone to wall instability. Since the adoption of formal slope design methodology in the early 1970s, the number of failures has generally decreased. This shows the importance of a detailed geotechnical engineering design that complies with legal regulations and safety standards.

Undoubtedly, the loss of life or injury to workers is the gravest potential consequence of any mining activity. Pit slope failures can also have further potential social impacts such as labor conflicts, detrimental relationship with local communities, loss of worker confidence and loss of credibility before shareholders (Ortiz et al., 2015). Safety will always be a prime objective in any mining operation and therefore be addressed at all scales of slope stability (Stacey, 2009).

While safety is the paramount consideration, a strong encouragement for the slope designer is the large economic incentives associated with maximizing slope angles. However, this should be commensurate with acceptable economic risk tolerance. The outcome of a potential pit slope failure must be minimized first and foremost.

2.2.1.2 Economic Impact

From an economic standpoint the impact of pit slope stability is simple: the steeper the slope the lower the stripping ratio, thus the more profitable the mine. The potentially large economic impact of slope angle changes is well recognized. Coates (1981), for example, gave a figure of five million tons decrease in stripping as a result of an average slope angle increment of 5° in a 300 m x 300 m x 125 m deep pit. Read and Stacey (2009) showed that an increase in the overall slope angle of 1° in a 50° wall of 500 m high results in a reduction of approximately 3600 m³ or 9000 ton of stripping per meter length of face.

The number of tons of material per running meter of pit slope represented by an increase in the overall slope angle is illustrated in Figure 2.5. Using an average density of 2.7 cubic meter per ton, which is the most

common value for most granitic rocks, the mathematical relationship expressed in tons per meter is given by Call (1972). For a slope increment from 40° to 50°, the amount of rock is 238 tons per meter of pit wall for a pit 500 meter deep.

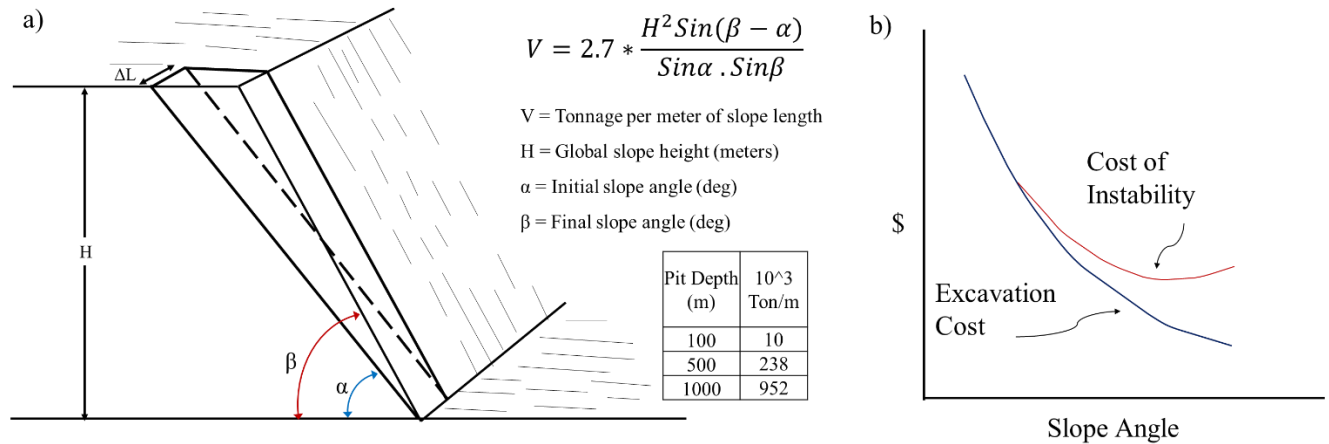


Figure 2.5 Effect of change in overall pit slope angle on stripping volume: a) Stripping volume calculation; b) Economic impact due to slope instability. (Call, 1972)

Although the economic effect of changes in slope angle is variable and must be computed for each mine and even for each sector of a mine, as a generalization, the steeper the slope the greater the profit. Thus, there is considerable economic incentive to utilize the maximum possible slopes. In this context, two concepts referred as to ultimate (final) pit wall and working (operating) pit slope should be distinguished.

Normally, during the initial stage of pit excavation, ‘operating slopes’ are cut with rather flatter angles either to provide additional operating width or to ensure stability where data to support the designs are limited. However, maintaining this ‘safer’ but ‘conservative’ design will almost always have negative economic consequences. That is why, it is of utmost importance to continuously refine the design with more information becoming available as the pit is being mined (Armstrong, 1990; Whittle, 1990; Hustrulid & Kuchta, 1995; Sjöberg, 1999). Increasing the angle of the working slopes can be advantageous since this will increase early revenues and delay mining of waste rock. On the other hand, an excessive increase of these slope angles is likely to heighten the risk of failure substantially. Slope failures at this early stage of mining could prove disastrous for the entire operation.

Ultimate pit limits are not achieved instantaneously. They are not reached until the last or final stage of the mining operation. They are worth the expense of conducting an optimization study. The ultimate pit limit

gives the shape of the mine at the end of its life. Usually this contour is smoothed to produce a stable final pit outline. Overall, the main benefits of steeper slope angles thus result from a minimizing of waste excavation for the final pit walls and delayed waste excavation for interim slopes, whereas the principal cost of having a steeper slope results from increased instability and costs associated with it (Coates, 1981).

2.2.1.3 Environmental and Regulatory Impact

In recent years the environmental component has made the development of mining projects, and with it the slope design component, both technically and “politically” more complex. Although not directly related to economics in the short term, environmental impacts will almost certainly affect the long-term mining business. Environmental impacts may result in air pollution, liquid spills that may lead to some of the social effects mentioned earlier. Slope instability may also result in more stringent regulations and closure considerations, both of which in turn will have adverse economic effects to keep the operation working (Ortiz et al., 2015).

Regulatory factors influencing slope design are typically related primarily to safety. The regulatory codes related to pit slopes vary significantly around the world. Most open pits are in jurisdictions where there are mining regulations that specify safety and environmental requirements, including those for mine closure. These regulations are aimed at providing correct mine management for all aspects of the operation, including the stability of pit slopes, or a requirement for “clean benches and stable faces” above the mining operation. More defined criteria, including minimum bench widths and maximum operating heights for benches, and even specific design methodologies can also be considered. The slope designer working on international projects must therefore be aware of the regulations under which he is working (Read & Stacey, 2009).

2.2.2 Open Pit Slope Design Procedure

The design of open pit slopes can be considered as the process whereby an optimal excavation configuration is sought while subject to constraints pertaining to safety, ore recovery, financial impact and environmental and safety regulations (Ortiz et al., 2015). In simple words, the optimum pit slope design should be “steep enough to be economically acceptable” and “flat enough to be safe” during the life of the mine.

Initially, the development of a formal geotechnical design method for pit slopes took place in the late 1960's and early 1970's, founded initially on the principles of soil mechanics. As open pits started to be mined at greater depths (>300 m) and failures became relatively common, public pressure and industry support led to the establishment of a better understanding of the factors contributing to pit slope failure. This research culminated in the preparation of two of the most world-wide famous rock mechanics books for pit slope analysis and design: Rock Slope Engineering by Hoek and Bray (1973) and the CANMET Pit Slope Manual by Herget (1977).

From the early 1980's onwards, research interest into pit slope designs entirely diminished in favor of underground rock mechanics, reflecting the need to resolve serious issues in that area. Having no British or Canadian researchers interested in pursuing further advancements in rock slope engineering, the Australians took over the task. In 2004 the Large Open Pit Project (LOP) was initiated under the leadership of Dr. John Read from CSIRO. The LOP has provided an updated framework for the stability assessment of large slopes associated with open pit mines. This can be found in the must-read book for any open pit mine engineer: Guidelines for Open Pit Design (Read & Stacey, 2009).

The following two sections explain the open pit slope design process in further detail. Although these are guidelines proving a general but relatively standard framework, they can be applicable, with modification to local geology and mining requirements, to all open pits.

2.2.2.1 Scale-Based Approach

In a typical open pit mine, several different mining units can be identified, each of which has an associated slope geometry (Figure 2.6.a). The smallest of these units is the bench slope (Figure 2.6.b.i). This is separated by catch benches which are constructed to retain rock spills from upper levels. The next unit in scale is the inter-ramp slope, which can be thought as a slope composed of a stack of benches or the slope between the haul roads or ramps (Figure 2.6.b.ii). The overall pit slope incorporates all ramps and benches (Figure 2.6.b.iii). It is defined as going from the toe or pit bottom to the crest of the pit.



Three scales of slope stability analysis for open pit mines:

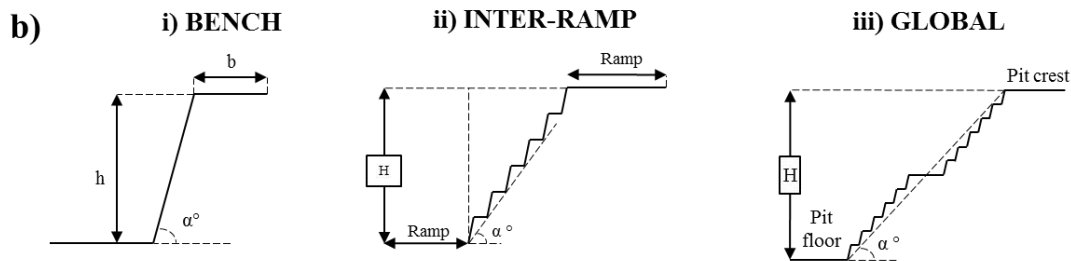


Figure 2.6 Typical open pit mine layout: a) Slope scale-based types and b) Bench, Inter-ramp and Global slopes geometry configuration

Each of these slope units defined above must be designed separately. This is simply because different failure mechanisms will prevail at different scales and thus affect different portions of the pit. For example, a single bench failure may have little or no impact on the overall operation of the mine if the berm is wide enough to prevent spalling rock from rolling down the pit wall. An inter-ramp failure, however, which cuts the haul road will have a greater impact on the operation by blocking the access to the mine. The overall failure usually occurs from the top to the bottom and damages tens of benches and one or more ramps. An overall slope failure may cost the mining company several months to clean the debris and recover. Therefore, mining companies usually allow some bench failures if they do not affect the mining activities, however, inter-ramp and overall slope failures are not allowed.

As will be seen in the upcoming section, the geotechnical slope design of an open pit wall starts at the bench scale configuration by considering minor geological structures (e.g. joints). Then, the design of larger scale slopes i.e. inter-ramp and global will focus on intermediate and major structures, respectively as well as the overall rock mass strength.

2.2.2.2 Design Steps: Current Practice

For a rational slope stability analysis, first and foremost the rock mass comprising the entire open pit mine should be divided into a selected number of *structural zones or domains*. Each of these zones is expected to be distinct and hold similar characteristics clearly differentiated from the ones of its neighbors in terms of the geometrical (orientation) features of the dominant joint sets and mechanical (strength) properties of the rock type. It is also important to consider the orientation of the proposed open pit slope face since different slope orientations within a structural domain require different design considerations. Therefore, the slope is divided into *design sectors* which contain one slope orientation and lie within one structural domain. Stability analysis and slope designs are then carried out for each design sector. It should be highlighted the division of an open pit into zones or sectors is first carried out based on limited surface mapping and drill holes core logging data. As more information is retrieved by exposing pit benches during excavation, the initial zoning may be updated and/or modified. This implies that the design sectors may have to be revised in an iterative process.

Current guidelines for open pit slope design requires that a representative geotechnical model is built based on four input components: the geological, structural, rock mass and hydrogeological models. Each of these four components includes different sub-components which are summarized in further details by Hudson & Harrison (2000), Wyllie & Mah (2004), Read and Stacey (2009). The geotechnical model with its four components is the first step in the process of open pit slope design. These are briefly summarized in Figure 2.7.

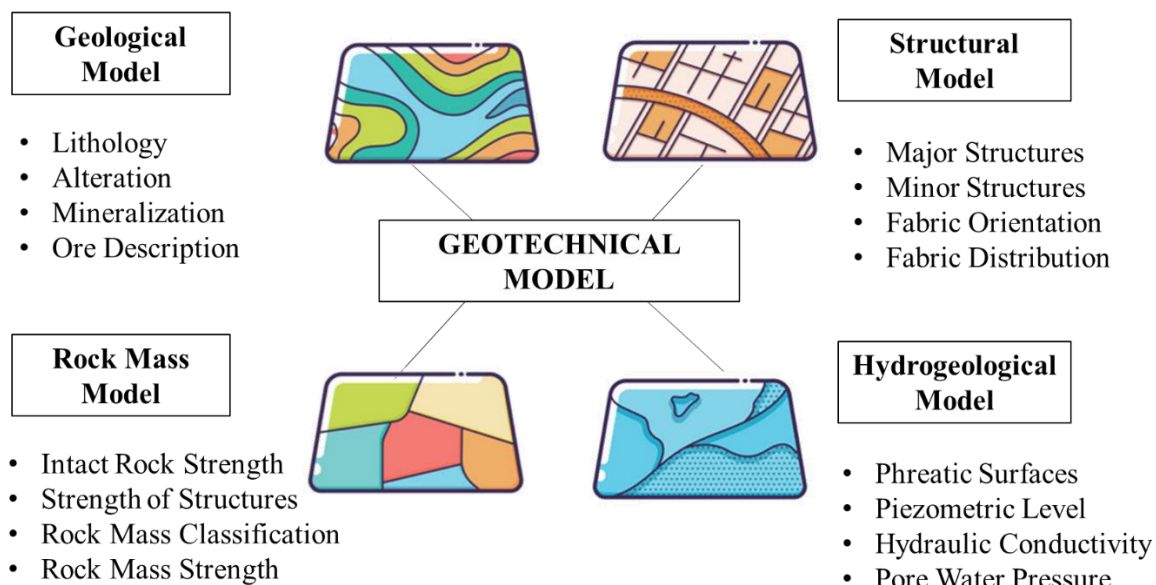


Figure 2.7 Inputs for the construction of an open pit geotechnical model (Guest and Read, 2009)

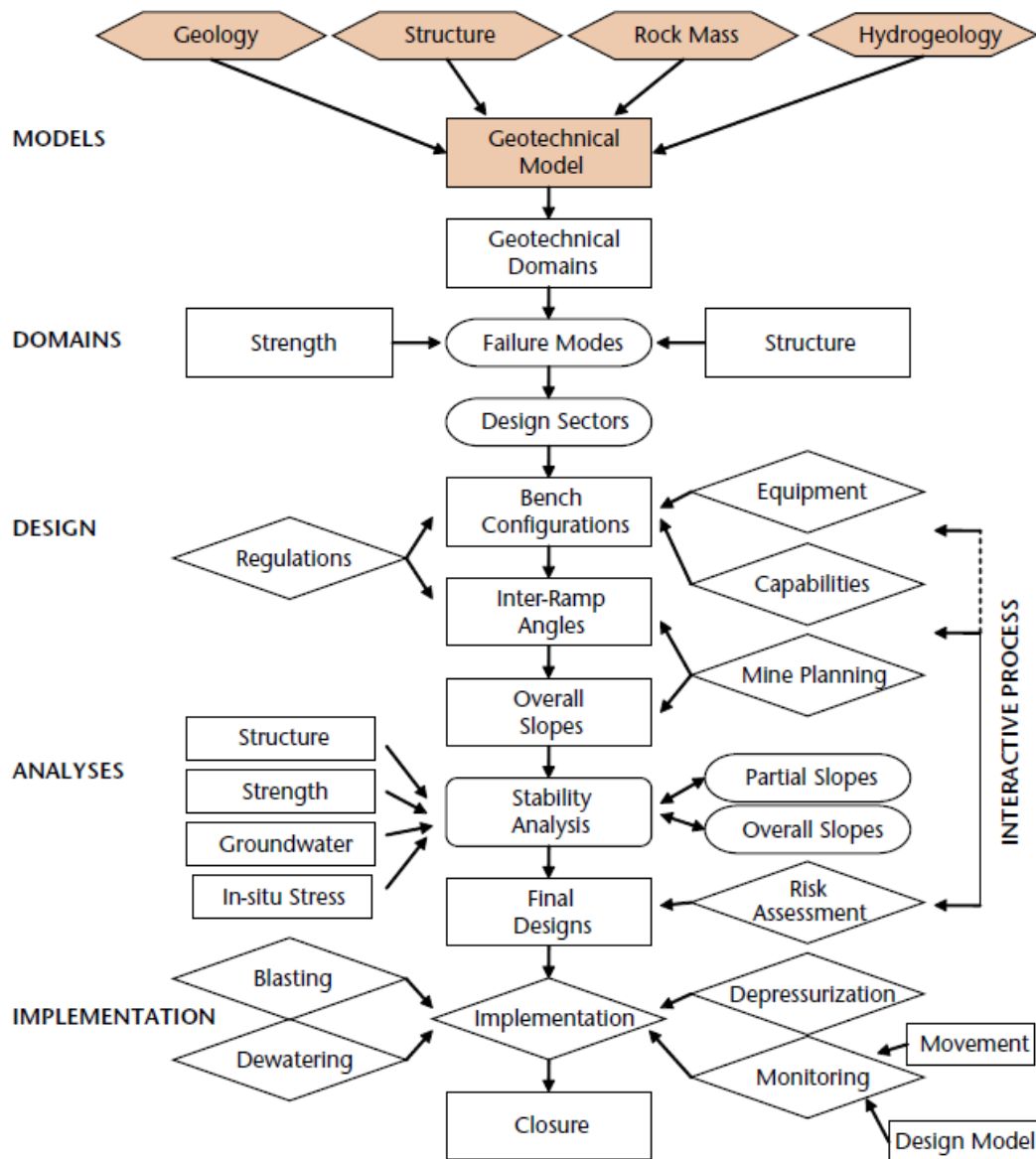


Figure 2.8 Open pit slope design process (Read and Stacey, 2009).

- **Geological Model:** The geological model depicts the 2D (geological section) or 3D (block model) distribution of rock types within the pit that will be exposed during mining operations. The material type categories can relate not only to lithology, but also to the degree and type of alteration, which can have a significant influence on rock strength, either by increasing it (silicification) or reducing it (argillization). The geological model will generally be provided by the mine geology staff and therefore, the information will probably be biased towards a description of ore genesis and

mineralization. The slope designer must carefully differentiate information that may be useful from a geotechnical point of view.

- **Structural Model:** This model is typically carried out by structural geology specialists. The objective of the structural model is to describe the dimensions (length and depth) and orientation of major geological structures such as faults and shear zones. It is important to highlight whether these major structures are expected to be intercepted by the projected pit geometry given that they controlled the global or overall stability of the pit mine. Information about the general orientation and spatial distribution of minor structures (e.g. joints) is also part of the structural model. This data is generally collected during field mapping and/or core logging campaigns and it becomes a major consideration for the design at a bench scale. The structural model provides invaluable information to the geotechnical engineer of both major and minor discontinuities that are likely to influence the slope stability.
- **Rock Mass Model:** The rock mass model characterises the mechanical strength of the materials of each of geotechnical units or domains. This needs the geological and structural model as a framework. It includes the execution of laboratory testing to measure properties such as the intact rock compressive strength and joint shear strength. The rock mass strength is then estimated based on laboratory testing and the use of a classification scheme (e.g. RMR or GSI). The purpose of this model is to define the engineering properties of the rock mass for later use in the stability analyses.
- **Hydrogeological Model:** Groundwater usually has negative effects on the stability of an excavation or rock slope. Its main effect on the pit slope is given by an increase in the existing pore water pressure within discontinuities and pore spaces in the rock mass. This in turn translates into a reduction of the effective rock mass shear strength and a resulting lower Factor of Safety (FoS). Although critical to the slope design process, groundwater conditions in the pit can be modified artificially (e.g. mine dewatering and pit slope depressurisation). Therefore, a clear understanding of the pore pressure distribution and potential means for modifying (reducing) any pressures is essential. The hydrogeological model provides valuable information of water table, piezometric surfaces and hydraulic gradients for open pit slope design and performance.

Figure 2.8 summarizes the process of open pit slope design. As shown in this figure, once the geotechnical model is built and the pit sectorization defined, subsequent steps involving slope stability analyses can be carried out. Thus, for each structural zone or domain, the potential failure mode is assessed based on

whether geological discontinuities or rock mass strength is expected to be the controlling factor. After this, the design at three different scales (i.e. bench, inter-ramp, overall) are evaluated based on the required acceptance levels (FoS or PoF) against instability (Read and Stacey, 2009).

For pits in moderately competent rocks, where the rock mass structure is expected to be the controlling factor in slope stability, the design process commences with a bench scale analyses and then the resulting design is translated up in scale into inter-ramp and global designs. For weaker rocks, on the other hand, the slope design is typically initiated by determining the overall slope angle and then moves through inter-ramp slopes to a bench design that meets the required acceptance criteria. It should be borne in mind that the open pit design is an iterative process in which as mining progresses and more data becomes available a re-assessment of the original design should be carried out.

2.3 Typical Modes of Failure in Open Pit Slopes

Many different slope stability problems can be encountered during the operation of an open pit mine. These problems have different origins and commonly have different effects on the design and operation of the pit. It has been found convenient to group the typical mine slope stability problems into three broad categories based on their scale. These are illustrated in Figure 2.9 and described below.

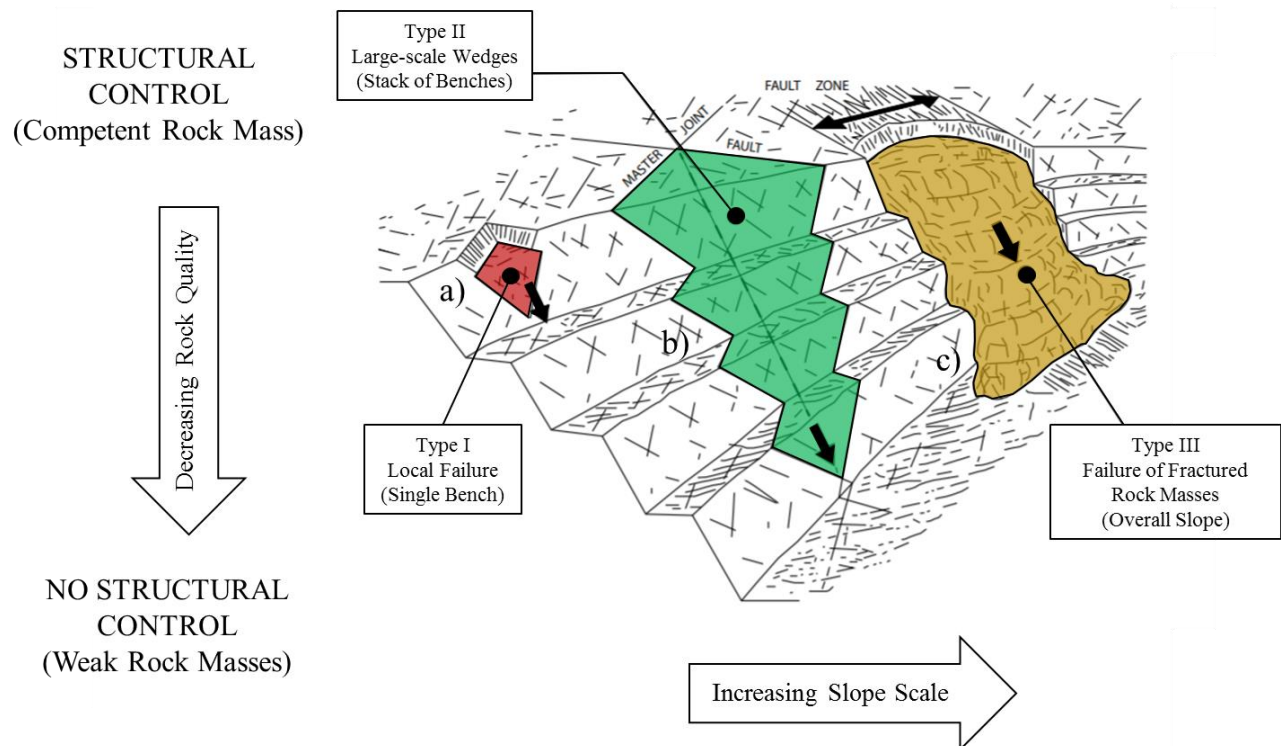


Figure 2.9 Three typical types of failures in open pit mines (Patton & Deere, 1970)

- Type I: Local slope failures involving a single bench.

Local slope failures of small rock blocks along one or more joint planes, such as the one illustrated in Figure 2.9.a, are common during the operation of open pit mines. These are almost impossible to eliminate completely without the use of excessive use of unpractically flat slopes or a costly slope-support system. In most cases, these types of failures are of the extent of less than the height of one bench. Such failures would not usually appreciably influence the overall mining operation. In general, good slope design will minimize local failures but it is unlikely that many mining operations could afford to eliminate all such failures. Safety considerations may require close observation and monitoring of certain individual bench slopes.

- Type II: Large-scale wedge failures affecting several benches.

The presence of two or more through-going discontinuities, such as a highly persistent bedding-plane or master joint combined with a fault, may lead to the situation illustrated in Figure 2.9.b. This geologic condition is potentially much more hazardous than the local failure explained above. This hazard results from a much larger rock block prone to slide. Geologic conditions leading to such failures are often difficult to detect in advance mainly because the two adverse geologic structures may be separated by long distances or the overburden may make them hard to detect. In the example shown in Figure 2.9.b the block failure probably would not occur until the excavation had reached the intersection of the fault and the master joint. A failure of such wedge block could stop mining operations for months and could conceivably change the economics of the entire operation.

- Type III: Global circular failures in highly fractured rock masses.

Rotational shear failure occurs in rock slopes whose intact rock strength is low and with a sparse or non-existent rock joint pattern (i.e. the geologic fabric is essentially randomly oriented). This generally applies to weak rock masses such as highly weathered or closely fractured materials (Figure 2.9.c). The failure surface in these cases generally take place along a surface that approaches the shape of a circular or log spiral arc. This is the most common type of slope failure in soil and soil-like materials.

Based on the geological conditions of the rock mass, rock slope failures can be either along pre-existing discontinuities, or through the rock mass itself. This classification highlights the importance of assessing the shear strength along discontinuities in some cases and the overall rock mass strength in others. A division into structurally and non-structurally controlled rock slope failures is explained below (Figure 2.10).

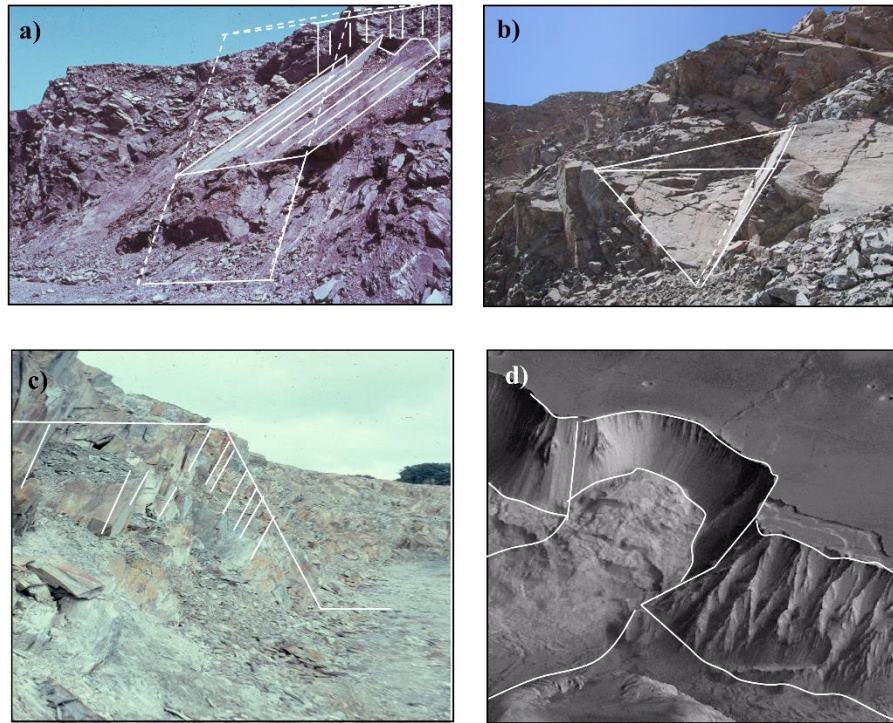


Figure 2.10 Main failure mechanisms in rock slopes: a) Planar, b) Wedge, c) Toppling and d) Circular.

2.3.1 Structurally Controlled Failure Mechanisms

Structurally controlled failure mechanisms are related to low stress environments such as those found in relatively shallow depth open pit mines. These are gravity-driven processes leading to the sliding of rock blocks along the rock mass discontinuities. Traditionally open pit mining in hard jointed rock masses faces structurally controlled failures at the bench scale due to the shear strength of natural discontinuities being exceeded by the imposed shear stresses acting upon them. The three basic modes of structural failure are: planar sliding, wedge sliding, and toppling. These three types are briefly address below.

2.3.1.1 Planar Failure

A planar failure can be considered as a special type of the more general case of wedge failure. Planar failure involves the movement of discrete rock blocks by single (i.e. one plane) sliding. In order that sliding should occur on a single plane, the following geometrical conditions must be met (Hoek & Bray, 1981):

- The plane on which sliding occurs should dip out of the slope face or ‘daylight’ into free space. This means that its inclination or dip angle must be smaller than the dip of the slope face.
- The inclination or dip of the plane of slip must be greater than the friction angle of that plane.

- The dip direction of the planar discontinuity must be within 20 degrees of the dip direction of the slope face, or, stated in a different way, the strike of the planar discontinuity must be within 20 degrees of the strike of the slope face.

Although not a geometrical condition per se, planar failure requires that additional cross-crossing discontinuities exist acting as lateral release surfaces (Figure 2.11). These surfaces do not contribute to the stability by adding shear strength, they just define the lateral boundaries and extension of the sliding rock block. Alternatively, the planar failure may be located on a nose of rock so that the slope forms the lateral termination of the failure mass (Wyllie & Mah, 2005).

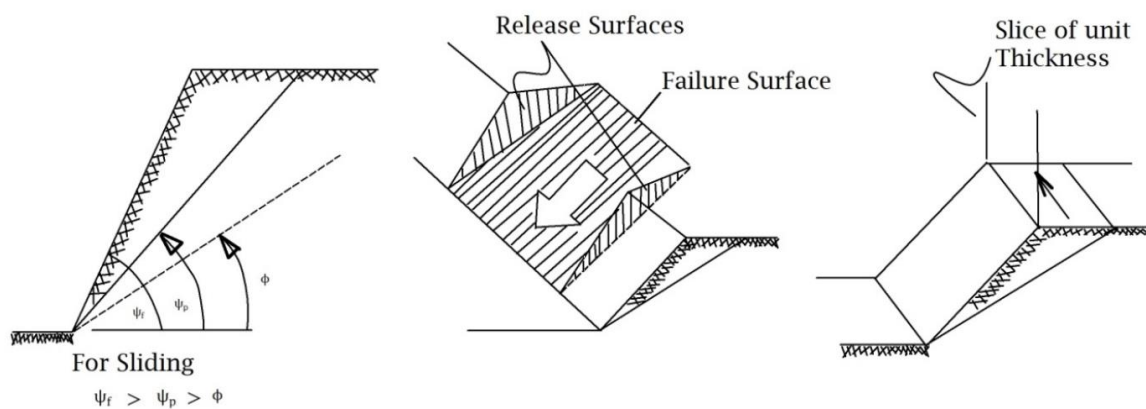


Figure 2.11 Geometrical conditions for planar failure (Hoek and Bray, 1981)

It should be noted that even if all the three above mentioned conditions are met, it only indicates the kinematic feasibility of rock blocks prone to single sliding and not that the actual instability will occur. In other words, the kinematic analysis solely indicates that the requisite geologic structural conditions are present. In most cases a further kinetic analysis would be performed in order to evaluate the potential of failure by considering the shear strength along the failure surface. This is done through a limit-equilibrium analysis whereby external effects such as pore-water pressure, seismic force, and reinforcing elements can be accounted for. This resolution can be carried out in either two or three dimensions, but the most common case is the former, in which the stability formulation considers a unit thickness of the slope.

In the author's experience, a pure planar failure is a comparatively rare instability type in rock slopes mainly because it is only occasionally that all three geometrical conditions required to produce such failure occur in an actual slope. Furthermore, in many cases there is not a single sliding plane, but rather a series of smaller features which create a step-path failure surface. Nevertheless, planar failure stability assessment

following the kinematic and kinetic analyses can be conducted to better understand the sensitivity of the slope to changes in shear strength, groundwater, and applied forces (both resisting and driving forces).

2.3.1.2 Wedge Failure

Unlike planar instabilities, wedge failures can occur over a wider range of geological and geometrical conditions (Wyllie & Mah, 2005). The wedge failure type in rock slopes is probably the most common type of failure involving block sliding (Hoek and Bray, 1981). This type of failure can be considered as a double sliding mechanism occurring along the intersection of two discrete planes, each dipping oblique to the slope (Figure 2.12). The shape of the sliding block is tetrahedron and failure can occur by sliding on both planes in a direction along the line of intersection or along one plane only with separation across the other plane (Piteau & Martin, 1982). The sides of which are defined by the two intersecting planes, the slope face, and the upper slope surface. For wedge failure slip can occur without any topographic or structural release features as long as the line of intersection of two discontinuities daylights into the excavation. The following kinematic conditions are required for a wedge failure to be formed:

- The trend of the line of intersection must approximate the dip direction of the slope face.
- The plunge of the line of intersection must be less than the dip of the slope face. Under this condition, the line of intersection is said to daylight on the slope.
- The plunge of the line of intersection must be greater than the friction angle of the surface.

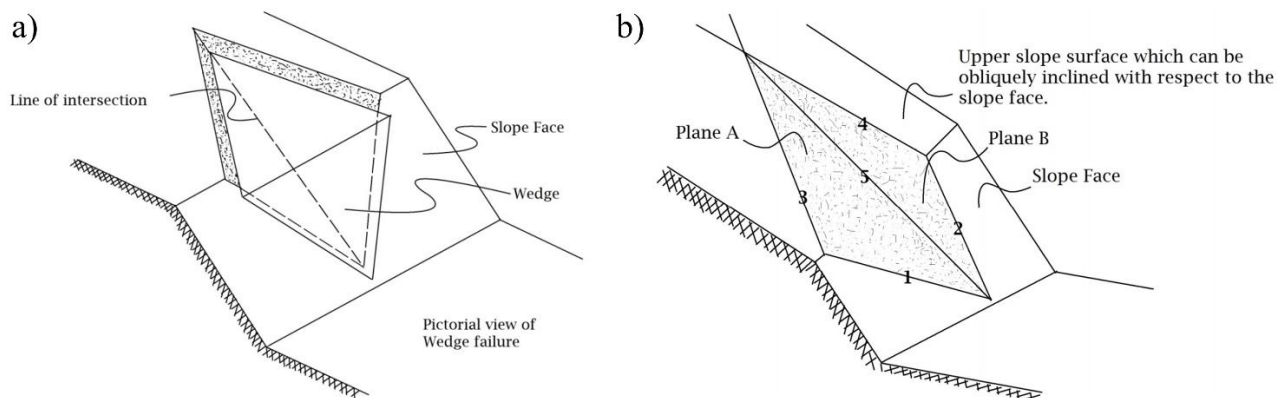


Figure 2.12 Wedge failure: a) Geometry of a biplanar wedge and b) Wedge geometry with an upper face (Hoek and Bray 1981)

When the rock block movement takes place along both planes simultaneously it can be considered as a pure wedge failure whereas if sliding is along the steeper of the two planes it would turn into a single (planar) sliding mode. Kinematic analyses determine whether sliding can occur and, if so, whether it will occur on only one of the planes or simultaneously on both planes, with movement in the direction of the line of intersection. Further details on the procedure can be found on Hoek and Bray (1981). Stereonet-based analysis can be useful for establishing the potential for wedge failure; however, a kinetic analysis will be needed to calculate the Factor of Safety of the rock slope against wedge failure. Again, the limiting equilibrium method of analysis can be used. Details on the method can be found on Wyllie and Mah (2004).

2.3.1.3 Toppling Failure

Toppling failure is possible whenever a set of well-developed (i.e. highly persistent) and through-going (i.e. regularly spaced) discontinuities dip steeply into and strike sub-parallel to the slope face (Piteau & Martin, 1982). Some of the authors that have propose this as a main failure mechanism are Goodman (1980), Hoek and Bray (1981) and Brown (1981). As opposed to planar and wedge sliding failure, toppling involves the overturning of interacting block columns. It is a failure model that relies on the development of thin slabs formed by bedding planes, rock joints, or foliation (Kliche, 1999).

In the experience of the author, a pure toppling mechanics is hardly ever encountered in open pit mines. The few cases this failure type can be observed are related to rock slope cuts in metamorphic rocks (e.g. slates or schists). Toppling is a more complex failure mechanism when compared to planar or wedge sliding. Often, it is seen in conjunction with planar or wedge sliding and not as a unique failure mode i.e. combination of sliding and toppling is most likely to occur.

Toppling failures can be classified into three main types (Figure 2.13). In rocks with one preferred discontinuity system, flexural toppling can occur as shown in Figure 2.13.a. Continuous columns break in flexure as they bend forward. Thinner layers transfer the gravitational load into thicker ones. Typically, erosion of the toe lets the failure begins and it moves backward into the rock slope. The lower portion of the slope is covered with disoriented and disordered fallen blocks. The outward movement of blocks produces interlayer sliding and a portion of the upper surface of each bed is exposed in a series of back facing scarps. Flexural toppling occurs most notably in slates, phyllites and schists. (Goodman,1976).

Block toppling depicted in Figure 2.13.b occurs mostly in competent rocks where the individual columns are formed by a major set of discontinuities dipping into the rock face and a less predominant, widely spaced and orthogonal joint set defining the column height. The toe of the slope, with short columns, receive the load from overturning and longer columns above. This thrusts the toe columns forward, permitting further

toppling to occur. The base of the disturbed mass is better defined than in the case of flexural toppling; it consists of stairway generally rising from one layer to the next. The steps of this stairway are formed by cross joints which occupy the positions of primary flexural cracks in flexural topples. Consequently, new rock breakage in flexure occurs much less markedly than in flexural topples. Thick bedded sedimentary rocks such as limestone and sandstone, as well as columnar jointed basalt exhibit block toppling failure. (Goodman,1976).

Block flexural toppling, depicted in Figure 2.13.c is characterized by pseudo-continuous flexure of long columns through accumulated motions along numerous cross joints. Sliding is distributed along several joint surfaces in the toe, while sliding and overturning occur in a close association through the rest of the mass. Sliding occurs because accumulated overturning steepens the cross joints. There are fewer edge-to-face contacts than in block toppling but still enough to create a loosened, highly open character within the disturbed zone. Interbedded sandstone and shale, interbedded chert and shale, and thin-bedded limestone, exhibit block flexural toppling. (Goodman,1976).

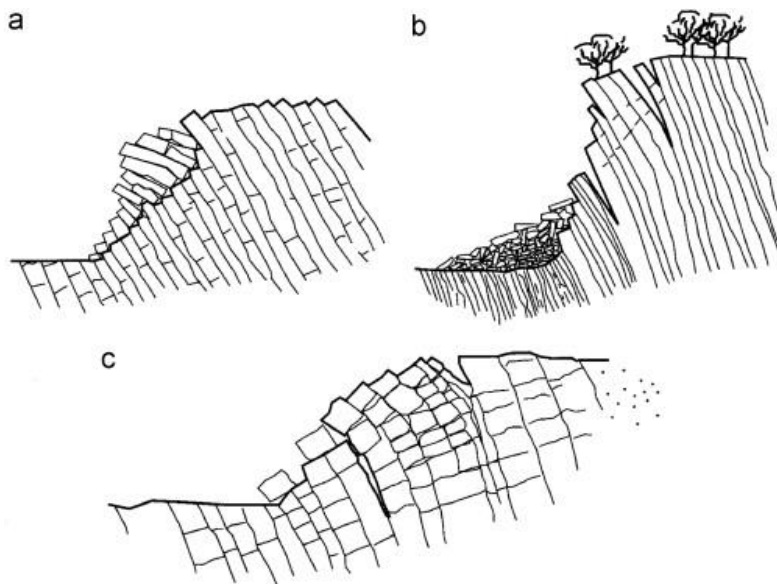


Figure 2.13 Common types of toppling: (a) block toppling, (b) flexural toppling and (c) block-flexural toppling (Wyllie & Mah, 2004; Goodman & Bray, 1976)

2.3.2 Non-Structurally Controlled Failure Modes

Non-structural failure modes include failure of moderately weathered and/or heavily fractured rock masses. Basically, this occurs when the slope dimensions are substantially larger than the individual intact rock pieces (Figure 2.14). In this type of failure, the shape of the slip surface will usually be curvilinear and its

location within the slope will now depend on the overall shear strength of the rock mass rather than that of the discontinuities.

Figure 2.14 shows six rock slopes with different jointing patterns. A slope cut in a massive rock such as the one shown in Figure 2.14.a can be expected to be stable and behave as continuum linear elastic material. The sketches in Figures 2.14.b to 2.14.e illustrate blocky rock masses with joint spacing progressively being reduced. In these four cases slope failure will be dictated by the presence pre-existing discontinuities and the rock mass would behave as a discontinuum media. However, as the rock mass gets more and more populated with rock fractures it gets back to the point of an equivalent continuum material. Figures 2.14.f depicts the case of a highly fractured rock mass in which the failure surface will be essentially of circular shape such as in soil-like materials.

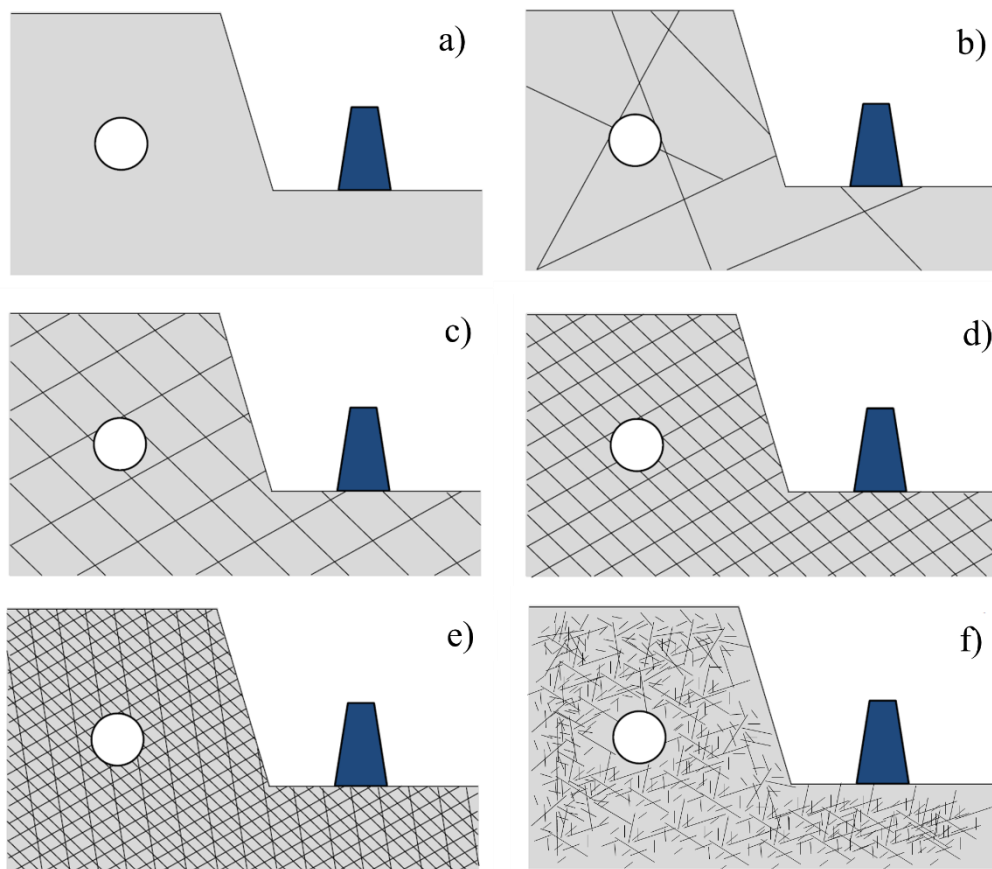


Figure 2.14 Rock mass fracture pattern at different slope scales: a) massive rock mass, b) competent rock mass with few discontinuities, c) and d) blocky rock masses, e) very blocky rock mass and f) highly fractured rock mass (Agharazi, 2013)

2.3.2.1 Rotational or Circular Failure

Although rotational failures are primarily associated with failures in soils, such failures may occur in rock masses if the failure surface is not predominantly controlled by structural discontinuities. If the mode of failure is not structurally controlled and the rock mass strength is of the same magnitude as the induced shear stresses, similar techniques as those used in soil slope stability analysis may be employed. The most widely used of these being the method of slices, where a critical slip surface is calculated based on the balance of driving forces/moments and resisting forces/moments. Several solutions exist (e.g. Bishop, Janbu, Spencer, Morgenstern-Price, etc.) with each differing in terms of the underlying assumptions taken in the force/moment balance to make the problem determinate. There are several books devoted to the method of slices for rock slopes (Hoek & Bray, 1981; Giani, 1992; Kliche, 1999; Wyllie & Mah, 2014).

2.4 Geotechnical Design Methods for Pit Slopes

Current approaches associated with rock engineering analysis and design include the empirical, analytical, numerical and observational methods. These are briefly reviewed in the following sections. This categorization based on four methods have been expanded by Jing & Hudson (2002) into eight approaches and two levels as illustrated in Figure 2.15. Although the same four broad categories are maintained, the classification by Jing & Hudson differentiates methods in which there is a one-to-one mechanism mapping in the model (Level 1) from methods in which such mechanism mapping is not totally direct (Level 2).

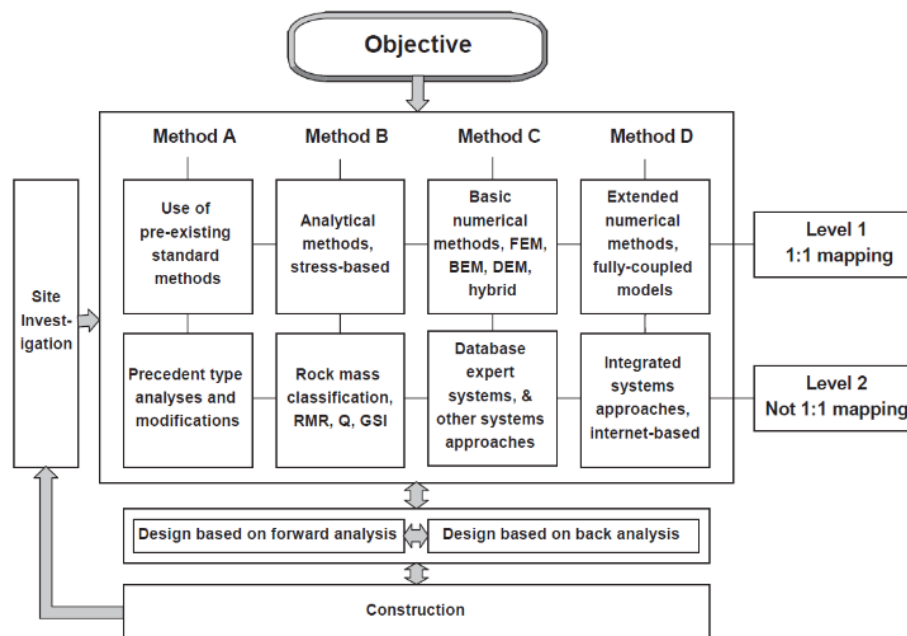


Figure 2.15 The four different basic methods to rock mechanics and rock engineering analysis and design (Jing & Hudson, 2002)

2.4.1 Empirical Methods

Perhaps the first and simplest of all the assessment methods, the empirical approach is all about learning from past experiences and field observations. This is an approach widely used in rock mechanics and is based on basically engineering experiences and critical judgement (E Sousa et al., 2012). It serves for example as a firsthand estimation of some mechanical properties such as rock mass strength or deformation modulus. Also, they are often employed to evaluate stability in rock slope projects by providing a semi-quantitative description of the rock mass.

The applicability of the empirical method is not based on physics laws or constitutive models. They are solely based on comparison and correlation with previous projects. It is in this regard that the engineer should be careful when it comes to selecting an empirical approach by ensuring that the site conditions that the method was based upon are similar to those of the site under study.

The most common empirical methods in rock mechanics are the vast number of rock mass classification schemes available e.g. RMR (Bieniawski, 1989), NGI Q-system (Barton et al., 1974), GSI (Hoek et al., 1995). The most popular ones pertaining to assess rock slope stability are the slope mass rating SMR (Romana, 1991) derived from the RMR; and the Q-slope (Barton, 2017) based on the Q-system. It is out of the scope of this thesis to give a deep review these two approaches since it that have been extensively covered in the literature.

Overall, empirical approaches constitute a useful tool for preliminary estimates of stability performance and for identifying the critical failure mode (Salmi & Saeed, 2015). Its application to design and stability prediction require; however, sound engineering judgment and experience in similar geotechnical settings (E Sousa et al., 2012).

2.4.2 Analytical Methods

Analytical methods use simplified mathematical models that can be solved by closed-form solutions (Nikolić et al., 2016). They idealized field conditions and rely on several assumptions such as shape and location of a failure surface, rigid block movement and uniform localization of shear stresses. If the underlying assumptions are applicable to the rock slope under study, a simple analytical estimate can be as valid as a sophisticated numerical model (Read & Stacey, 2009).

Analytical methods are routinely applied in conventional slope stability analysis and are widely accepted by the engineers, mainly because of its validity and simplicity (Yong et al., 2016). The most well-known analytical technique for geotechnical analysis is the Limit Equilibrium Method (LEM) whereby force or/and moment equilibrium conditions are examined on the basis of statics for a specific failure mechanism (Stead

et al., 2001). These analyses require information about material strength but no stress-strain behavior. Thus, failure modes that involve sliding of rigid blocks are most efficiently solved using the analytical methods (Wyllie & Mah, 2004). It is important to note that the limit equilibrium solution just give an estimate of the FOS with no information on the deformation of the slope, something which numerical models can do.

The limit equilibrium method for analyzing the stability of rock slopes remains up to date a useful tool for use in practice. However, its main limitations arise because the method does not consider the rock mass displacement, strain or deformation. It is the absence of a stress–strain relationship in conventional limit equilibrium analysis methods that is the fundamental piece of missing physics. Using a numerical method such as the finite element to compute stresses inside a limit equilibrium framework to analyze the stability of geotechnical structures is a major step forward to overcome this issue (Krahn, 2001).

2.4.3 Numerical Methods

Numerical methods of analysis used for rock slope stability have become widely used due to the advances in computing power and the availability of commercially available numerical modelling codes (Stead, 2001). To date not only 2D but also 3D numerical modelling software are used for rock mechanics problems. Since a rock mass is a discontinuous, anisotropic, inhomogeneous, and inelastic material, the prediction of its behavior has always been a challenge (Nikolić et al., 2016). There is not closed-form solution for this complex situation and consequently, numerical methods must be applied for solving this type of rock engineering problems.

Numerical methods are approximate solutions of the governing equations to a physical phenomenon given some initial conditions. The calculation process often involves solving partial differential equations (PDEs) that are non-linear and cannot be solved analytically. One advantage of numerical methods over analytical solutions is that they account for the nonlinear stress–strain behaviour of the rock mass and thus allows us to quantify the mining induced stresses as excavation of the pit slope progresses.

Numerical methods can be divided into continuous and discrete approaches depending on the assumption made with respect to the rock mass fracture system. While the continuum approach would be more suitable for massive rock masses or ones with very few fractures; the discrete approach would be more adequate in cases of moderately fractured and/or jointed rock masses with many naturally occurring fractures (Jing & Hudson, 2002).

The most commonly used numerical methods for rock engineering practices are:

- Finite difference method (FDM)
- Finite element method (FEM)

- Boundary element method (BEM)
- Discrete element method (DEM)

The FEM is arguably the most commonly used numerical method for rock mechanics problems. It is out of the scope of this thesis to provide a thorough description of each of the numerical methods mentioned above. A comprehensive review of the subject is given in Jing & Hudson (2002) and Nikolić et al. (2016) who provide a state-of-the-art review regarding the capability and utility of the numerical methods for rock mechanics purposes. The reader is also advised to consult the books by Desai & Christian (1979), Pande et al., (1990) among others.

While these techniques open new possibilities in terms of engineering design, it is critically important to understand the limitations of such geotechnical software and to be aware of the inherent assumptions in the design process.

2.4.4 Observational Method

When it comes to designing excavations in rock, the engineer must inevitably consider the uncertainties related to the rock mass properties. A common approach is to be conservative in the design, but this is not always economically sound or possible in practice (Spross et al., 2014). The observational method is normally applied when the prediction of the geotechnical behavior is difficult like when the ground conditions are complex or not sufficiently well known (Stille & Virely, 2014). This method was first outlined by Terzaghi (1961) and later defined by Peck (1969) with an initial focus on soil mechanics applications. However, it can be argued that an ‘observational’ method has long been used by field geotechnical engineers to some degree or another. In rock engineering, perhaps the best example of the observational approach is the so-called New Austrian Tunneling Method or NATM.

In short, the method embodies a preliminary design prepared on any available knowledge about the site conditions, then during the construction phase, the behavior of the structure is carefully observed and progressively modified until it is deemed appropriate to improve performance. The essential feature of the method is that it refines the original design as new data becomes available. These measures accommodate the structure to the actual conditions at the site.

The observational approach is the only way to validate or calibrate the results from either analytical or numerical methods (Bieniawski, 1984). It is strongly related to field monitoring and instrumentation programs since they are the main source of field data. Application of the observational approach to rock slope engineering would begin with the rock mass characterization via the RMR or GSI. Using this information, the most likely range of stability conditions are identified, and cut slopes angles defined. Exposing the slopes during excavation allows for a more detailed evaluation of the rock mass, from which

more accurate rock mass properties are derived. More accurate slope stability analyses can then be performed, and the original design refined as appropriate.

Case studies of the observational approach to rock slope stability problems can be found in Pease et al., (1995); Klar et al., (2011); Macciotta et al., (2016) among others.

2.5 Approaches in Slope Stability Analysis

Slope stability analysis can be classified into deterministic or probabilistic types depending on how uncertainties are incorporated and evaluated (Ceryan et al., 2018). In a deterministic analysis the input is a set of parameters that are fixed quantities, usually taken as the mean values of the data obtained from site investigation or laboratory testing. For a probabilistic analysis, on the other hand, the input parameters are described as random variables and defined by probability distributions.

Although, simple and straightforward, the deterministic analysis fails to account for the uncertainties and variability explicitly and sufficiently. In recent years, the probabilistic approach along with the calculation of probability of failure (PoF) instead of a Factor of Safety (FoS) has become more common (Nilsen, 2000). The main advantage of the probabilistic method is that it takes into consideration the natural variability and uncertainties of the rock mass properties.

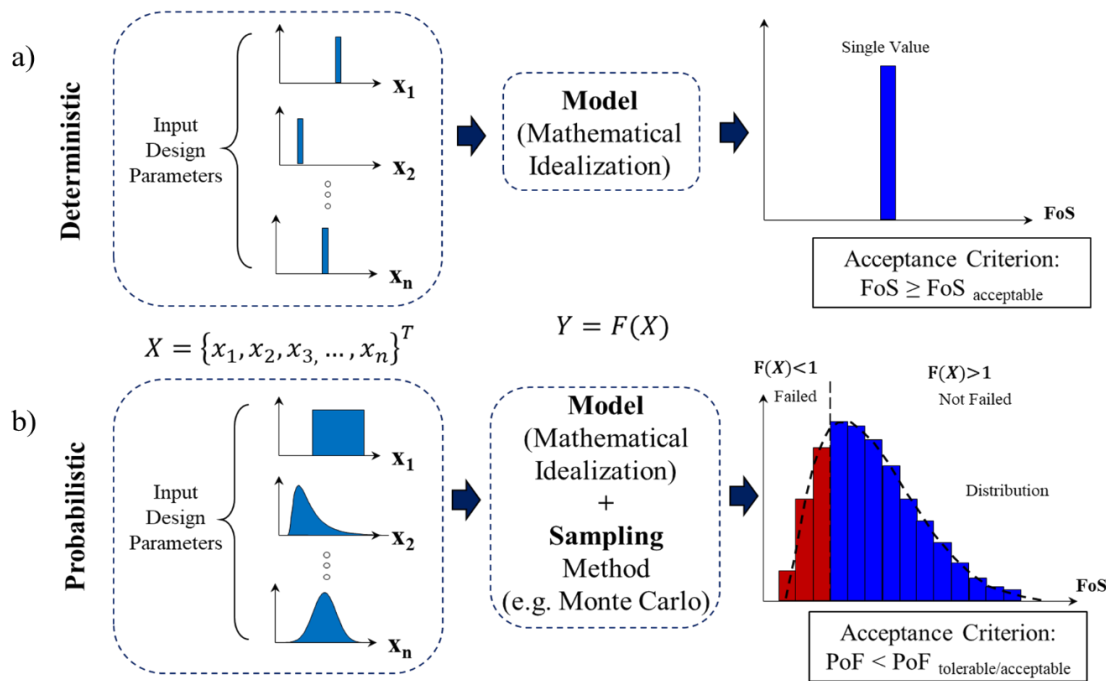


Figure 2.16 Approaches in slope stability analysis: a) Deterministic and b) Probabilistic.

2.5.1 Deterministic Analysis

In the deterministic approach, the stability of the slope is merely described by a single value i.e. the Factor of Safety (FoS). This type of analysis uses a mathematical model, typically the Limit Equilibrium Method (LEM), from which a FoS is obtained based on average values of the rock mass properties as input parameters (Figure 2.16.a). Thus, the uncertainty is not explicitly considered in a deterministic approach design, and the input variables taken as their average are assumed with certainty (Coates, 1977).

Deterministic analysis enjoys a long history of development, and acceptable levels of FoS for various conditions are well established. It has been taken as a routine step for slope stability analysis. However, a deterministic analysis can only cope with the uncertainty and variability of rock mass properties in an implicit way by requiring a large, and sometimes excessively conservative, FoS values (Qian, 2012; Read and Stacey, 2009). Overdesign is one way to compensate for uncertainty and increase relative reliance (El-Ramly, 2002)

2.5.2 Probabilistic Analysis

In a probabilistic slope stability analysis, the same input parameters as the ones for the determinist approach can be used with the only difference that the variability of the rock mass properties are accounted in the design processes (Sjöberg, 1996). These parameters are now described as input random variables and defined by a probability distribution. By using the same mathematical model (e.g. LEM) plus a sampling method such a Monte Carlo technique, the probability of slope failure ca be calculated (Chiwaye & Stacey, 2010). That is the area under the curve for a FoS less than 1 (Figure 2.16.b).

The use of a probabilistic approach for rock slopes was demonstrated, among others, by Leung and Quek (1995), Park and West (2001), Park et al. (2005), Tatone and Grasselli (2010), Grenon and Hadjigeorgiou (2010), Irigaray et al. (2012), Gravanis et al (2014), Zheng et al. (2015), Basahel and Mitri (2019), Obregon and Mitri (2019). In all these studies attention has been given on the calculation of the probability of failure associated with slip failures along rock discontinuities. A thorough and critical review of the different methods of analysis for open pit slope stability was carried out by Abdulai and Sharifzadeh (2018).

2.6 Acceptance Criteria for Open Pit Design

2.6.1 The Concept of Slope Failure

Failure of a slope is an ambiguous concept without a common universally accepted definition. Failure may have meanings related to some type of local malfunction, total collapse, unexpected behavior, or a major disaster; as well as being the opposite of a successful design (Adams, 2015). It should be highlighted, however, that not all slope ‘failures’ are catastrophic (Duncan, 2000). Some of these could be better

described as an unsatisfactory performance or a minor downslope movement of rock debris. Bench-scale slope failures, for instance, are generally expected during the operation of an open pit mine and they can be acceptable when adequately managed by catch berms. Large-scale failure, on the other hand, involving several benches or compromising the overall pit slope are important enough to be of major concern.

In recognition of this important distinction between catastrophic failure and less significant performance problems, it is important to keep in mind the real ‘consequences’ of the event and not to be misled by the word “failure”. This is specially the case in the geotechnical analysis of open pit slopes since the current design practice follows a scale-based approach (i.e. bench, inter-ramp and overall scale slopes). The real concept of ‘failure’ will therefore depend on the affecting scale and economic consequences of such failure.

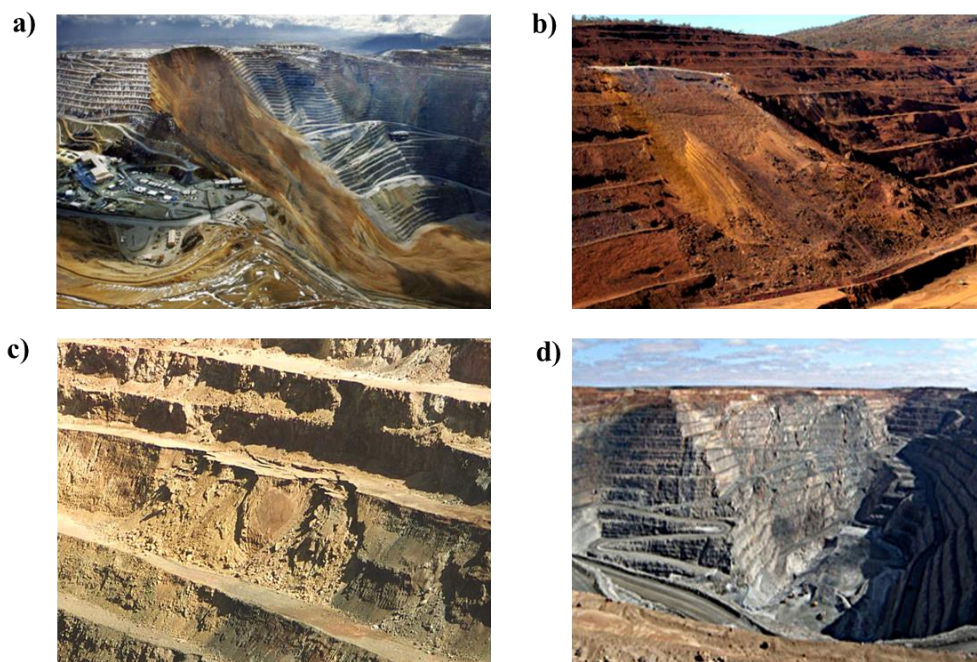


Figure 2.17 Different types of pit slope performance. a) Global circular failure, b) Inter-ramp scale failure, c) Bench slope local failure d) Stable open pit design

2.6.2 Factor of Safety (FoS)

The Factor of Safety (FoS) is the common metric in slope stability analyses. Most geotechnical engineers are accustomed to working with this as a design criterion which is defined as the ratio between the resisting forces (capacity, C) and driving forces (demand, D) of a system (Read and Stacey, 2009).

$$FoS = \frac{C}{D} \quad [Eq.2.1]$$

The FoS is currently an industry standard and the most basic design acceptance criterion in engineering (Read and Stacey, 2009). There has been a wide experience in its application to all types of geological conditions, for both rock and soil materials (Willy and Math, 2004). Furthermore, there are generally accepted factor of safety values for slopes excavated for different purposes i.e. for mining and/or civil applications (Priest and Brown, 1983). From the expression shown above and in a strict sense, a FoS less than unity implies that the slope is unstable whereas a FoS greater than one would be deemed as stable. The case for which the FoS equals one would represent a state of limit equilibrium (meta-stability). From a practical standpoint, however, a design FOS greater than one is required in order to account for the underlying uncertainties in both capacity and demand.

The minimum value of FoS for an engineering design should be selected consistently with the uncertainty involved in the input parameters such as the rock mass shear strength and the consequences of failure (local or global). The rationale to follow is that when the uncertainty and the consequences of failure are both small, it is acceptable to use small factors of safety. Conversely, when the uncertainties or the consequences of failure increase, larger factors of safety are necessary. In this regard, it has been suggested (Terbrugge et al., 2009; Steffen, 2014; Fillion, 2018) that high and therefore conservative values of FoS can be considered for the early stages of a mining project (e.g. scoping studies or pre-feasibility) given that data is limited and often too spread. As the project moves to further stages and as more data becomes available the selected FoS can be narrowed down (Figure 2.18)

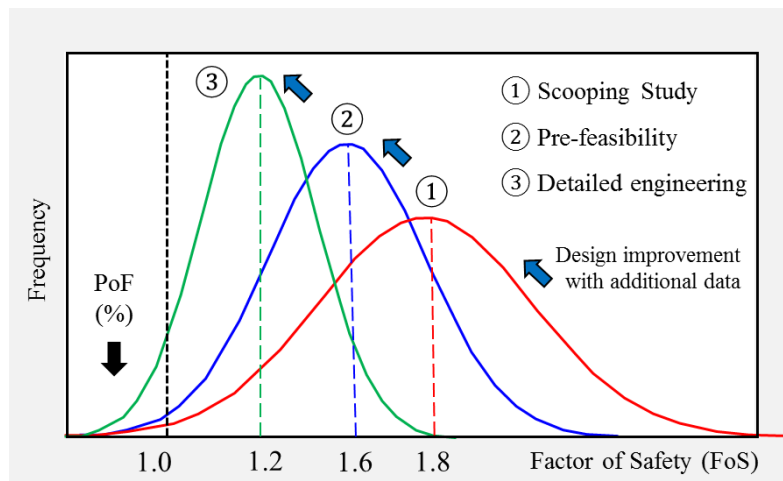


Figure 2.18 Variation of the Factor of Safety (FoS) at different stages of a mining project (Terbrugge et al., 2009 & Fillion, 2018).

2.6.3 Margin of Safety (MoS)

Stability analysis is basically a comparison of available strength to imposed stresses. These quantities could also be called capacity (C) and demand (D) of a rock engineering system. The Margin of Safety (MoS) is defined as the difference between the capacity and demand with the slope being unstable if the MoS is negative (Wyllie, 2017). This means that the limit case for the Margin of Safety is a value of MoS=0. The MoS is expressed in terms of probability and it is calculated as follows:

$$MoS = P[C - D < 0] \quad [Eq.2.2]$$

Where C and D are the two input random variables. The limit state, corresponding to the boundary between desired and undesired performance, would be when MoS = 0. If MoS \geq 0, the structure is safe (desired performance). Let us now assume that both the capacity and demand follow a normal distribution and that they are mathematically defined with the probability density functions f(c) and f(d), respectively as in Figure 2.19.a. When the capacity and demand distributions are compared, it is possible to calculate a third probability distribution for the margin of safety (Figure 2.19.b). It follows that for the special case in which C and D are normally distributed, f(MoS) is normally distributed as well (Baecher and Christian, 2005).

The mean of f(MoS) is:

$$\mu_{MoS} = \mu_C - \mu_D \quad [Eq.2.3]$$

And the standard deviation of the MoS is:

$$\sigma_{MoS} = \sqrt{\sigma_C^2 + \sigma_D^2 - 2\rho_{CD}\sigma_C\sigma_D} \quad [Eq.2.4]$$

Where:

μ_C and μ_D : mean values of C and D, respectively.

σ_C and σ_D : standard deviations of C and D, respectively.

ρ_{CD} : correlation coefficient between C and D.

A reliability index β which expresses the distance of the mean MoS from its critical value (MoS=0) can then be calculated following.

$$\beta = \frac{\mu_{MoS}}{\sigma_{MoS}} = \frac{\mu_C - \mu_D}{\sqrt{\sigma_C^2 + \sigma_D^2 - 2\rho_{CD}\sigma_C\sigma_D}} \quad [Eq.2.5]$$

Having determined the reliability index β , the probability for which P[MoS<0] is mathematically given by:

$$P[MoS < 0] = \Phi(-\beta) \quad [Eq.2.6]$$

Where $\Phi[Z]$ represents the area under the normal curve where the safety margin is less than zero. This area is obtained from the standard normal table or calculated using modern spreadsheets such as Microsoft Excel. This is also shown in Figure 2.19.b, with $P[\text{MoS} < 0]$ being proportional to the area of the shaded yellow area.

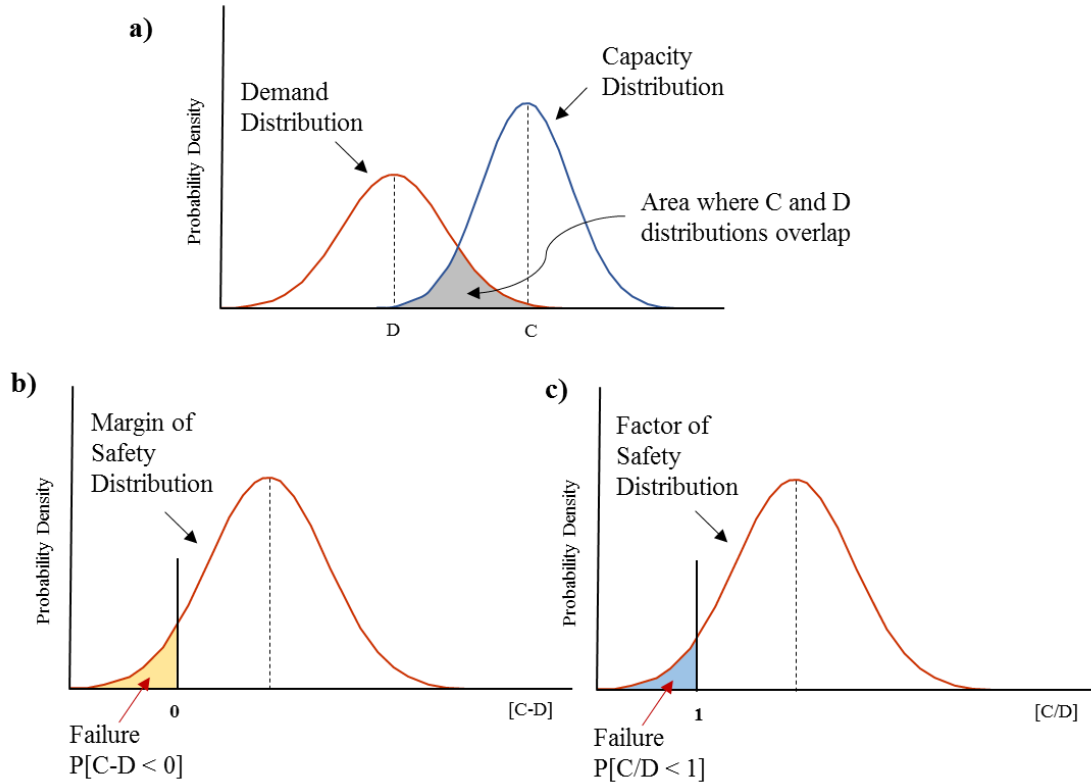


Figure 2.19 Probability density functions for: a) Capacity and Demand, b) Margin of Safety and c) Factor of Safety (Savely, 1987)

2.6.4 Probability of Failure (PoF)

The Probability of Failure (PoF) is also a relationship between the capacity (C) and demand (D) of a rock engineering system. The PoF is defined as the probability of the ratio C/D -also known as Factor of Safety FoS- being less than one (Read & Stacey, 2009). The PoF is calculated as follows:

$$PoF = P[FoS < 1] \quad [\text{Eq.2.7}]$$

$$PoF = P\left[\frac{C}{D} < 1\right] \quad [\text{Eq.2.8}]$$

Where C and D are the two input random variables. Let us now assume that both the capacity (C) and demand (D) follow a lognormal distribution, then $\ln C$ and $\ln D$ are normal variates. This means that the logarithm of their ratio (C/D) becomes the difference between their logarithms and the formulation becomes identical to the case of the MoS. For this case the reliability index β is given by:

$$\beta = \frac{\mu_{FoS}}{\sigma_{FoS}} = \frac{\ln\left(\frac{\mu_{FoS}}{\sqrt{1+CoV^2}}\right)}{\sqrt{\ln(1+CoV^2)}} \quad [\text{Eq.2.9}]$$

Where μ : mean; σ : standard deviation and $CoV = (\sigma/\mu)$ is the coefficient of variation of the distribution of the FoS . The probability for which $P[FoS < 1]$ is mathematically expressed as:

$$P[FoS < 1] = \Phi(-\beta) \quad [\text{Eq.2.10}]$$

Figure 2.19.c. shows the PoF with the critical area (i.e. $FoS < 1$) highlighted in blue. It should be noted that the above equations are only valid when C and D are lognormally distributed. In cases where this condition is not met, calculations get more complicated and tools such as the Monte Carlo sampling technique comes in handy.

2.6.5 Suggested Design Criteria

The FoS is the most common criterion for slope design, and there has been a wide experience in its application to all types of geological conditions, for both rock and soil materials. Furthermore, there are generally accepted factor of safety values for slopes excavated for different purposes i.e. mining or civil facilities. However, unlike civil slopes, where the emphasis is on the reliability and performance of the design and cost/benefit is less of an issue, open pit slopes are normally constructed to lower levels of stability, recognizing the shorter operating life spans involved and the high level of monitoring, both in terms of accuracy and frequency, that is typically available in the mine.

It could be said that all excavated pit walls have potential for failure. The acceptability of any given failure will depend on its consequence and perceived risk. If the failure of a given slope is deemed to have no impact on the surrounds, or the safety and production of a mine, there is likely to be minimal concern. Therefore, pit wall design is essentially governed by two factors: i) the probability of failure, and ii) the consequence of it. To accommodate these two design factors, it is usual practice to apply an appropriate factor of safety (FOS) and/or probability of failure (POF) to the design geometry of the pit wall. Recommendations exist in the literature for acceptable FoS and PoF values (Kirsten, 1983; Priest & Brown, 1983; Swan & Sepulveda, 2000; Christian, 2004; Sullivan, 2006). Table 2.1 describes the acceptance criteria for FoS and PoF at different scales for open pit slope design based on the work by Read & Stacey (2009).

Table 2.1 Suggested acceptable criteria for open pit slope design

Slope Scale	Consequence of failure	Acceptance criteria		
		FoS min (Normal Conditions)	Fos min (Extreme Conditions)	PoF max Pr[FoS<1]
Bench	Low-High	1.1	NA	25-50%
Inter-ramp	Low	1.15-1.2	1	25%
	Medium	1.2	1	20%
	High	1.2-1.3	1.1	10%
Overall	Low	1.2-1.3	1.05	15-20%
	Medium	1.3-1.5	1.10	5-10%
	High	>1.5	1.15	<5%

NA: Not Applicable.

Extreme refers to earthquake or heavy rainfall.

2.7 Chapter Summary

Chapter 2 covers a critical review of the wider literature on rock slope stability assessment.

- It started with formal definitions of epistemic uncertainty and aleatory variability for rock engineering systems and highlighted the reducible character of epistemic uncertainty with further laboratory and/or field measurements. It was also stated that this kind of uncertainty can be handled using probability theory and updated with additional data collected at different stages of the project.
- The main impacts of slope failures in open pit mining operations was addressed from an economic, environmental and regulatory standpoint. Also, a description the geotechnical design procedure was given following a scale-based approach i.e. bench, inter-ramp and global slope design.
- The importance of building a representative geotechnical model as the first step in the open pit design procedure was emphasized. The geotechnical model required four input components: the geological, structural, rock mass and hydrogeological models.
- The typical (i.e. structural and non-structural) modes of failure in open pit slopes was explained by considering joint fabric, rock mass conditions, scale of analysis and impact of failure.
- A summary of the main geotechnical design methods (i.e. empirical, analytical, numerical, and observational) was provided and compared in terms of their assumptions, limitations and advantages.
- The deterministic and probabilistic approaches for rock slope stability assessment was explained and compared in terms of the input and output parameters. Advantages of the probabilistic analysis to handle uncertainty and variability over the traditional deterministic approach was highlighted.
- Finally, a summary of the most common used acceptance criteria for open pit mine design was provided in terms of minimum Factor of Safety (FoS) and maximum Probability of Failure (PoF).

Chapter 3

Analysis of Structural Geological Data

The slope design in a jointed rock mass such as the one shown in Figure 3.1 requires a sound understanding of the geological discontinuities (Hoek and Bray, 1981; Nicholas & Sims, 2001). For data collection purposes, these geological structures can be grouped into two main types (Call, 1972; Call et al., 1976; Priest, 1980; Villaescusa, 1991; Cylwik et al., 2011). Minor discontinuities like joints and bedding planes are those that are relatively small and usually too numerous to be mapped and located individually whereas major discontinuities such as principal faults or shear zones are those that are long enough to be individually located on a geological map (Nicholas & Sims, 2001; Wyllie and Mah, 2004).

The term ‘discontinuity’ -as it is used throughout this thesis- is a collective or general term to refer to most types of natural breaks within the rock having zero or low tensile strength (Priest, 1993) meaning that failure tends to occur preferentially along these surfaces (Barton, 1978; Norrish & Wyllie, 1996; Gudmundsson, 2011). It is a very commonly used term for rock defects such as bedding planes in sedimentary rocks, cleavage and schistosity in metamorphic rocks, and joints often occurring in igneous rocks (Giani, 1992).



Figure 3.1 Jointed rock mass with three principal joint sets.

3.1 Methods of Field Data Collection

The principal methods of describing rock masses and their discontinuities from a slope engineering point of view are the survey of rock exposures and drill core description. More recent techniques allow us to

automate traditional outcrop mapping and manual core logging such as the use of terrestrial photogrammetry and down-hole televiewers (both acoustic and optical). All these methods will be briefly explained in the following sections and real-life case studies will also be presented in the following chapter.

3.1.1 Surface Structural Mapping

Geological mapping of structural data is required in almost all stages of a rock mass characterization program (Hoek et al., 2000). Structural data are a key input for kinematic, limit equilibrium and numerical slope design analyses (Read and Stacey, 2009). The fracture data are collected by mapping methods that provide the appropriate input parameters required for rock slope design. The geometrical characteristics and physical properties of each major-types discontinuity feature is usually established deterministically. Minor geological structures represent for practical purposes an infinite population in the area of design and their geometrical and physical features are therefore treated statistically in a slope-design analysis from a representative smaller sample (Priest, 1980; Villaescusa, 1991).

There are ten parameters selected to describe rock discontinuities as given in the ISRM publication: *Suggested methods for the quantitative description of discontinuities in rock masses* (Barton, 1978), these are: orientation, spacing, persistence, roughness, wall strength, aperture, filling, seepage, number of sets, block size (see Figures 3.2 and 3.3). A brief description of each of these parameters is provided below as given by Zhang, L (2016). Although all these are important a special attention will be given to three geometrical properties (i.e. orientation, spacing and persistence.) and one mechanical property (i.e. wall shear strength) in the following sections.

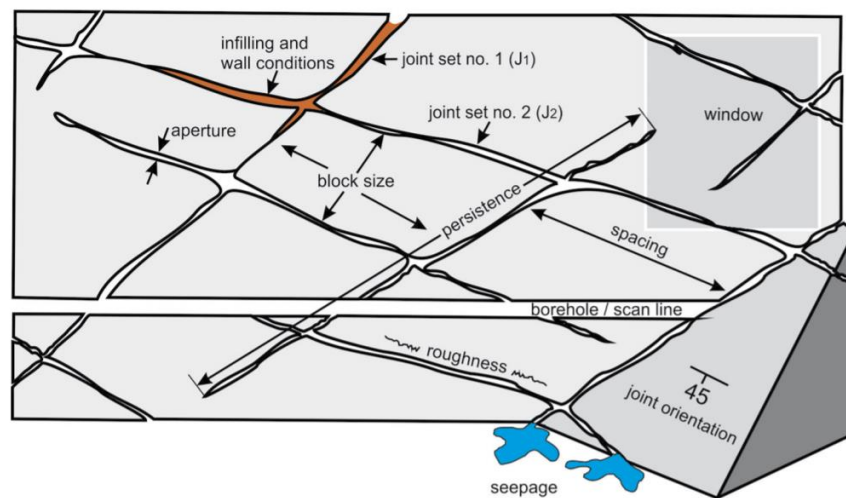


Figure 3.2 Recommended ISRM discontinuity properties to be described during structural field mapping (Harrison & Hudson, 1997)

1. Orientation: The attitude of a discontinuity in space. It is described by the dip direction (azimuth) and dip of the line of steepest declination in the plane of the discontinuity.
2. Spacing: The perpendicular distance between adjacent discontinuities. It normally refers to the mean or modal spacing of a set of discontinuities.
3. Persistence: The discontinuity trace length as observed in an exposure. It may give a crude measure of the areal extent or penetration length of a discontinuity. Termination in solid rock or against other discontinuities reduces the persistence.
4. Roughness: The inherent surface roughness and waviness relative to the mean plane of a discontinuity. Both roughness and waviness contribute to the shear strength. Large scale waviness may also alter the dip locally.
5. Wall strength: The equivalent compressive strength of the adjacent rock walls of a discontinuity. It may be lower than rock block strength due to weathering or alteration of the walls. It is an important component of shear strength if rock walls are in contact.
6. Aperture: The perpendicular distance between adjacent rock walls of a discontinuity, in which the intervening space is air or water filled.
7. Filling: The material that separates the adjacent rock walls of a discontinuity and that is usually weaker than the parent rock. Typical filling materials are sand, silt, clay, breccia, gouge, mylonite. It also includes thin mineral coatings and healed discontinuities such as quartz and calcite veins.
8. Seepage: The water flow and free moisture visible in individual discontinuities or in the rock mass.
9. Number of Sets: The number of discontinuity sets comprising the intersecting discontinuity system. The rock mass may be further divided by individual discontinuities.
10. Block Size: The rock block dimensions resulting from the mutual orientation of intersecting discontinuity sets and resulting from the spacing of the individual sets. Individual discontinuities may further influence the block size and shape.

The suggested methods for the quantitative description of discontinuities is rock masses, prepared by ISRM (Barton, 1978), provides a thorough description to the principal aspects of the discontinuity field measurement procedure. The report by the Geological Society Engineering Group Working (1977) entitled: Description of Rock Masses for Engineering Purposes, is a is another source the reader is forwarded to for further details on rock discontinuity property description. Minor structural features (e.g. rock joints) used

in the bench design are most commonly collected by using the scan-line method (Call, 1972) or window-mapping method (Mathis, 1988). These are further explained below.

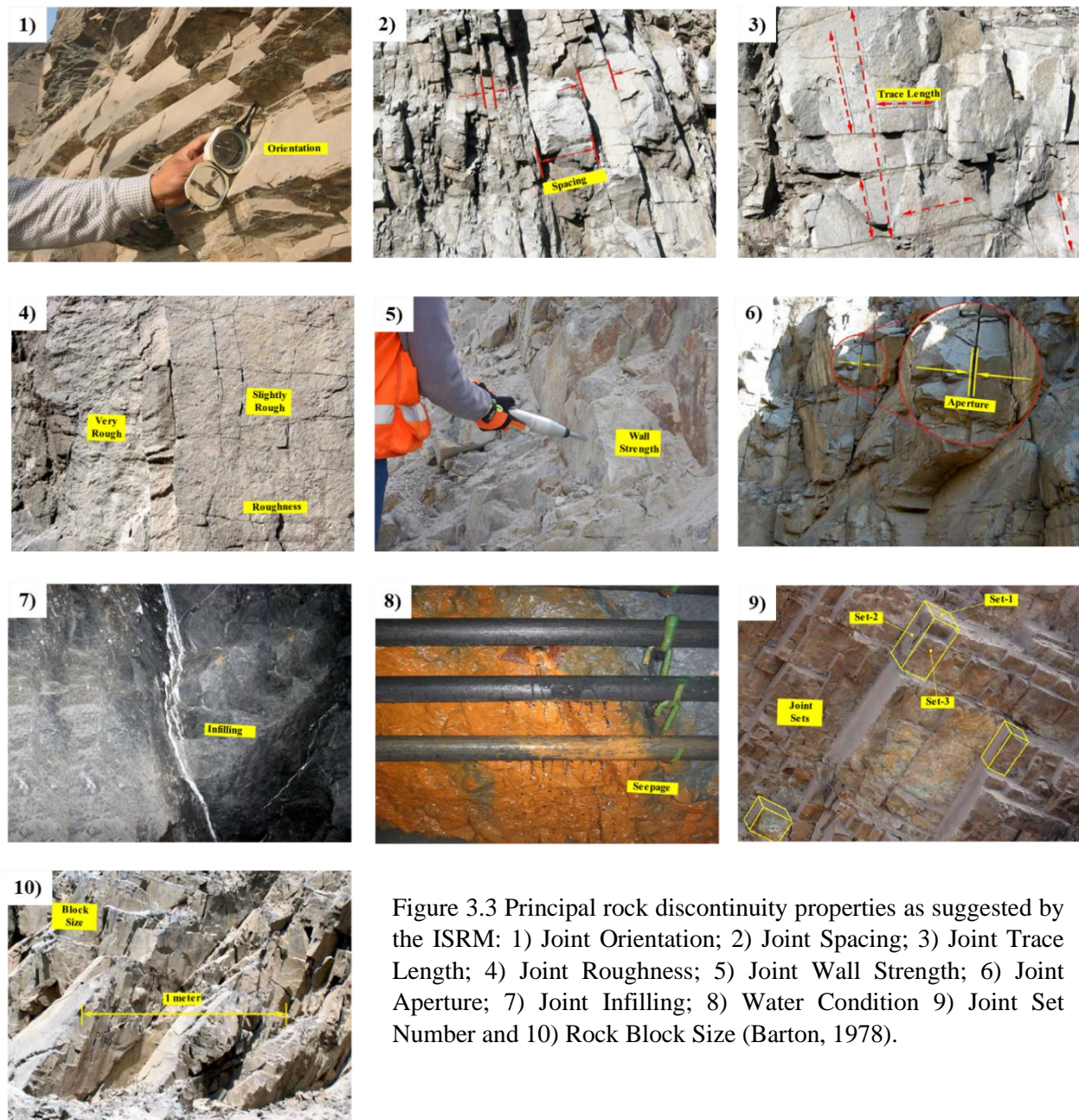


Figure 3.3 Principal rock discontinuity properties as suggested by the ISRM: 1) Joint Orientation; 2) Joint Spacing; 3) Joint Trace Length; 4) Joint Roughness; 5) Joint Wall Strength; 6) Joint Aperture; 7) Joint Infilling; 8) Water Condition 9) Joint Set Number and 10) Rock Block Size (Barton, 1978).

Window mapping involves measuring all discontinuities within a representative area or “window” (Figure 3.4). These are rectangular or square windows. The bench face or outcrop is divided into ‘cells’ and spaced at regular intervals along the excavation walls in order to collect the field data (Wyllie and Mah, 2004). Normally, the width of the cell is equal to one to two times the height of the cell (Nicholas & Sims, 2001).

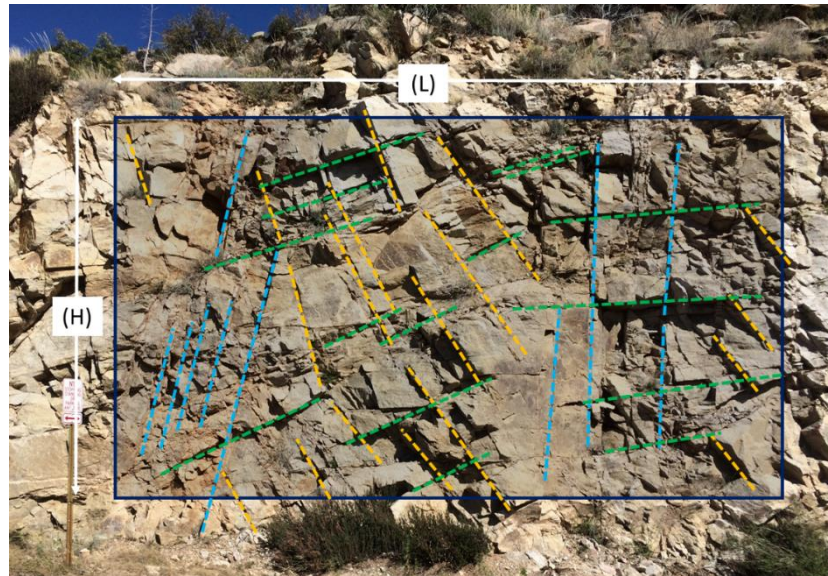


Figure 3.4 Example of a structural window mapping with joint traces highlighted.

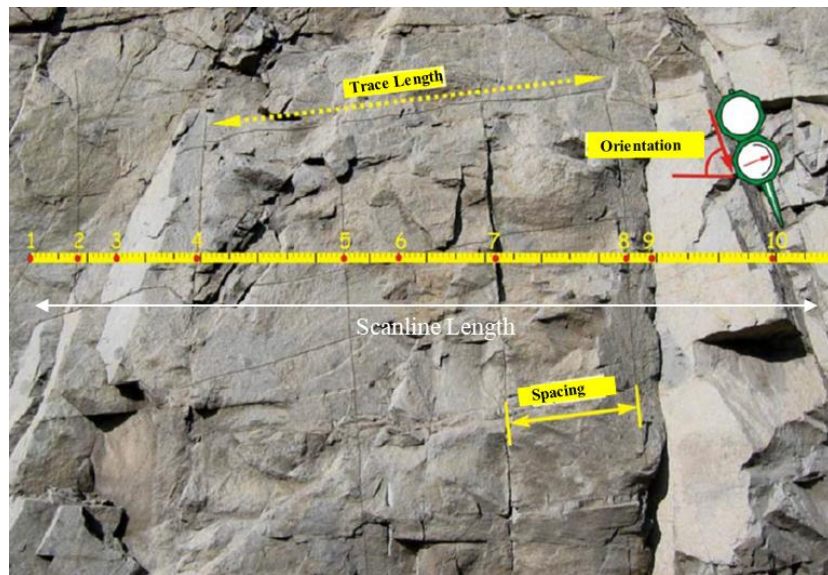


Figure 3.5 Example of a structural scanline mapping intersecting ten rock joints.

This is a form of a planar sampling or two-dimensional mapping tool. We begin by visually identifying the main discontinuity sets within each cell boundaries, and the orientation, length, and spacing characteristics are recorded. This process requires the grouping by eye of a family of discontinuities with similar orientational features in order to form a geological design set.

A detailed line survey (also commonly called scan-line mapping) is a systematic, one-dimensional spot sampling method which can be extended to two dimensions if the line is located inside a sampling window. This technique consists of stretching a measuring tape along the bench face or outcrop and recording the point of intersection, orientation, length, roughness, filling type, and thickness of each discontinuity crossed by the tape (see Figure 3.5). Ideally, the sampled sites would be randomly selected at three equal length and mutually orthogonal directions. Any discontinuity ignored by one line because of its orientation would be sampled preferably by one or two of the other lines. In practice, however this is often not the case, since rock exposures to be mapped are determined by availability and accessibility constraints. The dimensions of the observation window should be kept constant at each measured site if possible, since data from different sites is usually grouped together.

The scanline method has been described in detail by numerous authors (Call, Savely, and Nicholas 1976; LaPointe and Hudson 1985; Warburton 1980). The technique has been used in mining and civil engineering for many years and has been well documented by several authors (Priest & Hudson 1981; Windsor & Thompson 1997; Harries 2001; Brown 2003). Regarding the cell-mapping method, this has been summarized in the literature (Call, Savely, and Nicholas 1976; Call 1992). The reader is referred to these and other papers for further discussion of both surface mapping methods.

One key aspect in the collection of field structural data is the number of measurements being considered. In this respect, Savely (1972) stated that at least 60 observations of joint orientations are required to stereographically define discontinuity sets. Also, Villaescusa (1991) recommended at least 40 measurements per discontinuity set in order to construct experimental histograms and thus provide a sound statistical base of the discontinuity set characteristics. Considering that granitic rocks often exhibit three orthogonal joint sets, a minimum of 120 orientations should be mapped in this type of rocks. Priest and Hudson (1981) presented a method to calculate the number of observations required to estimate the precision of the mean discontinuity spacing value for a negative exponential distribution. Following their calculations, at least 41 measurements as shown in Figure 3.6 will be needed for a mean estimation within 20% error at an 80% confidence level. The required number of observations increases rapidly as the estimation error is decreased such that at 90% confidence with a 10% error estimation a total of 271 measurements should be made for design purposes. This quantity can easily be achieved by grouping data that belongs to the same structural domain and constructing composite stereoplots from them. When doing so, one must be careful to not group data from different rock types or previously established different structural domains.

It should be kept in mind that rock discontinuity properties are three-dimensional entities, but all field observations of rock structure are usually one-dimensional (as in the case of scan-line mapping) or at best two-dimensional when measurements are gathered from outcrop or excavation walls through window or cell mapping. It is worth noting then that data processing techniques based upon geometrical statistics and probability theory are required in order to make sound estimates of the 3D structural features (Einstein & Baecher, 1983; Davis & Sampson, 1986; Priest, 1993,). In this respect, some of the promising novel techniques for the geometrical representation of complex three-dimensional (3D) discontinuity systems are Discrete Fracture Network (DFN) models. DFNs are a mathematical representation of fracture characteristics in 3D space constructed from field data usually collected from limited exposures, e.g. one-dimensional (1D) borehole logging and two-dimensional (2D) outcrop mapping (Rogers et al., 2007; Elmo & Stead, 2010; Lorig, 2015).

The responsibility of the engineering geologist does not end with the gathering and compilation of data but must also include the representation of significant geologic factors in a form that is convenient, representative, and readily understandable to the slope stability analyst and the mine management. Basically, there are two graphical methods of presenting data: (i) maps and cross sections wherein the actual position of geological structures is shown and (ii) statistical data plots giving frequencies of orientation, spacing, persistence, etc.

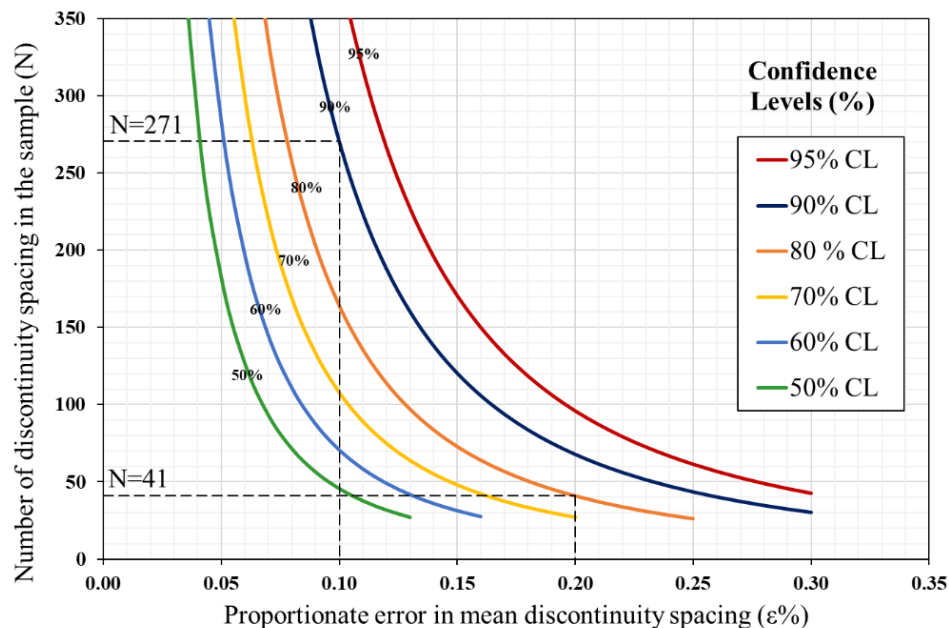


Figure 3.6 Number of observations required to estimate of the mean discontinuity spacing (Priest and Hudson, 1981)

3.1.2 Geomechanical Core Logging

As noted above, outcrop mapping is a key step in the collection of surface structural data that is commonly performed prior to mining (Read and Stacey, 2009). Even if surface mapping data are available and reliable, there is no guarantee that the rock-fabric data collected on surface will correspond to that at depth. Often the most cost-effective method to obtain the needed structural data at depth for rock slope design is through oriented borehole drilling and core recovery.

Boreholes represent line samples of the rock mass (Barton, 1978) and as such, it can be thought as a scanline that goes from surface to a given depth. Therefore, the same rock discontinuity parameters as described in a scanline are also reported for a borehole logging. It should be highlighted that mapping of exposed rock faces allows for the direct assessment of several rock mass characterization parameters that cannot be established by routine drill hole logging (Villaescusa, 2014). For example, joint persistence which defines the forming rock block's sizes will usually not be possible to be assessed from drill hole observations (Barton, 1985).

Core logging entails recording the orientation of geological structures in core samples to obtain the in-situ (actual) position of discontinuities to determine favorable or unfavorable conditions in the stability analysis of rock slopes (Ureel et al., 2013). The orientation of discontinuities encountered in a borehole can only be determined if it has been properly oriented. There are a variety of tools currently in use for core orientation e.g. Clay Imprint, Ball-Mark, EZY-Mark, ACT Reflex, etc. Commonly the process involves identifying the lowermost point ('bottom mark') on the top face of what is to be the next run of core (Davis & Cowan, 2012; Holcombe et al., 2013). After the core is extracted it is reassembled as far as possible and the 'bottom mark' used to subtend an orientation line along the core (known as the 'orientation mark' or 'ORI line'). This line is used to orient all other features in the core.



Figure 3.7 Reflex ACT II orientation tools (Reflex Instruments, 2013).

The Reflex ACT I, II, and III are core orientation devices developed by Reflex Instruments that are becoming increasingly popular and are now being applied worldwide in the mining industry (Figure 3.7). Once core orientation has been achieved and the reference line marked, the orientation of any structures along the core run can be measured using a goniometer. The following parameters are important when recording data for each core run: reference angle, alpha and beta angles (Figure 3.8). The alpha angle is the maximum angle of intersection between the discontinuity surface and the core axis. The beta angle is measured around the circumference of the core from the orientation line to the maximum down-hole apex of the discontinuity. The geologists, geological technicians, or geotechnical engineers log the recovered drill core. During the core logging process, a key factor is to distinguish between natural occurring joints and mechanical breaks induced by drilling or handling. Finally, the data can be processed, interpreted and plotted on stereographic projection to determine where adversely oriented joint sets with respect to the slope's direction may occur.

It is beyond the scope of this thesis to discuss all aspects of core logging. Readers who wish to pursue further detail on this matter are advised to consult the work by Bleakly, 1985; Nelson et al., 1987; Marjoribanks, 2002; and Ureel et al., 2013.

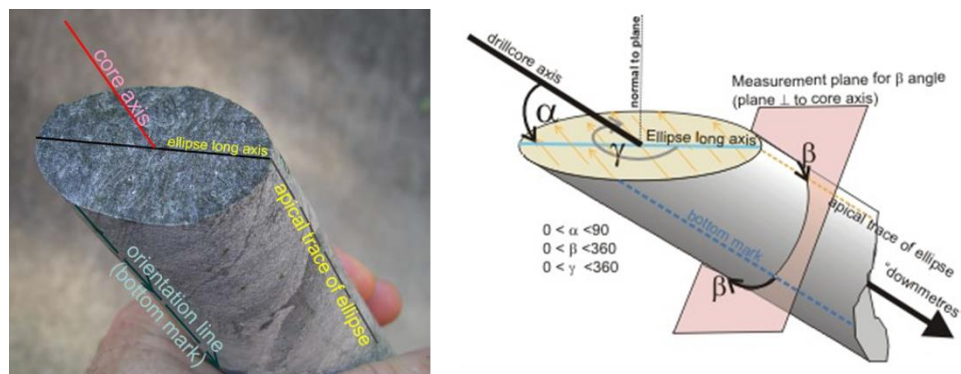


Figure 3.8 Angle conventions in oriented drill core (Holcombe et al., 2013)

3.1.3 Other Non-Traditional Methods

3.1.3.1 Televier Logging Methods

Traditionally, the only method to obtain structural data from drill holes has been via the logging of oriented drill core. Multiple instruments are now available to orient drill cores; however, the development and availability of televier technologies has provided new methodologies as opposed to the traditional (manual) methods for collecting reliable and accurate structural data. Although most widely used in the oil industry, televiers are now becoming routinely used to capture structural data for geological,

hydrogeological, and geotechnical investigations. Televueers are a digital marking technique capable of core orientation in angled vertical drill holes (Thomas et al., 2015).

Televueer surveys capture a continuous log of a downhole image of the internal drill hole walls. They can be grouped into optical (OTV) and acoustic (ATV) types. The optical type uses light and a camera to provide a direct image of the drill hole wall, and thus it can only be collected in air or clear water intervals. The acoustic type uses the amplitude of a reflected acoustic signal (Gaillot et al., 2007). The amplitude of the reflected acoustic signal is recorded as photographic-like images (Weir, 2015). Acoustic televueer can only be collected in borehole intervals where there is gas-free fluid. Figure 3.9 shows logs corresponding to these two types of televueer surveys.

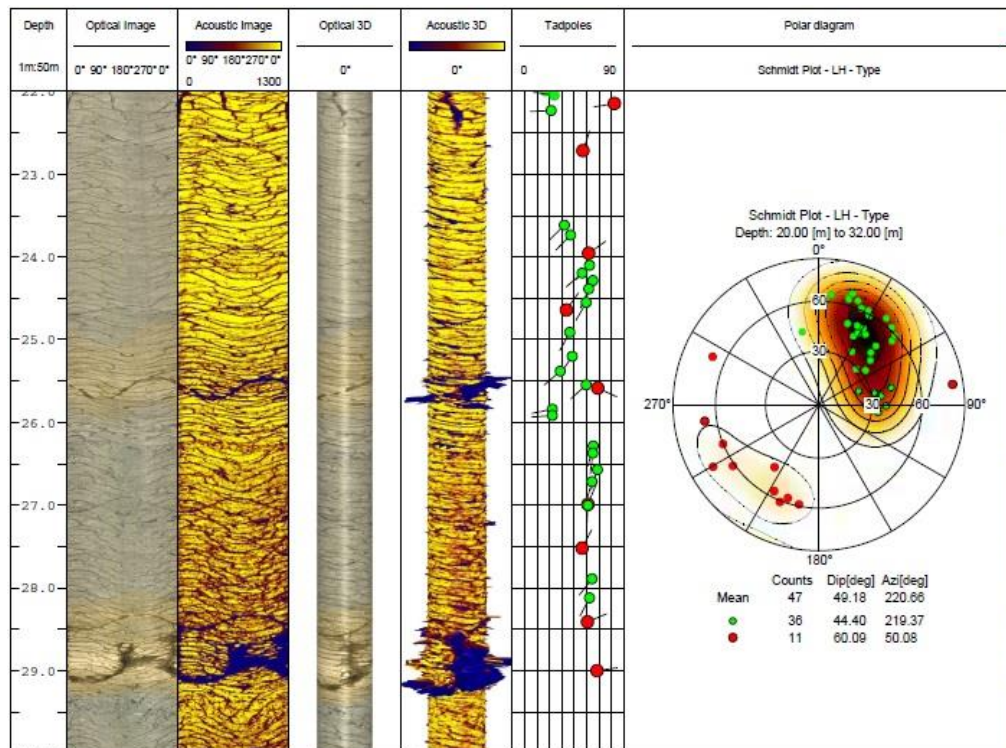


Figure 3.9 Example of ATV and OTV images of a vertical borehole (Piffer & Rinaldi, Waterstones Srl).

Planar features intersecting the borehole appear as sinusoids across the 2D image (Figure 3.10) and are derived from the image log by fitting sine waves interactively to the observed features (Williams and Johnson 2004). Each feature has its true orientation (dip & dip direction angles), which are calculated by considering the image orientation, and orientation of the well.

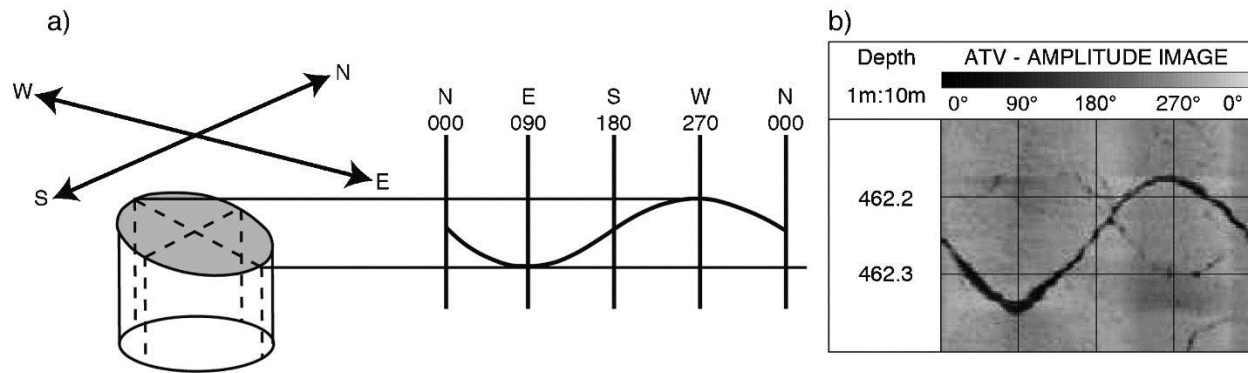


Figure 3.10 Orientation of discontinuity in borehole: (a) elliptical intersection between discontinuity and core; (b) 'unwrapped' view of borehole wall with discontinuity (Colog Inc. 1995).

Although televiewer surveys are believed to be expensive; it can actually be a cost-effective data collection tool in certain situations. The existence of broken zones and core loss during classical core logging present difficulties in obtaining orientation data, which can result in a paucity of structural data for significant intervals of the drill hole. In this situation, televiwers can provide the necessary structural data and thus resolve this issue. Televiewer logging by itself does not, however, replace drill core logging as it cannot provide the same level of data characteristics as physical assessment by an experienced engineering geologist. Televiewer surveys are therefore a complimentary tool for classical core logging. Also, important to be remarked is that the engineer should understand both the advantages and the limitations associated with the collection of structural data either through borehole imaging or traditional techniques.

Although the case studies presented in this chapter did not have televiewer data available at the time of preparation of this thesis, it was deemed worth it to provide a short summary of this useful techniques in the field of mining rock mechanics. Readers interested to dive into this topic are recommended to consult the work by Gochioco & Marks (2002), Su et al. (2005), Yongyue et al. (2010), Bae et al. (2011), Li et al. (2013).

3.1.3.2 Photogrammetry Mapping Techniques

Traditional hand measurements of geotechnical data typically collected by bench mapping can further be enhanced and supplemented by digital measurements from photogrammetric surveys. The use of 3D digital photogrammetric and laser imaging technology for structural mapping in open pit mines has increased dramatically within the last few years (Read & Stacey, 2009). Given the low cost for digital cameras and their ease of use in the field, the techniques using photogrammetric image processing are particularly useful for geotechnical characterization of rock slopes (Birch 2006, Haneberg 2008, Tannant et al. 2008, Sturzenegger and Stead 2009, Bahrani and Tannant 2011, Kim et al. 2013, Vasuki et al. 2014). This technology allows us to collect accurate structural data in areas where access is difficult and/or unsafe

without disrupting mine operations (Lee, 2011; Sturzenegger et al., 2011). This includes using traditional aerial, terrestrial, or Unmanned Aerial Vehicles (UAV's) platforms (Liu et al., 2019).

One major benefit of digital photogrammetry over traditional bench mapping is its capability to capture large-scale geological structures on the existing rock slopes (multi-bench scale) as shown in Figure 3.11 that would otherwise not be identified when mapping manually at a single bench scale. Geometrical properties of rock discontinuities such as orientation (dip/dip direction angles), trace lengths or plane area (also used to calculate joint persistence) and fracture set spacing, can be determined remotely and accurately over long areas of the pit. One disadvantage of this system is, however, that it cannot be used to determine the physical features of the structures, particularly surface roughness, joint aperture and nature of joint infilling.

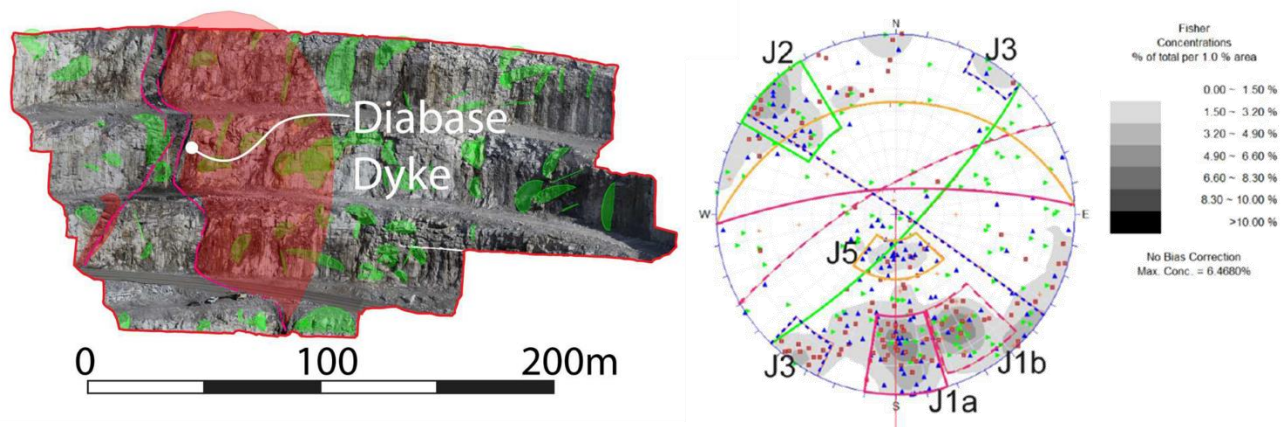


Figure 3.11 Example of a mapping window from camera imaging overlain with the 3-D terrain model of a pit sector. One major discontinuity (in red) and several rock joints (in green) were mapped (Tuckey, 2012).

Unfortunately, photogrammetric information was not at hand at the time of preparing this thesis. Nevertheless, it was considered useful to provide a brief outline of this technique in the field of rock slope engineering. Readers interested in photogrammetry-based techniques used for structural mapping in mining are advised to consult the work by Sturzenegger & Stead (2009), Grobler et al. (2003) and Tannant (2015).

3.2 Assessing the Geometrical Properties of Rock Joints

For the case of rock slope engineering with structurally controlled instabilities modes, i.e. planar or wedge failure, special attention should be given to the both the mechanical (strength) and geometrical (orientation) properties of natural discontinuities (Park et al., 2005; Basahel and H. Mitri, 2019).

The most measured geometrical properties of discontinuous rock masses are orientation, spacing and persistence or trace length. Authors such as Piteau (1970) and Baecher (1977) and Samaniego (1985) have pointed out that the above parameters are crucial for the design and stability of any structure built in or

above a discontinuous rock mass. This section will mostly cover the geometrical properties of rock joints with a special emphasis on joint orientation, joint spacing and joint persistence.

3.2.1 Joint Orientation

Discontinuity orientation is defined by two field measurements that can be expressed as either strike and dip, or most commonly, dip and dip direction angles. These can be easily determined from exposed outcrops or calculated from oriented rock cores. The overall purpose of surface mapping and/or geomechanical core logging is indeed to define sets of discontinuities that will control stability on a particular slope orientation (Wyllie & Mah, 2004). This section is primarily concerned with discontinuity orientation data processing, representation and interpretation.

Structural data collection techniques and procedures were covered in previous sections. After a set of dip and dip direction measurements have become available the next step involves a statistical analysis to identify the characteristic structural pattern of the rock mass. Quite often, joints occur in sets that are parallel or sub-parallel (clustered), while it is also possible for several joints to be oriented in different (random) directions (Hadjigeorgiou, 1992; Jaeger and Cook, 2009).

Although surface (scanline and or window) and sub-surface (borehole logging) structural data collection tools can produce an objective sampling strategy, they do introduce an orientation sampling bias as fractures with shallow angles of intersection with the scanline or borehole axis are seldom observed (Fisher et al. 2014; Priest 1985). Ruth Terzagui (1965) was one of the first to point out this bias for sampling lines, boreholes or planes.

This concept is better demonstrated in Figure 3.12 where three discontinuities A, B and C all with equal spacing, and different orientations are intersected by a sample line. It can be observed that Set A is sampled seven times, Set B five and Set C twice. This demonstrates that, although the hypothetical discontinuities are uniformly distributed, their sampling frequency is partially dependent on the relative angle between the sampling line and the discontinuity. Terzaghi (1965) also pointed out that there will be no intersections between the fracture set and the sampling line or plane when the sampling domain is parallel to the fracture set. The term blind zone is applied to the orientations of the poles of fractures in this situation (Yow, 1987; Priest, 1993).

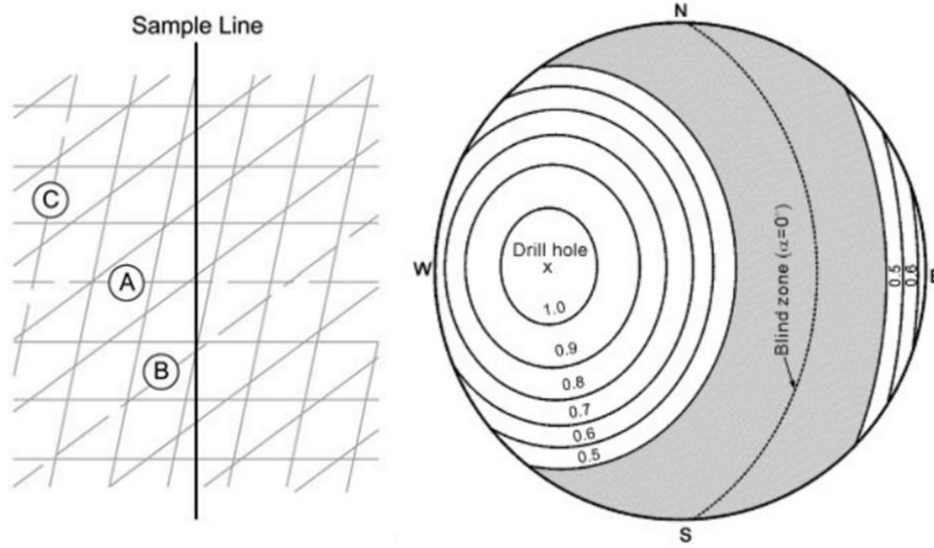


Figure 3.12 Sampling bias imposed by one-dimensional (linear) discontinuity sampling represented by a drill hole with a plunge of 45° to the west (Fowler, 2013).

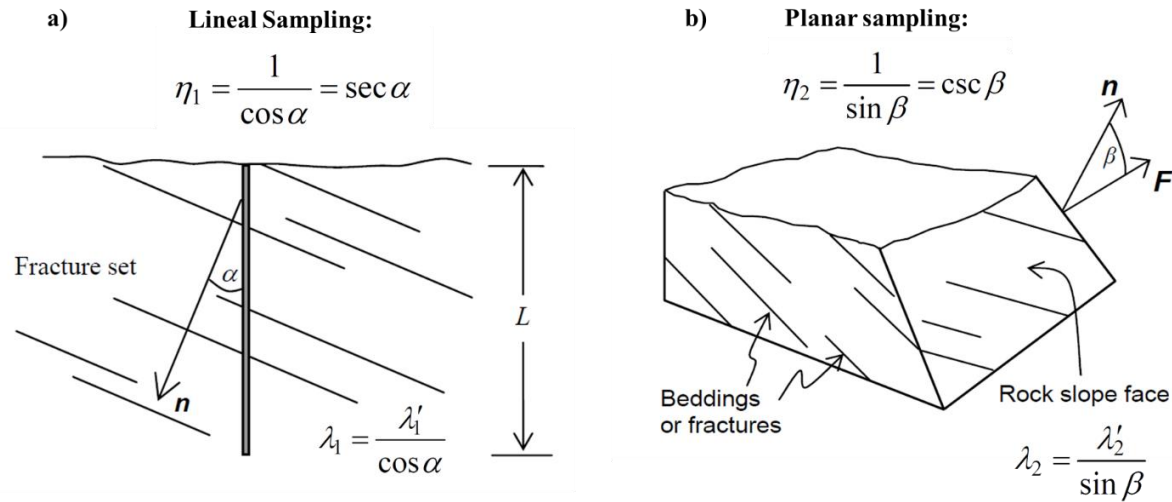


Figure 3.13 Terzagui correction factor for a) a scanline at an angle α with the normal to a fracture set and b) a rock slope whose normal F makes an angle β with the fracture normal n (Wang & Mauldon, 2006)

Figure 3.13.a. shows a drill hole, as a linear sampling line, at angle α with respect to the normal n to a set of fractures. If λ_1 is the fracture frequency measured along the fracture normal and λ_1' is the measured frequency along the drill hole, then the bias caused by the sampling orientation can be corrected by multiplying the field-measured frequency λ_1' by a correction factor η_1 . In Figure 3.13.b. the case for planar sampling is shown, such as for a natural or excavated rock slope. If β denotes the angle between the sampling plane normal F and the normal to a set of fractures n , λ_2 denotes the measured fracture frequency

on the plane perpendicular to the fracture set and λ_2' denotes the measured fracture frequency on the rock slope (sampling plane). Then the bias caused by the orientation of the sampling plane can be corrected with a weighting factor η_2 .

The commercially available software Dips developed by Rocscience Inc. offers an automatic calculation of the Terzagui weighting factors for the correction of bias in discontinuity orientation data sampled on scanlines, windows or boreholes. Figure 3.14 shows contour plots of rock joint clustering based on three oriented boreholes. The orientation of these boreholes has strategically been defined so that the blind zones created by each borehole is minimized (Figure 3.15). The two contoured stereographic projections present the same data, whereas Figure 3.14 is uncorrected, Figure 3.16 has been bias-corrected by means of the Terzaghi weighting factor. As can be seen on these two figures, different contouring and clustering patterns can be obtained when correcting orientation data for sampling bias. This is specially recommended when dealing with highly scattered structural data such as the one coming from core logging.

One of the simplest forms of graphical representation for 3D oriented geological data is the use of stereo plots by adopting a technique known as stereographic or hemispherical projection. The reader is forwarded to the work by Philips (1971), Goodman (1976), Priest (1985), and Lisle & Leyshon (2004) for further details on this technique. One advantage of stereo plots is that they allow for large amounts of data points to be plotted and contoured to identify main joint clustering sets. Visually the preferred orientations of joint sets are defined by peaks in the contour plot. Figure 3.17 correspond to the same stereo plot as in Figure 3.16 where the main joint sets have been highlighted. Three main joint sets have been identified, two subvertical (J1 and J2) and one sub horizontal (J3). The mean orientation is also shown in Figure 3.17.

Joint orientation data will always exhibit some degree on variability in its geometrical properties. However, this natural variability will not be the same and there will vary from site to site depending on the regional and local geological setting. This can be easily seen in Figure 3.18 where two different rock outcrops are shown, both having two main joint sets. In the case of outcrop #1 the orientation of the sub-horizontal and sub-vertical joint sets vary much more with respect to the mean or average (painted as a red line) than in the case of outcrop #2 which is much more tightly clustered. One could say that a probabilistic approach should be followed when assessing the stability in a rock mass such as outcrop #1 whereas a deterministic analysis could be reasonable for evaluating the stability in a rock mass such as outcrop #2. In either case, the natural variability should be quantified before deciding which approach to take.

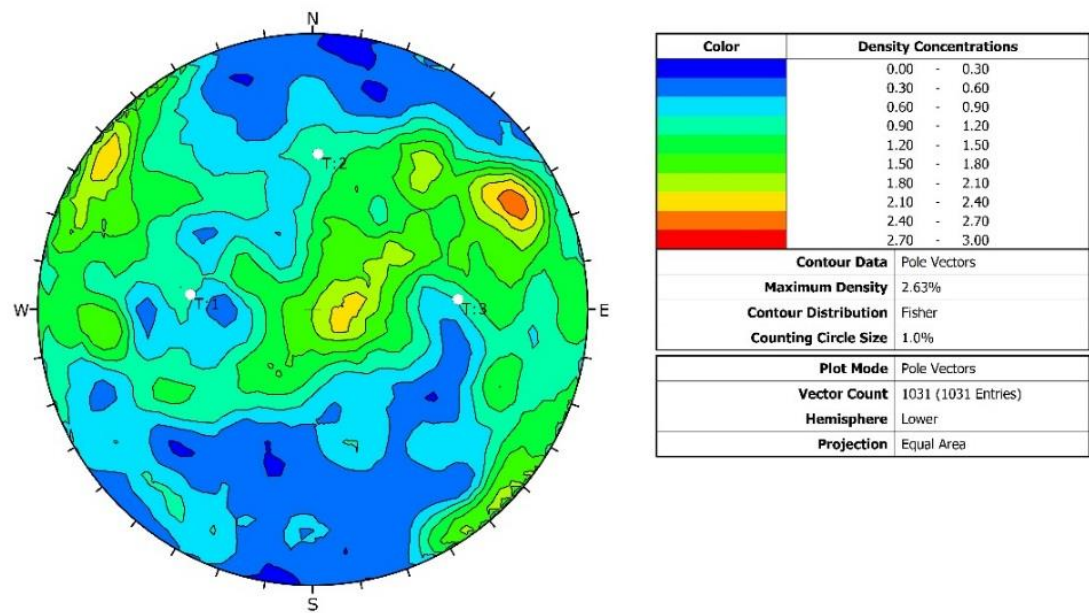


Figure 3.14 No bias-corrected contour plot corresponding to the three oriented boreholes.

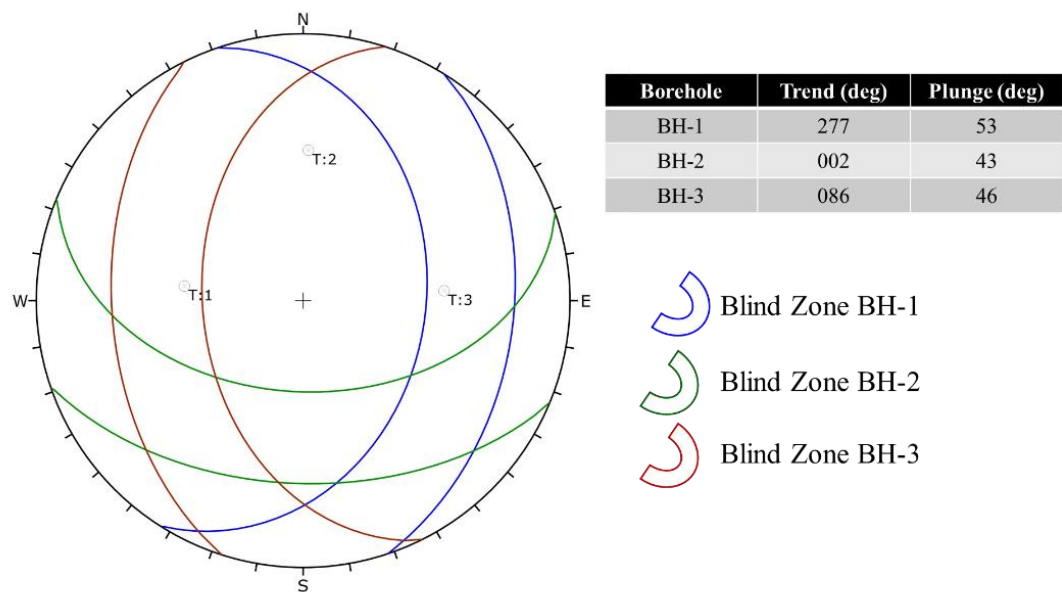


Figure 3.15 Blind zones associated to three oriented boreholes: BH1, BH2 and BH3.

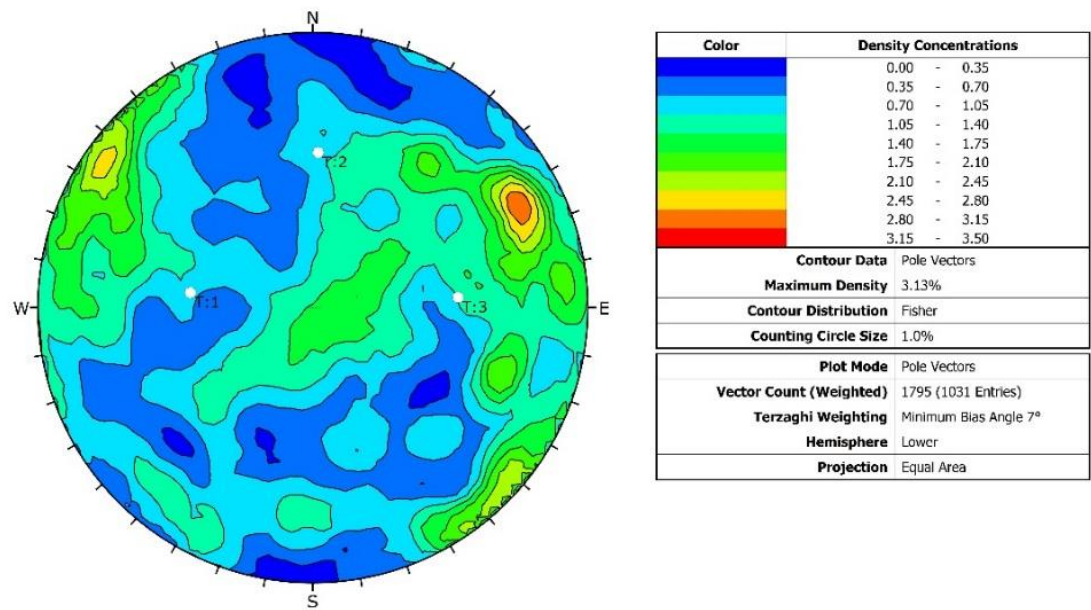


Figure 3.16 Bias-corrected contour plot corresponding to the three oriented boreholes

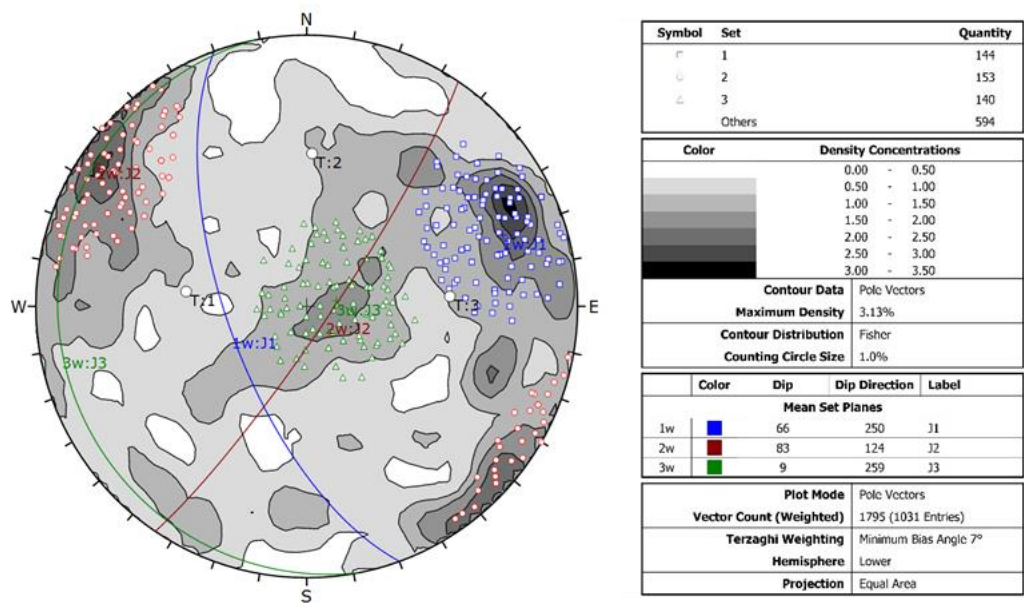


Figure 3.17 Equal-area contour plot for boreholes BH1, BH2 and BH3 with three identified main joint sets J1, J2 and J3.

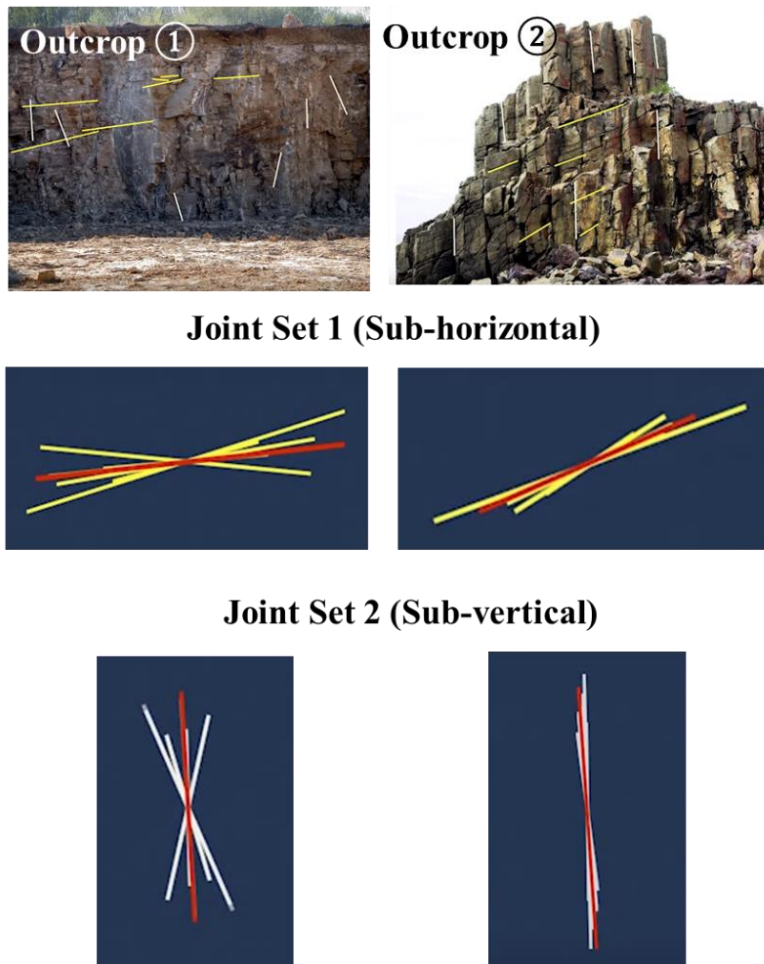


Figure 3.18 Example of variability in joint orientation (dip angles) for outcrop 1 (highly variable) and outcrop 2 (tightly clustered).

A problem basic to applications in geological engineering is finding the probability of occurrence of a joint normal in a given orientation once the preferred orientations have been determined. It is often encountered that joint orientation distributions such as the one shown in Figure 3.19 fit quite well to a normal distribution for both the trend and plunge values. Some skewness is observed, however, for special cases in which the joint set is subvertical (dips steeply) or sub horizontal (dips softly), having positive skewness for the first one and negative skewness for the second one. In these special cases, more sophisticated statistical distributions other than the symmetrical gaussian can be selected based on a χ^2 goodness-of-fit procedure.

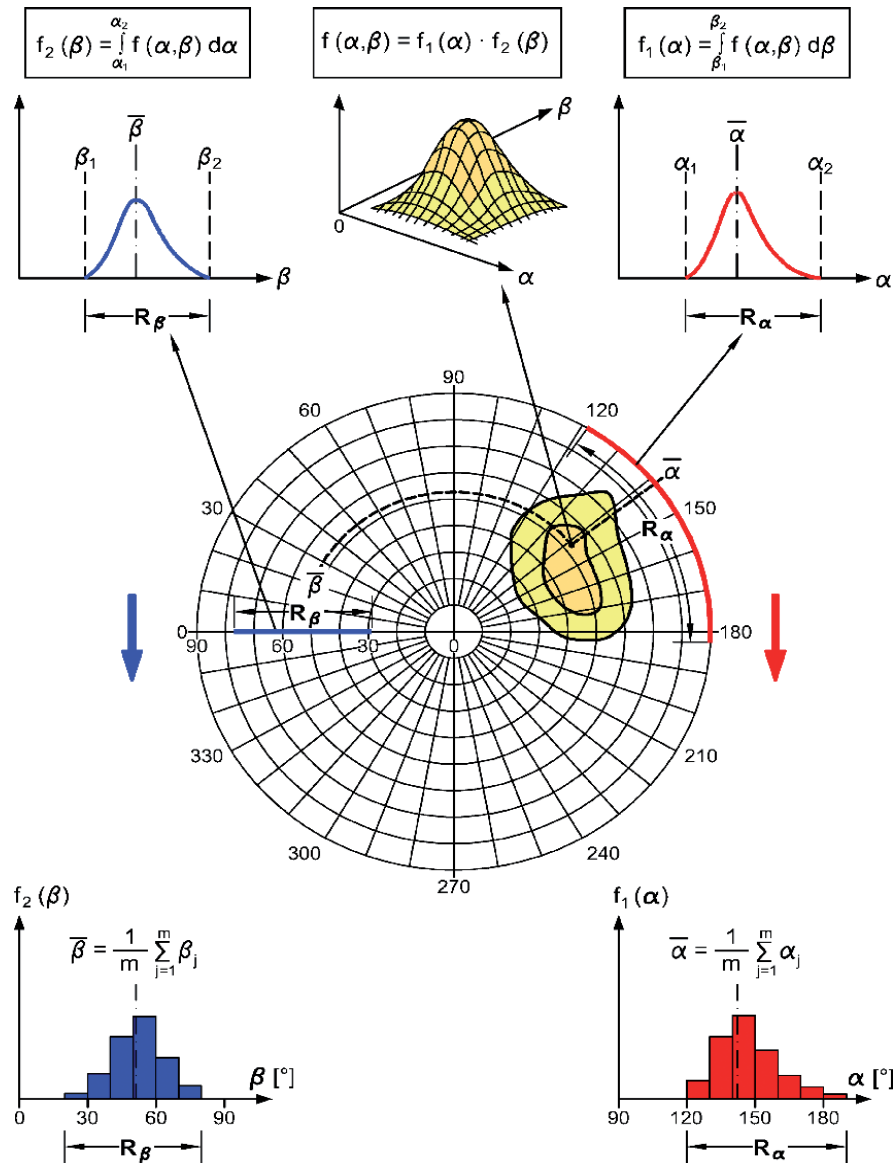


Figure 3.19 Normal distribution fit for the trend (R_β) and plunge (R_α) histograms (Wittke, 2014)

3.2.2 Joint Spacing

In a strict sense, discontinuity spacing is the orthogonal distance between two adjacent discontinuities that belong to a given joint set (Priest, 1993). This is also called the true or normal (i.e. perpendicular) spacing of the discontinuity set (see Figure 3.20). An apparent spacing would be one measured along a line of general orientation and different to the normal of the discontinuity set. Discontinuity spacing is closely related to the discontinuity frequency i.e. the reciprocal of mean spacing (Hudson and Priest, 1983). That being said, both discontinuity spacing (s) and discontinuity frequency (λ) are parameters sensitive to the orientation of the line of measurement as pointed out by several authors (Priest & Hudson, 1976; La Pointe

& Hudson, 1985; Dershowitz & Herda, 1992; Panda & Kulatilake, 1995; Ruf, et al., 1998; Bai et al., 2000; Peacock et al., 2003).

Measurements of discontinuity spacing can be made on rock exposures or drill cores. For the case of scanline mapping the length along the scanline is recorded for each intersected discontinuity. In the case of an oriented borehole the depth at which the discontinuity is intersected is measured and register in the core log. In both cases, the apparent spacing can be calculated by simply direct subtraction of the distance or depth of one joint with the one immediately after it.

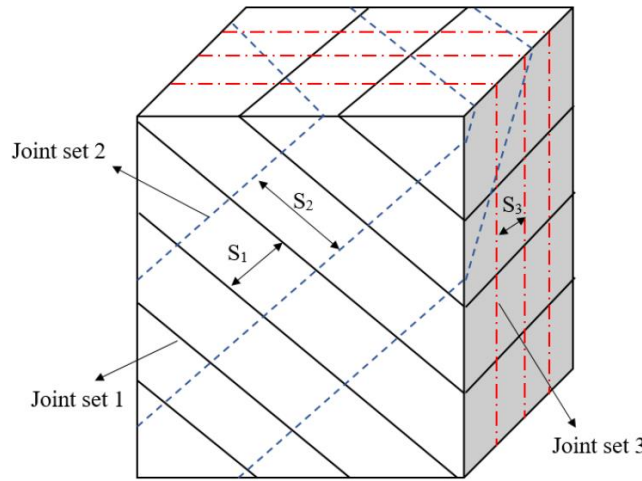


Figure 3.20 A jointed rock mass containing three main joint sets with their true spacing being indicated (Chang & Konietzky, 2018)

If only apparent spacing measurements are available (S_{ap}), such as the case of core logging data, the true joint spacing (S_{tr}) can be obtained by following the expression (ISRM, 1978, Giano, 1992, Wong, 2013):

$$S_{tr} = \lambda s \cos \theta \quad [\text{Eq.3.1}]$$

Where S_{tr} is the true joint spacing, λs is the joint frequency (i.e. # joints/meter) along the measuring line (e.g. scanline) and θ the angle between the sampling line and the normal to the joint set calculated as follows (see Figure 3.21).

$$\cos \theta = |\cos (\alpha_n - \alpha_s) \cos \beta_n \cos \beta_s + \sin \beta_n \sin \beta_s| \quad [\text{Eq.3.2}]$$

Where α_n and β_n : trend and plunge of joint set normal. α_s and β_s : trend and plunge of scanline or borehole axis.

If now two discontinuity sets are considered, as illustrated in Figure 3.22, and the spacing along an arbitrary sampling line is aimed at, the contribution from each set is resolved onto the sampling line as weighting summation. For calculation purposes it is easier to find the average fracture frequency (λs) along the scanline and this calculate the mean spacing. This procedure can be readily extended to any number of discontinuities sets as shown in Figure 3.22.

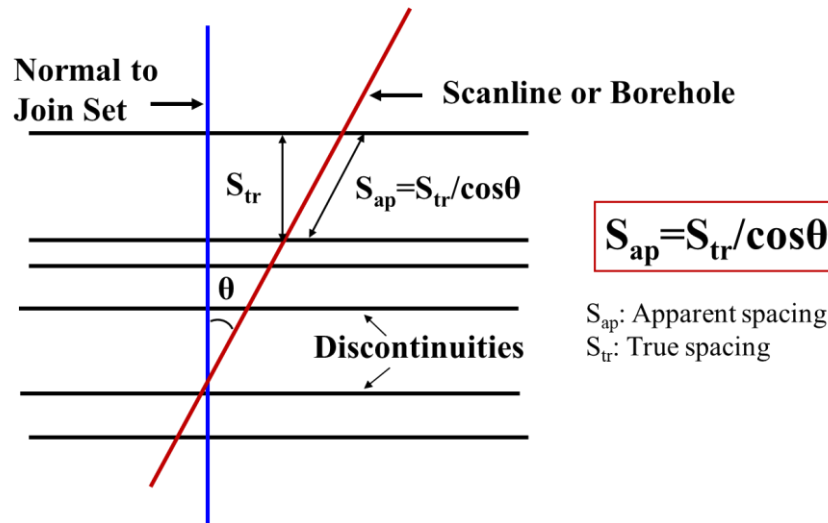


Figure 3.21 The true joint spacing (λ) calculation from apparent spacing (λs) for one joint set
 (Adapted from Hudson and Harrison, 1997)

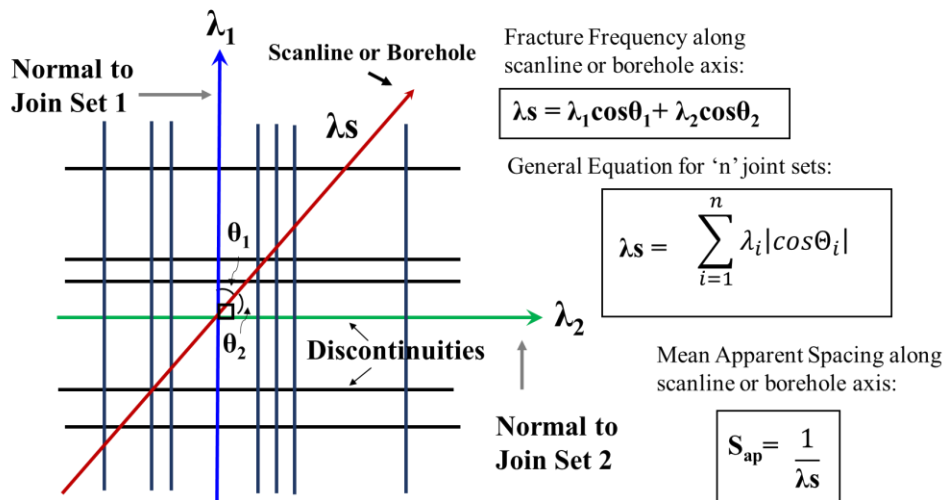


Figure 3.22 The true joint spacing (λ) calculation from apparent spacing (λs) for two joint sets.
 (Adapted from Hudson and Harrison, 1997)

For engineering purposes, we might wish to know in which direction is the maximum fracture frequency and in which direction is the minimal fracture frequency since this may define the shape and size of the forming rock blocks. Figure 3.23 shows a contour plot that displays the 3D distribution of fracture frequency (ff) in a rock mass with four main joint sets as given by Harrison et al (2002). It can be seen that the locus of the global minimum and maximum fracture frequency (ff) can be determined as 3.42 and 8.85 joints per meter, respectively. By taking the inverse of these values, we can state that the min and max spacing will consequently be 0.11 and 0.29 m. as shown in Figure 3.24.

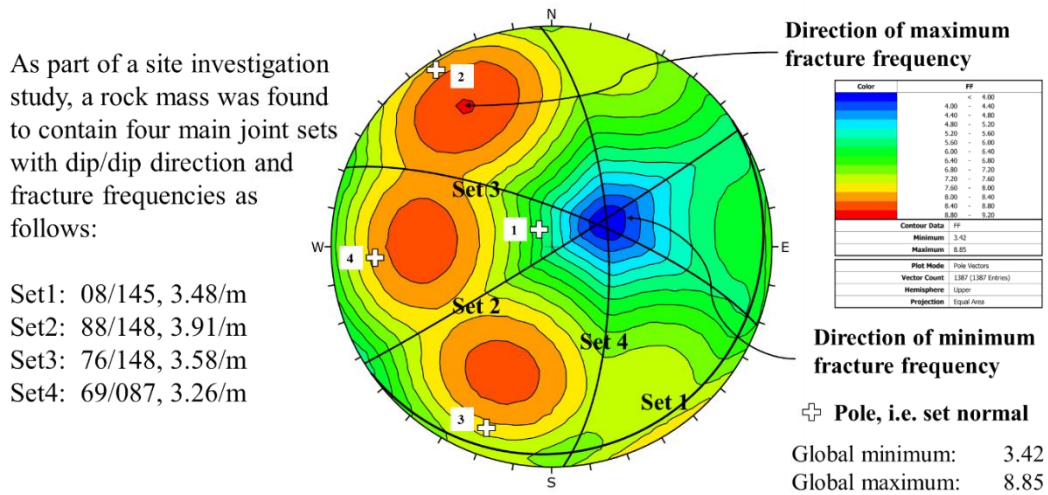


Figure 3.23 Fracture frequency counter plot for a rock mass with four joint sets.

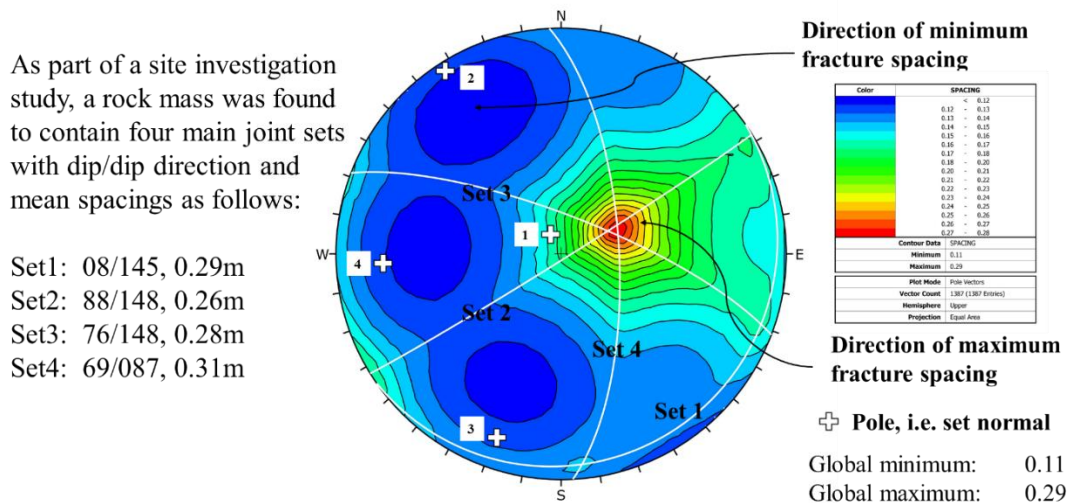


Figure 3.24 Joint spacing counter plot for a rock mass with four joint sets.

Although a mean discontinuity spacing provides a direct measuring of rock quality it has been found useful to investigate the distribution of discontinuity spacing by plotting histograms of the sampled values of total spacing (Priest, 1993). The histogram in Figure 3.25 comes from one oriented borehole of 228 m length. When fitting a probabilistic distribution to that histogram an exponential function is obtained which means that there are many small spacing values and very few large spacing values in the distribution. This is not too surprising since it has been suggested by Priest and Hudson (1900) among others that discontinuity spacing for a variety of rocks can be modelled by a negative exponential distribution as the one shown in Figure 3.25. It should be noted that a sufficiently large sample of individual spacing values (preferably more than 200 individual measurements) are often needed for a negative exponential distribution to be evident. This number can be easily obtained from regular oriented core logging.

Borehole Orientation
Trend: 007° / Plunge: 63°

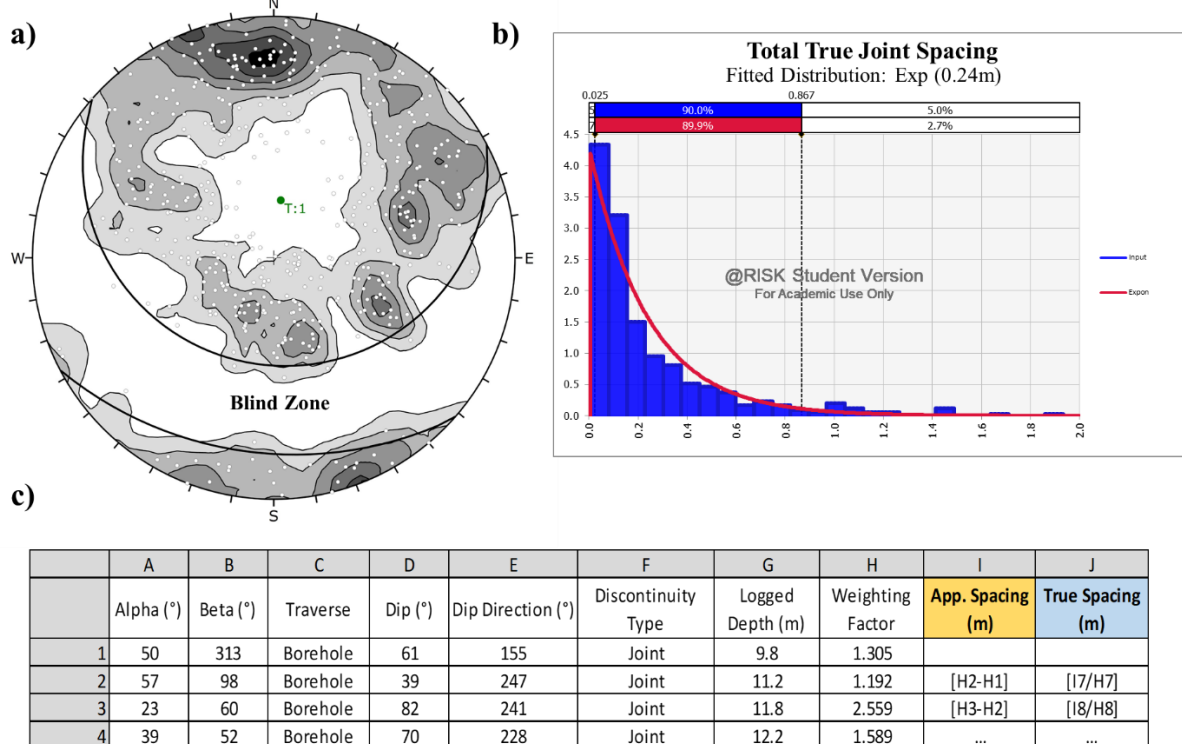


Figure 3.25 Statistical analysis of total joint spacing. a) Contour plot of corelogging data; b) Histogram of the total joint spacing; c) Spreadsheet for core logging data processing as an output of Dips software.

The fact that the observed distributions of total joint spacing tend to be of negative exponential form suggest, but does not confirm, that the discontinuity occurrences are random. It should be borne in mind that boreholes are a 1D sampling tool and therefore several boreholes oriented in different directions are needed in order to rely on the assumption that joint occurrences in 3D are random too. If so, the position of rock

joints in 3D space could be modelled as a stochastic Poisson process (Baecher et al., 1977; Dershowitz & Einstein, 1988; Dowd et al., 2007). There are however other patterns that the geologist could observed when plotting spacing values, these are uniform and clustered occurrences of rock discontinuities (Davis & Sampson, 1986). In the experience of the author, the uniform pattern could be expected in sedimentary rocks where the planes of stratification tend to occur at regular intervals. The clustered patter of rock joints occurrence can be present in all lithologies and it is related to faults or shear zones where the jointing or fracturing is more intensely closer the fault or shear zone and it gets less prominent when moving further out these major structures.

3.2.3 Joint Persistence

In a strict sense persistence refers to the areal extension of a discontinuity and thus implies a 3D sampling approach (Barton, 1985). This makes joint persistence one of the most difficult geometrical property to quantify given that only a small portion of the discontinuity surface is visible in scanline (1D) or window (2D) sampling. In the case of drill cores, it is worth noting that no information about persistence can be gathered.

For rock slope engineering, persistence is a very important parameter because it defines along with the discontinuity spacing the size of rock blocks that will be formed and which if unfavorably oriented may lead to stability problems. Hence, efforts should be made to measure discontinuity persistence. Unfortunately, it can be crudely approximated by observing the discontinuity trace lengths on surface exposures only.

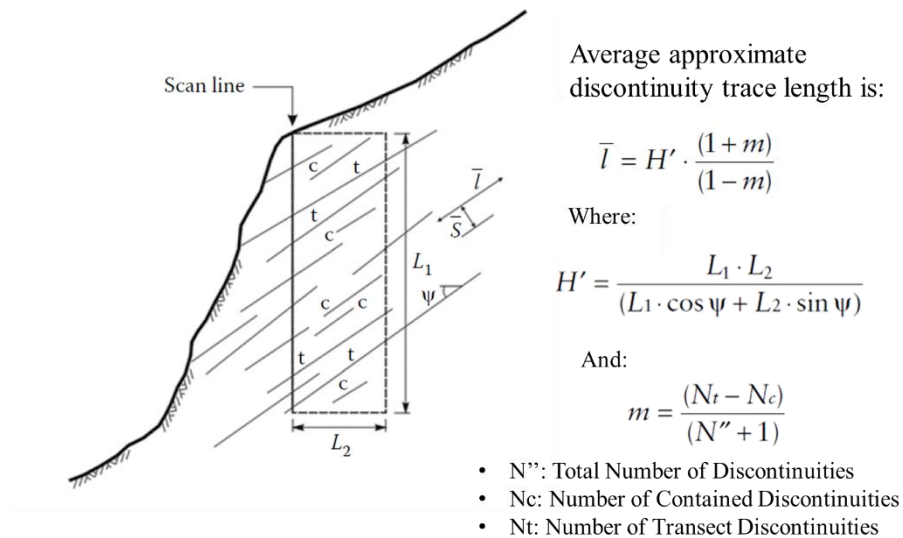


Figure 3.26 Mean joint trace length estimation based on the method developed by Pahl (1981)

A useful technique during the field mapping of discontinuity lengths is the one developed by Pahl (1981) and summarized by Priest (1993) and Willie & Mah (2004). This is one of the simplest and yet useful techniques to calculate the approximate average persistence of a set of discontinuity by measuring the exposed trace lengths on a rectangular rock face window as shown in Figure 3.26. Pahl's procedure is a distribution independent approach for which the type of termination within the sampling window needs to be recorded. In this respect, two classes of discontinuities should be differentiated: N_c is the number of discontinuities that are contained i.e. they have both ends visible within the area; N_t area transecting discontinuities and have neither end visible; N' refers to the total number of discontinuities of a particular joint set is simply the sum of N_t and N_c .

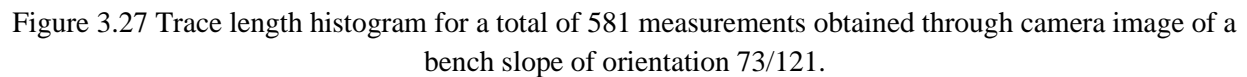
Recently new methods that have been proposed to estimate discontinuity persistence through traced lengths measurements involve circular window mapping; however, these go beyond the scope of this thesis. The reader is forwarded to the work by Mauldon (Mauldon, 1998; Mauldon et al., 2001; Mauldon and Mauldon, 1997; Rohrbaugh et al., 2002) and Einstein (Zhang and Einstein, 1998; Zhang et al., 2002) for further details.

As for spacing values, probability distributions can also be fitted to the mapped discontinuity trace lengths. Previously, it was stated that an exponential law will often be found in the spacing of random occurring discontinuities. For the case of joint trace length, however, a consensus about the best type of distribution that it would follow is less consistent. Historically, joint length distributions have been a topic of research for many authors and results were summarized by Hudson and Priest, 1979, 1983; Priest and Hudson, 1976, 1981). It can be found in this literature that exponential, lognormal and gamma distributions have been reported to fit discontinuity trace lengths.

This lack of consensus is perhaps partly caused the strong biases inherent in the sampling techniques. Authors such as Baecher and Lanney (1978) and Baecher (1980) pointed out two types of biases, these are: truncation bias, through which small discontinuities are systematically excluded from samples, and censoring bias, through which the full trace length of some discontinuities is not observable due to the scale of the mapping area e.g. multiple-bench through-going rock joints.

In the experience of the author, a lognormal distribution for joint trace lengths can be found if small and large-scale mapping tools are combined. Figure 3.27 shows the trace length histogram for a population 581 measurements obtained through a high-resolution scanner image and later detailed interpretation for a sector of a Peruvian open pit mine. From this plot, a lognormal fit with a mean and standard deviation of 2.74m and 2.73 m were obtained, respectively. This agrees with the results by Baecher et al. (1977) who fitted exponential, lognormal and gamma distributions to trace length data. He used maximum likelihood estimators

Bench Slope Orientation
Dip: 73° / Dip Direction: 121°



Discontinuities can be geologic in origin e.g., faults, bedding, schistosity, cleavage planes, and foliations or anthropogenic in origin e.g., blast-induced, stress-induced, or hydraulic-induced fractures (Muralha et al., 2014). Regardless of their origin, theoretical studies and practical experience of rock slope problems suggest that geological discontinuities are of paramount importance for stability purposes by defining the rock mass shear strength and deformation characteristics.

80

The following discussing is concerned with the determination of the shear strength of structural discontinuities and with the processing and interpretation of direct shear test results. It also describes the relationship between the shear strength and the properties of the discontinuities.

3.3.1 The Mohr-Coulomb Linear Model

Mohr–Coulomb is the most popular failure criterion that works quite well for geomaterials, especially soils, where the failure generally takes place in shear (Braja et al., 2013). Coulomb (1776) determined that soil and rock shear strengths are the sum of two main components, one due to constant cohesion, and the other one

due to a frictional strength dependent on the normal stress action on the plane on which the shear strength is mobilized (Giani, 1992). M-C is the simplest linear model applicable to model the shear strength of rock masses and rock joints (Brady and Brown, 2013). The M-C shear strength model is expressed in terms of normal and shear stresses as follows:

$$\tau = c + \sigma_n \tan \phi$$

Where c is the cohesive strength of the cemented surface and ϕ is the angle of friction.

The physical meaning of the two strength parameters in the M-C model is directly related to the discontinuity infilling (cohesion) and discontinuity roughness (friction angle). For example, in minor discontinuities such as ‘joints’, hard infilling types like quartz or calcite would have a beneficial effect by increasing the joint shear strength. This can be observed in the so-called ‘healed discontinuities’ such as veins. In the case of major structures such as faults the same logic applies. If the fault infilling is made of clay-like material (e.g. gouge), this would certainly reduce its overall shear strength as opposed to a mineralized-breccia type of infilling. This breccia will usually be composed of cemented angular rock fragments due to the precipitation of minerals and will therefore increase the fault’s shear strength. A distinction should be made for the so-called ‘apparent cohesion’ given by the rock bridges existing in the rock mass. This arises when joints are not fully persistent showing interruptions in their continuity by the presence of rock bridges. In this case, the joint’s shear strength increases considerably, and the contribution of the rock bridges has to be accounted for in the stability analysis (Bonilla-Sierra et al., 2015).

From the point of view of practical rock mechanics, it should be highlighted that the shear strength of joints is often estimated based on small-scale laboratory tests, whereas for faults or other major structures their shear strength is obtained through careful back analysis of failed or stables slopes. In this respect, there are some field conditions that cannot be modelled in a laboratory setting and where engineering judgment should be used.

The most commonly used method for the shear testing of minor discontinuities is the direct shear test. The specimen, either in the form of a core or an unprepared lump, containing the structural discontinuity surface being investigated, is aligned parallel to the direction of the applied shear force. The two halves of the specimen are fixed inside the shear box using a suitable encapsulating material, generally an epoxy resin or plaster. This type of test is commonly carried out in the laboratory, but it may also be conducted in the field, using a portable shear box. Methods of preparing samples and carrying out these various tests are discussed by the ISRM Commission (1974), Goodman (1976, 1989) and Hoek and Bray (1981).

Since the use of “cohesion” in rock slope design is only permissible when discontinuity features are cemented, a modified M-C model can be derived for cases in which joint infilling does not contribute to the overall joint shear strength and therefore shear strength relies solely on the frictional resistance of the joint surface. The M-C shear strength for cohesionless joints can be represented by:

$$\tau = \sigma_n \tan \phi$$

Figure 3.28 shows the M-C model where c and ϕ can be obtained graphically by calculating the y-axis intercept and the slope of the best-fit line through linear regression analysis of a given direct shear data set.

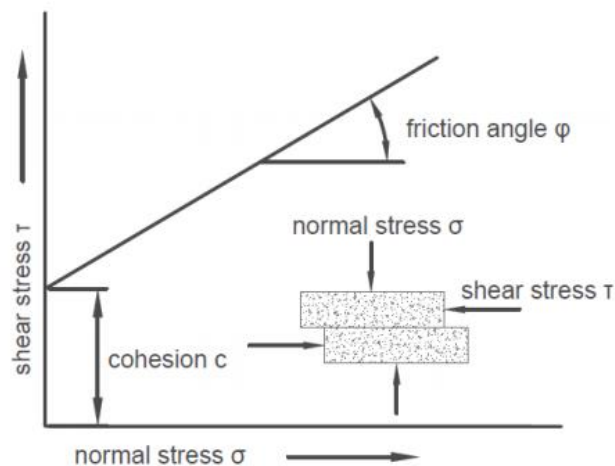


Figure 3.28 Mohr-Coulomb relationship between shear strength and normal stress (Hoek and Bray, 1981)

3.3.2 The Barton-Bandis Non-Linear Model

Joints are common and widespread in rocks, and unless they are healed and/or mineralized, they have weakening effects on the strength of rock masses due to their low or almost inexistent tensile strength (Priest, 1993; Singhal and Gupta, 2010; Prassetyo et al., 2017). Extensive laboratory experiments on rock joint behavior from the work by Drs. Nick Barton and Stavros Bandis provided insight into the effects of joint roughness and wall strength parameters, into the non-linearity of the shear strength of rock joints (Barton, 1973; Bandis, 1980; Bandis et al., 1981; Barton, 1982; Barton et al., 1985).

Seldom does one have to consider the nature of irregularities along failure surfaces in soils. Yet in rock the irregularities along a fault or joint surface can mean the difference between stability and failure of a mine slope. The Barton-Bandis (B-B) joint model is currently a widely known empirical model for predicting shear failure behavior of rough and clean joints (Barton, 1973; Barton and Choubey, 1977; Bandis, 1980; Barton et al., 1985). In the B-B model, the peak shear strength of a rock joint is determined by the following criterion:

$$\tau_p = \sigma_N \tan \left[JRC \log_{10} \left(\frac{JCS}{\sigma_N} \right) + \phi_r \right]$$

Where τ_p is the peak shear strength of the unfilled joint (that is, there is rock-to-rock contact across the plane), σ_n is the effective normal stress acting on the joint, JRC is the joint roughness coefficient, JCS is the joint wall compressive strength and ϕ_r is the joint residual friction angle. These three parameters have typical ranges of values from: JRC = 0 to 20 (smooth-planar to very rough-undulating), JCS = 10 to 200 MPa (weak-weathered to strong and unweathered) and $\phi_r = 20^\circ$ to 35° (strongly weathered to fresh-unweathered surfaces).

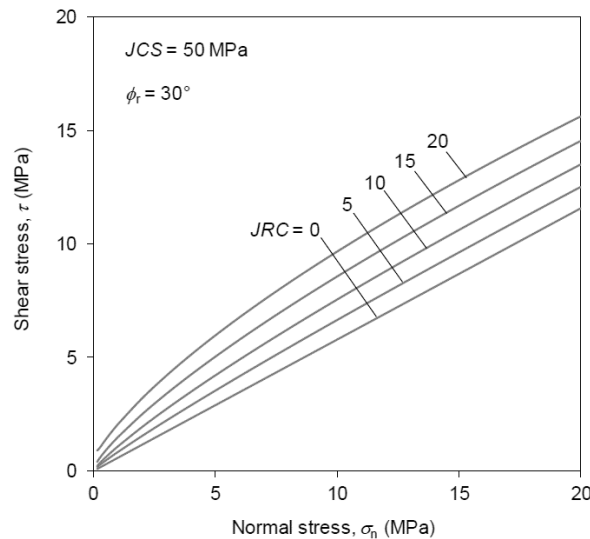


Figure 3.29 B-B criterion for different JRC values, JCS = 50 MPa and $\phi_r = 30^\circ$. (Prasetyo et al., 2017)

Figure 3.29 shows plots of the B-B empirical criterion as functions of different values of JRC and for typical values of JCS = 50 MPa and $\phi_r = 30^\circ$. With increasing JRC and σ_n , the B-B criterion becomes more curved and nonlinear. For JRC = 0, the B-B criterion corresponds to the M-C criterion with $\phi = \phi_r$ (cohesion is assumed zero). The main advantages of the B-B model as highlighted by Prasetyo et al. (2017) are: 1) it has been established based on an extensively verified and wide range of experimental results, 2) the

parameters involved have real physical meanings, and 3) the input parameters of the model can be easily determined using simple index tests or can be estimated by those with experience.

In the author's opinion, the use of this model is highly recommended when extensive and detailed discontinuity mapping plus field testing have been carried out. The easiness of the field measurements and relatively inexpensive index tests make the B-B a suitable and preferred model when more costly and time-consuming laboratory direct shear tests are not available.

The techniques available for estimating the three index parameters of the B-B criterion are briefly discussed below (Figure 3.30).

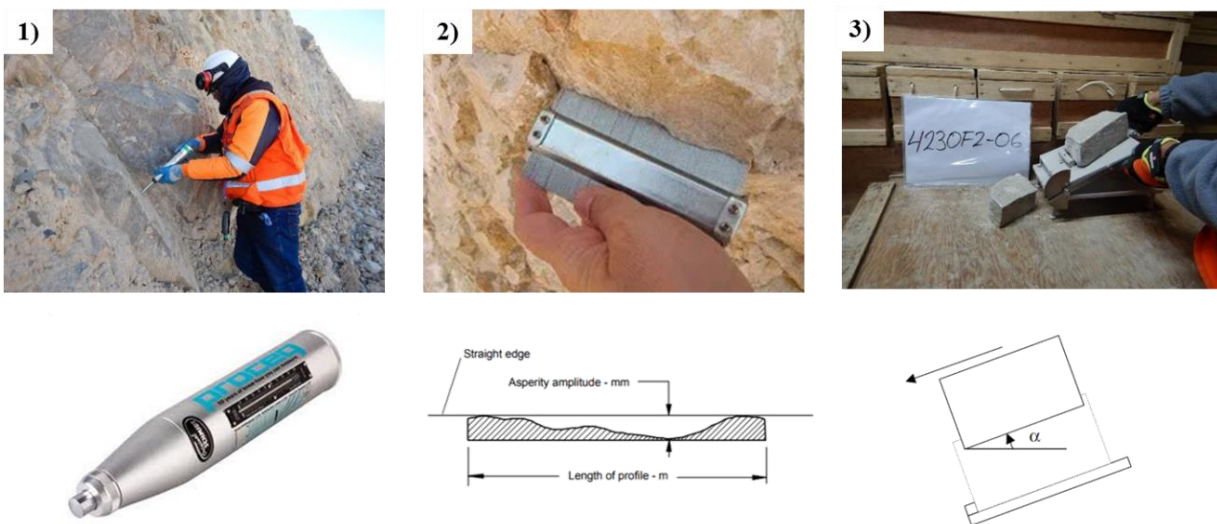


Figure 3.30 Field tests for B-B input parameters: 1) Schmidt hammer, 2) Barton's comb, 3) Tilt test.

The JCS value is mostly due to the thin layers of infilling or coating adjacent to joint walls. Thus, the JCS is an indirect measurement of the degree of joint weathering. Barton (1985) recommended the use of the Schmidt hammer to estimate the JCS value noting that it is not applicable for very weak rocks (i.e. $UCS < 25 \text{ MPa}$). The Schmidt hammer is basically a device for recording the rebound of a spring-loaded plunger after it has impacted on a surface. Originally designed to test the concrete rebound hardness, the technique was further developed to estimate the uniaxial compressive strength of rocks. Figure 3.31 shows an empirical chart between the Schmidt hammer rebound number, the hammer orientation, UCS and rock unit weight.

The joint roughness coefficient JRC is a unitless number for which two measuring methods are currently applied. The first consists of visually comparing the appearance of a discontinuity surface with typical joint profiles constructed by Barton and reproduced in Figure 3.32. The second approach, as given by the ISRM

Suggested Methods for the Quantitative Description of Discontinuities in Rock Masses (Barton, 1985), considers joint profiling. In this approach a profilometer, also known as a Barton comb, is pressed against the joint surface. Here JRC is determined by based on the joint profile length (L) and maximum amplitude (A) after plotting them on Barton's log-log scale graph (Figure 3.33).

As a result of extensive testing of natural joints and joint replicas, Barton and Bandis (1982) proposed a scale correction curves for JRC and JCS as shown in the following equations:

$$JRC_n \approx JRC_0 \left[\frac{L_n}{L_0} \right]^{-0.02 JRC_0}$$

$$JCS_n \approx JCS_0 \left[\frac{L_n}{L_0} \right]^{-0.03 JRC_0}$$

Where subscripts (0) and (n) refer to lab scale (100 mm) and in situ block sizes, respectively.

Barton and Choubey (1977) developed an empirical relationship for estimating the residual friction angle ϕ_r from the results of Schmidt Hammer L-type rebound tests:

$$\phi_r = (\phi_b - 20) + 20 \left(\frac{r}{R} \right)$$

Where r = rebound on wet or weathered joint surfaces; R = rebound on dry or unweathered rock joint surfaces and ϕ_b = basic friction angle estimated from residual tilt tests or dry unweathered sawn surfaces.

Wines & Lilly (2003) summarized the main constraints on the use of the criterion, as follows:

- Barton and Choubey (1977) recommended that the peak shear strength curves should be truncated for design purposes at a maximum allowable shear strength given by $\arctan(\tau/\sigma_n) = 70^\circ$.
- For unfilled joints the roughness and compressive strength of the walls are important, whereas in the case of filled joints the physical properties of the material separating the joint walls are of primary concern. Barton's criterion is only valid where joint walls are in rock-to-rock contact.
- Due to the relatively low normal stress levels involved in the determination of the criterion, Hoek and Bray (1981) reported that the criterion is valid for the normal stress range $0.01 < \sigma_n/JCS < 0.3$.

The reader is urged to revise the work by Barton and Choubey (1977) who describe at length recommended procedures for the required tests.

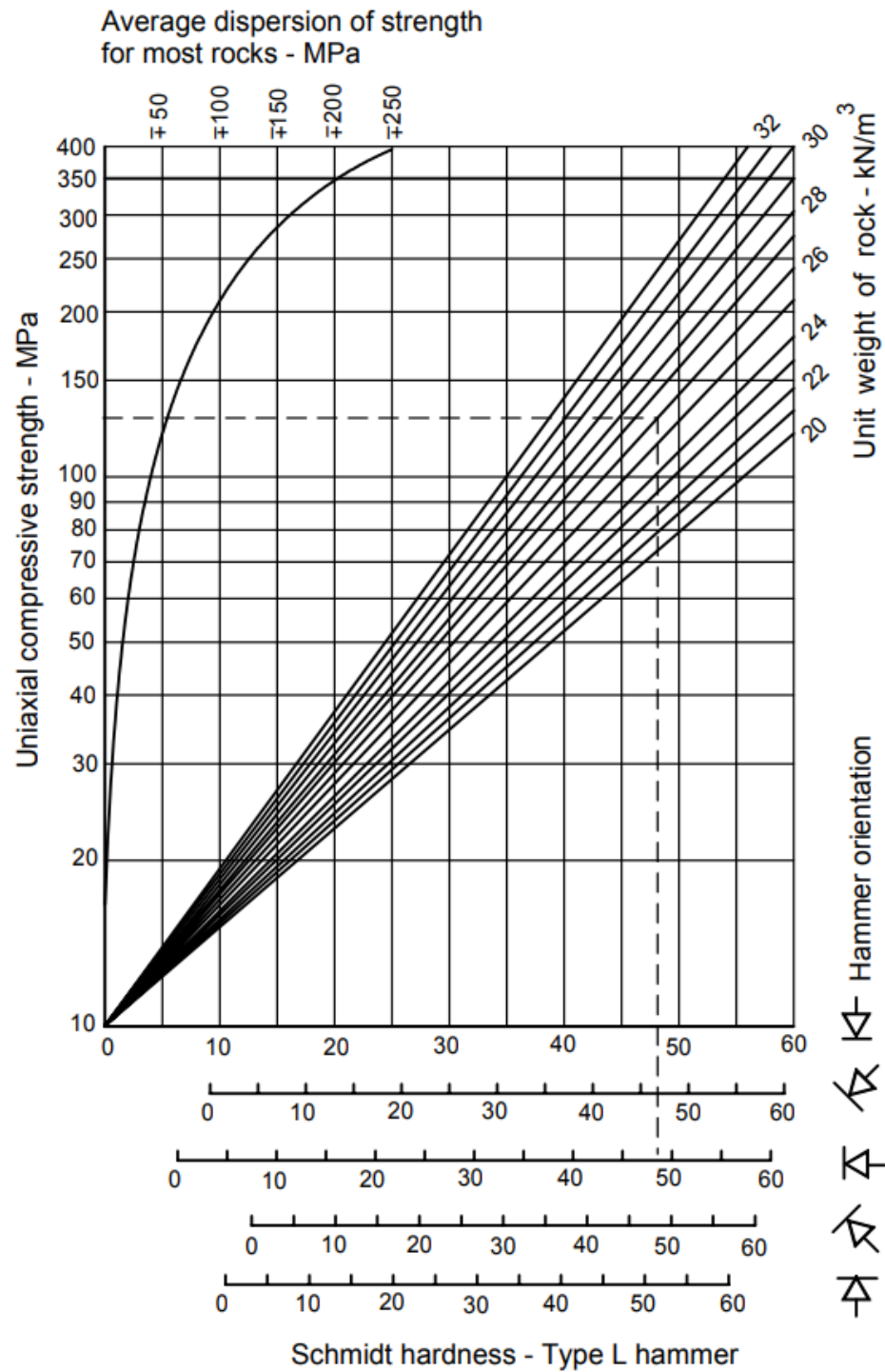


Figure 3.31 JCS from Schmidt hammer test. (Deere & Miller, 1966)

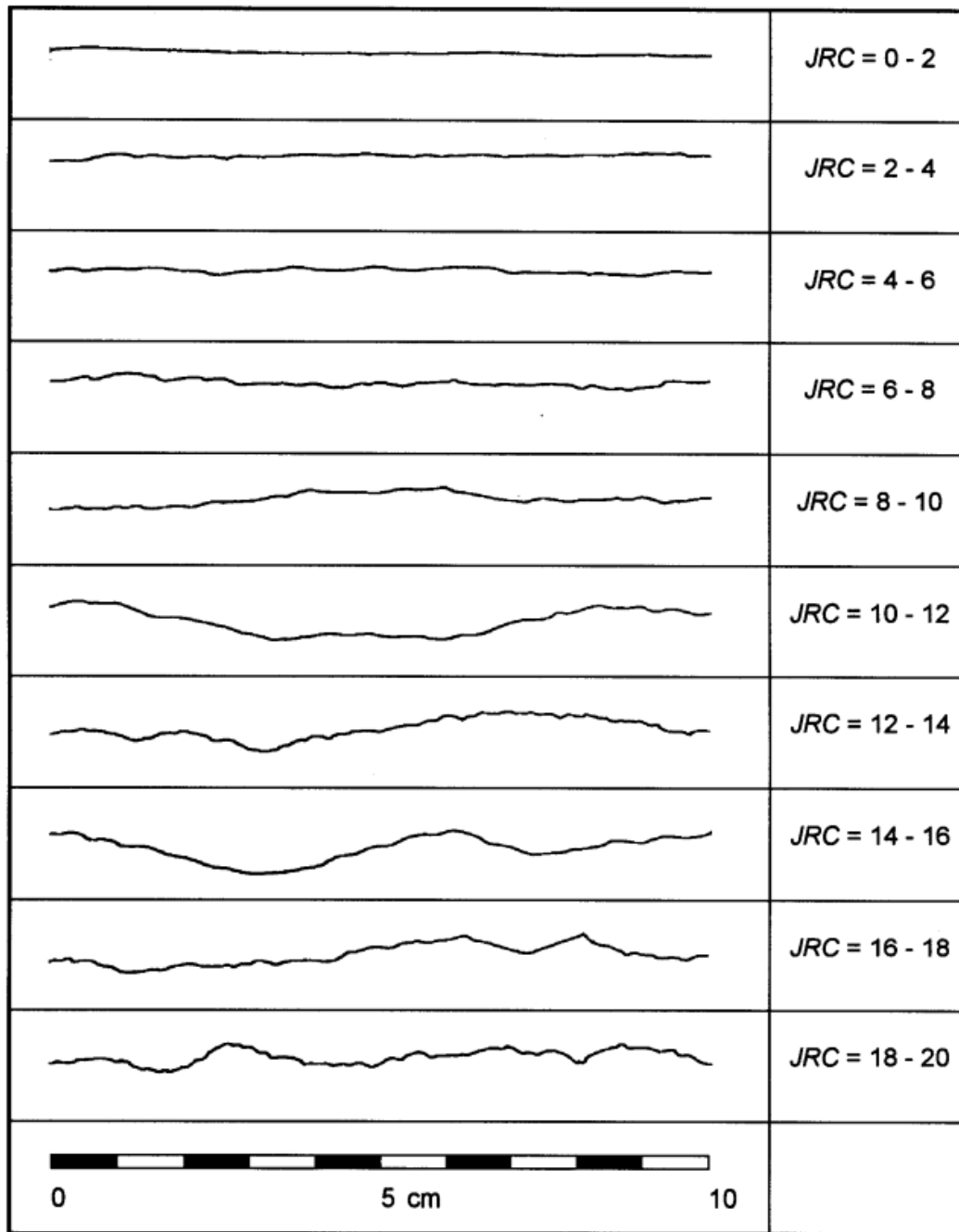


Figure 3.32 JRC from visual comparison with standard profiles (Barton & Choubey, 1977)

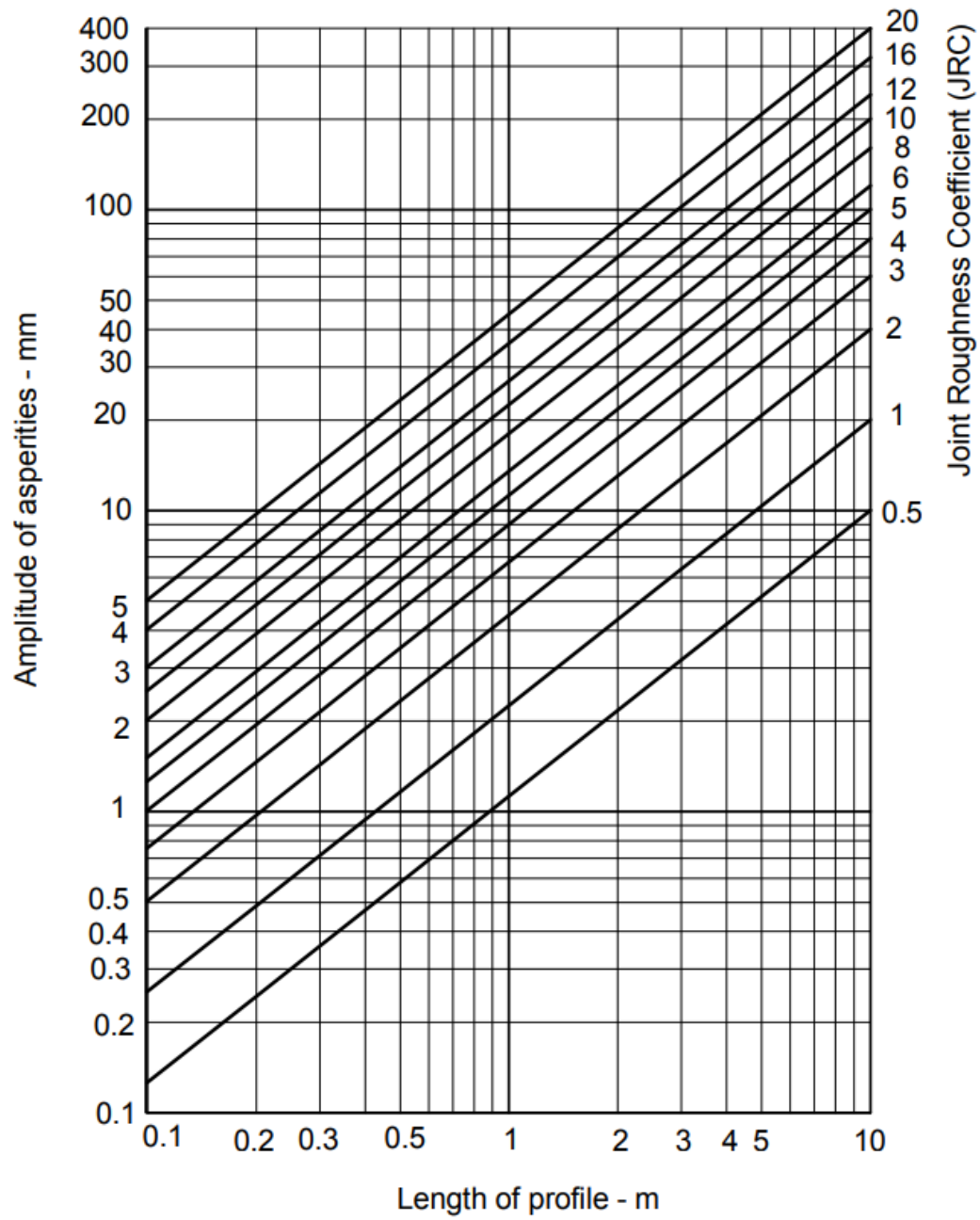


Figure 3.33 JRC from measurements of surface roughness using Barton's comb (Barton,1982)

3.3.3 The General Power Curve Model

Accurate prediction of shear strength is fundamental to mine slope design. Although a linear model such as the Mohr-Coulomb is widely used in analyzing the shear strength of rock joints, some direct shear data would be more adequately described by a non-linear model particularly in the range of small normal stresses (Barton, 1976; Hassani, 1980; Udd et al., 1981).

This curvature is generally more pronounced over the low normal stress range of 0 to 1000 kPa which is the typical stress levels acting on a bench slope scale. The traditional, M-C linear criterion exhibits the most divergence from actual curvilinear strength envelopes at these levels of stresses. The general power law representation of shear strength envelopes appears to be the simplest and most accurate means of accounting for such curvilinearity (Denby & Scoble, 1984). Such a model, of a general power curve form, can be expressed as:

$$\tau = c + a (\sigma_N + b)^d$$

Where σ_N is the normal stress, τ is the predicted shear strength for a given σ_N and a , b , c and d are the parameters of the model obtained from a regression analysis. This formula, describing a general power curve with the y-intercept equal to c (i.e. constant cohesion), readily degenerates to a linear M-C model if $b=0$ and $d=1$ or to a modified power curve if $c=0$ (i.e. cohesionless joints). A modified version of the general power curve equation of the form $\tau = a (\sigma_N + b)^d$ was originally proposed by Jaeger (1971). This author stated that the true relationship between normal and shear stresses acting on surface at failure followed a power law which has been proven to be valid for sliding on rock discontinuities.

Figure 3.34 shows data sets from two different specimens being tested. The modified power curve for specimen one shows no intercept with the y-axis meaning that the discontinuities have no cohesion. This is the case when direct shear tests are performed on saw-cut ('simulated') discontinuities created from intact rock samples. In the same figure, the general power curve model has been fitted to specimen number two which shows a constant cohesion of 0.42 ton/m² which equals 4.12 kPa. This is the case when direct shear tests are performed on natural discontinuities that exhibit some type of hard infilling. Although low, this calculated average cohesion value can be critical at the time of calculating Factors of Safety for potentially unstable rock blocks.

When performing a probabilistic geotechnical stability analysis for the bench slopes, one should not just rely on the results of a single direct shear test. Rather, several test results (preferably five or more) should be combined to produce a regression curve representative of the discontinuity type. This procedure defines the specimen's expected shear strength at any given normal stress for which envelopes of +/- 1, 2 or 3 standard deviations can be added to account for shear strength variability (Figure 3.35).

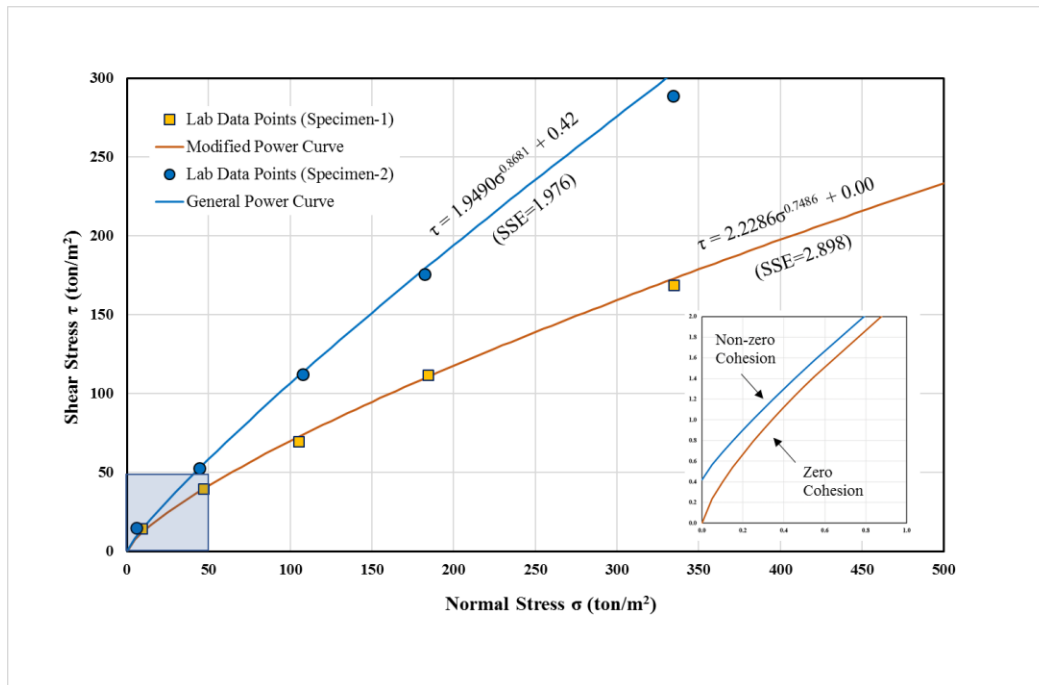


Figure 3.34 Examples of modified power regression curves for describing shear strength of a single test for two specimens. Adapted from Miller & Borgman (1984).

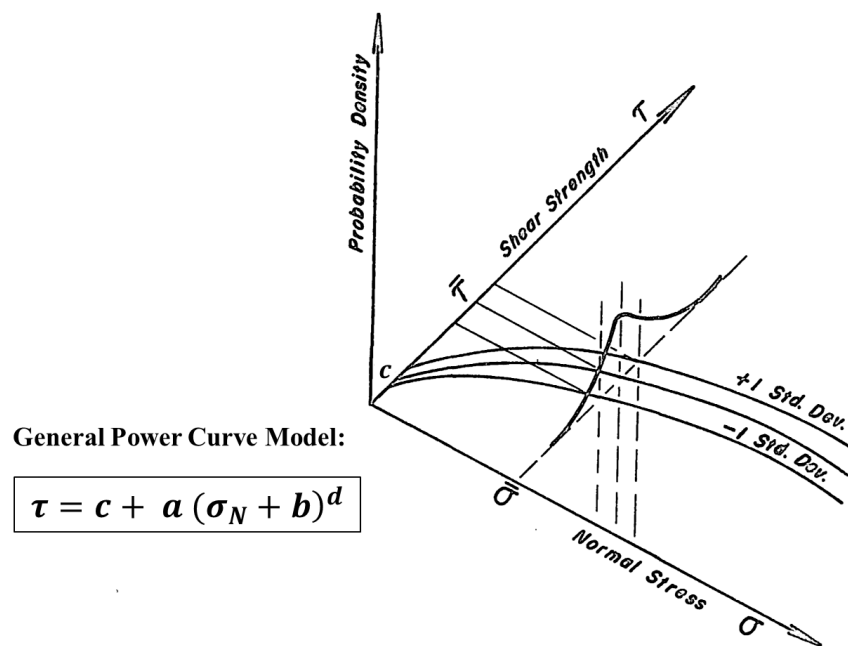


Figure 3.35 Power shear strength criteria showing variability for a specific normal load (Savely, 1987)

3.4 Chapter Summary

Chapter 3 covers an extensive and comprehensive review of structural data collection, processing and interpretation for structurally controlled rock slope stability assessment purposes.

- The importance of assessing the geometrical and strength properties of geological discontinuities in the slope design of a jointed rock mass was highlighted. A clear distinction between major (e.g. fault or shear zones) and minor (e.g. rock joints) geological structures was made as well as the proper definition of geological ‘discontinuity’ given.
- The main sources for structural data was explained. Traditional i.e. surface mapping and core logging techniques and less conventional e.g. photogrammetry and televiewer logs were described in quite detail. Also, each of the ten main geometrical and physical characteristics of discontinuities, as suggested by the ISRM, was explicated. These included: orientation, spacing, persistence, roughness, wall strength, aperture, filling, seepage, number of sets and block size.
- Further emphasis was given to three geometrical joint properties: orientation, spacing and persistence, since these define the shape and size of the potential forming unstable rock blocks.
 - Joint orientation was said to be most commonly expressed in terms of dip and dip direction angles and typically be assessed through stereographic projection techniques. A Terzagui correction factor for orientation bias for linear and areal mapping was explained and the generating blind zone around boreholes defined.
 - Joint spacing was defined as the orthogonal distance between two adjacent discontinues that belong to a given joint set discontinuity frequency. This was related to the discontinuity frequency which is the reciprocal of mean spacing Joint true and apparent spacing was linked through simple trigonometric relationships.
 - Joint persistence was defined as the areal extension of a discontinuity, implying a 3D sampling approach. Due to sampling constraints joint persistence could only be estimated by measuring their trace lengths on scanline (1D) or window (2D) sampling methods.
- Determination of reliable shear strength values for rock discontinuities was exemplified using three different models based on the available information at hand.
 - The Mohr-Coulomb model was presented as the simplest and oldest mathematical idealization of rock joint shear strength, requiring important amount of laboratory data.
 - The Barton-Bandis model was presented as an alternative to the M-C model, since the former is mostly based in field index tests of simple and quick execution.
 - The General Power curve model was also presented as the general case of non-linear fitting to laboratory or field data.

Chapter 4

Bench-Slope Scale

Rock slope instabilities at the bench scale mostly occur as the result of failure along structural discontinuities (Herget, 1977; Goodman, 1989; Kliche, 1999). In this context, several authors have recognized the importance of acquiring detailed knowledge of the rock mass structural features for slope design purposes (Hoek & Bray, 1981; Glastonbury & Fell, 2000; Grenon & Hadjigeorgiou, 2010; Cylwik et al., 2011; Wyllie & Mah, 2014; Stead & Wolter, 2015). Figure 4.1 highlights the main two stages i.e. field data collection and laboratory data analysis within a rock engineering design framework.

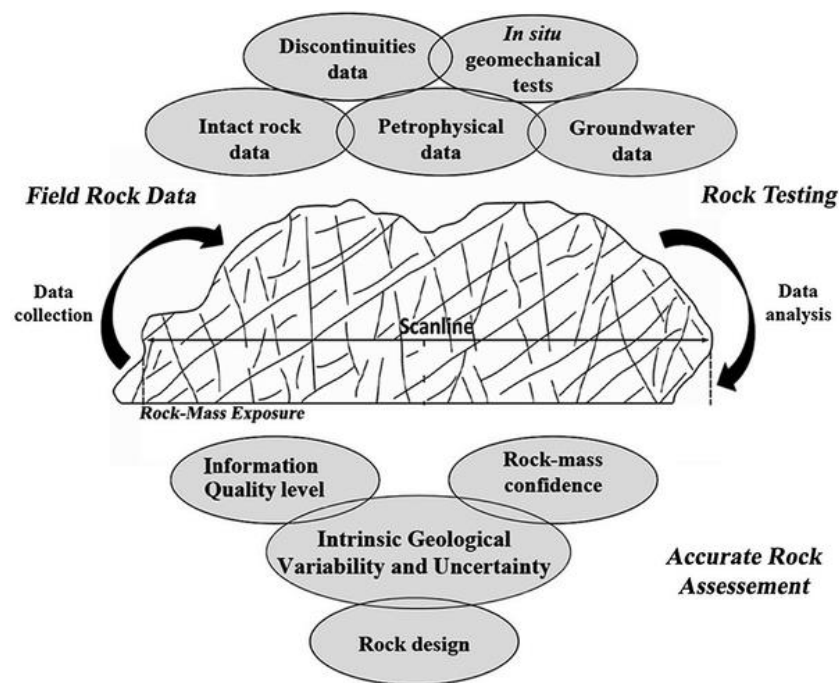


Figure 4.1 Input rock mass properties for rock engineering surveys (Chaminé et al., 2015)

4.1 Analysis of Structurally Controlled Failure Mechanisms

Structurally controlled failure mechanisms include e.g. planar, wedge and toppling. These are classically analyzed by means of a kinematic approach based on stereographic projection techniques, and a kinetic approach that uses the limit equilibrium method. Recently, Discrete Fracture Network modelling has provided a tool to perform a 3D kinematic and kinetic stability analysis in rock masses. These three approached are briefly summarized below and case studies presented at the end of this chapter.

4.1.1 Kinematic Analysis of Rock Blocks

Kinematic analysis identifies a potential -structurally controlled- failure mechanism for an existing or proposed rock slope direction (Kliche, 1999; Park & West, 2001). This is commonly carried out using stereographic projection techniques (Goodman, 1989) for which three tests have been proposed by Markland (1972), Hocking (1976) and Goodman (1976) to identify planar, wedge and toppling failure mechanisms, respectively (Figure 4.2.a). All these conditions are also shown stereographically in Figure 4.2.b. The zones highlighted in red represent the critical failure condition. If the pole or intersection of the mean joint set lies on the critical area it can be reported as a potential failure.

The conventional kinematic analysis shown in Figure 4.2.b can be considered as a deterministic approach since it uses the mean (average) discontinuity sets. Taking the average of a discontinuity set can only be representative in the case of tightly clustered structures that follow a clear trend and where there is no much variation in their orientation. However, in most cases, the orientations of the discontinuities measured in the field - either by surface mapping or core logging - are not clustered tightly. There is in fact a varying degree of scatter in these orientations due to both the inherent natural variability of the rock structural properties (Baecher & Christian, 2005) and the imprecise (imperfect) field data collected through mapping (Bedi, 2014). As a result, the conventional deterministic stereonet-based analysis cannot properly deal with the uncertainty and variability of the problem, and it can potentially yield to misleading conclusions (Park et al., 2016).

A closer look at Figure 4.2.b reveals that if a conventional (deterministic) kinematic analyses were to be performed, no potential failure would be reported. This is simply because the mean orientation of the joint sets all lies outside their corresponding critical zones. A careful observation of the density contours shows that in effect part of the joint orientation distribution lies within this critical zone (Figure 4.2.c). This means that there are in fact some combinations of dip and dip direction angles leading to a potential failure.

When aiming to consider the uncertainties and variability in the orientation of a discontinuity within a discontinuity set, a probabilistic analysis should be used as part of a probabilistic kinematic analysis procedure. The first step for a probabilistic kinematic analysis is to determine the probability density function of the joint set orientations. Joint orientation can be modeled as a Fisher distribution, which is usually presented in a lower hemisphere stereonet as a series of circles around the average joint pole orientation (Figure 4.3.a). This distribution can be visualized as a combination of two normal distributions – one for dip direction, and one for dip (Figure 4.3.b). A Fisher Distribution describes the angular distribution of orientations about a mean orientation vector and is symmetric about the mean.

It is a one-parameter distribution with K being the "Fisher constant". The Fisher K value describes the tightness or dispersion of an orientation cluster. A larger K value (e.g. 50) implies a tighter cluster, and a smaller K value (e.g. 20) implies a more dispersed cluster, as shown in Figure 4.4.

Once the probability density function for dip and dip direction values have been determined, the kinematic instability can be quantified as the probability (Pr) of a pole or intersection lying within the critical zone for a given failure mechanism. In terms of probabilities, this can be written as follows.

For planar failure,

$$\Pr [\phi_d < \beta_j < \beta_s] \times \Pr [\alpha_s - 20^\circ < \alpha_j < \alpha_s + 20^\circ] \quad [\text{Eq.4.1}]$$

Where:

α_j, β_j : Dip direction and dip of joint.

α_s, β_s : Dip direction and dip of the slope.

ϕ_d : Friction angle of the discontinuity.

For wedge failure,

$$\Pr [\phi_d < \alpha_i < \beta_s] \times \Pr [\alpha_s - 80^\circ < \beta_i < \alpha_s + 80^\circ] \quad [\text{Eq.4.2}]$$

Where:

α_i, β_i : Trend and Plunge of intersection.

For toppling failure,

$$\Pr [90^\circ - \beta_s + \phi_d < \beta_j] \times \Pr [(\alpha_s + 180^\circ) - 20^\circ < \alpha_j < (\alpha_s + 180^\circ) + 20^\circ] \quad [\text{Eq.4.3}]$$

4.1.2 Kinetic Analysis of Rock Blocks

Unlike a kinematic analysis which only describes the motion of rock blocks without considering the forces that cause them to move, a kinetic analysis does consider the effects of forces acting upon them. A kinetic analysis will quantify and compare the resisting (capacity) and driving (demand) forces acting on the discontinuity surfaces at the time of failure. In this evaluation a ratio between these two forces (i.e. the FoS) is calculated based on a limit-equilibrium method (LEM).

A detailed review of LEM calculation for planar, wedge and toppling failure will not be given in this section since there is an extensive literature that already covered these topics. The reader is forwarded to consult the books by Hoek and Bray, 1981; Kliche, 1999; Willye and Mah, 2014 among others.

Calculations for planar, wedge and toppling failures at the bench scale were carried out using the commercially available software RocPlane, Swedge and RocTopple from Rocscience Inc.

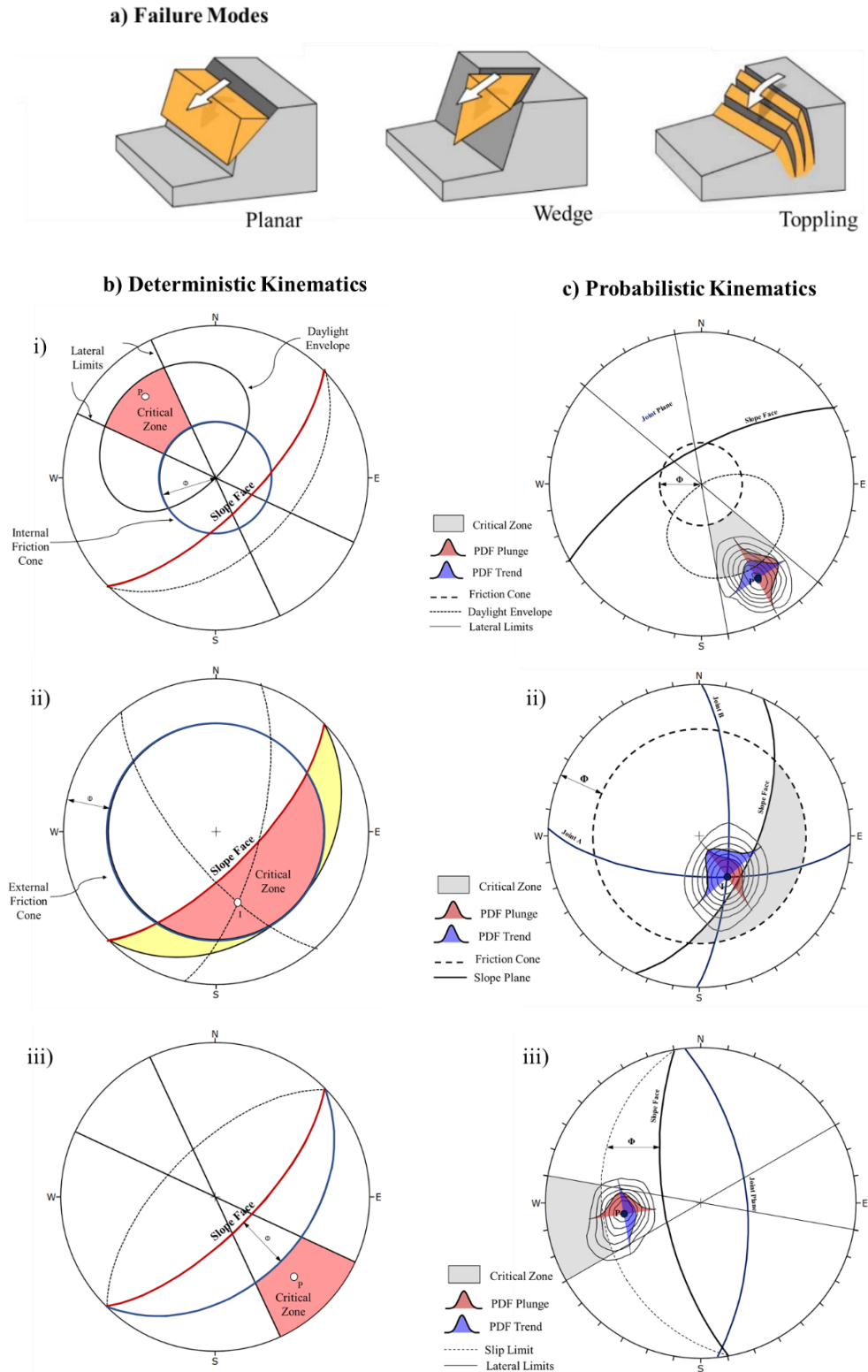


Figure 4.2 a) Modes of different structurally controlled rock slope failures. Stereographic projections for both the a) Deterministic and c) Probabilistic kinematic analysis approaches are shown

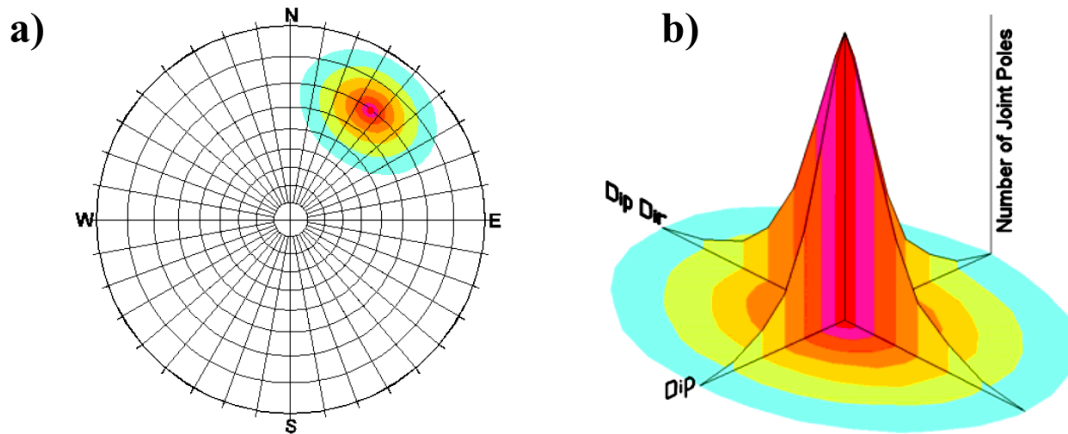


Figure 4.3 Joint Pole Orientation. a) Fisher distribution as concentric circles. b) Three-dimensional view of dip and dip direction distribution on the sphere (Ron Crouse, 2008)

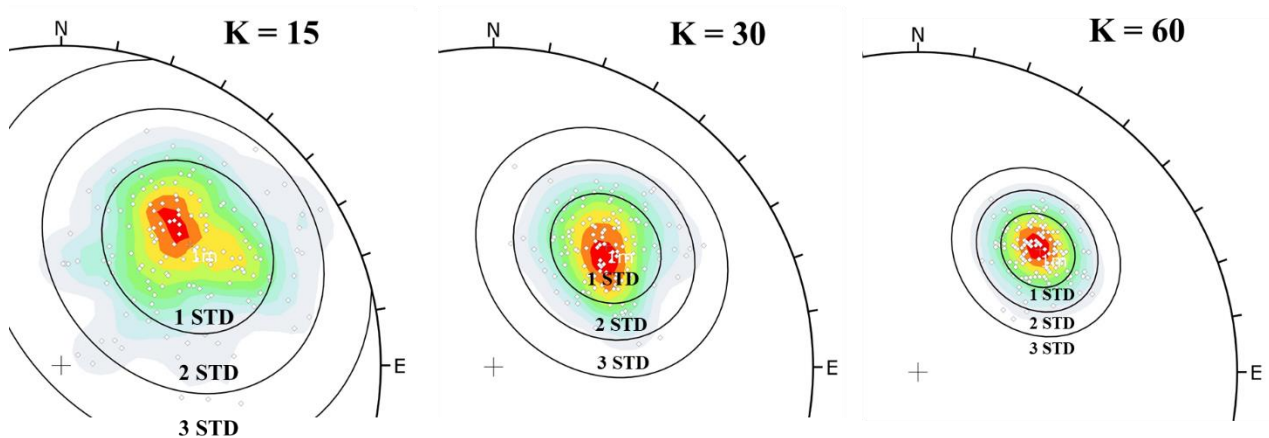


Figure 4.4 Variation in the degree of joint orientation clustering for varying Fisher 'constant values of 15, 30 and 60

4.1.3 Discrete Fracture Network (DFN) Modelling

DFN modelling is a recent developed tool for the three-dimensional (3D) stochastic representation of discrete fractures within rock masses. DFN models were first introduced in the late 1970s for fluid flow modelling purposes in fractured rock masses (Dershowitz et al., 2004; DeGraff, 2007). Since then, the DFN approach has been developed continuously, and its applications extended to various engineering problems (Miyoshi, 2018). Some examples of these applications in the field of mining include (Lorig et al., 2015):

- Estimate rock mass strength and deformation modulus
- Quantify natural rock mass fragmentation distribution.
- Perform 3D kinematic and kinetic block stability analysis.

A comprehensive review on DFN modelling and applications are provided in (Elmo et al., 2007; Jianhua, 2008; Styles and Pine, 2011; Bonilla et al., 2015, Lorig, 2015).

In summary, the steps to follow to generate a DFN model include:

1. Structural data collection
2. Discontinuity data characterization
3. DFN model construction
4. DFN model validation

The author would like to highlight that even though DFN models require the classical information gathered during field mapping (e.g. joint orientation, joint length, etc.), the way in which these parameters are described or reported should be redefine. The joint length is one critical parameter for constructing DFN models. It is required that the actual trace length is measured as opposed to the conventional intervals of 1 m, 1 to 3 m, 3 to 10 m, 10 to 20 m, and greater than 20 m long as suggested in the ISRM methods. This discretization of joint length in unequal intervals adds subjectivity in the characterization of data and makes difficult to fit an adequate distribution to the created histograms (Figure 4.5).

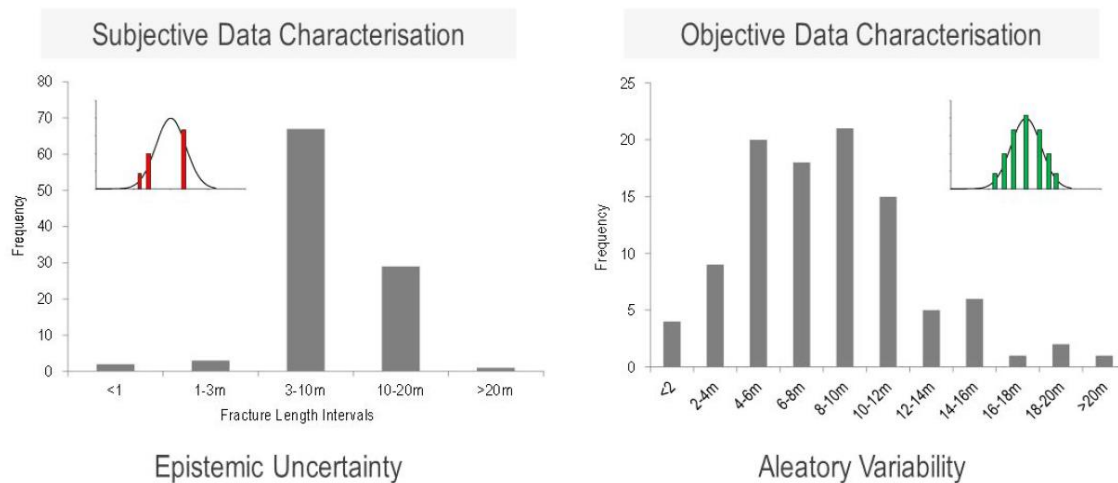


Figure 4.5 Example showing the limitations of ISRM suggested methods (Elmo et al., 2015)

The advantage of a DFN model when performing a kinematic and kinetic analysis is that rock blocks are delimited by discontinuities whose size (i.e. length) is not infinite but finite following a given statistical distribution. This is more realistic and less conservative than the classical LEM analysis in which rock blocks are assumed to be of the maximum size possible (see Figure 4.6).

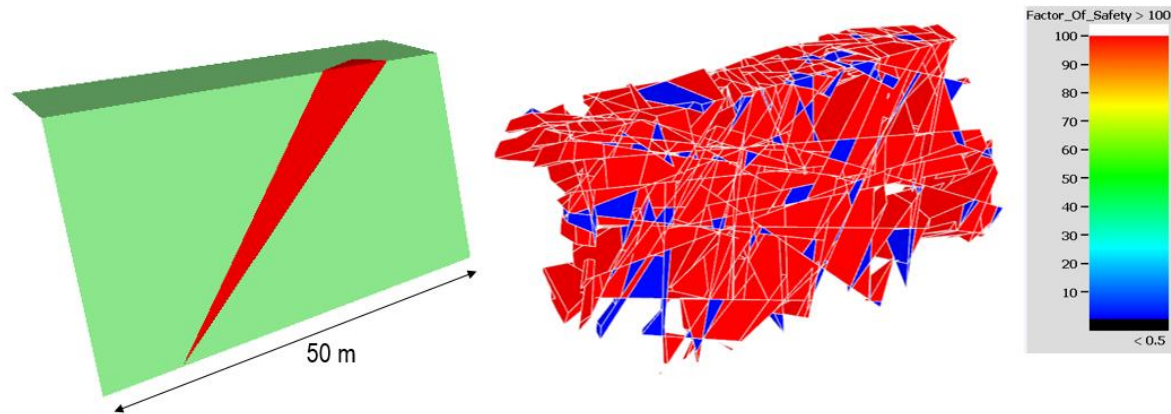


Figure 4.6 Comparison of limit equilibrium analysis and DFN modeling approach (Miyoshi, 2018)

There are various DFN software packages commercially available. Some examples are FracMan (Golder Associates, 2019), SiroModel (CSIRO, 2017), FracSim 3D (Xu and Dowd, 2010), and MoFrac (MIRARCO, 2013). For the case study that will be shown in the next section Fracman software was used.

4.2 Case Studies

Real-life case studies are presented in the following sections to compare and put in perspective the results obtained by combining structural field data and rock laboratory testing for the design of bench slopes in open pit mining. These will show how depending on the type, quantity and quality of information (field or laboratory data) available at the time of analysis, adequate results can be achieved with yet simple but practical analytical calculations (e.g. LEM).

Three case studies are presented. The first one deals with the geotechnical reconciliation of an existing open pit mine. Since some benches were already excavated, field data was collected from direct mapping on exposed benches. The second case study was an open pit mine project with more than fifty geological and geotechnical diamond drill holes (DDH) with structural field data coming mainly from oriented core logging. The third case study is an attempt of the author to construct an approximate DFN model with available data from classical bench mapping.

4.2.1 Case Study #1

Geological Setting

The first case study shown in this section corresponds to an open pit mine located in the Peruvian Andes at an elevation of 3500 m. This is a gold mineral deposit classified as an epithermal high sulphidation system with an extension of @ 2.5 km x 1 km and a depth of 250 m for the first stage of ore recovery. Rock types present within this deposit range in age from late Eocene to early Miocene, typically consisting of pyroclastic rocks such as tuff or ignimbrite. Also, locally in extension in the north part of the pit there is a

crushed rock (breccia) material cemented with a fine grain matrix and associated with a subvertical fault system. Significant hydrothermal alteration has occurred in this region due to the mineralizing fluids which has attacked the country rock as they moved up to the surface. This has resulted in three main hydrothermal alteration types of the parent (host) rock. These are: strong silicification, moderate and advanced argillic. The difference amongst these three depends on the mineral assemblage occurring. For example, in silicification crystalline quartz replaces or fills voids in the rock whereas in argillic alteration the original feldspar minerals of the rock breaks down to clays. It will be shown later in this thesis that hydrothermal alteration has a great effect on the geomechanical properties of rocks by either increasing or reducing the rock's compressive strength. Figure 4.7. shows the geological map of the open pit mine which has been divided into seven zones based on similar lithological features. The case study presented here corresponds to the bench-scale slope stability analysis for zone 05 only (see Figure 4.8).

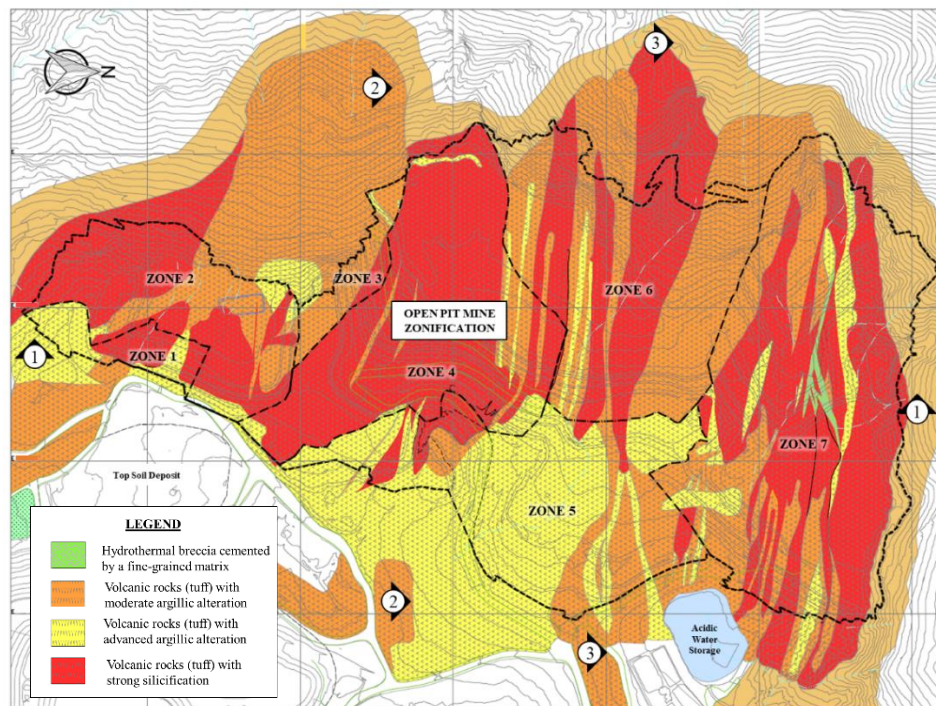


Figure 4.7 Geological map of the open pit mine with zoning limits. The study area corresponds to zone 05



Figure 4.8 Perspective 3D view of the open pit mine. The study area corresponding to zone 05 is shown

Structural Geology

Geological features such as faults, dikes, shear zones, and contacts that have dimensions of the same order of magnitude as the area being characterized are regarded as ‘major’ structures. These structures are treated as individual elements for design purposes, as opposed to joints, which are considered as ‘minor’ structures and handled statistically. From the structural mapping information, there are not known regional structural features within the immediate area of the pit. Intermediate scale structures (>25 m in length), related to a local faulting system is, however, evident in the area of the pit. This system corresponding local faulting is believed to have influence at the inter-ramp scale analysis which will be addresses in chapter 05. The structurally controlled stability analysis at the bench scale presented in this section will only account for the minor geological structures such as rock joints. The rock mass of this case study has been described as a very blocky type according to the GSI classification scheme (Figure 3.9). This will be useful later on when assessing the overall (global) stability of the pit slope covered in chapter 06.



Figure 4.9 Very blocky rock mass type in the open pit mine

Structural Field Data Collection

The field data collection program was developed for rock mass characterization purposes to support the development of a geotechnical model suitable for the open pit slope stability evaluation. Rock mass structural characteristics were measured by surface mapping on the existing bench slope faces. In the present case study, the field data collection consisted of extensive structural mapping of minor geological structures (e.g. rock joints) conducted at 36 different sites that were strategically located to cover most of the study area. The structural field data was collected following the ISRM suggested procedures (Barton, 1985).

Figure 4.10 shows the window (cell) mapping locations within zone 05 of the existing pit wall. A total of 622 discontinuities were mapped in this area and their orientation reported in terms of Dip and Dip Direction angles. Lower hemisphere equal-area stereographic projections constructed from these data were used to define the predominant joint sets. Contoured plots such as the ones shown in Fig. 4.11 were examined visually to identify clusters of subparallel discontinuities. A correction bias (Terzaghi, 1965) was applied to all orientation data since features that are perpendicular to the direction of surveying are favored over those which are parallel. This bias correction calculates a geometrical weighting factor for each measured discontinuity, with the highest correction applied to the structures that are parallel to the direction of surveying. Figure 4.11.a shows the corresponding contour plot for the case of no bias correction factor being applied (unweighted) and Figure 4.11.b the contour plot with the Terzaghi (1965) correction applied.

It should be noted that these two concentration pole density plots vary importantly, being the corrected the one to be used for later analysis. In both plots three main joint sets (J1, J2 and J3) are identified. Their mean values, range, and other statistical characteristics are summarized in Table 4.1.

Table 4.1 Summary of mean joint sets orientation – case study 1

Joint Set		Mean Dip (°)	Mean DipDir (°)	Dip Range (°)	DipDir Range (°)	K Fisher	Angular Deviation (°)	Relative Occurrence (%)	N° Poles in Set	N° Total Entries
J1	1m	83	183	50-90	150-215	13.37	22.2	33%	204	Unweighted
	1w	86	184		330-035	13.87	21.7	35%	348	622
J2	2m	88	97	56-90	065-130	14.14	21.5	25%	158	
	2w	90	276		245-310	14.53	21.2	24%	243	Weighted
J3	3m	34	336	04-67	260-054	13.89	21.7	18%	111	1002
	3w	36	337			13.72	21.9	17%	167	

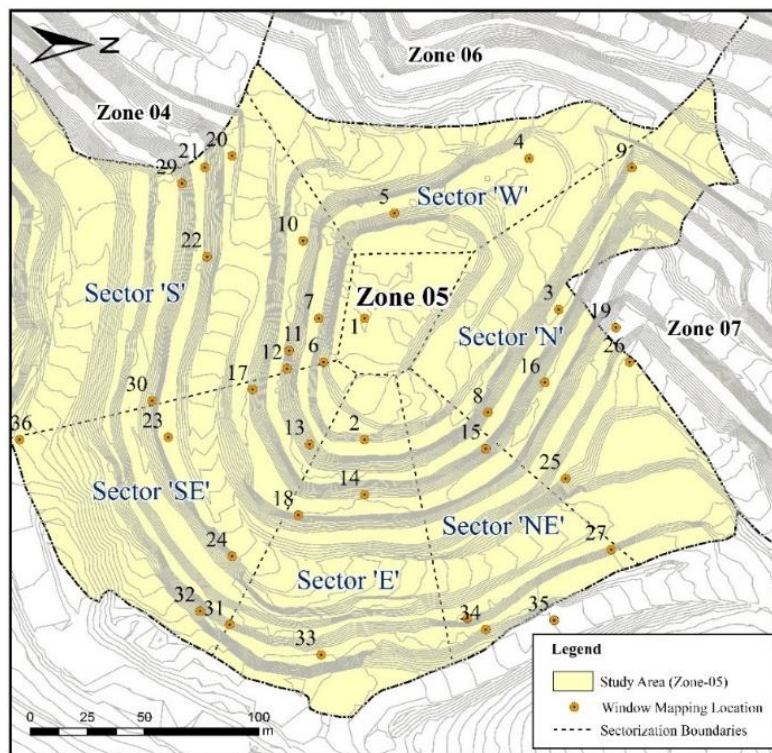


Figure 4.10 Structural window mapping (WM) point locations within zone 05 of the open pit mine

Structural Zones & Design Sectors

The rock mass comprising the entire open pit mine was divided into a number of *structural zones* or domains. Each of these zones is expected to be distinct and hold similar characteristics clearly differentiated from the ones of its neighbors in terms of the geometrical (orientation) features of the dominant joint sets and mechanical (strength) properties of the rock type. It is also important to consider the orientation of the proposed open pit slope face since different slope orientations within a structural domain require different design considerations. Therefore, the slope is divided into *design sectors* which contain one slope orientation and lie within one structural domain. Stability analysis and slope designs are then carried out for each design sector. Then, the open pit mine was divided in 07 different zones as shown in Figure 4.7. The design sectors for the case study area (zone 05) is shown in Figure 4.10. These are in total 06 sectors named: North, North East, East, South East, South and West.

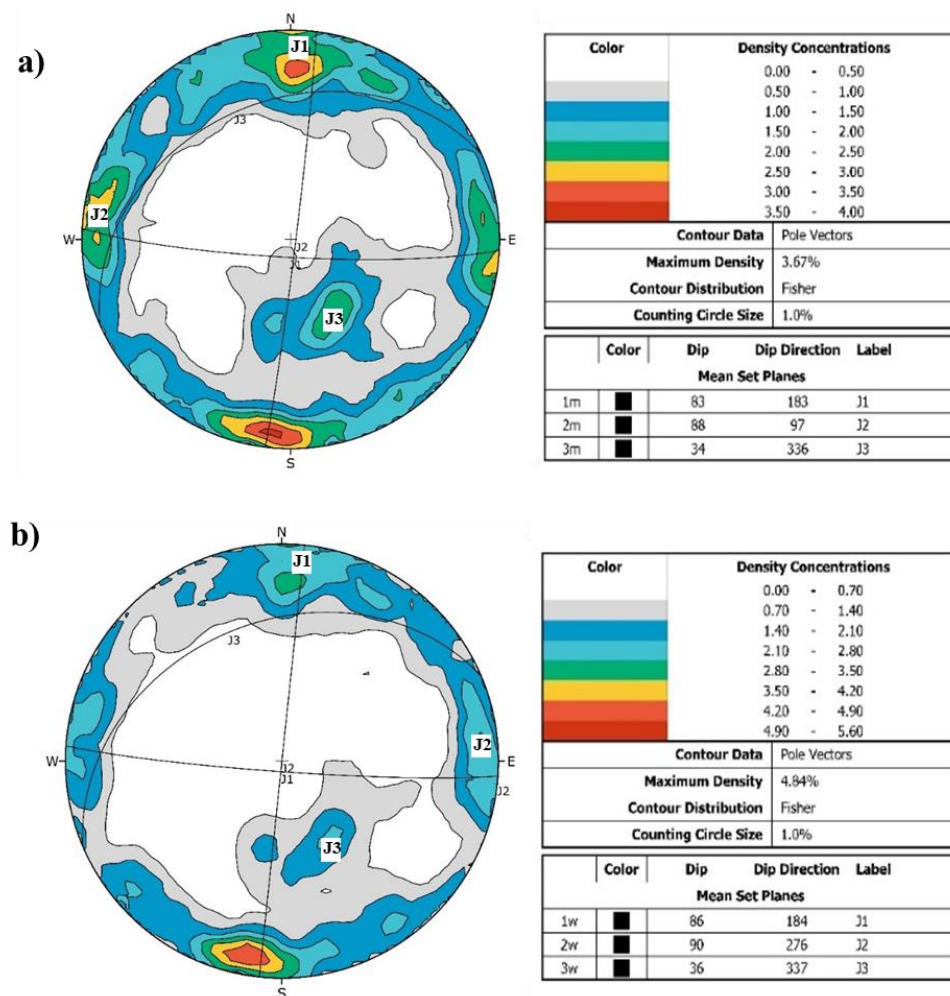


Figure 4.11 Composite stereonet plots for the orientation of joint sets in zone 05 of the open pit mine. a) Unweighted contour plot. b) Weighted contour plot

Rock Laboratory Testing

Geomechanical laboratory testing was conducted in order to determine the mechanical characteristics for the intact rock and rock joints. The overall laboratory program consisted of physical properties, direct shear and uniaxial compressive strength of the rock. A total of 79 laboratory tests were conducted on samples selected to represent the range of the rock conditions observed in the study area (zone 05). A summary of rock unit weight and direct shear tests results are given below since these are important input parameters for the bench slope stability analysis.

Unit Weight Measurements

Prior to actual testing of rock samples, sample dimensions and weights were measured and used to calculate total unit weights for each one. The combined data set included 09 tests with measurements ranging from 21.4 to 25.8 kN/m³ with a mean value of 24 kN/m³. Unit weights are summarized in Figure 4.12.

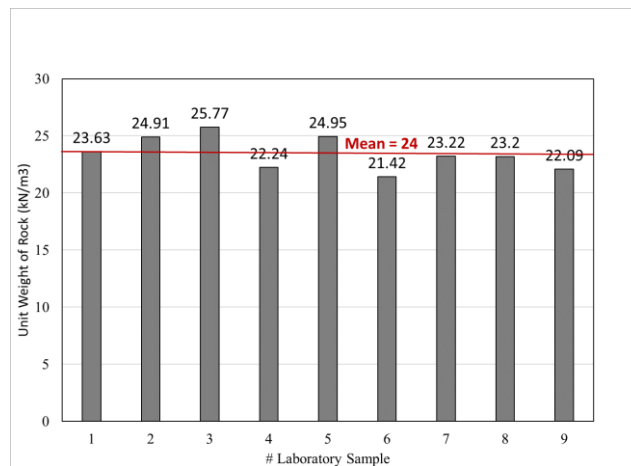


Figure 4.12 Laboratory tests results for unit weight measurements

Direct Shear Testing

For this project, 40 rock samples were selected for direct shear tests (ASTM Method D5607). To facilitate the estimation of a lower bound discontinuity shear strength envelope, saw-cut discontinuities were created in the rock samples prior to testing. The range of normal stresses applied during testing was selected according expected in-situ stresses within the slopes. The maximum selected normal load was set to 6 MPa. This value corresponds to a vertical weight due to a 250 m high slope (considering an average unit weight of 24 kN/m³).

Direct shear test data were fitted to both the linear Mohr-Coulomb(M-C) and non-linear Power Curve (PC) models. Both models (linear and non-linear) were adjusted to intersect the origin (i.e. $c=0$) given that direct shear tests were carried out on saw cut surfaces. The results from the linear M-C model give an average

friction angle of 31° with a minimum and maximum of 27° and 34° , respectively as shown in Figure 4.13. The 95% prediction interval for the data set is also shown in solid lines. They represent a range that is likely to contain the value of a single new observation (i.e. there is a 95% chance that a new lab test result will lie within the PI). A non-linear power curve model was fitted to the direct shear lab data ensuring that the derived curve intersect the origin (i.e. $c=0$) owing to the inexistent joint infilling during testing. The following average nonlinear fit was obtained $\tau = 0.615 (\sigma_N)^{0.977}$ and this is also shown in Figure 4.14. The corresponding 95% prediction interval for the data set is also shown in the same figure.

For the rock slope stability calculations both deterministic and probabilistic values of joint shear strength are defined. The first ones correspond to the average values obtained from the linear and nonlinear model. Both M-C and P-C joint shear strength models are defined directly as a random variable, rather than defining the individual parameters of the strength criterion as random variables. For a given normal stress, a random value of shear strength will be generated using the mean shear strength, coefficient of variation, and the selected statistical distribution (Lognormal or Gamma). This will be the actual value of shear strength used in the safety factor calculation. The random shear strength option is schematically illustrated in Figure 4.15. Basically, a variability of shear strength about the mean strength envelope is defined. This is intuitively simpler to grasp than defining variability of individual strength parameters. This approach eliminates the need for defining statistical distributions for individual strength parameters (which may be difficult to obtain or unavailable). Furthermore, the issue of statistical correlation of the strength parameters is avoided.

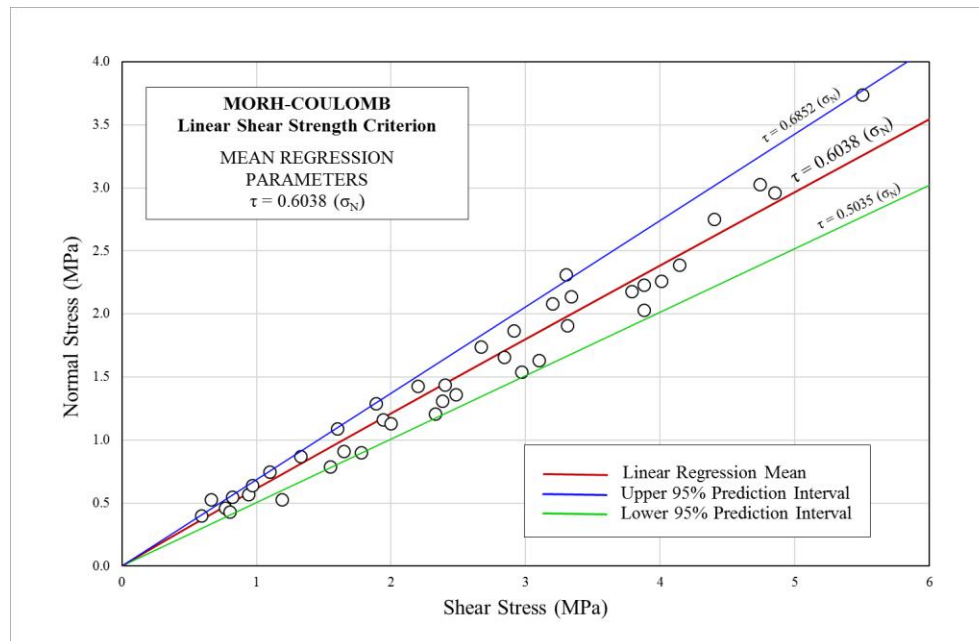


Figure 4.13 Mohr-Coulomb linear regression analysis for direct shear tests on joint samples.

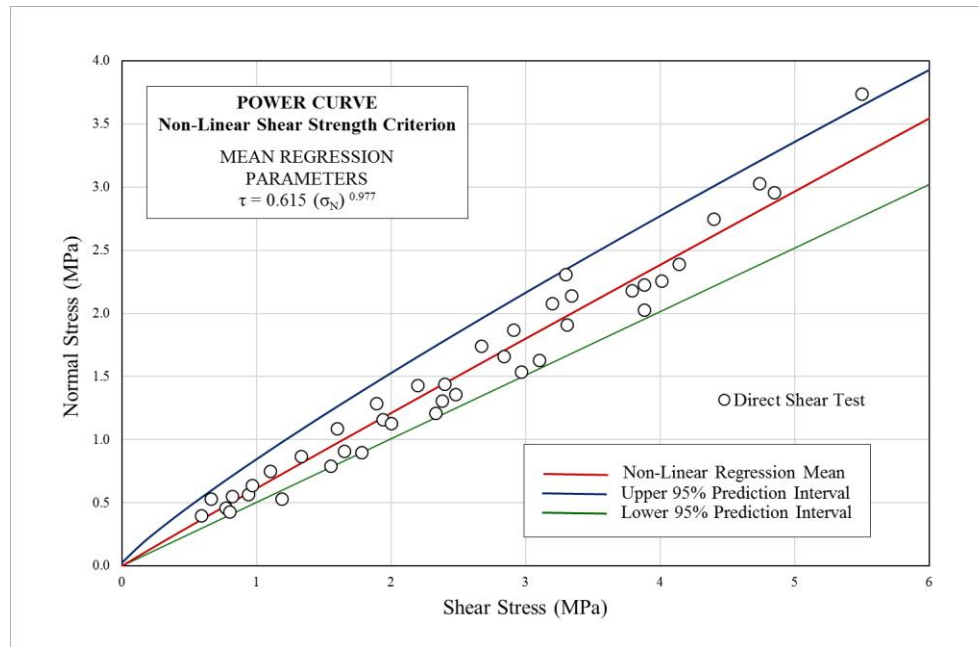


Figure 4.14 Power Curve regression analysis for direct shear tests on joint samples.

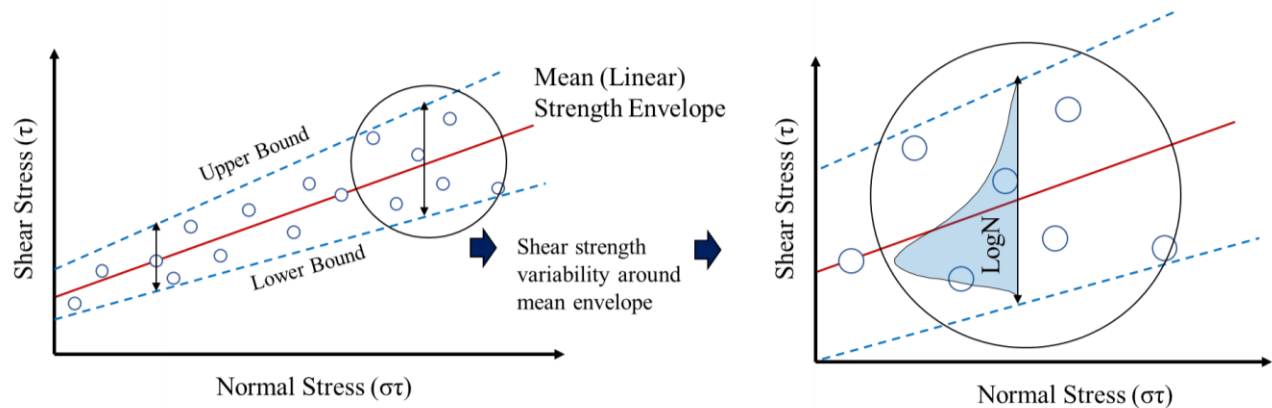


Figure 4.15 Random shear strength envelope model

Bench Slope Stability Analysis

Kinematic analysis following both the deterministic and probabilistic approach were carried out for the bench face slopes within zone 05. The benches in this area were excavated at a 65° slope angle with a height of 15m. Only the mean joint set orientations were used for the deterministic analysis. Figure 4.16 shows the results of the deterministic approach as equal area stereoplots for each of the 06 designing sectors.

For the probabilistic kinematic analysis, all the joint orientations belonging to each of the three main joint sets previously identified were used for fitting a theoretical probability distribution. Figure 4.17 shows the experimental histograms for the orientation of joint sets: J1, J2 and J3. It can be clearly seen that steeply

dipping joints such as J1 and J2 exhibit some skewness and therefore a non-symmetrical probability function can be expected to fit this shape. The fitted probability density function and its parameters are summarized in Table 4.2 for each joint set.

Table 4.2 Summary of statistical distribution for joint orientation – Case study 1

Joint Set	Dip (°)		Dip Direction (°)	
	Distribution	Parameters	Distribution	Parameters
Joint Set 01	Beta	$\alpha=3.63, \beta=1.48$	Weibull	$\alpha=3.18, \beta=52.99$
Joint Set 02	Beta	$\alpha=4.24, \beta=1.44$	Weibull	$\alpha=2.82, \beta=48.93$
Joint Set 03	Normal	$\mu=37.71, \sigma=14.11$	Normal	$\mu=335.85, \sigma=32.40$

With the given PDF shown above, the corresponding probability of kinematic instability was computed by using classical probability theory. It should be highlighted that for the present study dip and dip direction values were found to be independent variables and thus the multiplication rule for the probability calculation was used. The reason why independence was assumed is because no correlation was observed in the scatter plots for these two values. Figure 4.18 shows the scatter plot for joint set 03 in which a very weak correlation of 0.17 was found. Similarly, for joint set 01 and 02 correlation values of 0.06 and 0.08, were respectively obtained. All of these can be considered negligible and close to a no correlation pair-data set.

The kinetic analysis was carried out by a limit equilibrium approach in which both the factor of safety and probability of failure i.e. sliding along the discontinuities were considered. The joint shear strength envelope was assumed to be variable with the characteristics shown in Table 4.3.

Table 4.3 Summary of joint shear strength envelope – Case study 1

Parameters	Power Curve Model	M-C Linear Model
a	0.615	0.6038
b	0.977	1.000
c	0	0
d	0	0
Coefficient of Variation (CV)	0.25	0.25

The commercially available software RocPlane v.4, Swedge v.7 and RocTopple v.2 from Rocscience Inc. were used to model planar, wedge and toppling failure mechanisms, respectively. Both a deterministic and probabilistic analysis was carried out using the Rocscience software package. For the first one, all input parameters (i.e. joint orientation and shear strength) were set as their mean values. For the second one, a

Monte Carlo simulation technique was used to generate random samples from the user-defined probability distributions.

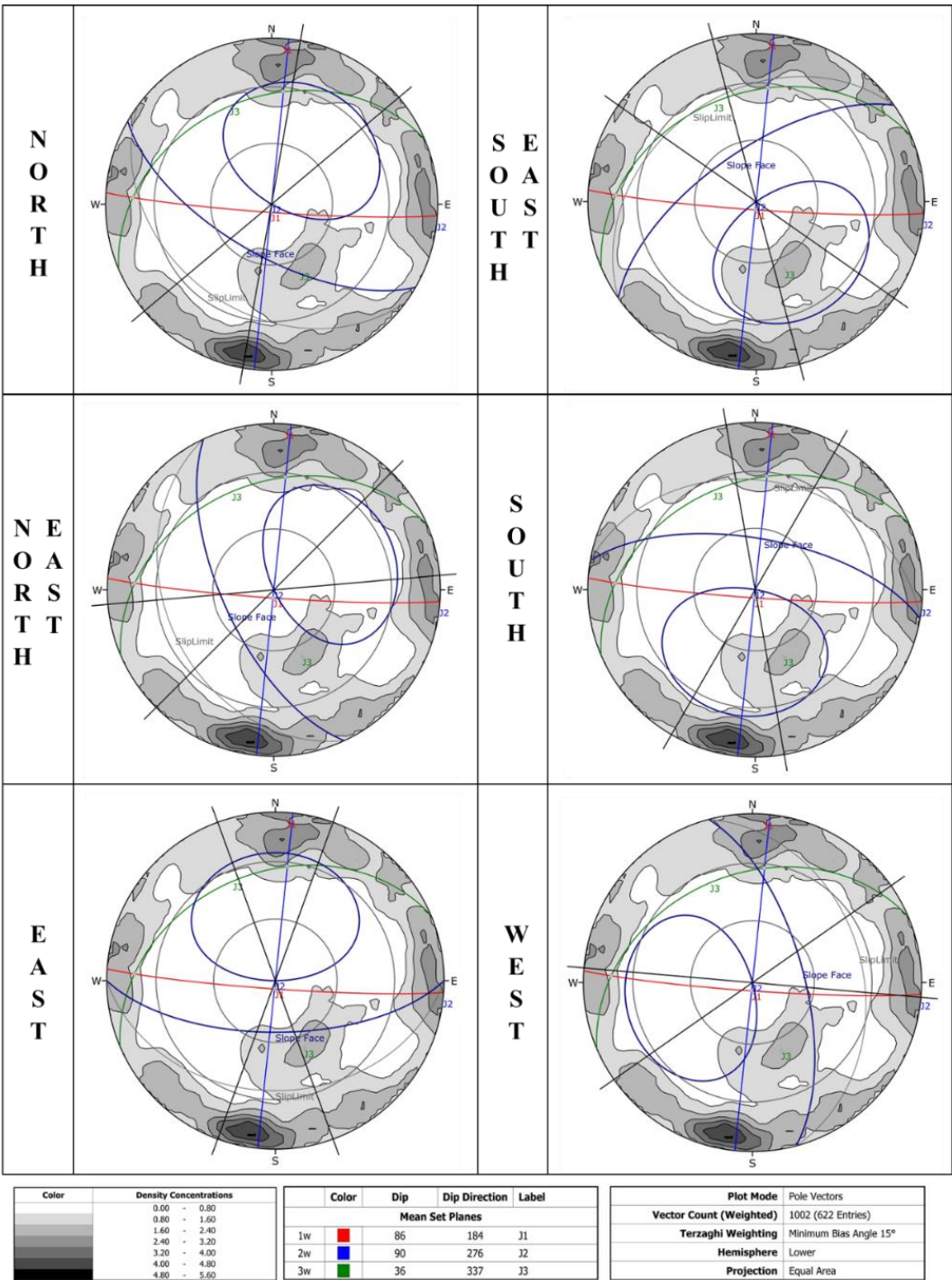


Figure 4.16 Deterministic kinematic stereographic analyses plots.

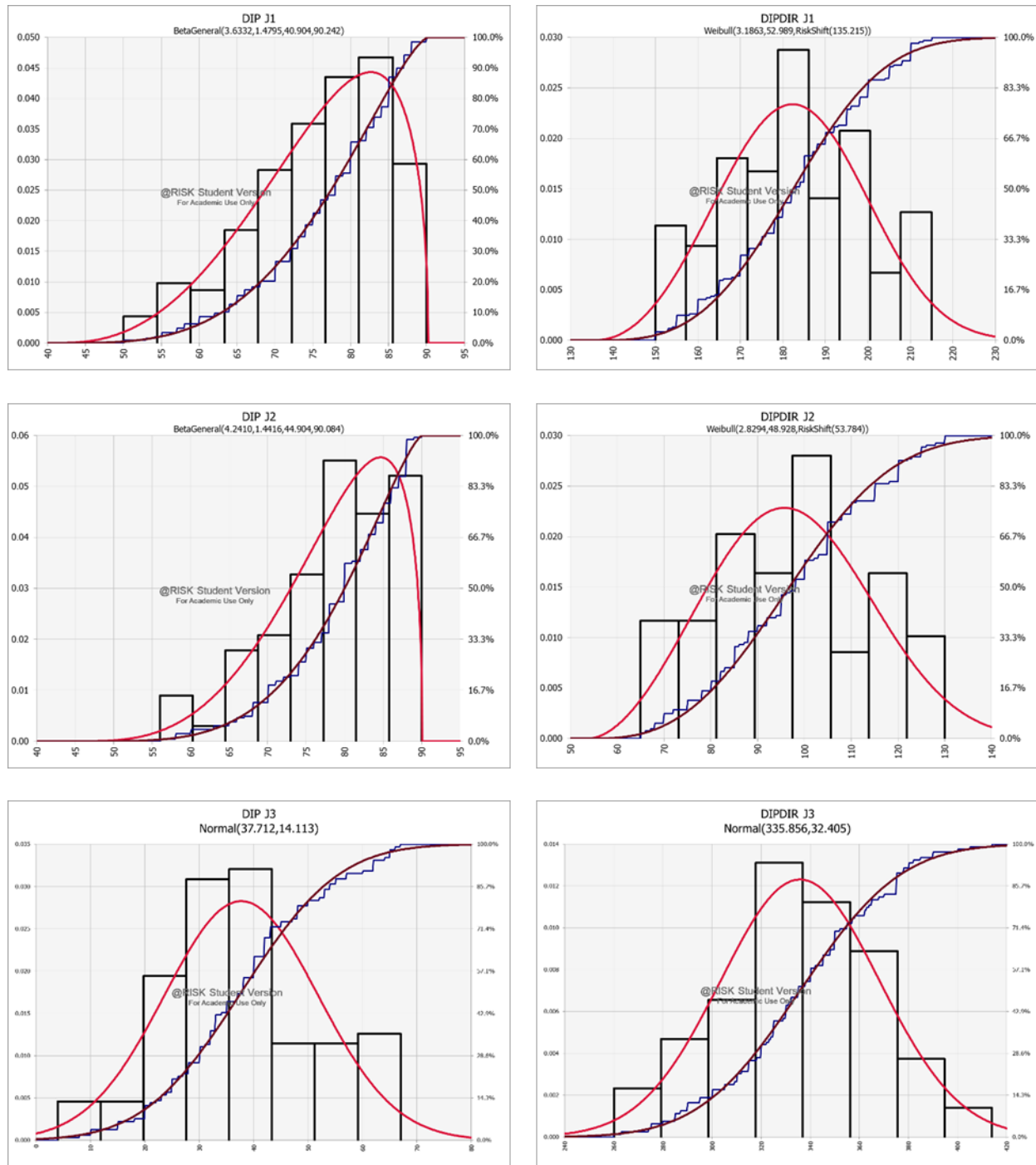


Figure 4.17 Experimental histograms for dip and dip direction angles of joint sets J1, J2 and J3.

A summary of the kinematic analysis results is shown in Table 4.4, whereas the results of the kinetic analysis is shown in Table 4.5. Finally, Table 4.6 shows the results of the total Probability of Failure (PoF) obtained by multiplying the kinematic and kinetic probabilities, respectively.

Table 4.4 Summary of deterministic and probabilistic kinematic analysis

Zone	Sector	Set #	Deterministic				Probabilistic			
			Potential Instability Mechanism				Potential Instability Mechanism			
			Planar	Wedge		Toppling	Planar	Wedge		Toppling
Zone 5	N	J1	No	J1&J2:	No	Yes	25.84%	J1&J2:	11.04%	19.02%
		J2	No	J2&J3:	No	No	22.70%	J2&J3:	3.67%	0.00%
		J3	No	J3&J1:	No	No	80.94%	J3&J1:	58.01%	0.00%
	NE	J1	No	J1&J2:	No	No	19.77%	J1&J2:	9.06%	0.00%
		J2	No	J2&J3:	No	No	28.50%	J2&J3:	4.87%	11.69%
		J3	No	J3&J1:	No	No	91.78%	J3&J1:	74.85%	0.00%
	E	J1	No	J1&J2:	No	Yes	28.51%	J1&J2:	11.16%	40.59%
		J2	No	J2&J3:	No	No	15.55%	J2&J3:	3.59%	0.00%
		J3	No	J3&J1:	No	No	83.82%	J3&J1:	20.64%	0.00%
	SE	J1	No	J1&J2:	No	No	34.23%	J1&J2:	4.24%	11.02%
		J2	No	J2&J3:	Yes	No	24.80%	J2&J3:	87.24%	3.32%
		J3	Yes	J3&J1:	No	No	86.50%	J3&J1:	73.68%	0.00%
	S	J1	No	J1&J2:	No	Yes	36.52%	J1&J2:	3.62%	38.75%
		J2	No	J2&J3:	Yes	No	13.66%	J2&J3:	90.84%	0.00%
		J3	No	J3&J1:	No	No	69.17%	J3&J1:	25.56%	0.00%
	W	J1	No	J1&J2:	No	No	26.31%	J1&J2:	4.48%	0.00%
		J2	No	J2&J3:	Yes	Yes	30.28%	J2&J3:	48.77%	29.68%
		J3	No	J3&J1:	No	No	60.20%	J3&J1:	18.06%	0.00%

Kinematic Probability

>25%
 5% - 25%
 <5%

The results of the deterministic kinematic analysis summarized in Table 4.4 shows that there is a high probability for the formation of: planar failure through set 03, wedge failure through sets 02 and 03, and toppling failure through sets 01 and 02. Now, based on the probabilistic kinematic results, the highest probabilities are for planar and wedge failure, and the smallest for toppling. It should be noted that these probabilities are associated with the chance of satisfying unstable conditions based solely on the joint orientation distribution and the slope geometry (i.e. probability of occurrence or formation).

Table 4.5 Summary of deterministic and probabilistic kinetic analysis

Zone	Sector	Set #	Deterministic				Probabilistic			
			Potential Instability Mechanism				Potential Instability Mechanism			
			Planar	Wedge	Toppling		Planar	Wedge	Toppling	
Zone 5	N	J1	No	J1&J2:	No	>1.1	22.72%	J1&J2:	81.54%	1.50%
		J2	No	J2&J3:	No	No	9.02%	J2&J3:	1.12%	0.00%
		J3	No	J3&J1:	No	No	0.23%	J3&J1:	3.24%	0.00%
	NE	J1	No	J1&J2:	No	No	8.31%	J1&J2:	80.50%	0.00%
		J2	No	J2&J3:	No	No	13.82%	J2&J3:	13.71%	2.00%
		J3	No	J3&J1:	No	No	0.17%	J3&J1:	7.75%	0.00%
	E	J1	No	J1&J2:	No	>1.1	28.13%	J1&J2:	79.96%	4.30%
		J2	No	J2&J3:	No	No	25.69%	J2&J3:	0.17%	0.00%
		J3	No	J3&J1:	No	No	0.56%	J3&J1:	3.42%	0.00%
	SE	J1	No	J1&J2:	No	No	3.25%	J1&J2:	82.84%	1.70%
		J2	No	J2&J3:	1.78	No	2.73%	J2&J3:	39.84%	3.32%
		J3	>1.1	J3&J1:	No	No	0.08%	J3&J1:	22.89%	0.00%
	S	J1	No	J1&J2:	No	>1.1	6.45%	J1&J2:	76.91%	1.20%
		J2	No	J2&J3:	1.98	No	8.86%	J2&J3:	28.45%	0.00%
		J3	No	J3&J1:	No	No	0.16%	J3&J1:	24.51%	0.00%
	W	J1	No	J1&J2:	No	No	3.06%	J1&J2:	78.83%	0.00%
		J2	No	J2&J3:	2.57	>1.1	8.35%	J2&J3:	11.19%	1.70%
		J3	No	J3&J1:	No	No	0.11%	J3&J1:	1.06%	0.00%

Kinetic Probability

>25%
 5% - 25%
 <5%

If a kinematically unstable condition is found to exist from a deterministic point of view, a kinetic analysis using the limit equilibrium method (LEM) is used to evaluate the factor of safety (FoS). Table 4.5 shows the FoS for the previously identified kinematically feasible blocks. It shows that all FoS are above 1.1 which is considered as the minimum acceptable criteria at the bench scale analysis. Table 4.5 also shows the kinetic probability which assessed whether the shear strength was exceeded or not by the induced shear stress for a given slope geometry. Thus, the kinetic probability is associated with the probability of sliding.

Table 4.6 Total probability of failure

Zone	Sector	Set #	Total Probability of Failure			
			Planar	Wedge		Toppling
Zone 5	N	J1	5.87%	J1&J2:	9.00%	0.29%
		J2	2.05%	J2&J3:	0.04%	0.00%
		J3	0.19%	J3&J1:	1.88%	0.00%
	NE	J1	1.64%	J1&J2:	7.30%	0.00%
		J2	3.94%	J2&J3:	0.67%	0.23%
		J3	0.15%	J3&J1:	5.80%	0.00%
	E	J1	8.02%	J1&J2:	8.92%	1.75%
		J2	4.00%	J2&J3:	0.01%	0.00%
		J3	0.47%	J3&J1:	0.71%	0.00%
	SE	J1	1.11%	J1&J2:	3.51%	0.19%
		J2	0.68%	J2&J3:	34.76%	0.11%
		J3	0.07%	J3&J1:	16.86%	0.00%
	S	J1	2.36%	J1&J2:	2.78%	0.47%
		J2	1.21%	J2&J3:	25.84%	0.00%
		J3	0.11%	J3&J1:	6.27%	0.00%
	W	J1	0.81%	J1&J2:	3.53%	0.00%
		J2	2.53%	J2&J3:	5.46%	0.50%
		J3	0.06%	J3&J1:	0.19%	0.00%

Total Probability of Failure

>25%
 5% - 25%
 <5%

Table 4.6 shows the results of the total Probability of Failure (PoF) obtained by multiplying the kinematic and kinetic probabilities, respectively. In other words, the total PoF results from a rock block that is kinematically feasible to move (i.e. probability of formation) and whose shear strength is exceeded by its shear strength (i.e. probability of sliding). As can be seen in Table 4.6, although we started with high kinematic probabilities for planar failure when linked with their respective kinetic probabilities, we end up with low total PoF. Likewise, the total PoF for wedge has importantly decreased to values below 10% except for two critical sectors (i.e. SE and S).

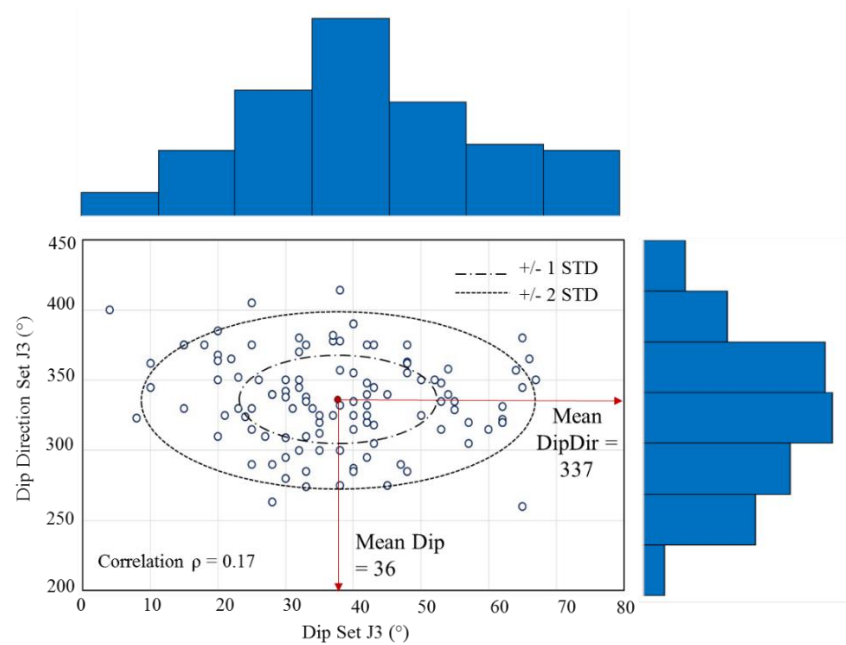


Figure 4.18 Scatter plot for dip and dip direction angles for Joint Set 3. One and two standard deviation ellipses are drawn centered at the mean values.

Figure 4.19 shows the summary of the total Probability of Failure (PoF) for each design sector of the open pit mine. Taking as maximum allowable PoF for the excavated benches a value of 25%, all except for sector SE and S are below this threshold. Recommendations can be put forward to steepen the bench angle from its current 65° or to increase the bench height above 15 m. provided in both cases that regular clean-ups of rock spills and daily ground control monitoring are implemented, especially for sector SE and S.

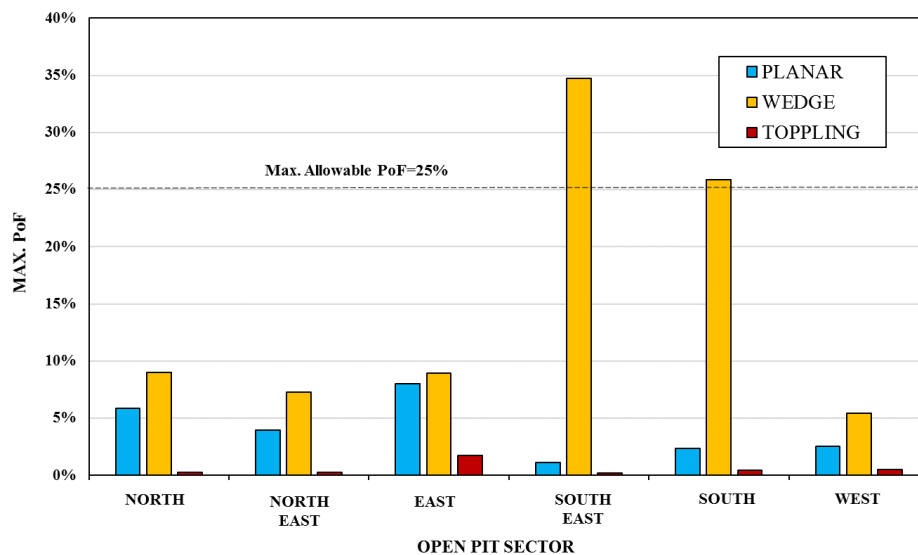


Figure 4.19 Total Probability of Failure (PoF) for each design sector of the pit.

4.2.2 Case Study #2

Geological Setting

This second mine case study is located in the central Andes of Peru at an altitude of 4600 m.a.s.l. Sedimentary rocks such as limestone are the predominant lithology in the area. These sequences have been intruded by a pluton of quartz-monzonite nature leading to a contact metamorphism in the surrounding area of the intrusion. This mine classifies as a polymetallic (Zn, Pb and Ag) ore deposit associated with a skarn mineralization type given by the contact metasomatism of the surrounding country rocks by ore-bearing hydrothermal solution adjacent to a felsic intrusive body. The extension of the ore body is @ 150 m length and 100 m width and a projection in depth of about 500 m. The skarn aureole (transition) between the host rock and the orebody has an approximate width of 100 m. Thus, three main geological units are differentiated: the host rock (limestone), transition (skarn) and ore body (Figure 4.20)

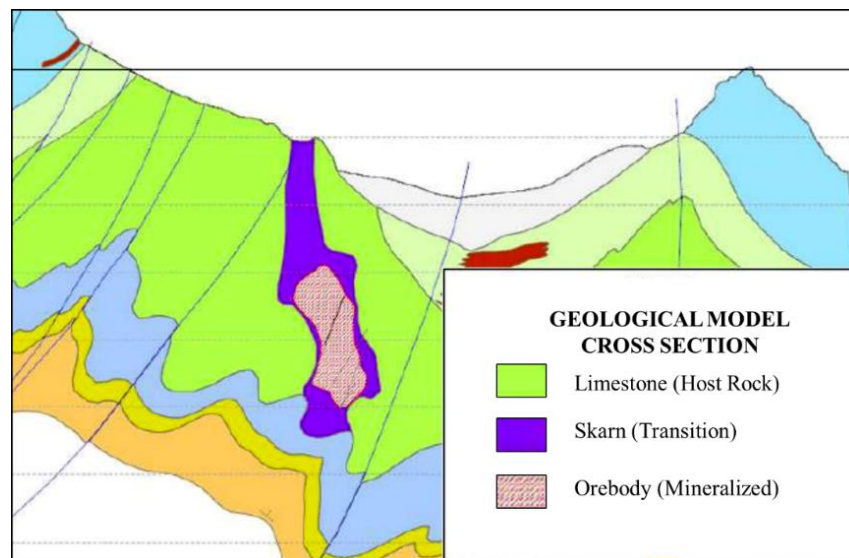


Figure 4.20 Geological cross section of the mine project.

Structural Geology

The area in which this case study is located has undergone intense faulting and folding. Major inverse faults striking NNE SSW were identified in the area suggesting that the maximum principal stress is horizontal. These major faults acted as mineralization pathways and while they will be disregarded for bench-scale slope stability analysis, they will be considered for the overall analysis of the pit. Also, regional and local symmetrical folds trending NW-SE have been reported.

Structural Field Data Collection

This second case study was at the feasibility stage of design and therefore an important number of oriented drill cores were performed as part of the field geotechnical investigation campaign. Surface mapping was restricted to few accessible outcrops and therefore very limited data could be gathered. As a consequence, the bench slope analysis and design for this case study #2 will mostly rely on core logging data as opposed to the first case study that had bench mapping information at hand.

A total of 52 geotechnical oriented boreholes were performed, in two consecutive years: 22 in 2016 and 30 in 2017. Surface mapping was conducted at 39 outcrops mainly in limestone (see Figure 3.21). A comparison is shown between minor discontinuities (rock joints) that were measured through outcrop mapping shown in Figure 4.22 and the ones registered during core logging shown in Figure 4.23. Although, they both provide evidence of two subvertical joint sets for the limestone, the core logging data shows a lot more scatter when compared to the surface mapping data. This is almost always the case since core logging data is subject to drilling rotation effects of the rock core and therefore a robust statistical analysis should be carried out to reduce bias and data scatter. Figures 4.24 and 34.25 show the contour plots of the structural data logged in the drill cores for the transition (skarn) and ore body lithologies. Again, a high degree of dispersion is observed for these two contour plots as expected from drill core information. Nonetheless, a joint clustering pattern can be identified leading to four and three main joint sets in the skarn and ore body, respectively.



Figure 4.21 Outcrop of a limestone rock type.

Tables 4.7, 4.8 and 4.9 show the summary of joint set orientation for each rock type.

Structural Zones & Design Sectors

The design sectors for case study #2 are shown in Figure 4.26. These are in total ten sectors from which five are going to be excavated in limestone, four in skarn and finally one (#10) that correspond to the bench slopes cut in overburden (soil-like) material.

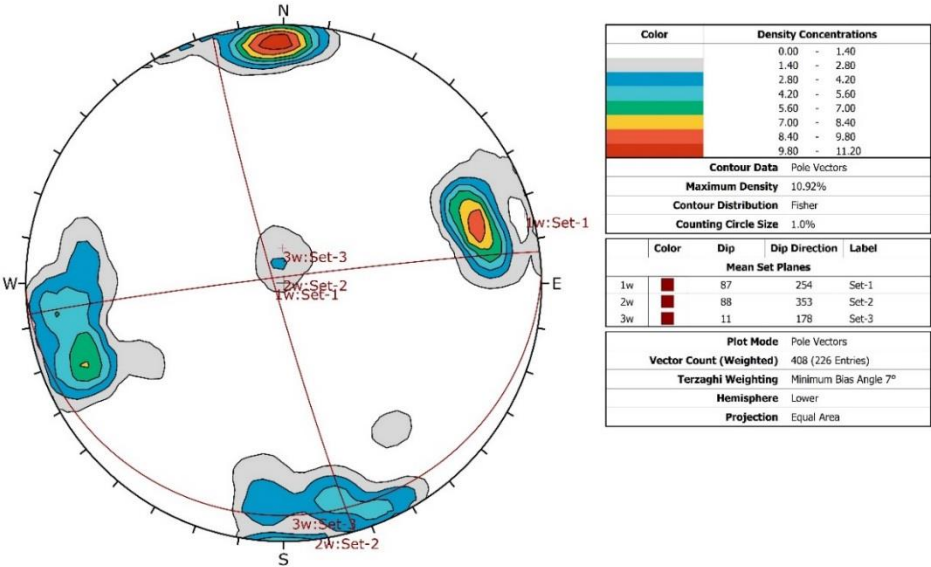


Figure 4.22 Contour plot based on surface mapping data for the limestone.

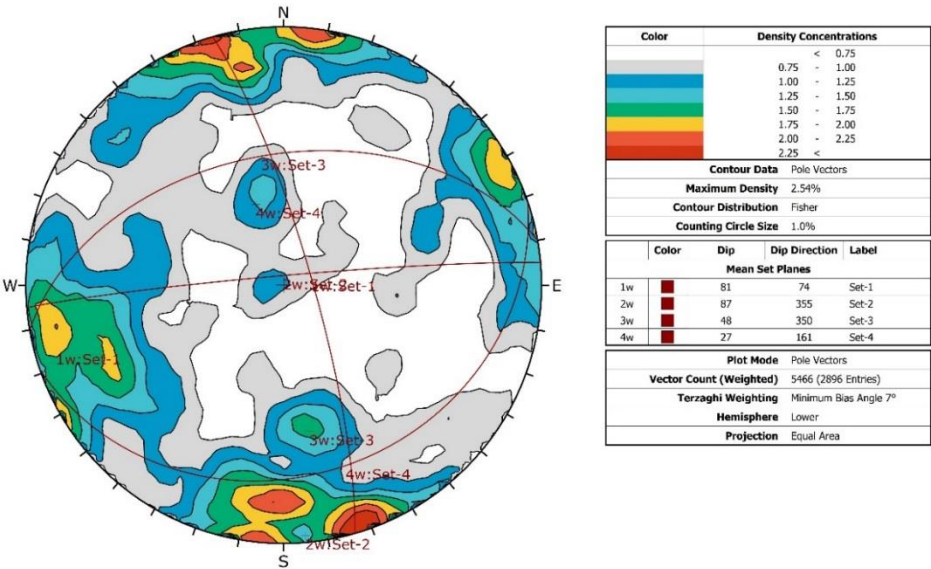


Figure 4.23 Contour plot based on core logging data for the limestone.

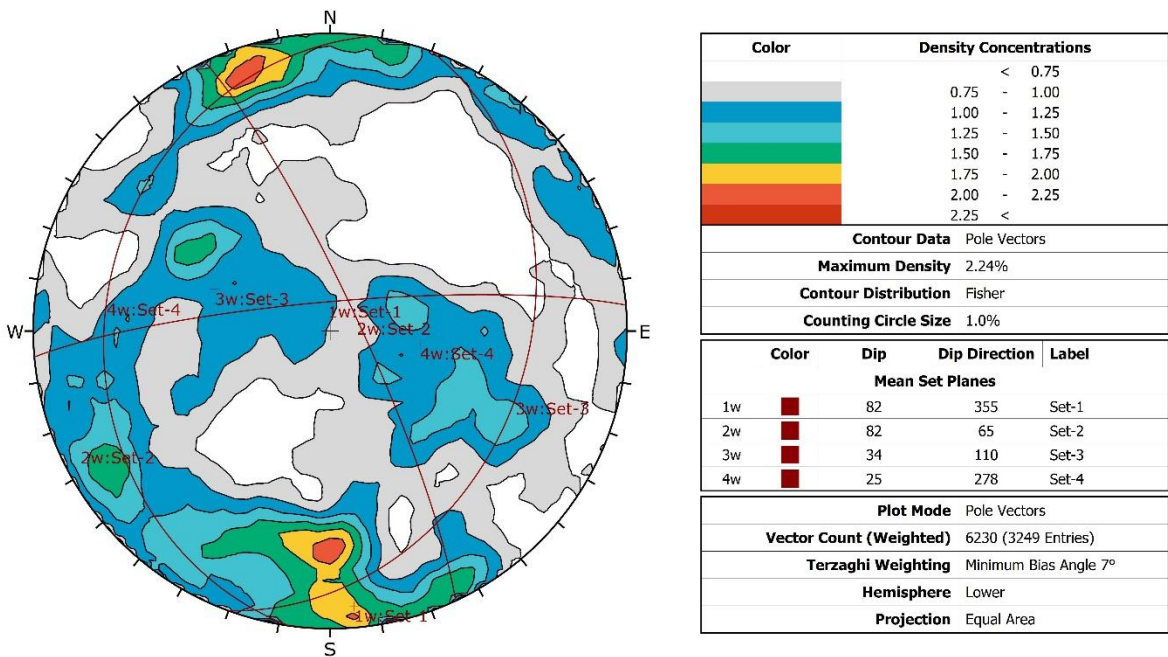


Figure 4.24 Contour plot based on core logging data for the skarn.

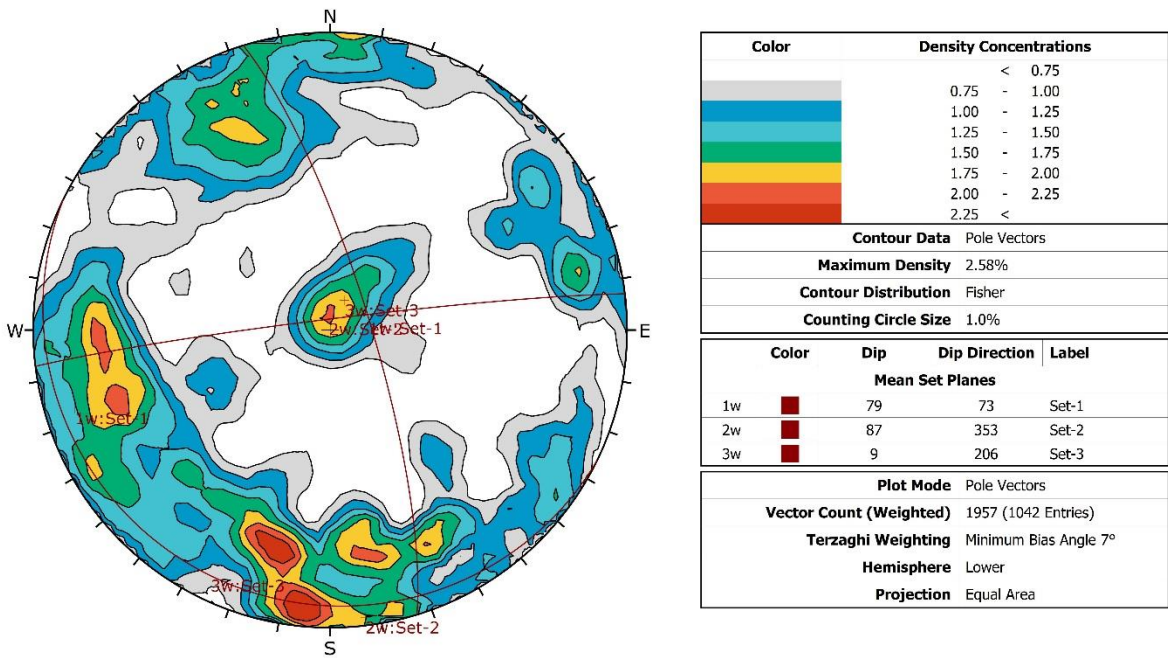


Figure 4.25 Contour plot based on core logging data for the ore body.

Table 4.7 Summary of joint orientation for limestone – Case study 2

Set N°		Mean Dip (°)	Mean DipDir (°)	Dip Range (°) @95%Confidence		DipDir Range (°) @95%Confidence		K Fisher	Relative Occurrence (%)
Set-1	1m	78	73	51	89	049	099	14.27	24%
	1w	80	73			229	279	14.22	22%
Set-2	2m	85	357	62	89	147	208	13.23	20%
	2w	87	356			327	388	13.74	25%
Set-3	3m	17	155	2	39	049	262	22.80	11%
	3w	17	157					22.91	8%
Set-4	4m	46	348	33	59	332	004	69.49	4%
	4w	46	348					71.65	4%

Table 4.8 Summary of joint orientation for skarn - Case study 2

Set N°		Mean Dip (°)	Mean DipDir (°)	Dip Range (°)		DipDir Range (°)		K Fisher	Relative Occurrence (%)
Set-1	1m	81	357	54	89	145	207	11	18%
	1w	82	355			325	027	11	26%
Set-2	2m	81	65	60	90	041	089	18	14%
	2w	82	65			221	269	18	13%
Set-3	3m	34	109	13	55	069	148	23	14%
	3w	34	110					22	10%
Set-4	4m	24	275	3	46	203	333	23	12%
	4w	25	278					22	10%

Table 4.9 Summary of joint orientation for ore body - Case study 2

Set N°		Mean Dip (°)	Mean DipDir (°)	Dip Range (°)		DipDir Range (°)		K Fisher	Relative Occurrence (%)
Set-1	1m	76	75	51	89	048	105	13	28%
	1w	79	73			228	285	12	23%
Set-2	2m	88	174	51	88	145	208	8	22%
	2w	87	353			325	028	8	32%
Set-3	3m	8	199	2	35	007	328	19	16%
	3w	9	206					19	12%

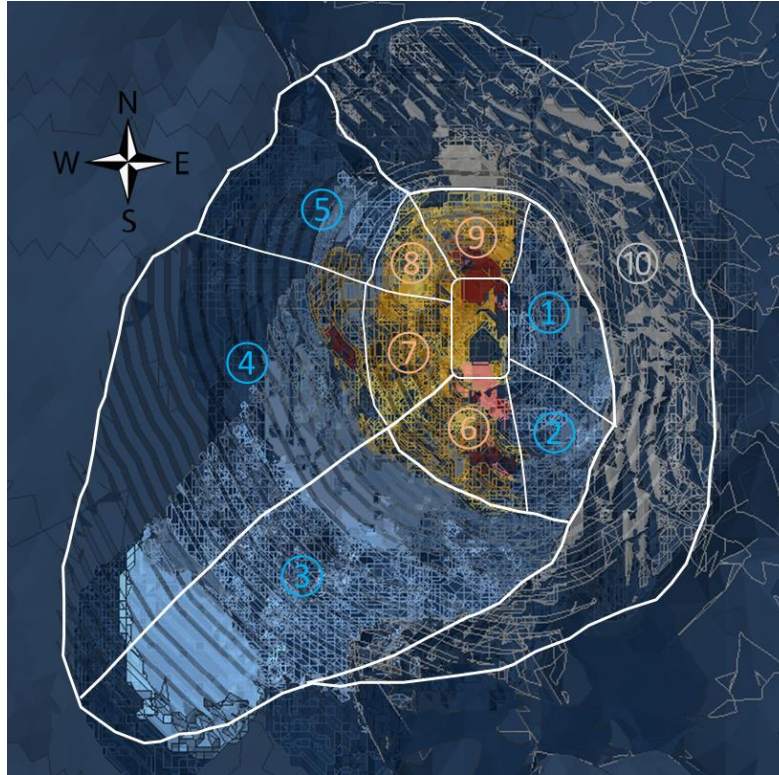


Figure 4.26 Open pit sectorization for case study 2

Rock Laboratory Testing

Geomechanical laboratory testing was conducted in order to determine the mechanical characteristics for intact rock and rock joints samples. The overall laboratory program consisted of physical properties, direct shear, uniaxial and triaxial compressive strength tests. A total of 79 laboratory tests were conducted on samples selected to represent the range of the rock conditions observed in the study area. The parameters that are of interest for bench slope design are the unit weight of rock and shear strength of joints. Thus, laboratory tests related to these two properties are reported below.

Unit Weight Measurements

The combined data set for measuring physical properties i.e. unit weight of rock samples included 29 tests: 13 in limestone, 10 in skarn and 6 for the orebody with mean values of 27 kN/m³, 30 kN/m³ and 36 kN/m³, respectively. Figure 4.27 shows a summary of unit weights measurements for all rock samples.

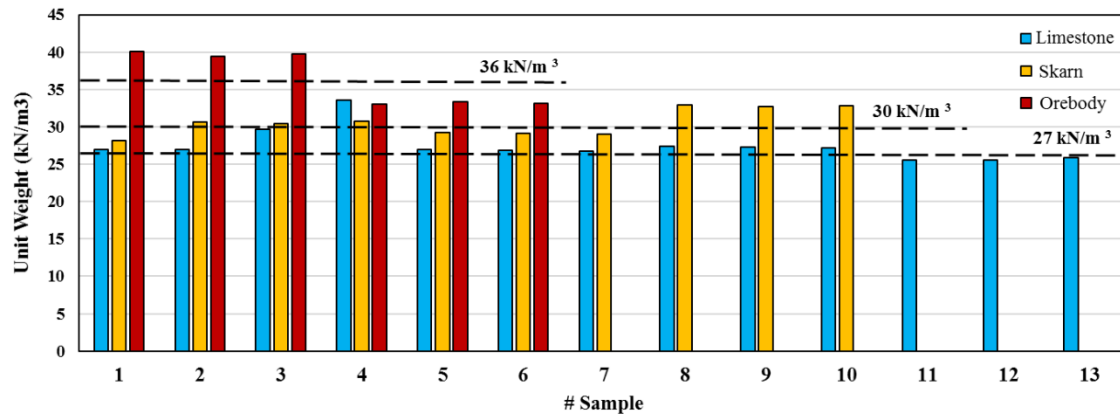


Figure 4.27 Unit weight values

Direct Shear Testing

For this project, 55 rock samples were selected for small scale direct shear tests (ASTM Method D5607) to obtain discontinuity shear strength data. The range of normal stresses applied to the samples varied from 0.75 to 12.5 MPa. Since not a sufficient number of direct shear test points were conducted on each lithology to define a shear strength envelope individually, an approach that uses a composite of all direct shear test information was followed to define the overall joint shear strength regardless of lithology. For this purpose, laboratory data points were subject to both a linear and curvilinear regression analysis. Both fitting models (linear and non-linear) were adjusted to intersect the origin (i.e. $c=0$) given that all direct shear tests were carried out on saw cut surfaces.

Figure 4.28 shows the direct shear test points for all three lithologies with the corresponding equations for each regression model. Although not conclusive, a trend for the limestone rock samples close the lower bound shear strength is observed. Likewise, the skarn rock samples seem to follow the upper bound, whereas the samples that belong to the orebody would apparently fit to the mean shear strength envelope specially for normal stresses greater than 5 MPa.

The linear regression corresponded to the Mohr-Coulomb model whereas the non-linear was of the form of a general power function. The average friction angle following the Mohr-Coulomb model is 34 deg. The maximum and minimum values for this model are 30 and 39 deg, respectively. The selected shear strength model for the overall minor discontinuities (i.e. joints) is non-linear (power curve type) since this minimizes the value of the Sum of Squares Errors (SSE).

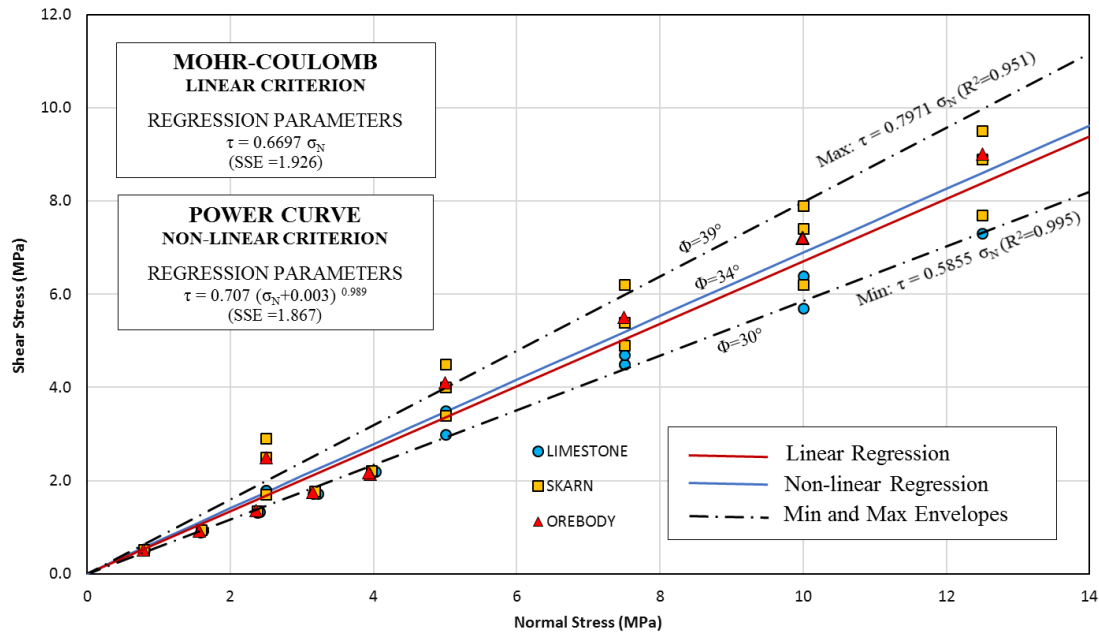


Figure 4.28 Joint shear strength envelopes

Bench Slope Stability Analysis

Both the kinematic (stereographic) and kinetic (limit equilibrium) analyses for planar and wedge failure was performed following the probabilistic approach. The joint shear strength envelope was assumed to be variable with the characteristics shown in Table 4.10. Also, bench Face Angles (BFA) were varied from 65 to 75 at 5 degrees interval while keeping slope height fixed as 10 m. The total Probability of Failure (PoF) was obtained by multiplying the kinematic and kinetic probabilities, respectively.

Table 4.10 Summary of joint shear strength envelope – Case study 2

Parameters	Power Curve Model	M-C Linear Model
a	0.707	0.6697
b	0.989	1.000
c	0	0
d	0.003	0
Coefficient of Variation (CV)	0.20	0.20

It should be noted that the calculated PoF's are an upper bound value since the joints were assumed to be of infinite persistence. A threshold value of Max. PoF = 25% was chosen for the bench design. From the analysis, sectors 2-3-8 are deemed potentially unstable for the case of planar failure (Figure 4.29). The remaining sectors (1-4-5-6-7-9) are considered to be stable for a BFA up to 75 degrees. For these last cases,

there is room for an optimization of the bench design. Regarding wedge failure, sectors 2 -3 are deemed potentially unstable and sector 6 is considered unstable for a BFA greater than 70° (Figure 4.30). The remaining sectors (1-4-5-7-8-9) are considered to be stable for a BFA up to 75 degrees. For these last cases, there is room for an optimization of the bench design.

It can be recommended that the optimum BFA is 70° . for which stable conditions at the bench scale are assured for most of the design sectors. For the critical remaining sector 2, 3 and 8 the bench width can be increased in order to account for unforeseen rock spills.

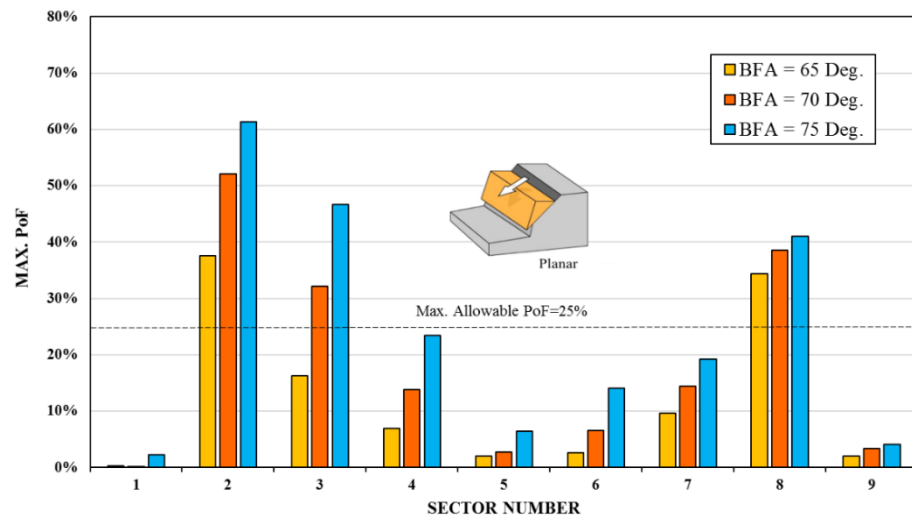


Figure 4.29 Total Probability of Failure (PoF) for planar failure

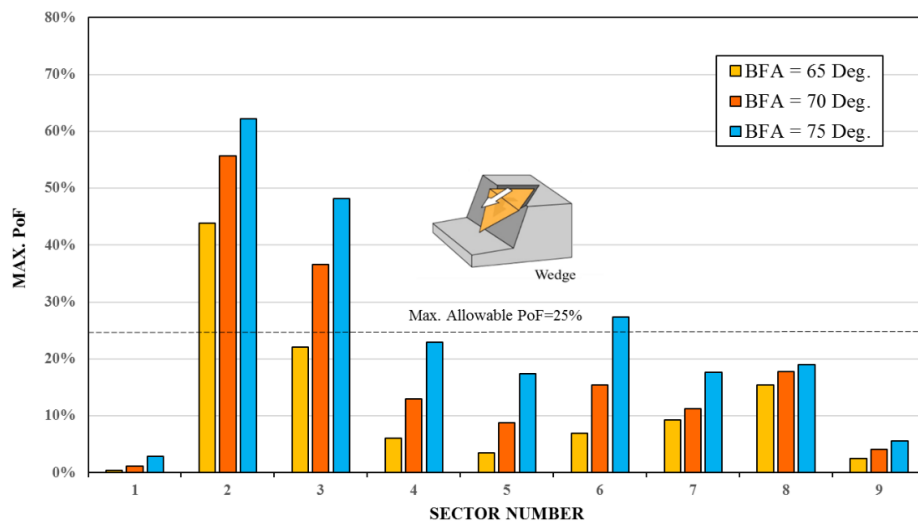


Figure 4.30 Total Probability of Failure (PoF) for wedge failure

4.2.3 Case Study #3

Geological Setting

The third case study is an iron open pit mine located in the coastal belt of Peru at an average elevation of 800 m.a.s.l. This belongs to the central Andean cordillera where the Nazca plate subducts beneath the South American Plate, forming an active seismic region. The mineralization is hosted by moderate fractured metasedimentary rocks (hornfels) overlain by a series of volcano-sedimentary sequences (see Figure 4.31). This is an Iron Oxide Copper Gold (IOCG) deposit associated with high-grade magnetite ore. The open pit extends over an area of approximately 700 m in a NE-SW direction by approximately 300 m in a NW-SE direction. The mineralization is close to the surface extending to depths approaching 550 m.



Figure 4.31 Mapping a bench face in an hornfels rock type

Structural Geology

A review of the regional structural geology of the mine site suggests that it is part of a NE-oriented monoclinial that plunges 40 degrees to the NNW. The compressional tectonic stresses the site was subjected to are translated into faulting and folding of the rock strata. Local faults that have been mapped in the study area have a nominal strike of N060 with dip angles between 75 and 85 deg. This faulting system will be considered for the inter-rampa and global scale analyses. The area in which this open pit mine is located has undergone moderate fracturing of the host rocks where principal structurally controlled discontinuities are those associated with faulting.

Structural Field Data Collection

The field data collection campaign consisted of extensive structural mapping of minor (i.e. rock joints) and intermediate (i.e. local faults) geological discontinuities. A total of 42 exposed bench faces cut in hornfels were mapped following the ISRM suggested procedures (Barton, 1985). Figure 4.32 shows the bench mapping locations within the open pit mine. A total of 575 rock joints and 79 local faults were mapped in this area and their orientation reported in terms of Dip and Dip Direction angles. Lower hemisphere equal-area stereographic projections constructed from these data were used to define the predominant sets.

For the purpose of bench-scale slope analysis only minor rock joints are presented in this section. Figure 4.33 shows the corresponding contour plot for these structures. From this figure, it can be observed that there is one well-defined discontinuity cluster corresponding to the bedding planes of the metasedimentary rock (hornfels). Also, a second cross-crossing joint set of higher dispersion (low clustering) was identified along with several random fractures. Since random fractures represent around 44% of the total collected structural data, they will be considered for further analysis as a highly scattered (i.e. very low Fisher K value) joint set. The main discontinuity orientation statistics are summarized in Table 4.11. for each set.

During structural field mapping the discontinuity properties were described in order to arrive at an RMR value (Bienawski, 1989) for each mapping site. Since the purpose of case study #3 is to construct an approximate DFN model, besides joint orientation, joint persistence is also necessary as an input parameter of the model. The discontinuity trace length was described at intervals of 1 m, 1 to 3 m, 3 to 10 m, 10 to 20 m, and greater than 20 m long as suggested in the ISRM methods. Not actual trace length measurements were taken and therefore an estimated value and distribution had to be selected for the joint persistence. Figure 4.34 and Figure 4.35 show a bar graph for the trace lengths and spacing values described during classical field mapping, respectively. Although they may look like a histogram and what is more, they may appear to visually fit to a normal distribution, this is not the case given that the class width of the chart is not constant but rather variable.

Most of the persistence values lie on the interval between 3 and 10m. It would be assumed that set-1 and set-2 will have an average persistence values of 10.0 m and 5.0 m, respectively and the random fractures a mean persistence value of 3.0 m. It would also be assumed that they will follow a lognormal distribution as this has been reported to fit field data as presented in chapter 3.

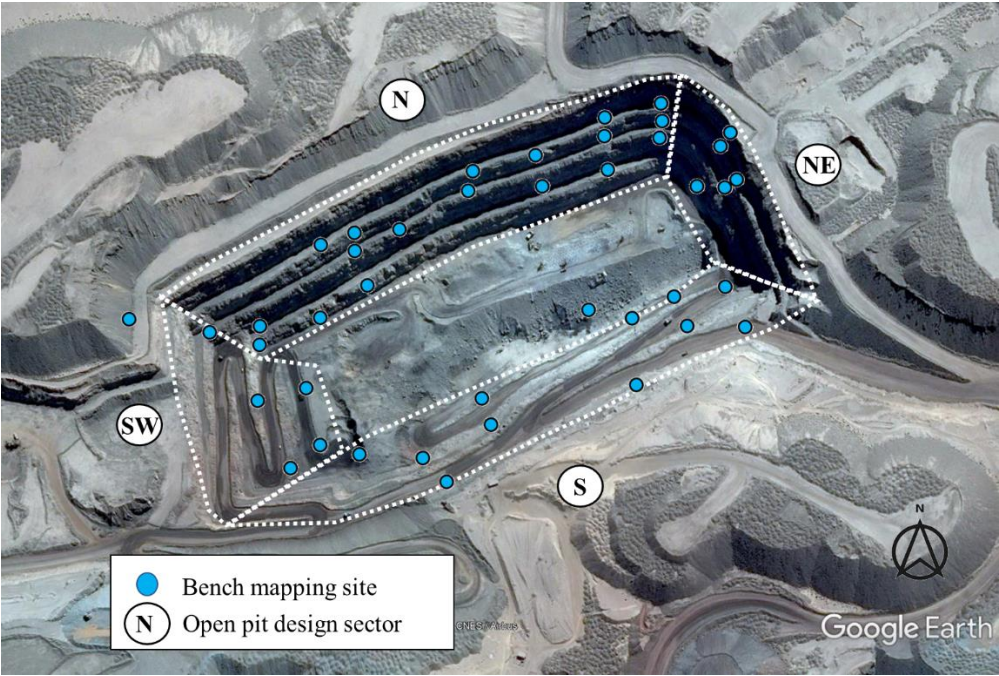


Figure 4.32 Bench mapping sites distribution within the pit. The open pit design sectors are also shown

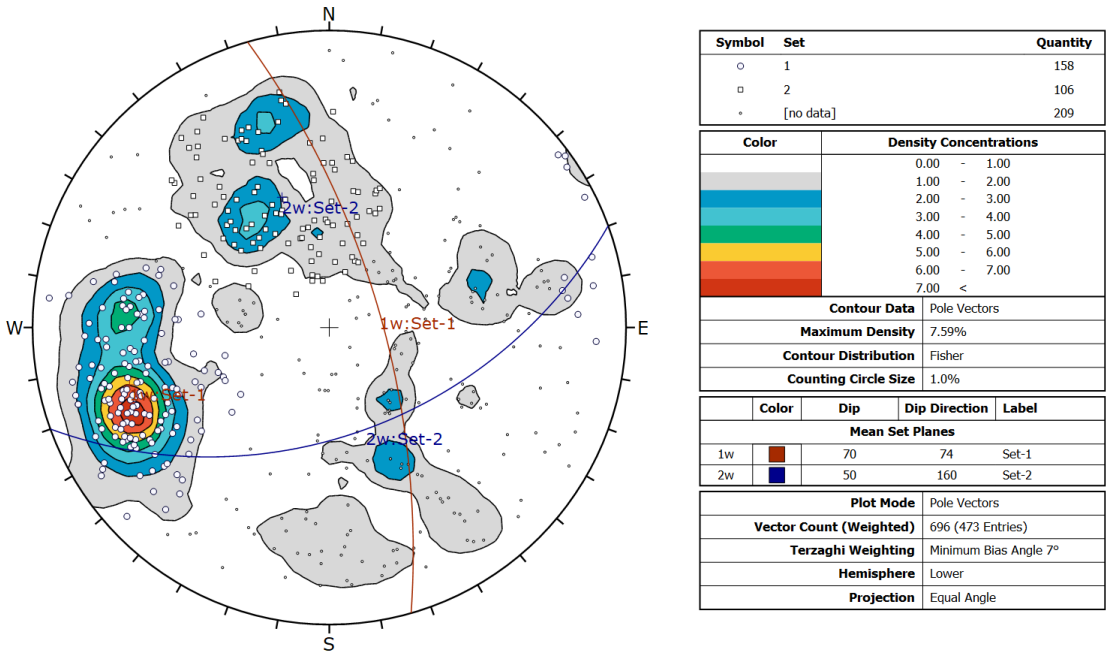


Figure 4.33 Composite contour plot for all minor discontinuities mapped in exposed benches

Table 4.11 Summary of mean joint sets orientation – Case study 3

Set N°	Mean Dip (°)	Mean DipDir (°)	Dip Range (°)		DipDir Range (°)		K Fisher	Relative Occurrence (%)
Set-1	70	74	40	89	42	93	19.2	33.4
Set-2	50	160	18	79	112	204	12.4	22.4
Random Set	33	311	-	-	-	-	2.5	44.2

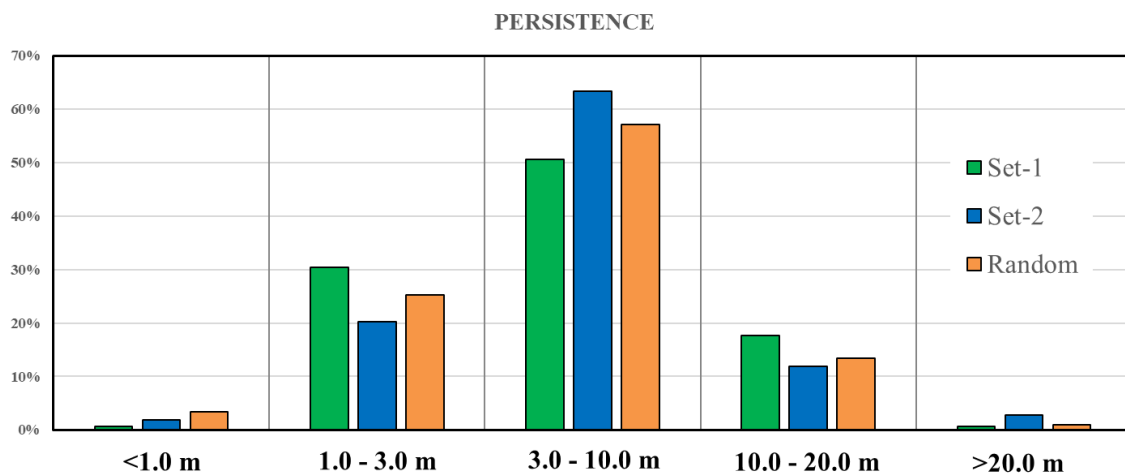


Figure 4.34 Bar graph of the persistence distribution of rock joints

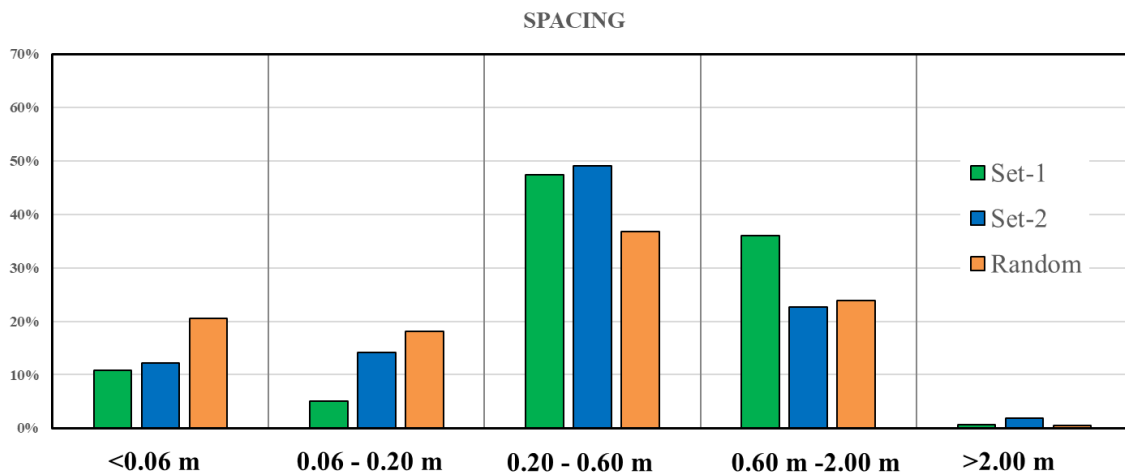


Figure 4.35 Bar graph of the spacing distribution of rock joints.

Structural Zones & Design Sectors

The design sectors for case study #3 are shown in Figure 4.32. These are in total four sectors named North (N), South (S), North East (NE) and South West (SW).

Rock Laboratory Testing

Geomechanical laboratory testing was conducted in order to determine the mechanical characteristics for intact rock and rock joints samples. The overall laboratory program consisted of physical properties, direct shear, uniaxial and triaxial compressive strength tests. The parameters that are of interest for bench slope design are the unit weight of rock and shear strength of joints. Thus, laboratory tests related to these two properties are reported below.

Unit Weight Measurements

A total of 27 (hornfels) rock samples were tested to measure their unit weight. Figure 4.36 shows a histogram for unit weights measurements of all rock samples showing a mean value of 27 kN/m³.

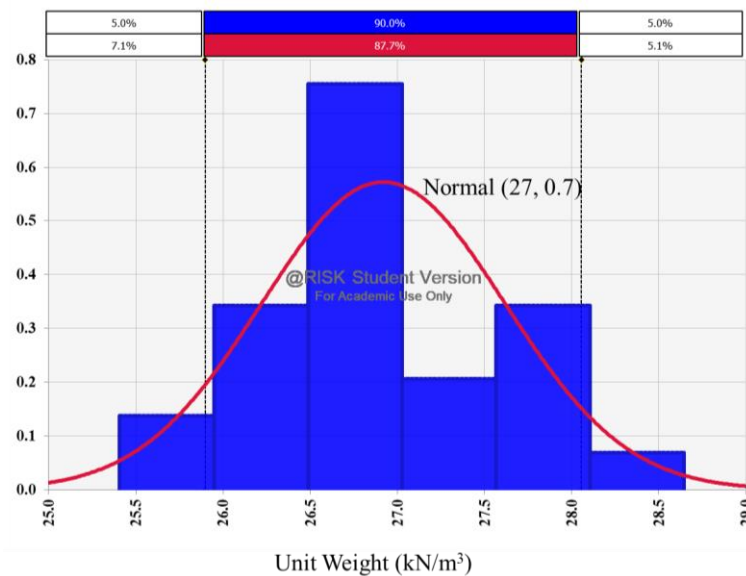


Figure 4.36 Histogram of rock unit weight measurements

Direct Shear Testing

Shear strength properties of minor discontinuities were estimated using field data of joint roughness coefficient (JRC) and joint compressive strength (JCS) for later incorporation into the Barton – Bandis model. This model was selected based on field observations given that most rock joints were in wall-to-wall rock contact along their surfaces. For this project, detailed characterization of joint roughness and strength was collected during field work by means of the Barton comb and Schmidt hammer.

Figure 4.37 and 4.38 show the distribution of JRC and JCS values for all 42 mapping sites. It is important to highlight that the JRC and JCS values shown in these figures have been already been scaled to an average joint persistence of 5.0 m as this is the assumed mean value for the analysis. Also, basic friction angles were measured in the field by performing numerous tilt tests on natural discontinuities. Figure 4.39 shows the distribution of basic friction angle values.

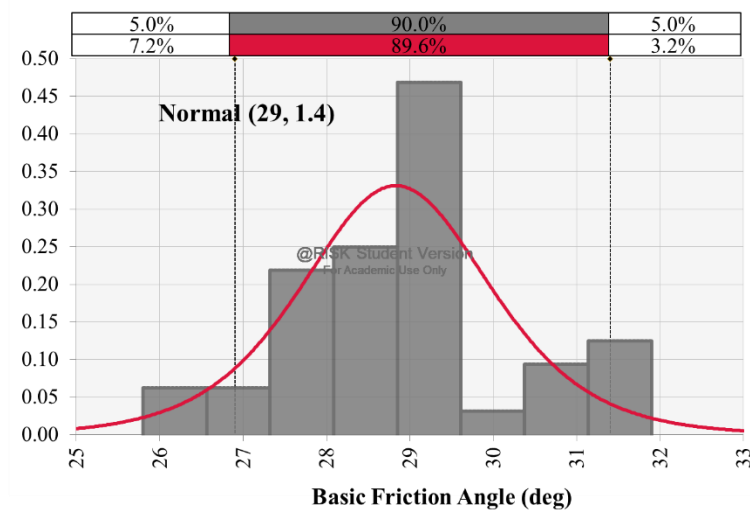


Figure 4.37 Distribution of basic friction angle as measured in tilt tests

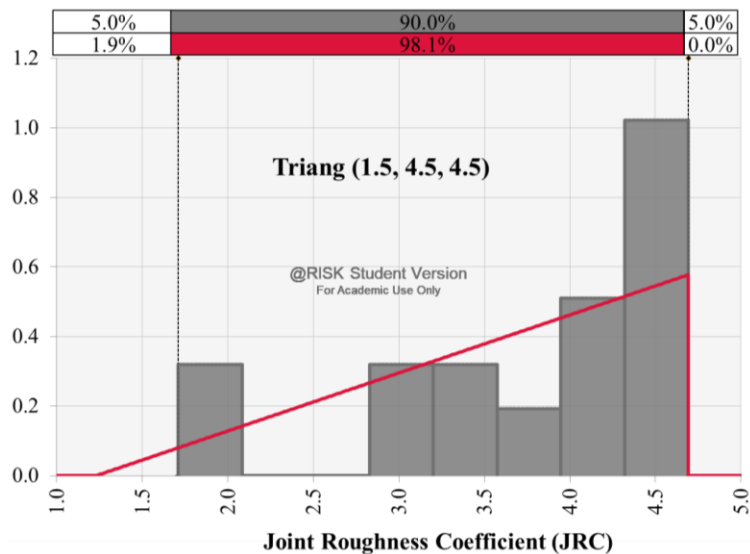


Figure 4.38 Distribution of scaled values of JRC from Barton's comb measurements

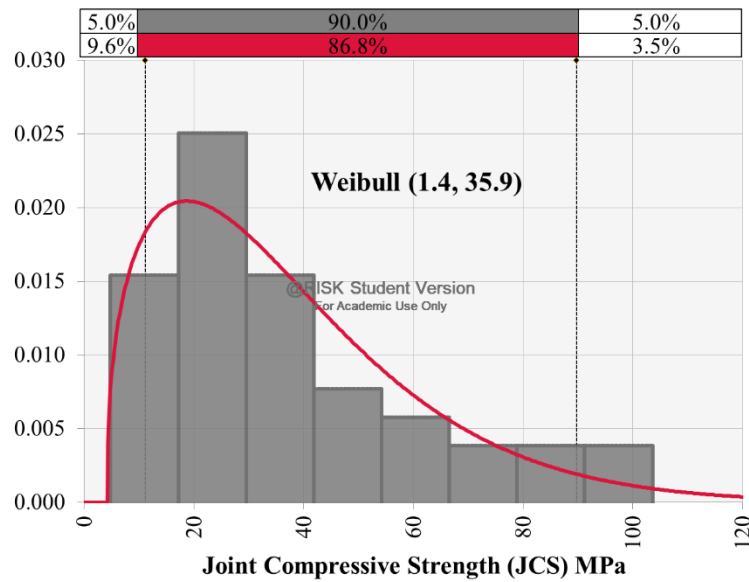


Figure 4.39 Distribution of scaled values of JCS from Schmidt hammer measurements.

Bench Slope Stability Analysis

Bench scale slope stability assessments were carried out by means of a Discrete Fracture Network Model (DFN). Joint orientation, joint size and joint shear strength were treated as stochastic input parameters in order to conduct a kinematic and then a kinetic analysis. The software Fracman by Golder Associates was used for the creation of a DFN model at the bench scale for the open pit. The input statistical distribution for the software are summarized in Table 4.12 below.

Table 4.12 Summary input parameters for DFN model – Case study 3

Joint Property	Set-1	Set-2	Random Set
Joint Orientation Distribution	Fisher K = 19.2	Fisher K = 12.4	Fisher K = 2.5
Joint Size Distribution	LogNormal (10.0, 5.0)	LogNormal (5.0, 5.0)	LogNormal (3.0, 3.0)
Joint Shear Strength Distribution	Barton – Bandis Model Phib = Normal (29, 1.4) JRC = Triangular (1.5, 4.5, 4.5) JCS = Weibull (1.4, 35.9)		

A single bench scale model was created in Fracman for each design sector of the open pit mine. The following dimensions were considered: Bench height = 15 m; Slope angle = 65 deg; Bench width = 7.0 m; Bench length = 40 m. Figures 4.40 to 4.43 shows the DFN model for each design sector of the mine with the critical forming rock blocks (i.e. $FoS \leq 1$) highlighted in red.

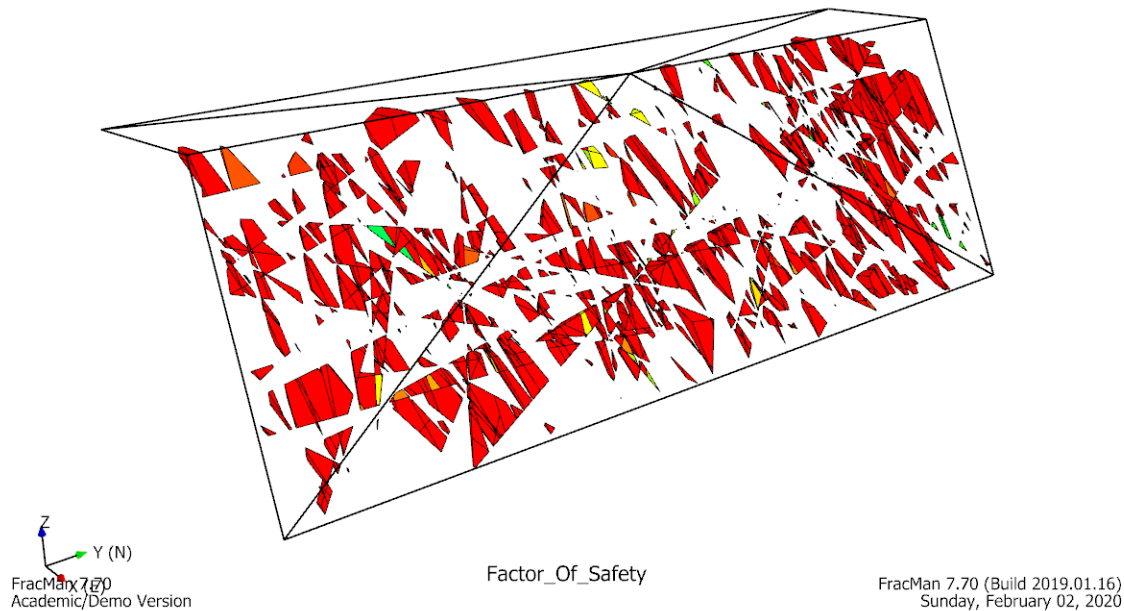


Figure 4.40 North Bench slope DFN model with rock blocks of $FoS \leq 1$ highlighted

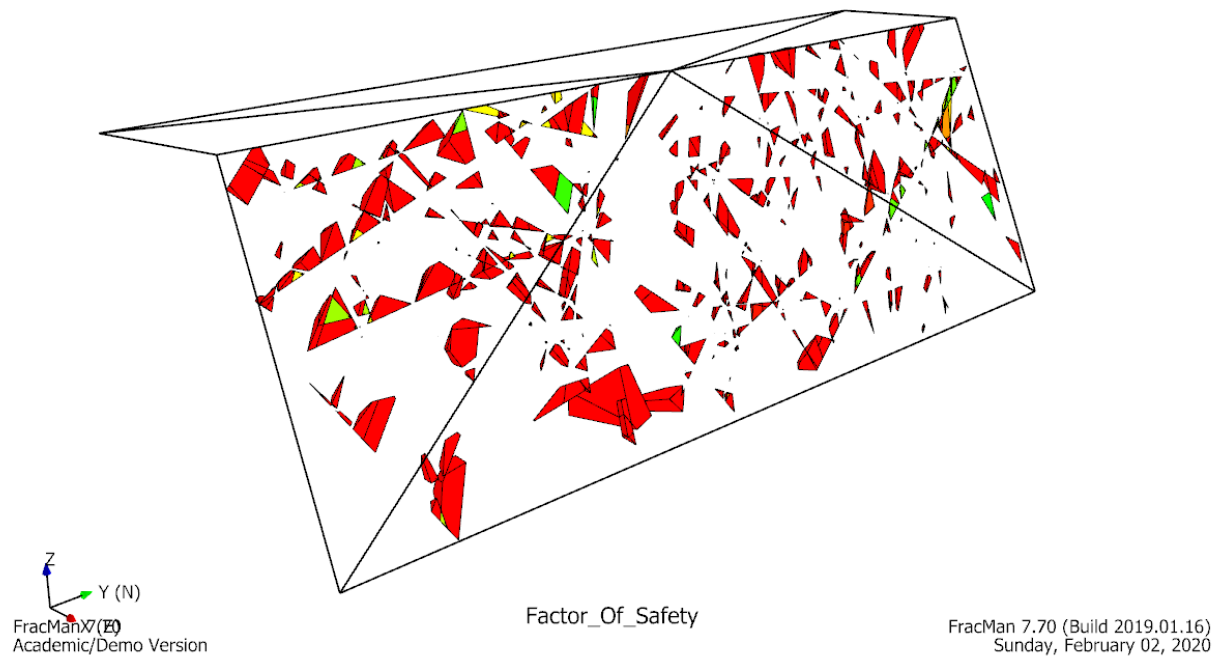


Figure 4.41 South-West Bench slope DFN model with rock blocks of $FoS \leq 1$ highlighted

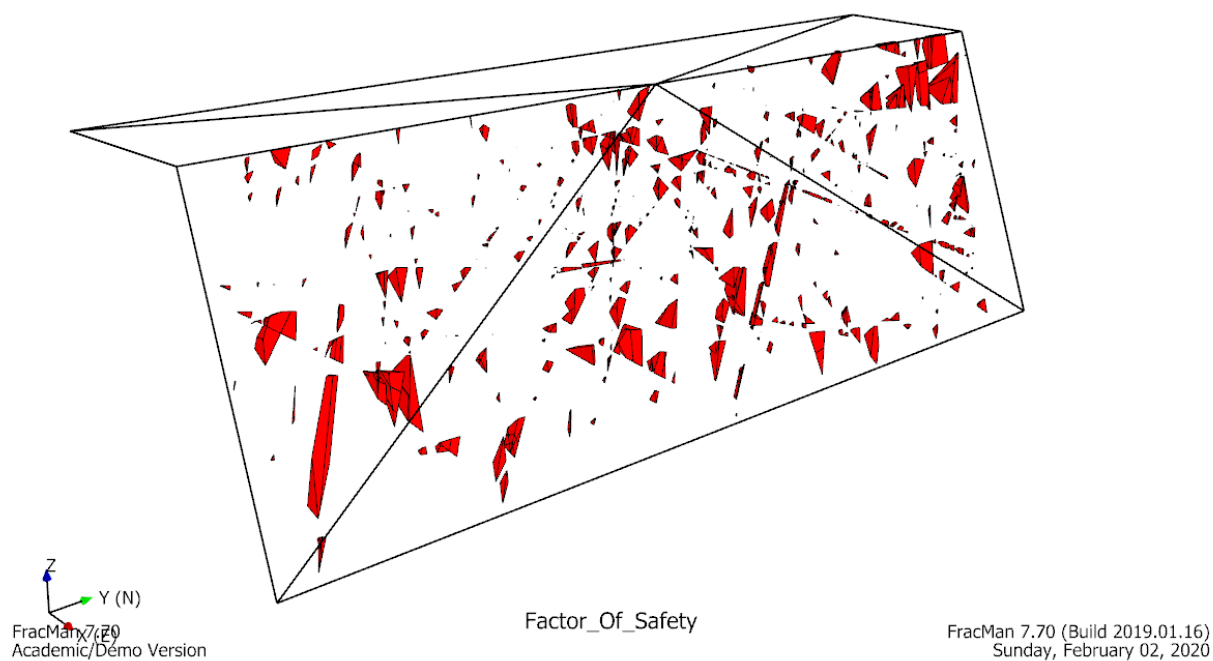


Figure 4.42 South Bench slope DFN model with rock blocks of $FoS \leq 1$ highlighted

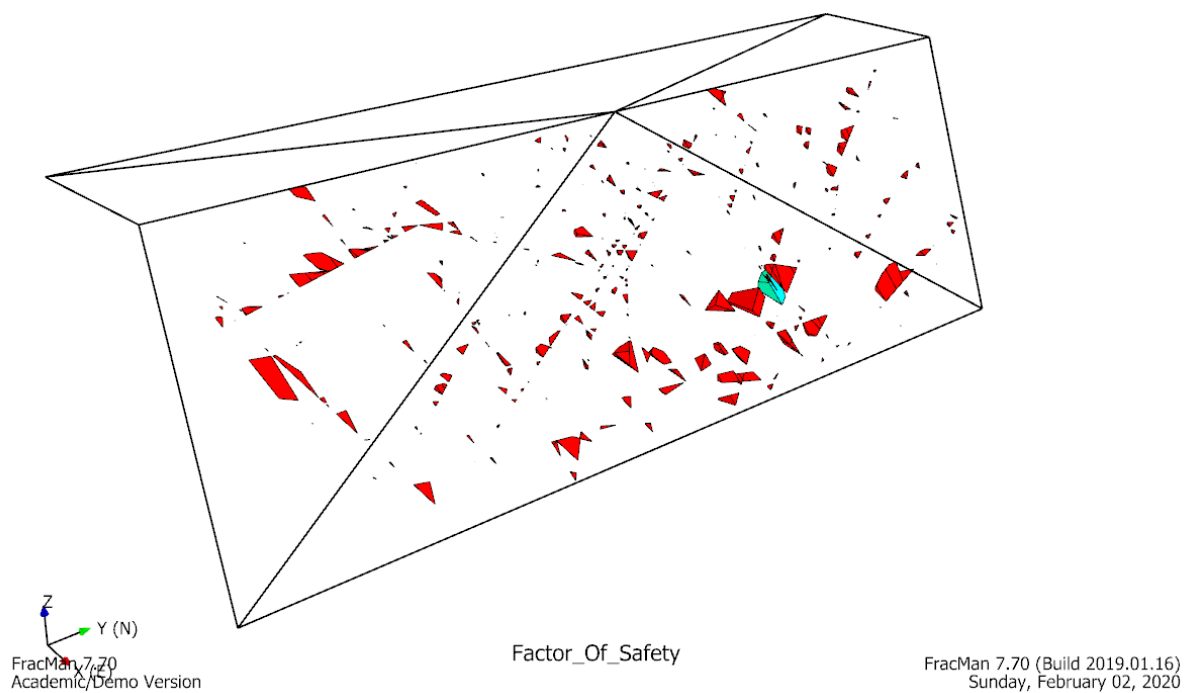


Figure 4.43 North-East Bench slope DFN model with rock blocks of $FoS \leq 1$ highlighted.

The analysis approach in FracMan can simulate rock block stability on slopes allowing a truly and comprehensive probabilistic assessment of the kinematic and kinetic stability conditions in surface excavations. The workflow employed in the analysis starts by determining the rock block geometry and its mode (i.e. single or double sliding). For each rock block identified, FracMan computes a FoS which differentiates between those blocks that are: a) Unstable or sliding ($FoS < 1$), b) metastable ($FoS = 1$), and c) Stable against sliding ($FoS > 1$). Kinematically inadmissible blocks (i.e. those whose shape and/or position doesn't allow them to slide) are assigned a $FoS = 100$.

From Figures 4.40 to 4.43 we can clearly observed that the North bench slope is the most critical owing to the formation of several unstable rock blocks. A total of 1277 rock blocks with a $FoS \leq 1$ for this sector. This is followed by the South, South West, and North East pit sectors with 726, 593 and 379 critical rock blocks formed. Also, it should be noted that the block volume distribution tends to be greater for the North and South West slope pit sectors than for the other two.

Table 4.13 shows the summary of the static kinetic and kinematic analysis for each of the four DFN models. A detailed description of the number of sliding ($FoS < 1$), metastable ($FoS = 1$), stable ($FoS > 1$) and Inadmissible ($FoS = 100$) rock blocks is given. From these, the probability of rock block formation (i.e. kinematic) and probability of rock block sliding (i.e. kinetic) can be calculated by taking a ratio as the corresponding number of valid to total generated blocks and another ratio between the unstable blocks to valid rock blocks. The total Probability of Failure (PoF) is given as the multiplication of the kinematic and kinetic probabilities as illustrated in case study #1.

Table 4.13 Summary of static kinetic and kinematic analysis DFN approach – Case study 3

Pit Sector	FoS<1 Sliding (1)	FoS=1 Metastable (2)	FoS>1 Stable (3)	FoS=100 Inadmissible (4)	Total Generated Blocks (5)	Prob. Block Formation (kinematic) (6)	Prob. Block Sliding (kinetic) (7)	Total PoF (8)
NE	5	374	10	5643	6032	6%	97%	6%
S	9	717	37	6385	7148	11%	95%	10%
SW	80	513	51	3324	3968	16%	92%	15%
N	80	1191	149	3658	5078	28%	90%	25%

Notes:

- Kinematic Probability (6) = $[(1) + (2) + (3)] / (5)$
- Kinetic Probability (7) = $[(1) + (2)] / [(5) - (4)]$
- Total PoF (8) = (6) * (7)

A pseudo-static kinetic and kinematic analysis using the DFN approach was also conducted given the area in which the mine is located corresponds to a highly active seismic region. A seismic coefficient of 0.22g was used for the pseudo-static of bench slopes. This value corresponds to 1/3 of the expected peak ground acceleration (PGA) at the mine site. For the pseudo-static analysis, Fracman multiplies the seismic coefficient with the rock block weight to obtain a driving force which is then considered in the calculation of the FoS as a driving force. Table 4.14 shows the summary of the pseudo-static kinetic and kinematic analysis for each of the four DFN models. The total Probability of Failure (PoF) given as the multiplication of the kinematic and kinetic probabilities is shown.

Table 4.14 Summary of pseudo-static kinetic and kinematic analysis DFN approach – Case study 3

Pit Sector	FoS<1 Sliding (1)	FoS=1 Metastable (2)	FoS>1 Stable (3)	FoS=100 Inadmissible (4)	Total Generated Blocks (5)	Prob. Block Formation (kinematic) (6)	Prob. Block Sliding (kinetic) (7)	Total PoF (8)
NE	14	456	18	5544	6032	8%	96%	8%
S	9	894	53	6192	7148	13%	94%	13%
SW	141	554	38	3235	3968	18%	95%	18%
N	199	1270	94	3515	5078	31%	94%	29%

Notes:

- Kinematic Probability (6) = [(1) + (2) + (3)] / (5)
- Kinetic Probability (7) = [(1) + (2)] / [(5) - (4)]
- Total PoF (8) = (6) * (7)

Figure 4.44 shows the Summary of the total PoF calculated with the DFN modelling approach under static and pseudo-static conditions. It is seen that PoF's associated with seismic conditions are greater than that of the static scenario. Also, the North sector is identified as the one with the highest PoF. It should be noted that the static PoF for this sector is just close to the threshold value selected as 25% maximum PoF for the bench scale. Only in the pseudo-static condition this sector does exceed the maximum allowable PoF. The other remaining sectors i.e. North East, South and South West are below the 25% PoF threshold in both static and pseudo-static conditions. Recommendations can be put forward as to increase the current bench design of the pit sectors deemed stable (i.e. NE, S and SW) whereas a less steep bench slope angles should be considered for the potential unstable North slope pit sector.

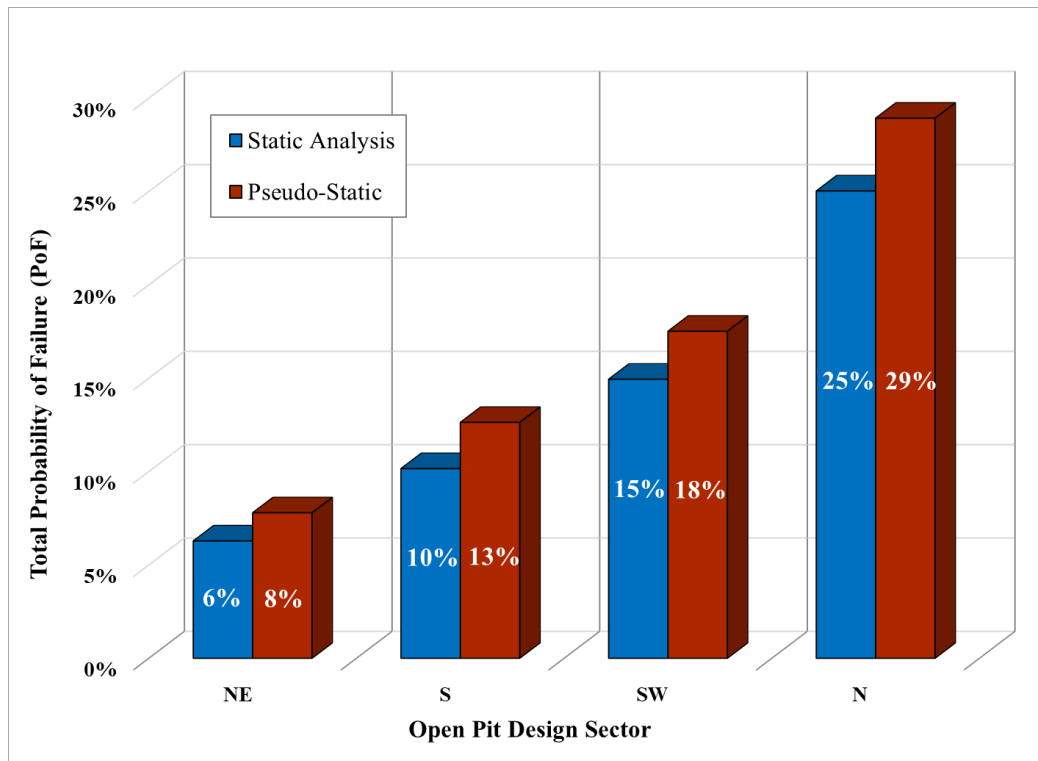


Figure 4.44 Summary of the PoF based on the DFN approach under static and pseudo-static conditions

4.3 Chapter Summary

Chapter 4 covers a brief review of kinematic and kinetic analysis for evaluating structurally controlled failure mechanisms in bench slopes, highlighting the deterministic and probabilistic approach for these types of analyses. This was followed by an introduction to the novel Discrete Fracture Network (DFN) Modelling technique for rock slope engineering applications. All the concepts and theory were then illustrated with three case studies of real open pit mining operations and projects.

- Case study 01 dealt with the bench slope analysis of an existing open pit mine. Therefore, field data was collected from direct mapping on exposed benches as part of the geotechnical reconciliation program of the mine. Window mapping was conducted at 36 different sites within sector 05 of the pit mine. A total of 622 minor discontinuities were mapped and three main joint sets identified. Information from laboratory testing comprising unit weight measurements and direct shear tests was available. The joint shear strength was fitted to both linear (Mohr-Coulomb) and non-linear (Power Curve) models. Both kinematic and kinetic rock slope stability analysis was carried out using the deterministic and probabilistic approaches. The commercially available software RocPlane v.4, Swedge v.7 and RocTopple v.2 from Rocscience Inc. were used to model planar,

wedge and toppling failure mechanisms, respectively. the total Probability of Failure (PoF) for each design sector of the open pit mine. The resulting FoS for all design sectors are above 1.1 which is considered as the minimum acceptable criteria at the bench scale analysis. Taking as maximum allowable PoF for the excavated benches a value of 25%, all except for sector SE and S are below this threshold. Recommendations were put forward to steepen the bench angle from its current 65° or to increase the bench height above 15 m. provided in both cases that regular clean-ups of rock spills and daily ground control monitoring are implemented, especially for sector SE and S.

- Case study 02 dealt with the bench slope analysis of a pit mine project. This comprised three different rock types i.e. limestone, skarn and ore body. Structural field data came mainly from the core logging of 52 geotechnical oriented diamond drill holes (DDH). Surface mapping was conducted at 39 outcrops mainly in the host rock (i.e. limestone). The open pit was divided into ten sectors, five in limestone, four in skarn and one corresponding to the overburden (soil-like) material. Both kinematic and kinetic rock slope stability analysis was carried out using the deterministic and probabilistic approaches. From these analyses, sectors 2-3-8 were found to be potentially unstable for planar failure. The remaining sectors (1-4-5-6-7-9) were stable for a BFA up to 75 degrees. For wedge failure, sectors 2-3 were deemed potentially unstable and sector 6 was found to be unstable for a BFA greater than 70° . The remaining sectors were found to be stable for a BFA up to 75 degrees. For these last cases, an optimization program for the bench design was suggested.
- Case study 03 showed the application of DFN modelling to bench slope analysis. Field data was collected from 42 exposed benches cut in hornfels. The discontinuity trace length was described discretely in the form of intervals. Not actual trace length measurements were taken and therefore a lognormal distribution was assumed for the joint persistence. Joint shear strength was estimated using field data of ϕ_b , JRC and JCS into the Barton – Bandis model. Static and pseudo-static bench stability assessments were carried out by a DFN model created with the software Fracman. Joint orientation, joint size and joint shear strength were treated as stochastic input parameters in order to conduct a kinematic and then a kinetic analysis. The number of sliding ($FoS < 1$), metastable ($FoS = 1$), stable ($FoS > 1$) and inadmissible ($FoS = 100$) rock blocks was obtained from the DFN model. From these, the probability of rock block formation (i.e. kinematic) and probability of rock block sliding (i.e. kinetic) was calculated. Finally, the total Probability of Failure (PoF) was obtained by multiplying the kinematic and kinetic probabilities, respectively.

Chapter 5

Inter-Ramp Slope Scale

Multi-bench or inter-ramp instabilities include failures that involve more than one bench, whereas for the bench-scale design, the controlling (minor) geological structures are mostly dealt with using a probabilistic approach. Inter-ramp slope design is typically performed through a deterministic analysis of (major) large-scale discontinuities. In this chapter, inter-ramp slope scale stability assessment is carried out for the three previously presented case studies using stereographic projection and limit equilibrium analyses.

5.1 Structural Stability Analysis of Major Discontinuities

Stability at the inter-ramp slope is still controlled by the rock mass discontinuities leading to relatively simple failure modes (e.g. planar, wedge or toppling). The discontinuities impacting on the stability of the inter-ramp slope are mainly comprised by through-going structures, such as highly persistent bedding-planes or master joints combined with a fault, affecting several benches of the open pit mine. Major geological discontinuities are usually mapped as single features. The location, frequency and continuity of these major structures should be defined from data collected during field mapping.

Inter-ramp stability analysis examines the potential failure of macro-block geometries, usually greater than one bench and which can include the entire inter-ramp height. Almost similar input parameters to those of the bench analysis are required for the inter-ramp stability analysis with the exception of the slope angle and height. Also, adjustments for the discontinuity shear strength might be needed since major discontinuities (e.g. faults) are likely to have different properties as those of minor structures (e.g. joints).

Kinematically possible failure modes for the inter-ramp slope including planar, wedge and toppling failures is assessed in the same fashion as for the bench-scale analysis. However, the inter-ramp kinematic analysis focuses on single structural features (e.g. poles or intersections) and not on the entire distribution of minor joint clustering.

5.2 Case Studies

In the following sections three case studies, previously presented in chapter 4, will be assessed at the inter-ramp scale slope using minor faults fabric. The purpose of these analyses is to establish the optimum inter-ramp angle (IRA) which undercuts as few daylighting planes, wedges or blocks as possible. Both deterministic stereographic and limit equilibrium-based analyses are used for each pit sector. All kinematic analyses for the case studies presented herein have been carried out using the DIPS software whereas the LE analyses were done using RocPlane, Swedge and RocTopple software from Rocscience Inc.

5.2.1 Case Study #1

The first case study presented before deals with the geotechnical reconciliation of an existing open pit mine. Since some benches were already excavated, field data was collected from direct mapping on exposed benches. Apart from the structural mapping of minor discontinuities (i.e. rock joints), intermediate scale structures (>25 m in length), related to a local faulting system was also mapped within the area of the pit. Figure 5.1 shows the distribution of these faults in the pit area. No faults were identified in the West sector. A total of 24 faults were mapped and described according to the ISRM suggested methods (Ulusay, 2014). The faults pole distribution is shown as an equal area stereo plot in Figure 5.2. These are colored according to pit sectors.

From the bench scale analysis, the recommended bench face angle (BFA) is 65° for case study #1. For a 15 m height bench slope with a 7.5 m of bench width, the resulting inter-ramp angle is 46° . The inter-ramp stability assessment is carried out for a slope of 5 benches which adds up to a 75 m high inter-ramp slope (Figure 5.3).

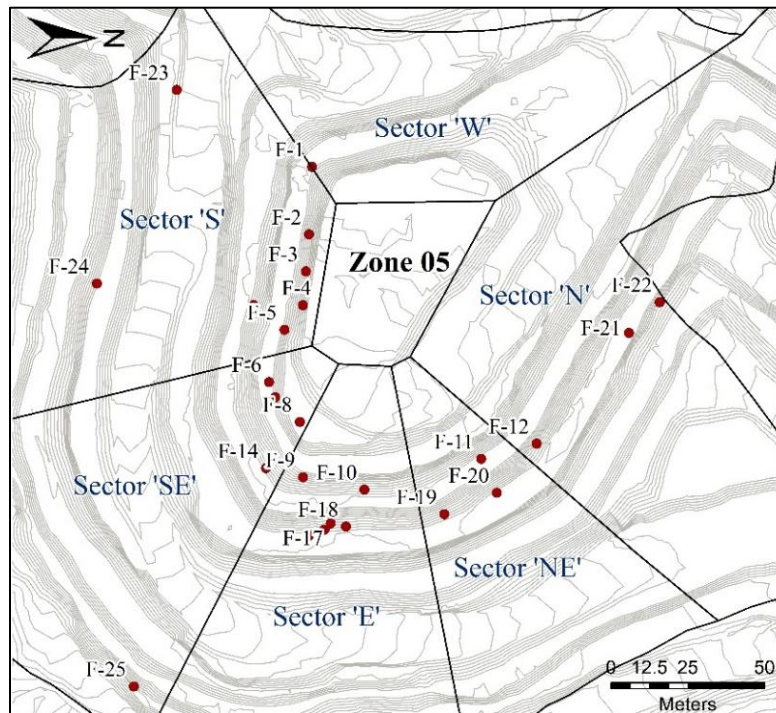


Figure 5.1 Distribution of mapped faults within the open pit mine – case study #1

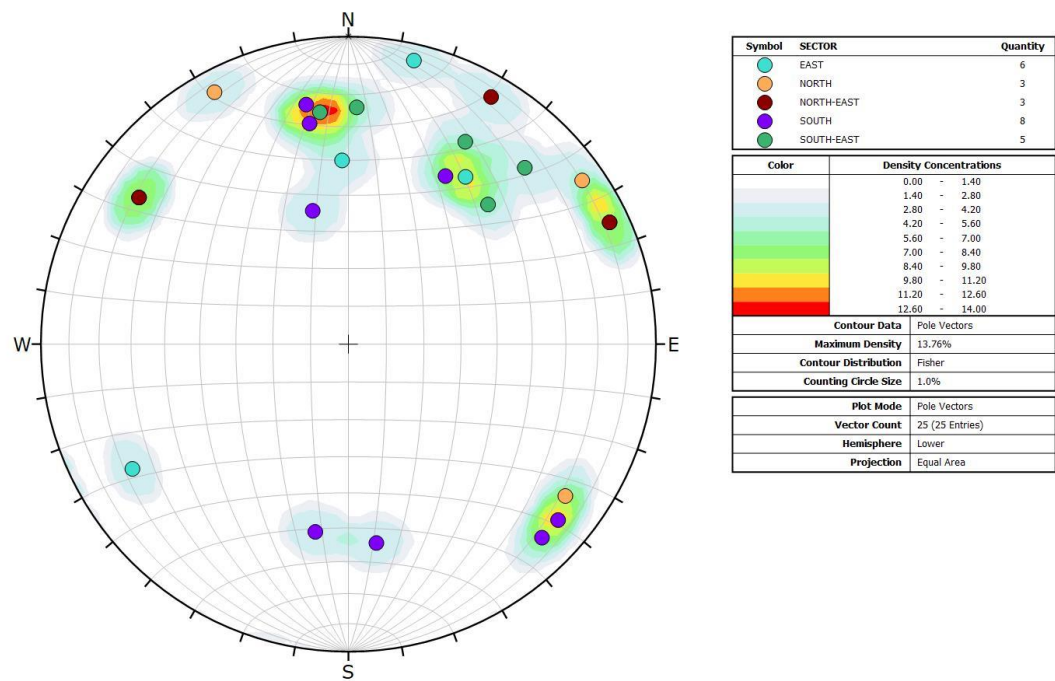


Figure 5.2 Equal area stereo plot of mapped faults within the open pit mine – case study #1

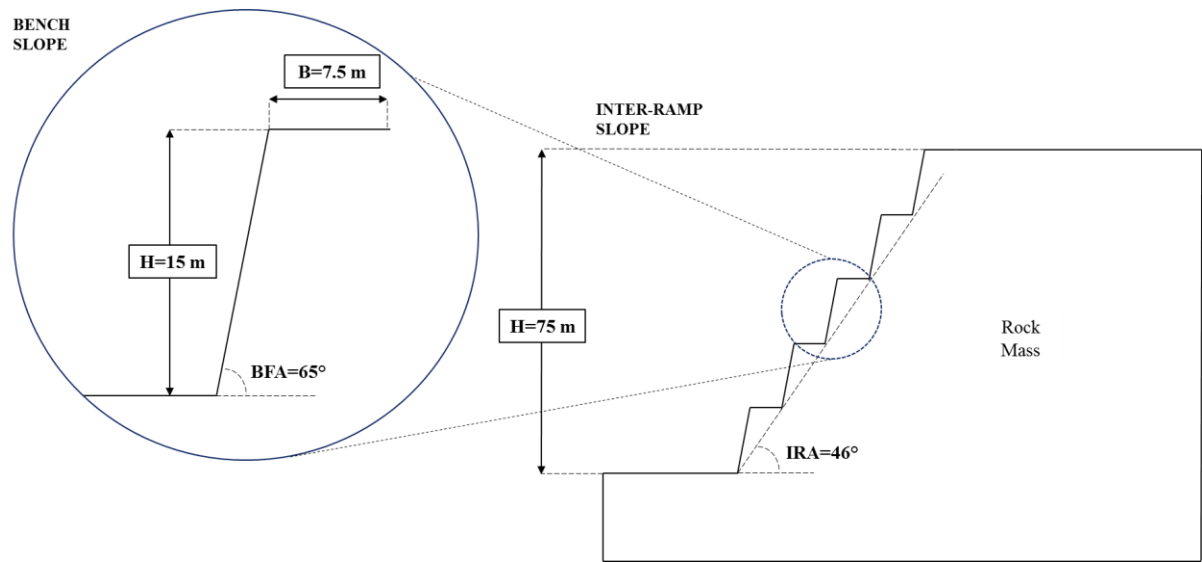


Figure 5.3 Inter-ramp slope configuration – case study #1

Kinematic Analysis

The open pit for case study #1 was divided in 5 design sectors named: North, North East, East, South East, South and West. These are shown as a radar plot on Figure 5.4. Once all mapped faults were selected upon the pit sector they belong to, a deterministic kinematic analysis was carried out for planar wedge and toppling potential failure mechanisms.

Figure 5.5 shows the results for planar kinematic analysis. For all pit sectors no potential planar failure was identified with an IRA of 46° . Therefore, the inter-ramp slope configuration is deemed stable against planar failure.

Figure 5.6 shows the results for wedge kinematic analysis with the intersection points between faults being plotted. One potential wedge in the East sector is identified. This will need further analysis by a LE approach. For all other sectors no potential wedge failure was observed in the stereo plots with an IRA of 46° .

Figure 5.7 shows the results for flexural toppling kinematic analysis. For all pit sectors no potential toppling failure was identified with an IRA of 46° . Therefore, the inter-ramp slope configuration is deemed stable against toppling failure.

A summary of the deterministic kinematic analysis for the inter-ramp slope scale is given in Table 5.1.

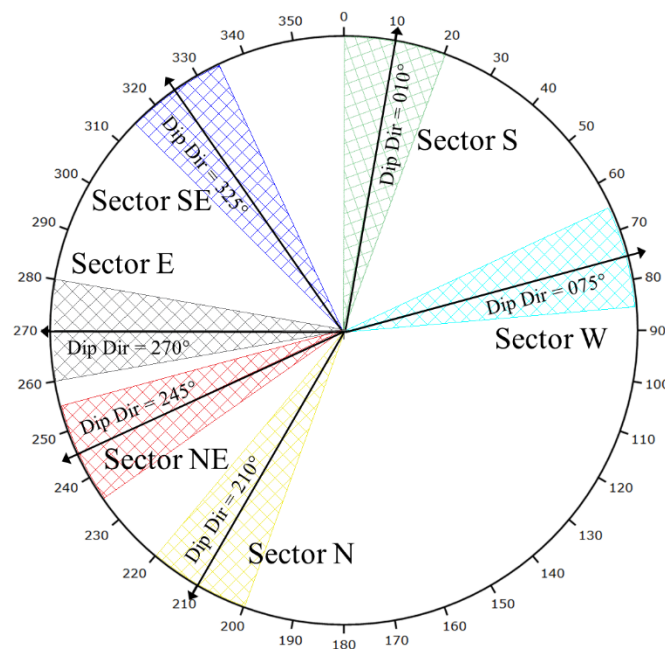


Figure 5.4 Radar plot of design sectors for the open pit mine – case study #1

Table 5.1 Summary of kinematic analysis for the inter-ramp slope – case study #1

Sector	Planar	Wedge	Toppling
South	No	No	No
West	-	-	-
North	No	No	No
North East	No	No	No
East	No	Yes	No
South East	No	No	No

Limit Equilibrium Analysis

Since the kinematic analyses of the previous section identified a potential wedge failure in the East sector of the pit formed by faults F-15 and F-16, a limit equilibrium analysis is now performed. The LE analysis for the faults used conservative shear strength values of zero cohesion and 35° friction angle. The Swedge software from Rocscience Inc was used for the calculation of the Factor of Safety (FoS) which is found to be 3.02 (Figure 5.8). Therefore, the inter-ramp slope configuration in the East sector of the pit is deemed stable against wedge failure. A summary of the deterministic kinetic analysis is given in Table 5.2.

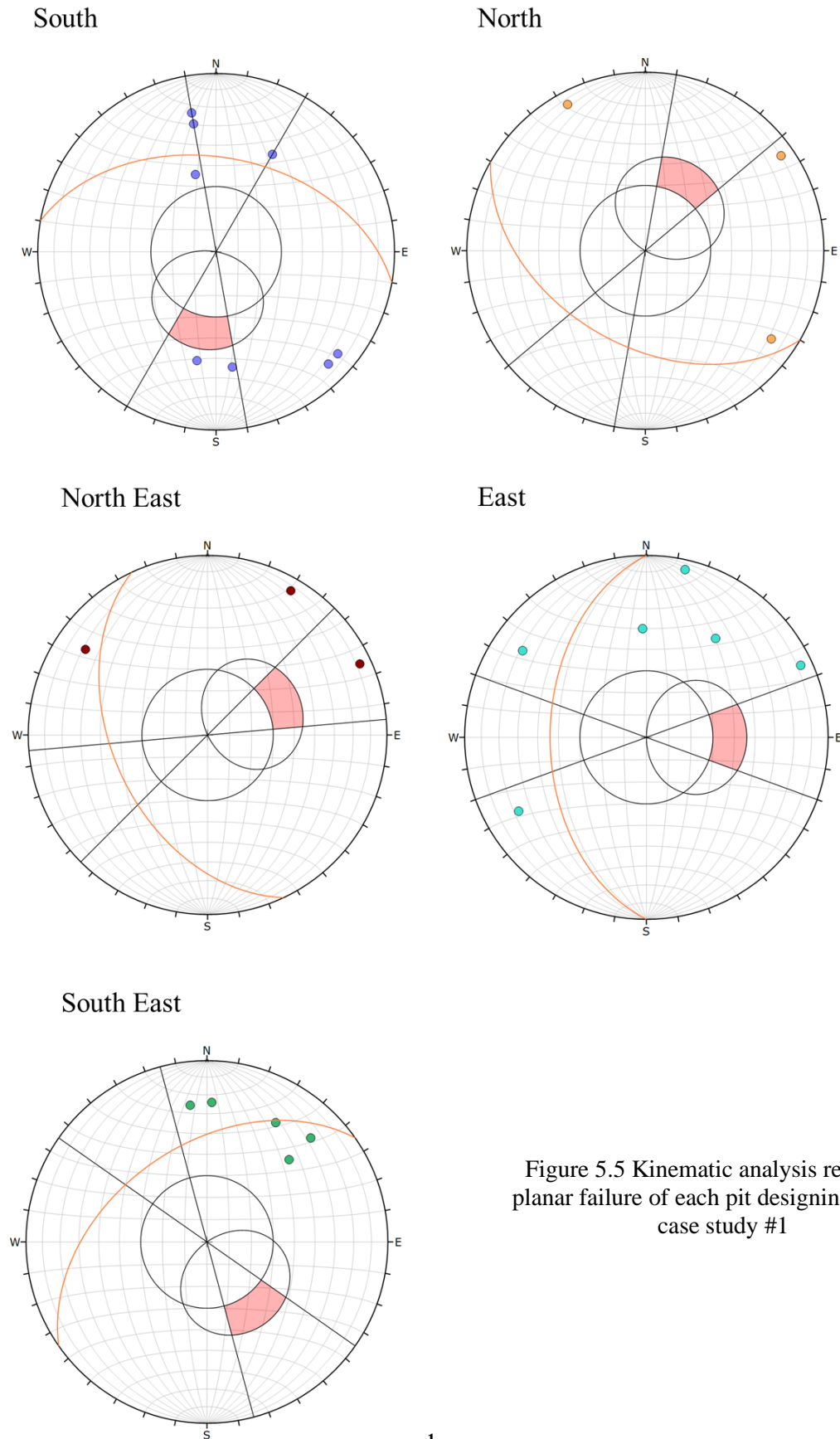


Figure 5.5 Kinematic analysis results for planar failure of each pit designing sector – case study #1

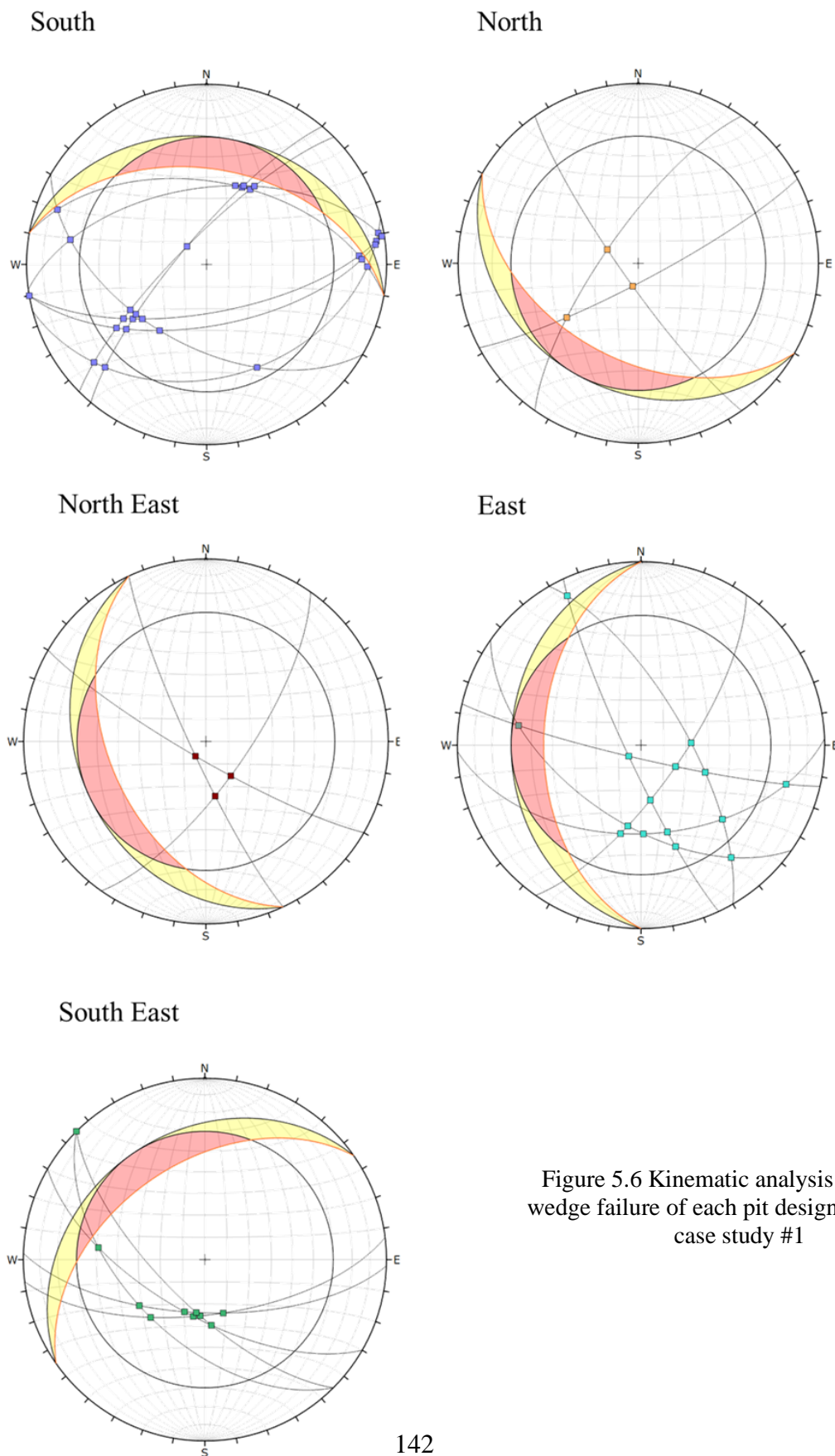


Figure 5.6 Kinematic analysis results for wedge failure of each pit designing sector – case study #1

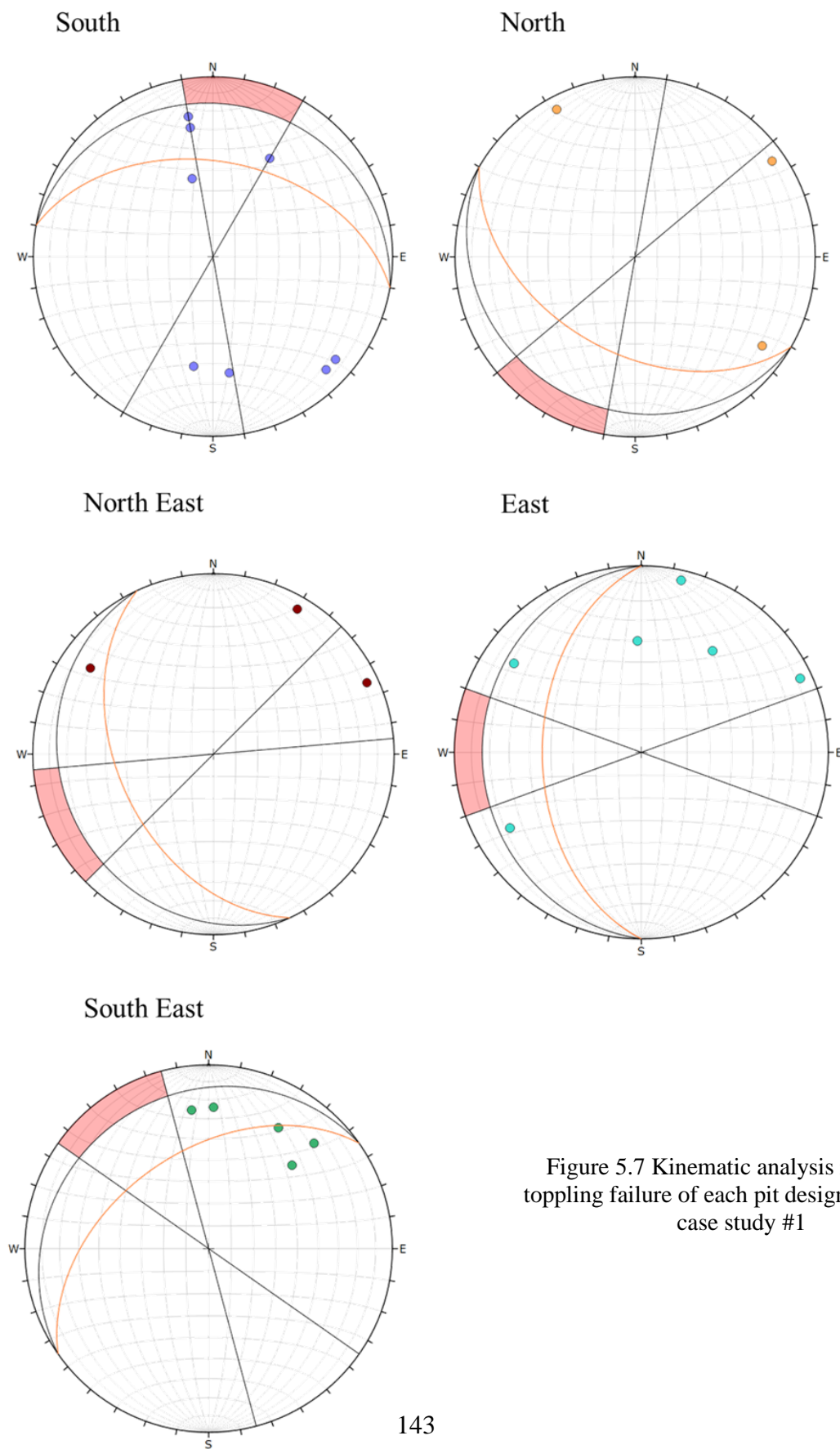


Figure 5.7 Kinematic analysis results for toppling failure of each pit designing sector – case study #1

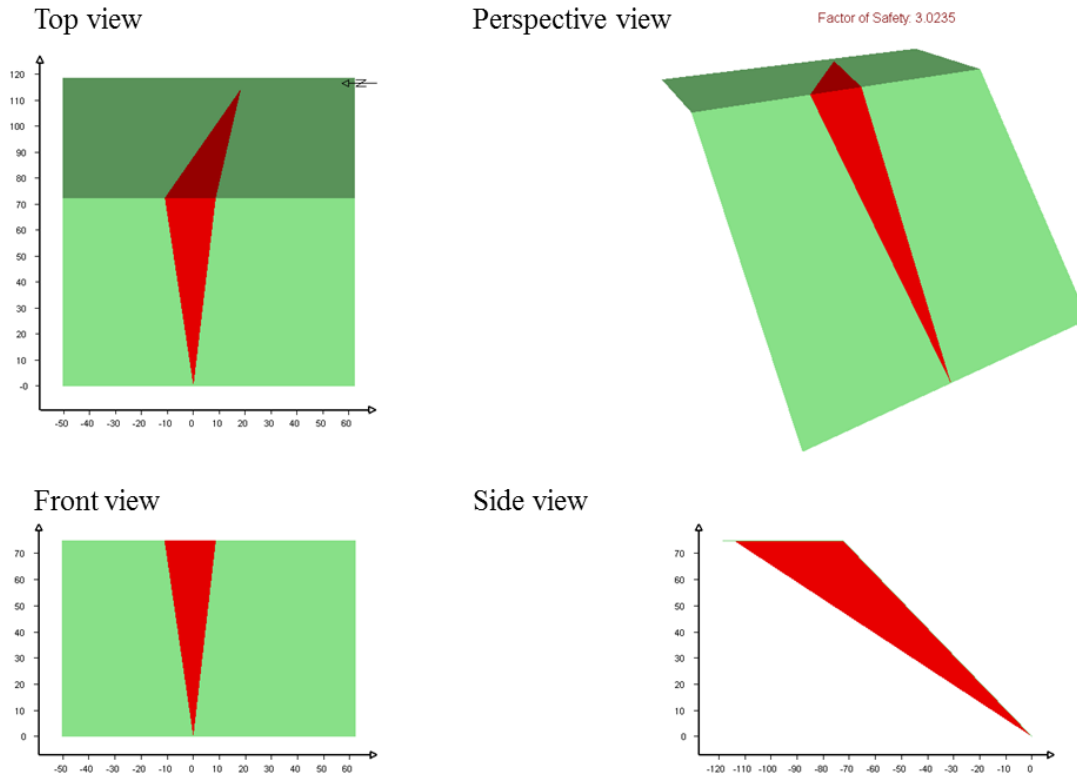


Figure 5.8 LE analysis results for wedge failure formed by F-15 & F-16 faults.

Table 5.2 Summary of LE analysis for the inter-ramp slope – case study #1

Sector	Failure Mode	Faults	FoS
East	Wedge	F-15 & F-16	3.02

5.2.2 Case Study #2.

The second case study is of an open pit mine project with structural information mainly based on geological and geotechnical diamond drill holes (DDH) with limited outcrop mapping sites. Since no exposed benches were available, the inter-ramp slope analysis will be based only on surface mapping information given that core logging data cannot provide reliable information regarding major geological structures. From the geological field reconnaissance program, four major steeply dipping faults were identified in the future open pit area $85^{\circ}/100^{\circ}$; $65^{\circ}/115^{\circ}$; $70^{\circ}/155^{\circ}$ and $70^{\circ}/070^{\circ}$ (Figure 5.9). Although these structures are thought to be of importance for the overall scale analysis, an inter-ramp stability analysis is also carried out.

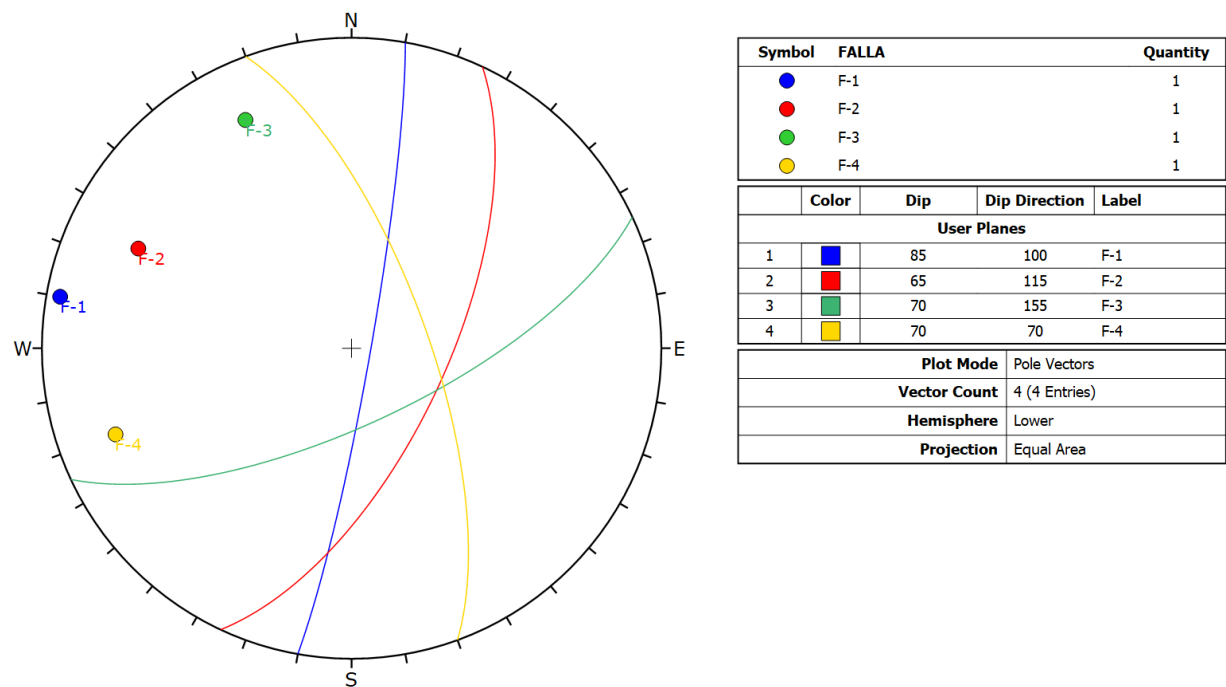


Figure 5.9 Equal area stereo plot of mapped faults within the open pit mine – case study #2

From the bench scale analysis, the recommended bench face angle (BFA) is 70° for case study #2. For a 10-meter high bench slope with a 6.5-meter wide bench, the resulting inter-ramp angle is 45°. The inter-ramp stability assessment is carried out for a slope of 5 benches which adds up to a 50 m high inter-ramp slope (Figure 5.10).

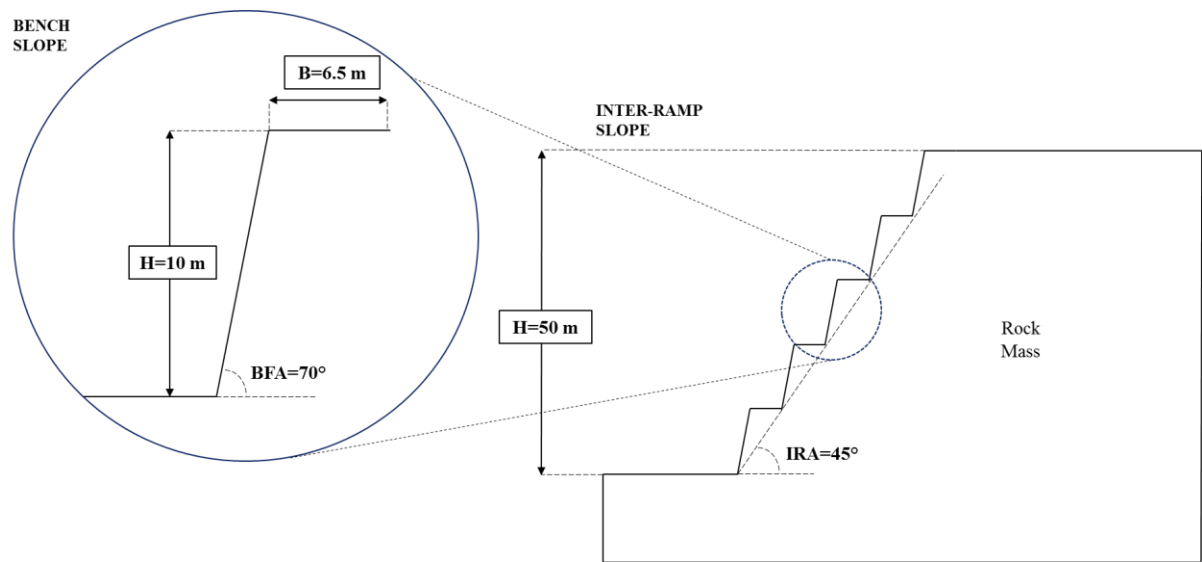


Figure 5.10 Inter-ramp slope configuration – case study #2

Kinematic Analysis

The open pit for case study #2 was divided into 9 design sectors from which 5 are in limestone, 4 in skarn and one (#10) that corresponds to the slope cuts in overburden (soil-like) material (Figure 5.11). With the 4 mapped faults, a deterministic kinematic analysis was carried out for planar wedge and toppling potential failure mechanisms of each sector that is going to be excavated in rock (i.e. sectors 1-9).

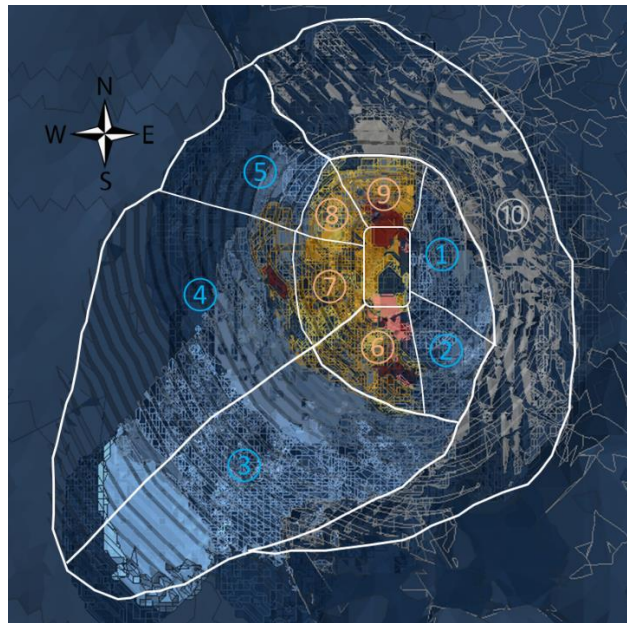


Figure 5.11 Open pit design sectors – case study #2

Figure 5.12 shows the planar kinematic analysis results. For all pit sectors no potential for planar failure is identified. The inter-ramp slope configuration is deemed stable against planar failure for an IRA of 45°.

Figure 5.13 shows the results for wedge failure. One potential wedge in sector #9 is identified for faults 1 and 2. This will need further analysis by a LE approach. For all other sectors no potential wedge failure was observed in the stereo plots with an IRA of 45°.

Figure 5.14 shows the results for flexural toppling kinematic analysis. For all pit sectors no potential toppling failure was identified. Therefore, the slope is deemed stable against toppling for an IRA of 45°.

A summary of the deterministic kinematic analysis for the inter-ramp slope scale is given in Table 5.3.

Limit Equilibrium Analysis

Since the kinematic analyses of the previous section identified a potential wedge failure in sector #9 formed by faults F-1 and F-2, a limit equilibrium analysis is now performed. The LE analysis for the faults used

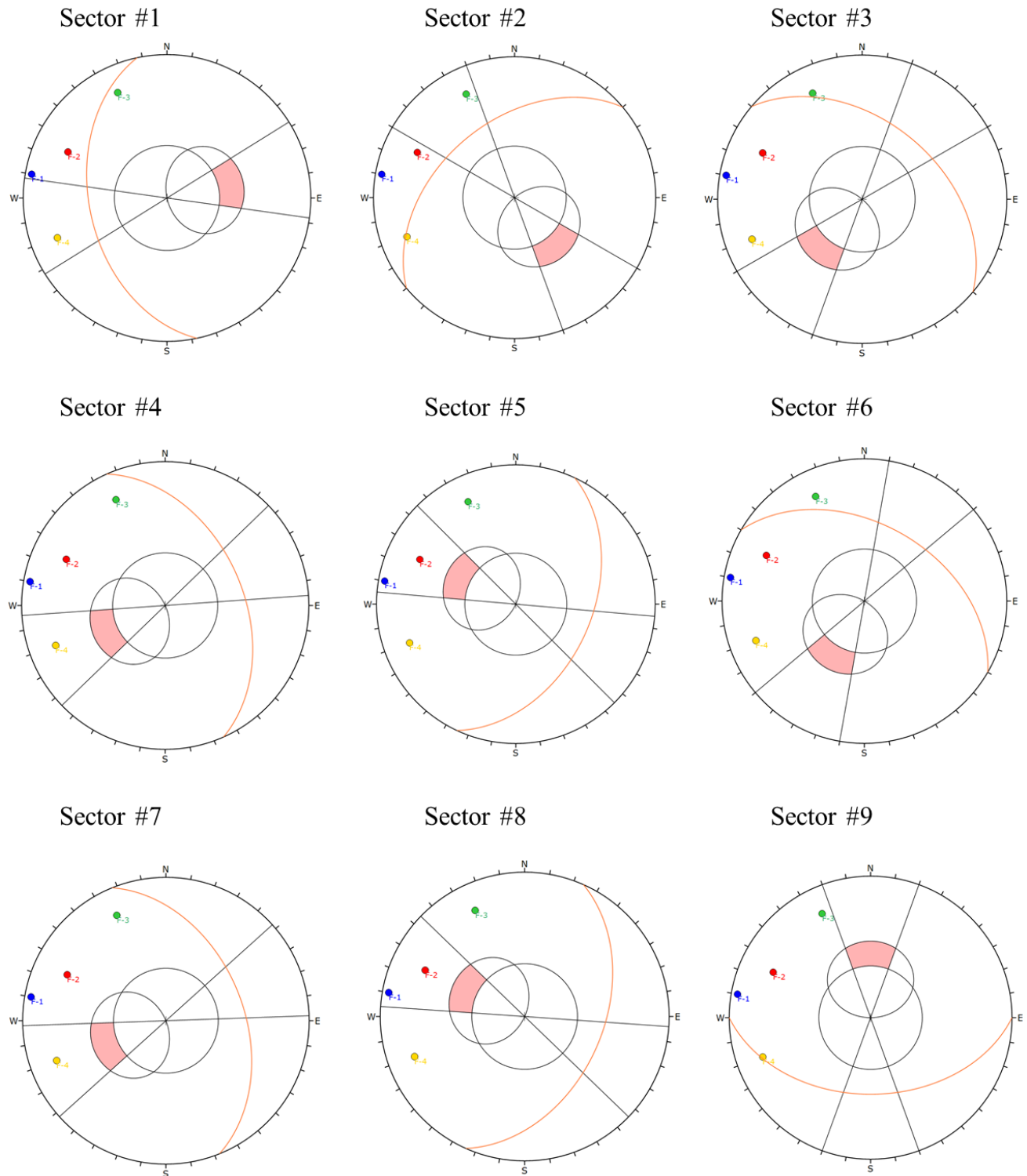


Figure 5.12 Kinematic analysis results for planar failure for each sector – case study #2

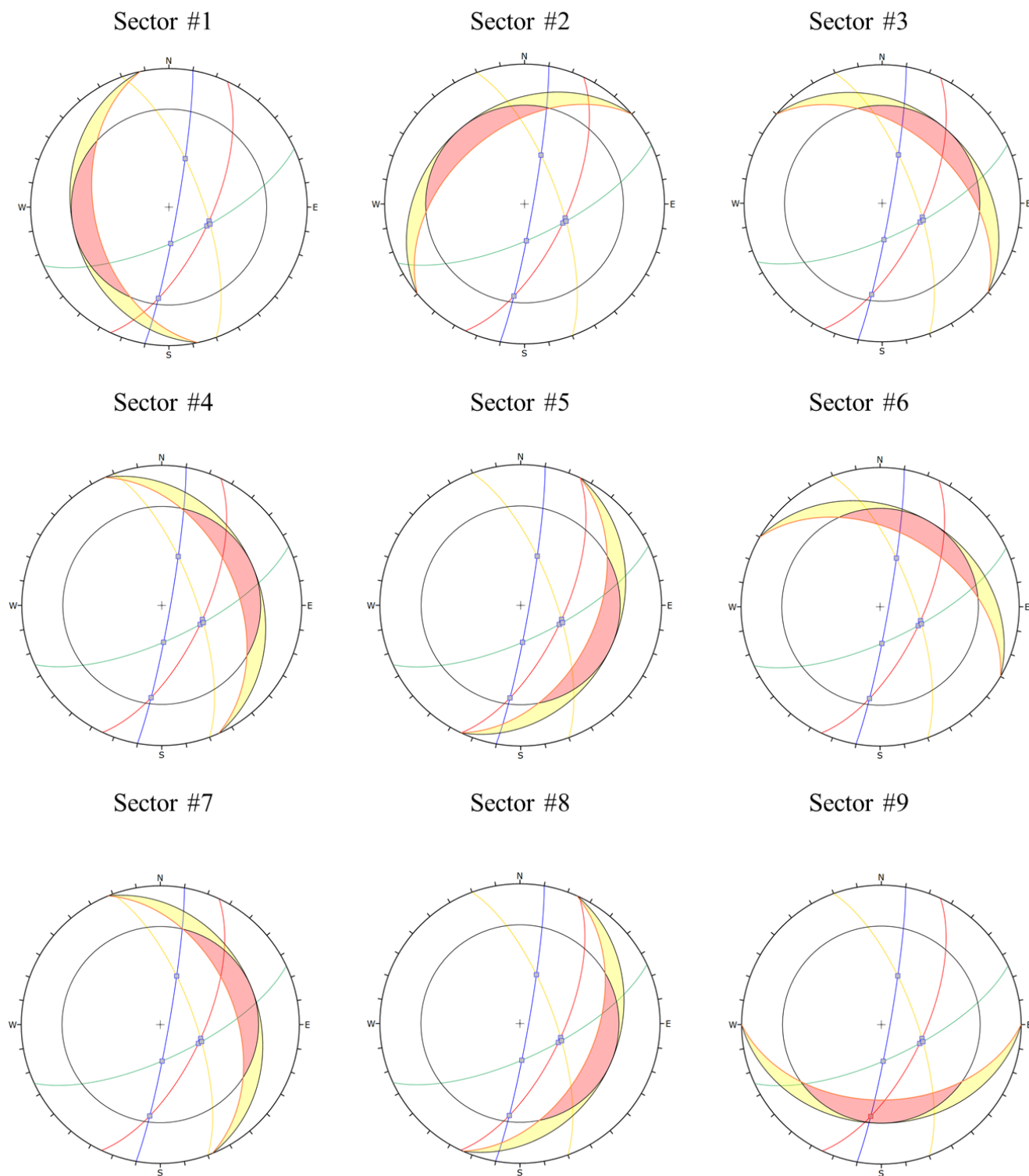


Figure 5.13 Kinematic analysis results for wedge failure for each sector – case study #2

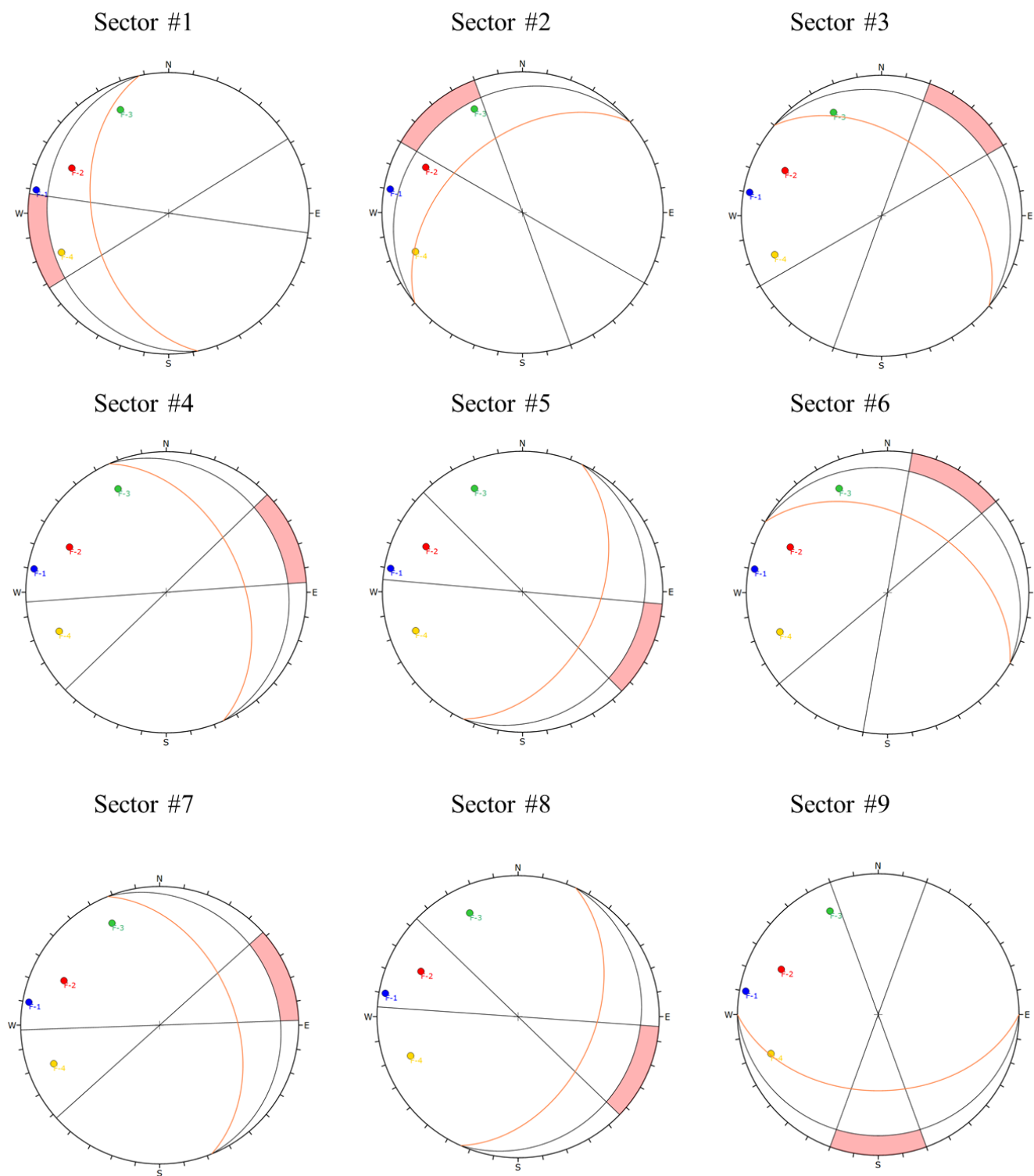


Figure 5.14 Kinematic analysis results for toppling failure for each sector – case study #2

conservative shear strength values of zero cohesion and 35° friction angle. The Factor of Safety (FoS) was found to be 3.79 (Figure 5.15). Therefore, the inter-ramp slope configuration is deemed stable against wedge failure. A summary of the deterministic kinetic analysis is given in Table 5.4.

Table 5.3 Summary of kinematic analysis for the inter-ramp slope – case study #2

Lithology	Sector #	Slope DipDir	Planar	Wedge	Toppling
Limestone	1	258	No	No	No
	2	320	No	No	No
	3	040	No	No	No
	4	066	No	No	No
	5	115	No	No	No
Skarn	6	030	No	No	No
	7	068	No	No	No
	8	114	No	No	No
	9	180	No	Yes	No

Table 5.4 Summary of LE analysis for the inter-ramp slope – case study #2

Lithology	Sector #	Slope DipDir	Failure Mode	Faults	FoS
Skarn	9	180	Wedge	F-1 & F-2	3.8

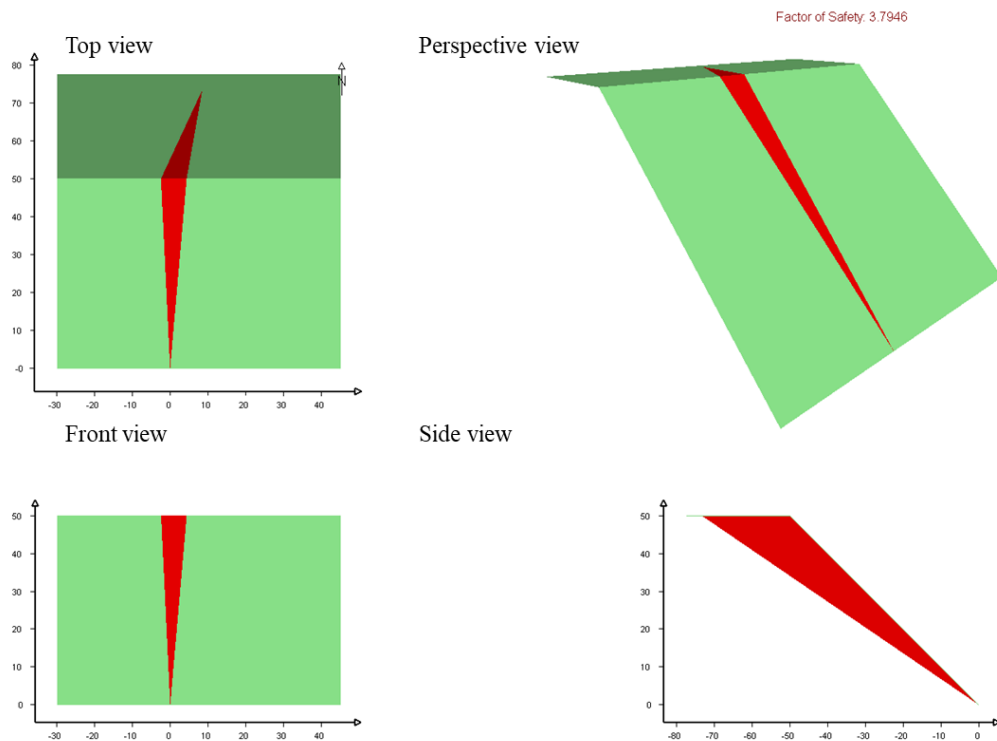


Figure 5.15 LE analysis results for wedge failure formed by F-1 & F-2 faults – case study #2.

5.2.3 Case Study #3

The area in which this open pit mine is located has undergone moderate fracturing of the host rocks where intermediate geological discontinuities are those associated with faulting. The third open pit case study relied on data from classical bench mapping of minor (i.e. rock joints) and intermediate (i.e. local faults) geological discontinuities. Figure 5.16 shows the distribution of these faults in the pit area. A total of 79 local faults were mapped and described according to the ISRM suggested methods (Ulusay, 2014). The faults pole distribution is shown as an equal area stereonet plot in Figure 5.17. These are colored according to the four open pit design sectors i.e. North, North East, South and South West.

From the bench scale analysis, the recommended bench face angle (BFA) is 65° for case study #3. For a 15-meter high bench slope with a 7.5-meter wide bench, the resulting inter-ramp angle is 46° . The inter-ramp stability assessment is carried out for a stack of 4 benches which adds up to a 60 m height inter-ramp slope (Figure 5.18).

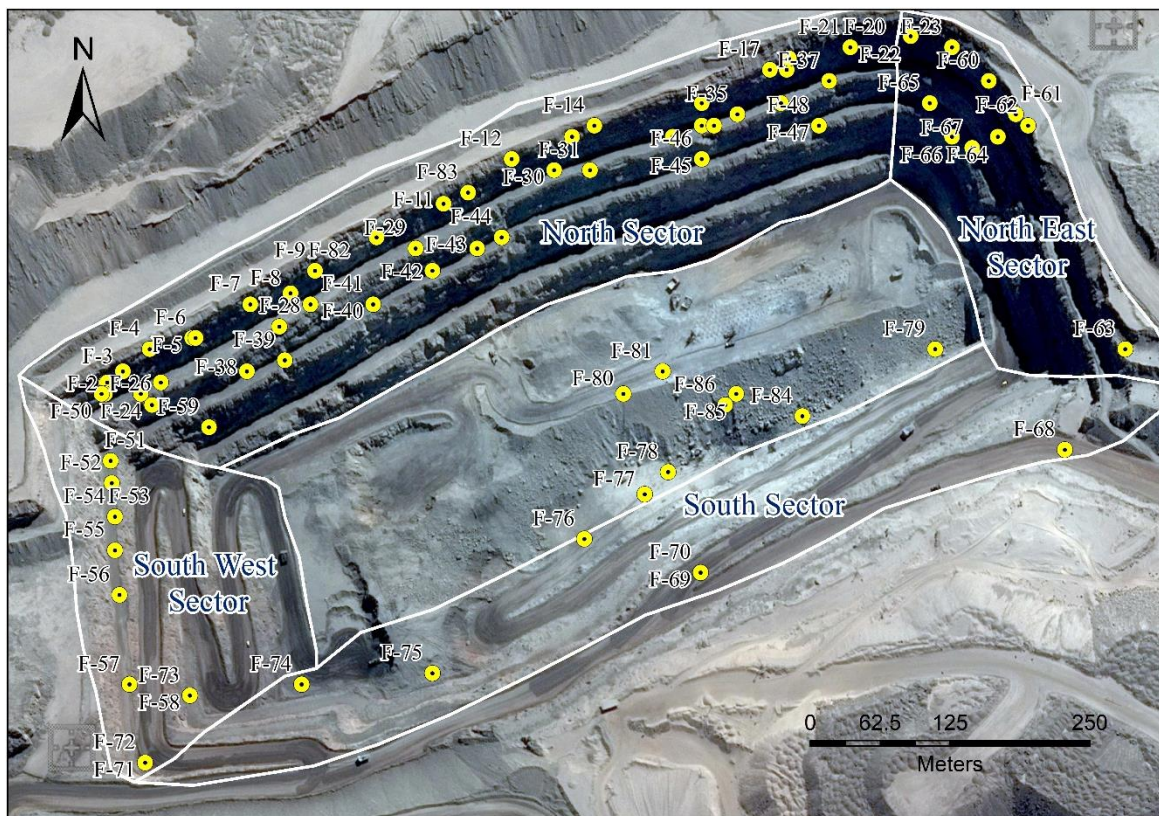


Figure 5.16 Distribution of mapped faults within the open pit mine – case study #3

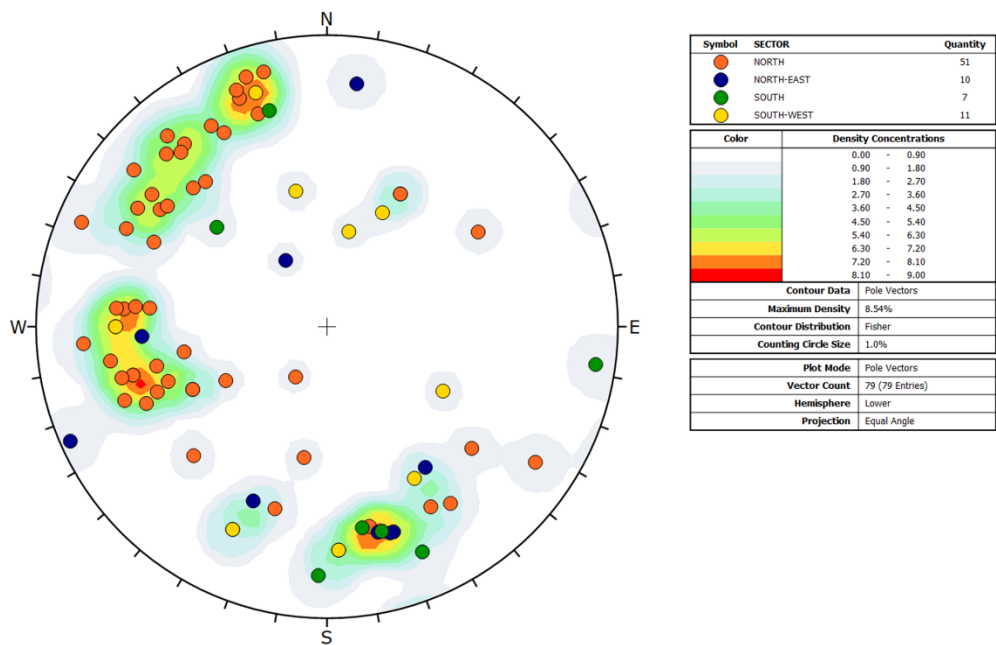


Figure 5.17 Equal area stereo plot of mapped faults within the open pit mine – case study #3

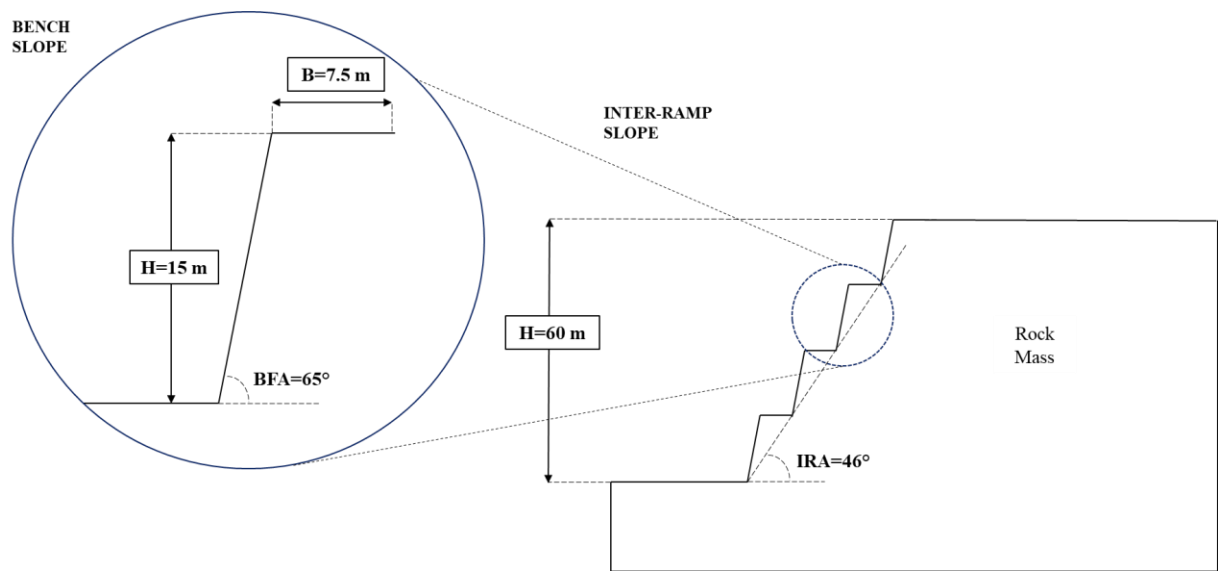


Figure 5.18 Inter-ramp slope configuration – case study #3

Kinematic Analysis

The open pit for case study #3 was divided into 4 design sectors named: North, North East, South and South West. These are shown as a radar plot on Figure 5.19. Once all mapped faults were selected upon the pit sector they belong to, a deterministic kinematic analysis was carried out for planar wedge and toppling potential failure mechanisms.

Figure 5.20 shows the planar kinematic analysis results. For all pit sectors, no potential for planar failure is identified. Therefore, the inter-ramp slope configuration is deemed stable with an IRA of 46° . Figure 5.21 show the results for wedge failure with the intersection points between faults plotted. No potential wedge failure is identified for the South West and South sectors. For the two remaining sectors North and North East, potential for wedge failure is observed with 21 and 2 critical intersections identified in the stereo plots for an IRA of 46° . These two sectors will need further analysis.

Figure 5.22 shows the results for flexural toppling kinematic analysis. No potential toppling failure is identified for the South West and North sectors. For the two remaining sectors South and North East the potential for toppling failure formation is observed for an IRA of 46° . These two sectors will need further analysis by a LE approach.

A summary of the deterministic kinematic analysis for the inter-ramp slope scale is given in Table 5.5.

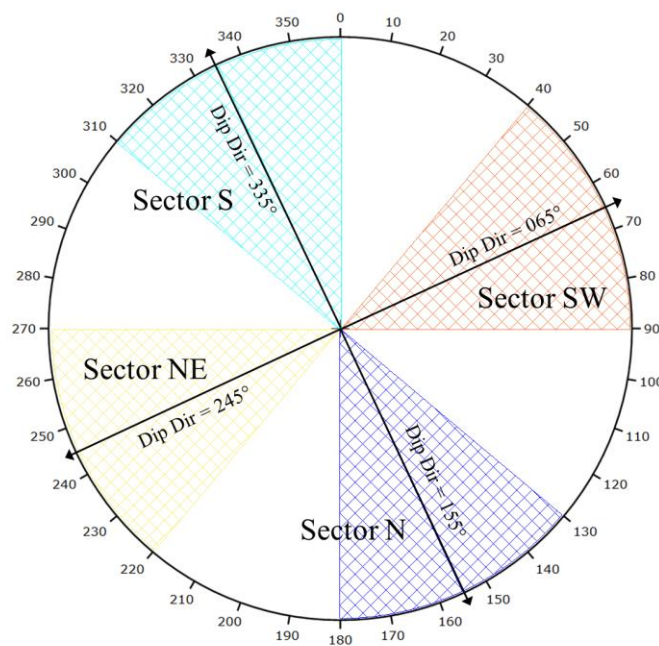


Figure 5.19 Radar plot of design sectors for the open pit mine – case study #3

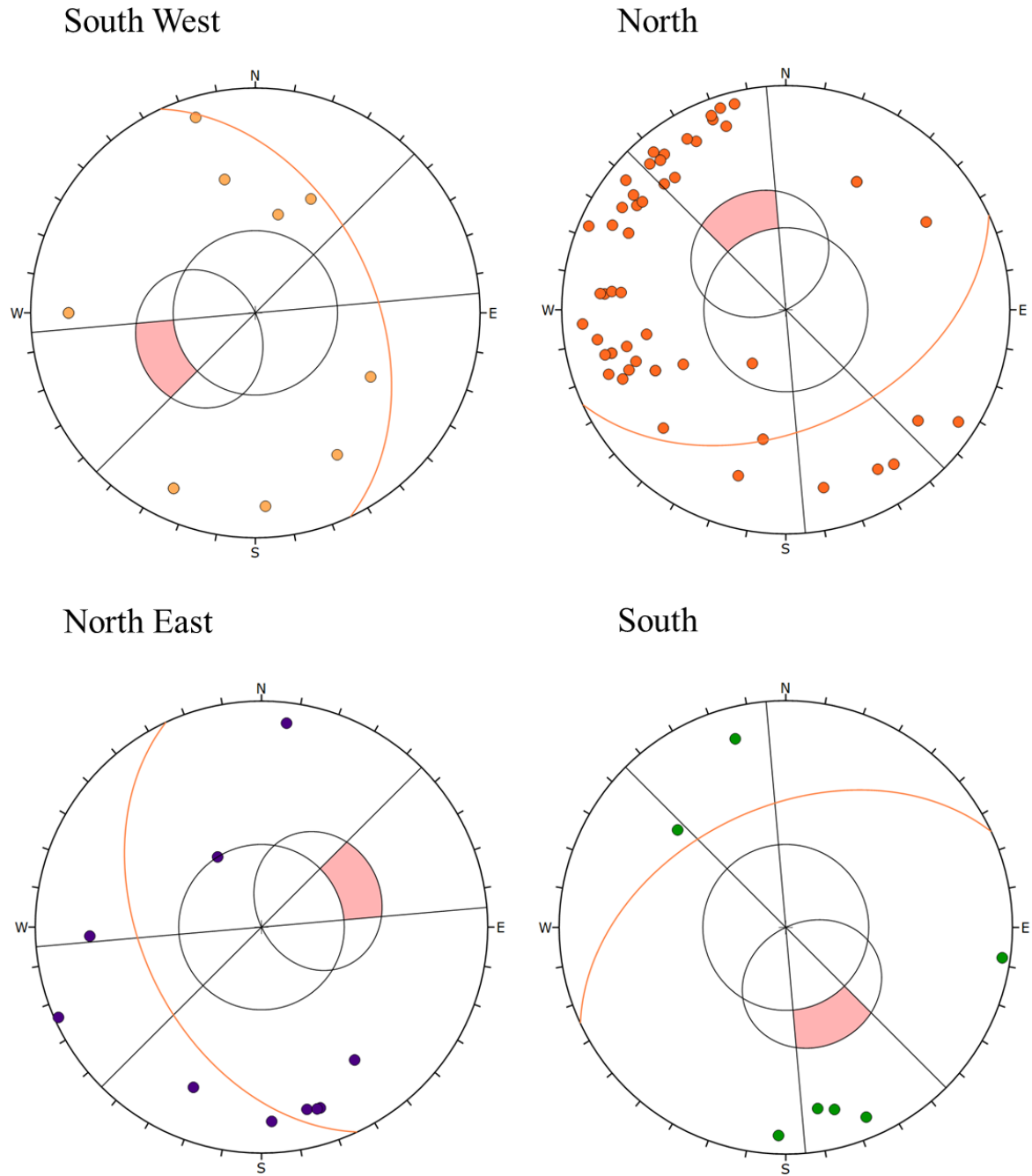


Figure 5.20 Kinematic analysis results for planar failure for each sector – case study #3

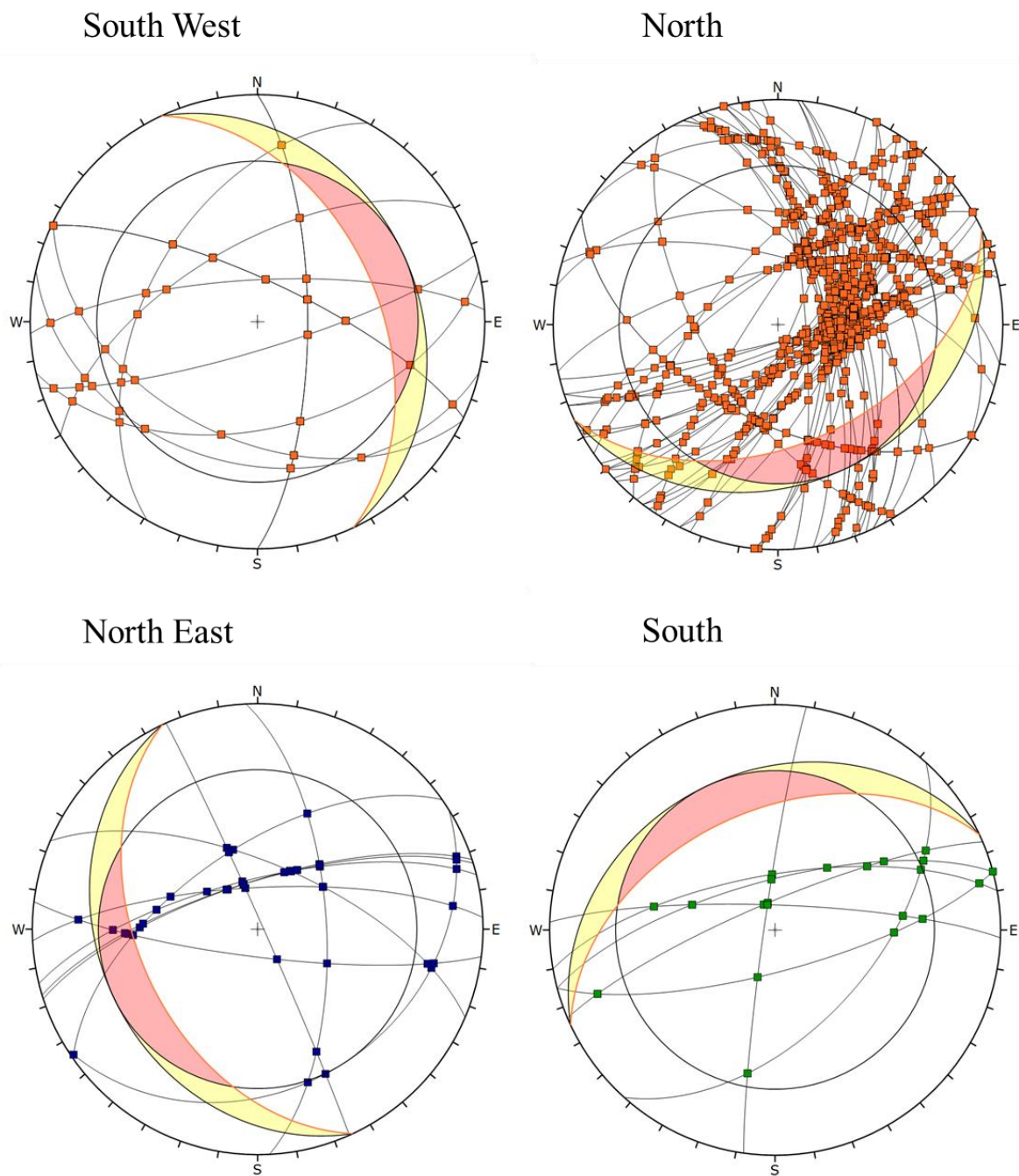


Figure 5.21 Kinematic analysis results for wedge failure for each sector – case study #3

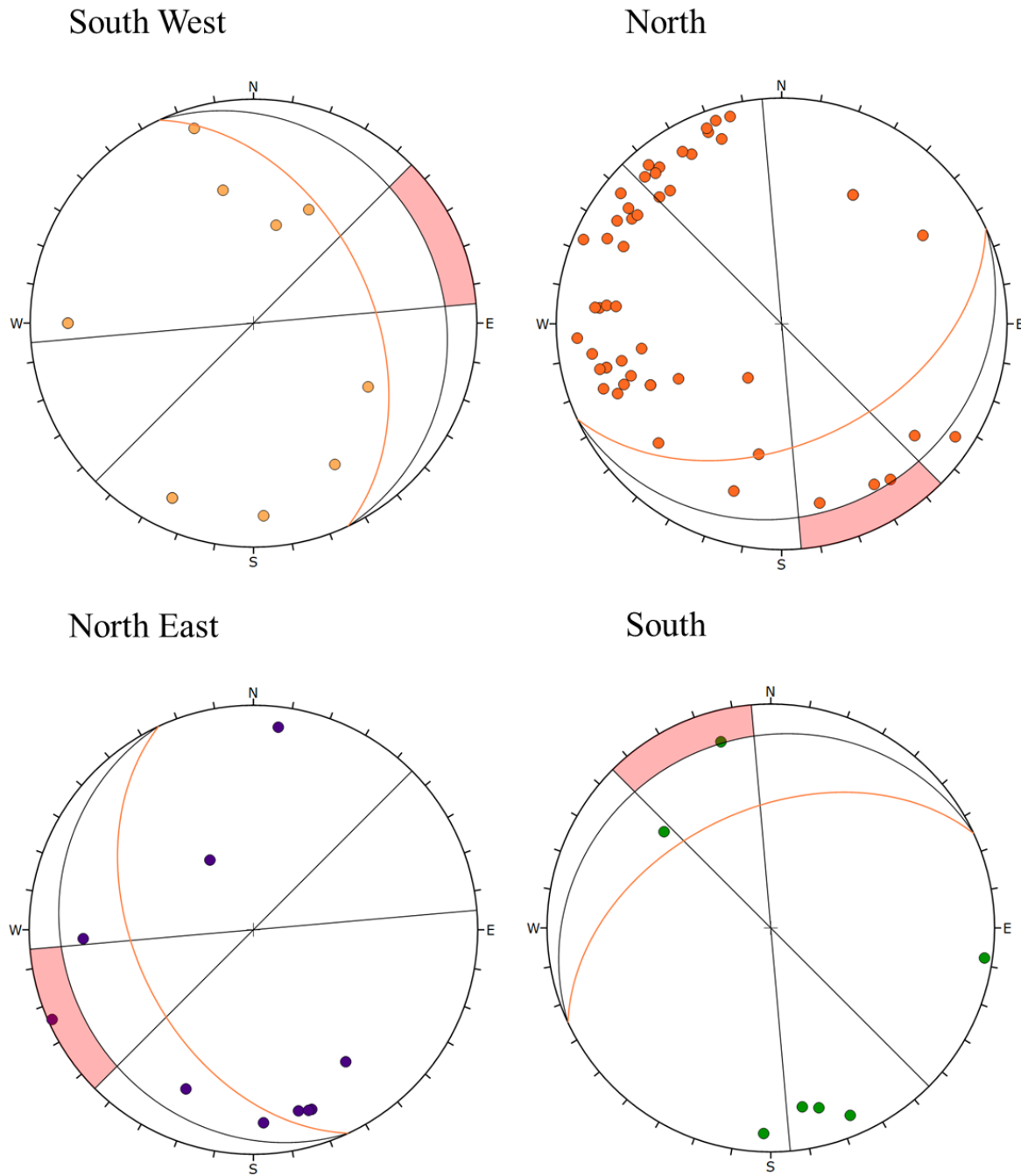


Figure 5.22 Kinematic analysis results for toppling failure for each sector – case study #3

Table 5.5 Summary of kinematic analysis for inter-ramp slope – case study #3

Sector	Planar	Wedge	Toppling
South West	No	Yes	No
North	No	Yes	No
North East	No	Yes	Yes
South	No	No	Yes

Limit Equilibrium Analysis

Since the kinematic analyses of the previous section identified a potential wedge failure for the South West and South sectors of the pit formed with 21 and 2 critical intersections, a limit equilibrium analysis is now performed. The LE analysis for the faults used conservative shear strength values of zero cohesion and 35° friction angle. Swedge software of Rocscience Inc. was used for the calculation of the Factor of Safety. Flexural toppling kinetic analysis for the South West and North sectors was performed with RocTopple software of RocScience. A summary of the deterministic kinetic analysis is given in Table 5.6.

From Table 5.6 most FoS values are greater than 1.3 which can be considered as the minimum required FoS at the inter-ramp slope scale. However, three wedges were found to be in a metastable condition with FoS values between 1.03 and 1.10. Although these cases do not meet the stability criteria, the wedges form thin slabs as can be seen in Figures 5.23-5.25. These may not pose a high risk to the slope performance. Also, it should be noted that the shear strength values considered for the faults are conservative ($c=0$ and $\phi=35^\circ$). Kinematically feasible toppling mechanisms are in fact stable with FoS greater than 1.3 (Figures 5.26-5.27).

Table 5.6 Summary of LE analysis for the inter-ramp slope – case study #3

Sector	Failure Mode	Faults	FoS
South West	Wedge	F-51 & F-58	5.64
		F-55 & F-72	1.97
North	Wedge	F-3 & F-30	1.03
		F-3 & F-39	1.04
		F-3 & F-48	1.10
		F-3 & F-31	1.35
		F-3 & F-59	1.57
		F-3 & F-26	1.62
		F-4 & F-3	1.62
		F-3 & F-40	1.69

		F-2 & F-3	1.73
		F-3 & F-17	1.85
		F-9 & F-37	1.91
		F-9 & F-39	1.95
		F-9 & F-30	1.95
		F-9 & F-48	2.03
		F-3 & F-14	2.13
		F-9 & F-20	2.52
		F-2 & F-14	5.79
		F-2 & F-27	6.60
		F-20 & F-39	6.81
		F-20 & F-30	7.02
		F-2 & F-11	7.34
North East	Wedge	F-61 & F-65	2.99
	Wedge	F-65 & F-66	2.39
	Toppling	F-23	>1.30
South	Toppling	F-76	>1.30

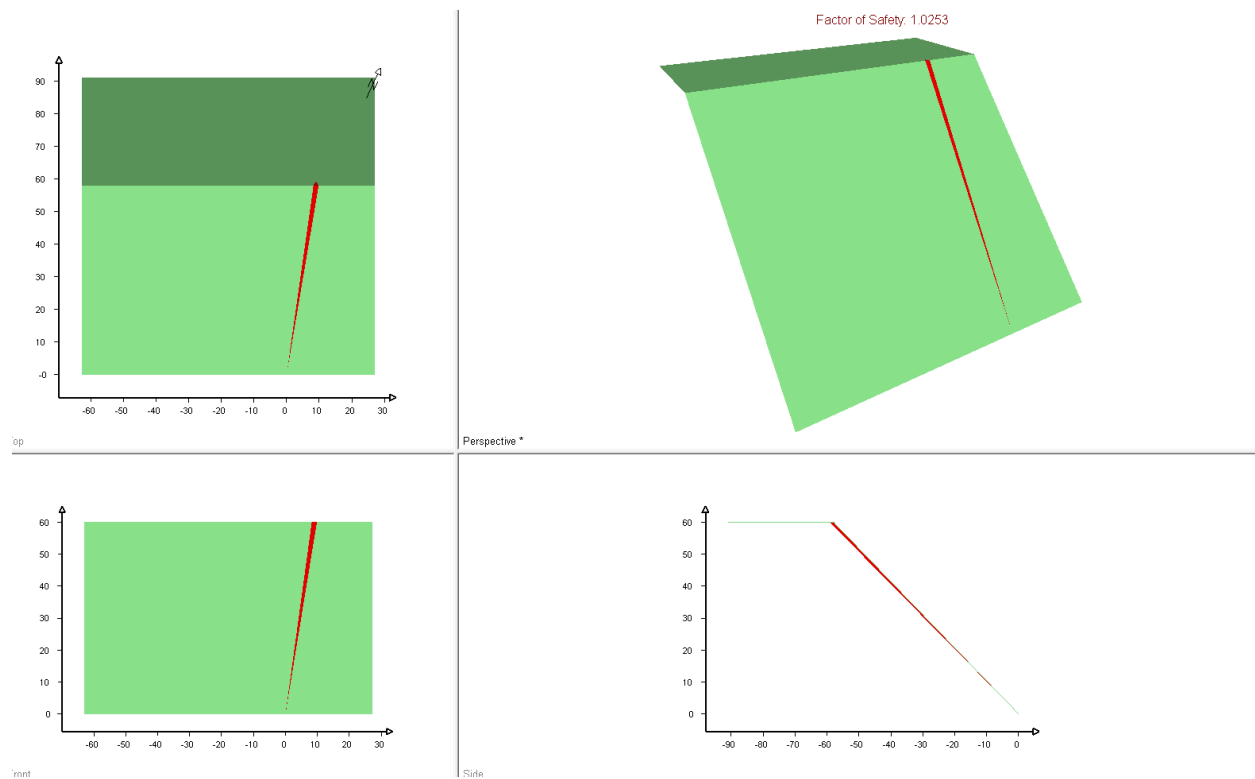


Figure 5.23 LE analysis results for wedge failure formed by F-3 & F-30 faults – case study #3

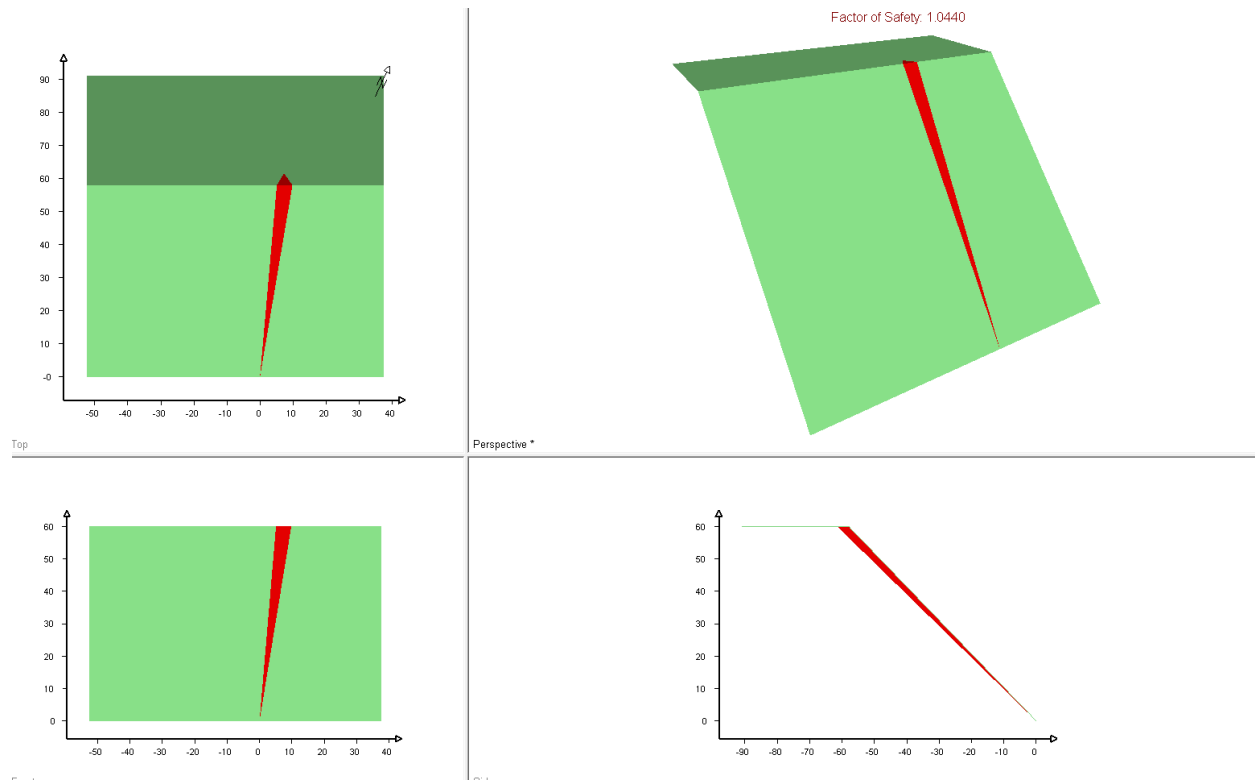


Figure 5.24 LE analysis results for wedge failure formed by F-3 & F-39 faults – case study #3

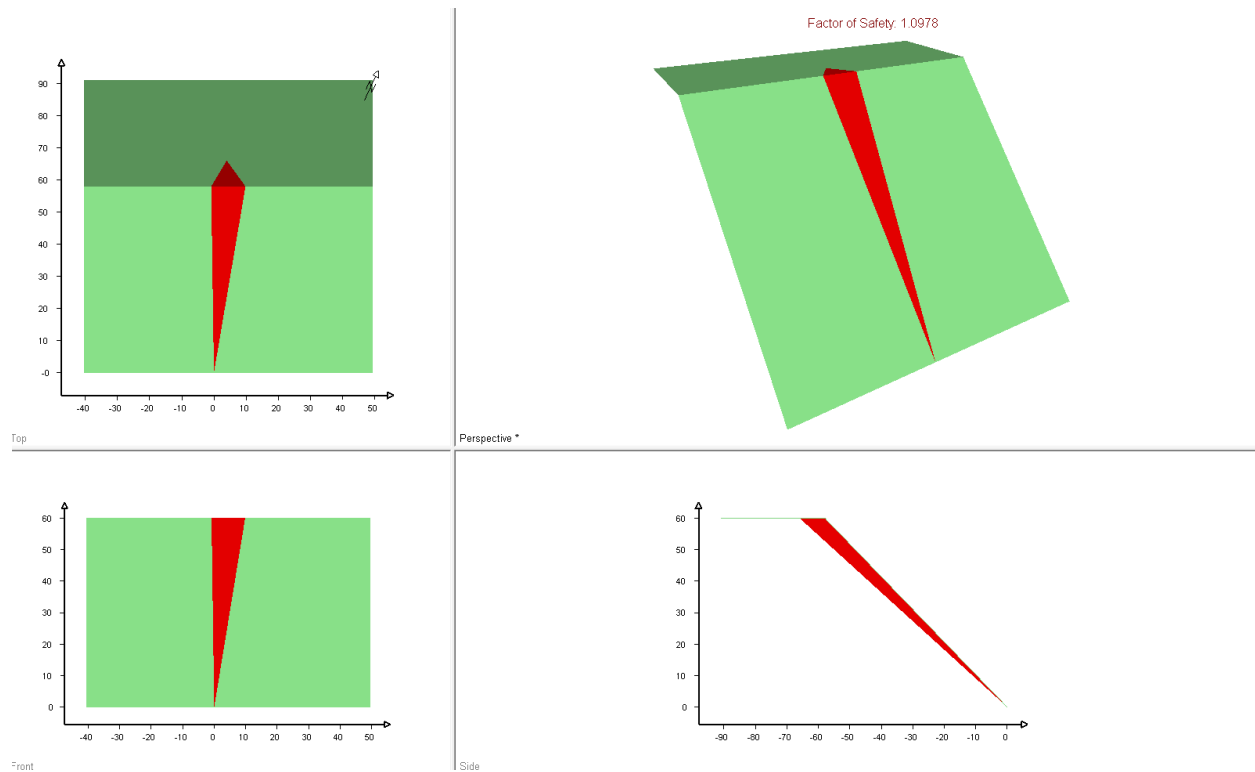


Figure 5.25 LE analysis results for wedge failure formed by F-3 & F-48 faults – case study #3

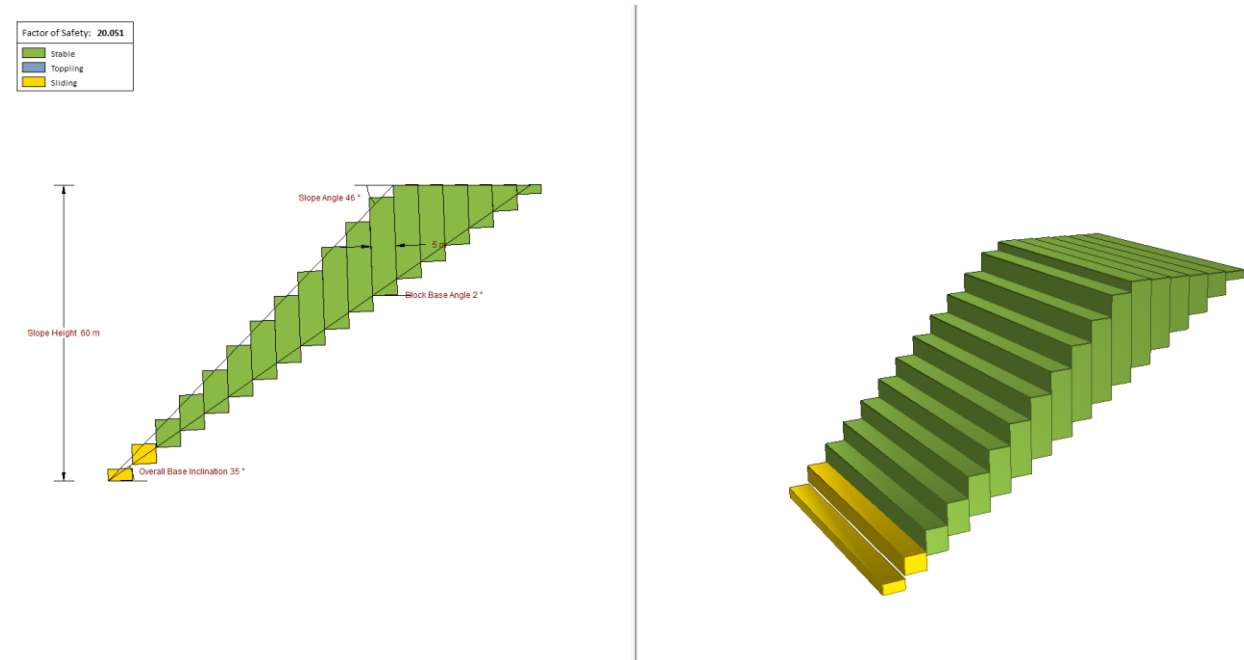


Figure 5.26 LE analysis results for toppling failure formed by F-23 fault – case study #3

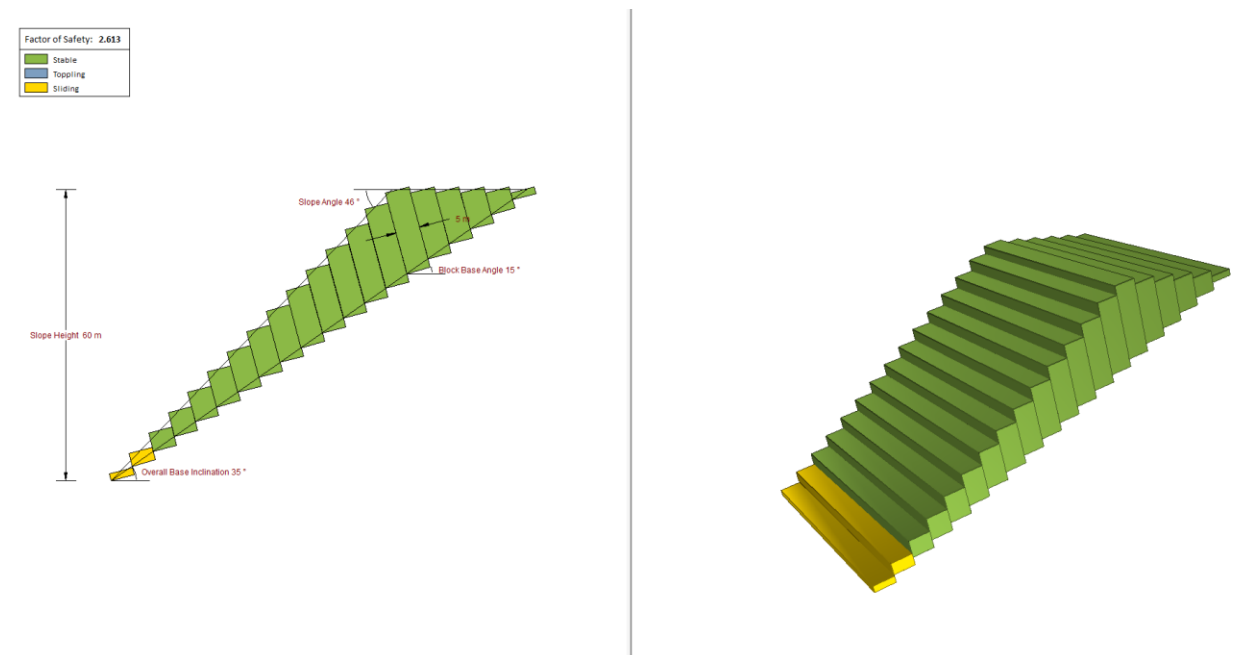


Figure 5.27 LE analysis results for toppling failure formed by F-76 fault – case study #3

5.3 Chapter Summary

In this chapter, the results of kinematic and kinetic analyses for evaluating structurally controlled failure mechanisms at the inter-ramp slope scale are presented for the three previously described case studies. Slope stability analyses were performed through a deterministic approach of major, large-scale discontinuities mapped during field geological characterization.

- The first case study dealt with the geotechnical reconciliation of an existing open pit mine. Intermediate scale structures (>25 m in length), related to a local faulting system were also mapped within the area of the pit. The inter-ramp stability assessment was carried out for a slope of 75 m in height and 46° inter-ramp angle. The results of the deterministic kinematic analysis show one potential wedge in the East sector formed by faults F-15 and F-16. For all pit other sectors, no failure potential was identified. A subsequent Limit Equilibrium (LE) analysis yielded a FoS of 3.02 for the critical wedge. Therefore, the inter-ramp slope configuration was deemed stable.
- The second case study is of an open pit mine project with limited outcrop mapping sites. From the geological field reconnaissance program, four major steeply dipping faults were identified in the future open pit area. The inter-ramp stability assessment was carried out for a slope of 50 m in height and 45° inter-ramp angle. The results of the deterministic kinematic analysis show one potential wedge in the sector #9 formed by faults F-1 and F-2. For all other pit sectors, no failure potential was identified with an IRA of 45° . A subsequent Limit Equilibrium (LE) analysis yielded a FoS of 3.79 for the critical wedge. Therefore, the inter-ramp slope configuration was deemed stable.
- Case study #3 is an open pit mine where intermediate geological discontinuities are those associated with faulting. A total of 79 local faults were mapped and described according to the ISRM suggested methods. The inter-ramp stability assessment was carried out for a slope of 60 m in height and 46° inter-ramp angle. The results of the deterministic kinematic analysis show potential wedge failure in the North and North East sectors. Also, potential for toppling failure was identified for the South West and North sectors. A subsequent Limit Equilibrium (LE) analysis of these potential failure mechanisms found FoS values to be greater than 1.3 which can be considered as the minimum required FoS at the inter-ramp slope scale. Therefore, the inter-ramp slope configuration was deemed stable.

Chapter 6

Global Pit Slope

Global scale failure mechanisms in open pit slopes are mainly controlled by the strength of the rock mass. As such, the engineering characteristics of both intact rock and discontinuities must be considered to arrive at good estimates of the rock mass strength properties. This chapter covers a summary of the main rock laboratory tests and rock mass classification schemes. Emphasis is given to the assessment of uncertainty in intact rock and rock mass Hoek-Brown strength envelopes. Finally, the global pit slope stability analysis is carried out for three case studies.

6.1 Assessment of Rock Mass Properties

The overall strength of the rock mass is determined from the characteristics of both the intact rock material and geological discontinuities. As shown in Figure 6.1, the rock mass characterization stage involves an estimation of the intact rock strength (typically obtained from rock laboratory testing) and the mechanical properties of the discontinuities (commonly assessed through mapping of surface outcrops and/or oriented core logging). A rock mass classification scheme is then used to define the rock mass quality empirically by degrading and scaling the intact rock strength envelope to that of the rock mass. Once the rock mass strength envelope is defined, the engineering design of the rock structure can be started.

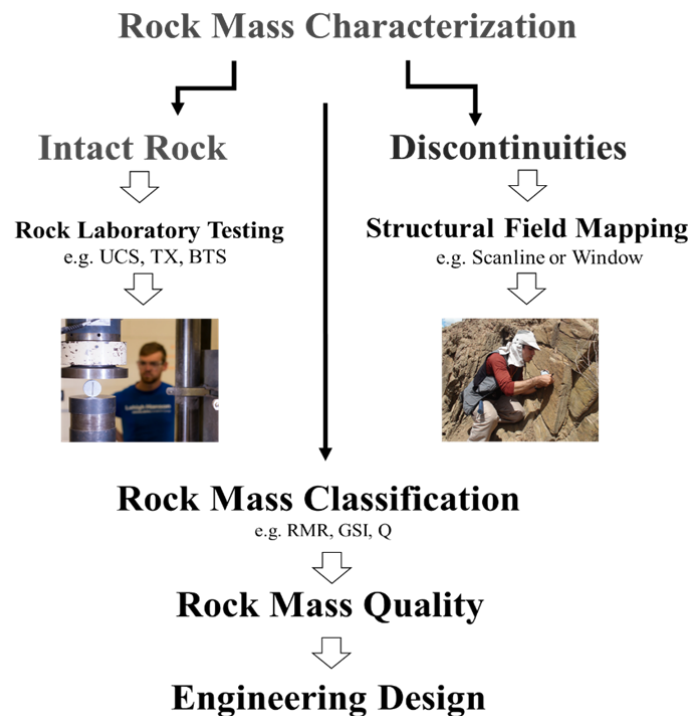


Figure 6.1 Rock mass characterization framework

6.2 Intact Rock Strength

6.2.1 Uniaxial Compressive Strength (UCS)

The UCS is one of the most commonly used parameters in calculation schemes associated with the analysis and design of rock engineering structures (Andreev, 1995). The UCS is arguably the oldest and simplest mechanical rock test that serves as a proxy for intact rock strength (Kahraman, 2001). It depends on the loading rate (e.g., Bieniawski, 1967), specimen geometry (e.g., Hudson et al., 1971), specimen size (e.g., Bieniawski 1968), and several other factors (Bewick et al., 2015). The UCS testing procedure is generally well established and it has been standardized by both the American Society for Testing and Materials (ASTM-D7012) and the International Society for Rock Mechanics (ISRM 1979). The reader is forwarded to these two references for further details on the UCS test procedure, data analysis and reporting format.

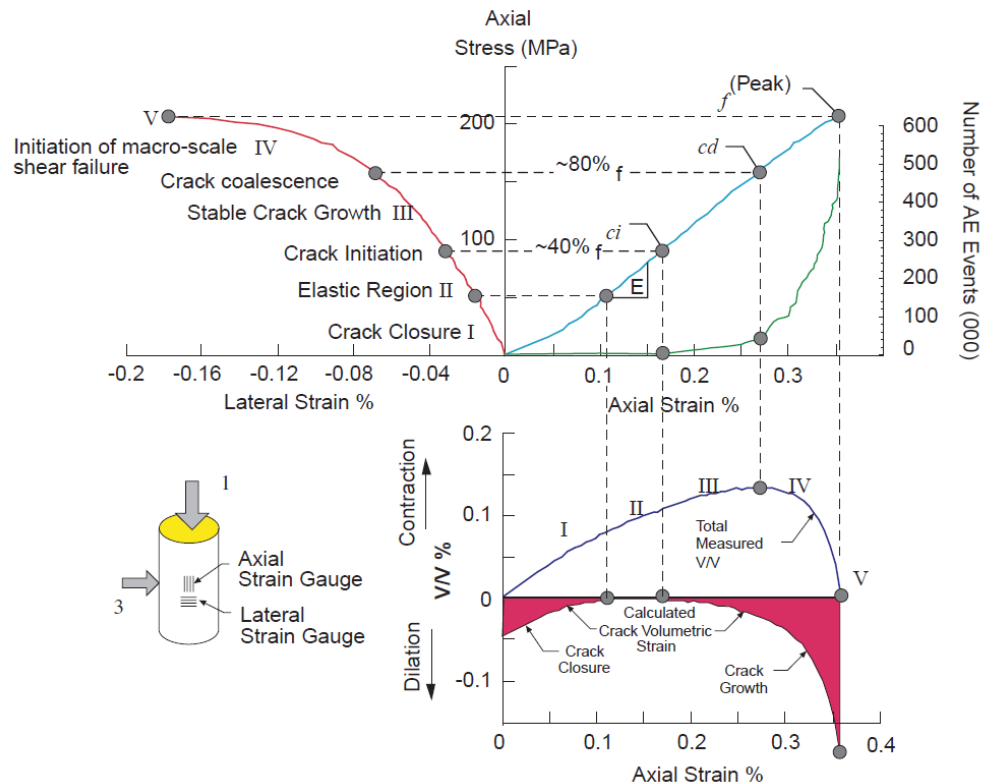


Figure 6.2 Stress–strain diagram showing the different stress levels of a rock subjected to uniaxial compression (Cai et al., 2004)

Stress-strain curves such as the one given in Figure 6.2 serve as the basis for obtaining the compressive strength, Young's modulus of elasticity and Poisson's ratio of the rock material. In this figure, it should be noted that the deformation increases almost linearly with increasing load. Nevertheless, at the very beginning of the uniaxial compression test, the stress-strain curve has a subtle and smooth concave shape that corresponds to the crack closure (σ_{cc}) stage. Eventually, a stress level is reached at which fracture

is initiated, i.e. existing cracks start to propagate, and new cracks initiate (σ_{ci}). With increasing deformation, the crack propagation is stable which means that if the stress increase is stopped, the crack propagation is also stopped. Further increasing the stress, however, leads to another stress level called the crack damage (σ_{cd}) stage, which corresponds to the long-term rock strength. At this stage unstable crack growth begins and the resulting cracks start to coalesce which means that crack propagation continues even if the stress increase is stopped. Next, macrocracks are formed followed by the failure of intact rock specimen at a stress level equal to its peak strength. This stress level at which the intact rock material fails is known as the unconfined or uniaxial, compressive strength – UCS (Jaeger et al., 2009).

6.2.2 Triaxial Compressive Strength (TX)

Triaxial compression tests have been widely used by researchers and practitioners alike to gain an understanding of the strength behavior of rocks under stress conditions simulating those encountered in surface or underground mining excavations (Elliott, 1993; Bewick et al., 2011). Triaxial testing allows to quantify the significant increase in rock strength with increasing confining pressure. Also, triaxial testing on intact rock is typically conducted to estimate the input parameters of empirical failure criteria such as the Hoek-Brown criterion considered later in this chapter. Despite its name, which implies a state of three independent principal stresses, the conventional ‘triaxial test’ simulates a special case of crustal condition, in which the intermediate and minor principal stresses are equal so that: $\sigma_1 > \sigma_2 = \sigma_3 > 0$ (Haimson & Chang, 2000). A general triaxial state of stress where all three principal stresses are varied independently is often referred to as a true triaxial or polyaxial test. Further discussion regarding true triaxial or polyaxial testing is provided by Hunsche & Albrecht (1990), Wawersik et al (1997), Kwasniewski et al (2012), Li et al (2015). These authors - among others - have studied the influence of the intermediate principal stress on rock strength behavior.

In the conventional triaxial test, a right-cylindrical rock specimen sample, prepared in the same manner as for the UCS test, is subjected to an axial stress (σ_1) while a hydrostatic (confining) stress ($\sigma_2 = \sigma_3$) is being applied on the lateral surface of the rock specimen by a pressurized fluid (Jaeger et al., 2009). Typically, several triaxial tests over a range of confining pressures should be carried out, usually up to a σ_3 magnitude of 0.3 and ideally 0.5 times the value of the expected UCS. The rock core is usually jacketed in thin latex rubber, so that the confining fluid does not penetrate the rock pore space. Also, the slenderness ratio of the rock specimen usually varies between 2:1 and 2.5:1 so that bending of the specimen under the axial load is avoided. It is not the purpose of this chapter to provide detailed guidelines of how to carry out a triaxial test and interpret the results. Such guidelines and discussion are available elsewhere, e.g. ISRM (1979) and ASTM (D4543) standards.

Figure 6.3 shows the widely used Hoek cell as a triaxial testing apparatus. This is a hollow cylinder test cell which provides an internal hydrostatic pressure. Originally developed by Hoek and Franklin (1967) at the Rock Mechanics Centre of Imperial College (London), the Hoek cell is widely used for testing cylindrical specimens of rock under triaxial compression. The popularity of the cell may be due to its proven efficiency and remarkable practicality. Its main advantage is that it does not require drainage between the tests allowing many specimens to be tested. In addition, the Hoek-Franklin cell is readily available commercially and in a variety of core sizes. The variables to be measured during the triaxial testing include the confining and the axial stress, typically measured with pressure gauges and the axial and lateral strain, commonly measured with strain gauges.

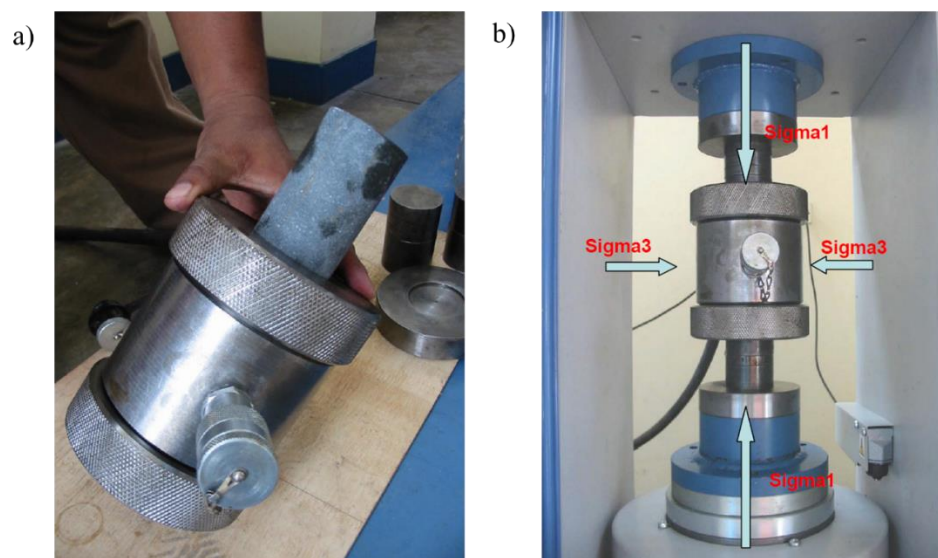


Figure 6.3 Triaxial test for rock samples a) Hoek cell and b) loading machine.

6.2.1 Brazilian Tensile Strength (BTS)

Direct tensile strength (DTS) testing is rarely carried out in practice mainly because of two main difficulties i) the preparation of the rock specimen and ii) the gripping of the rock core (Perras & Diederichs, 2014). Gripping can cause stress concentrations at the ends near the grips which may result in an invalid test. A valid direct tensile test should result in failure at the midpoint of the specimen. The Brazilian tensile strength (BTS) test is a simple indirect testing method for assessing the tensile strength of brittle material such as rocks (Li & Wong, 2013). Because of its simplicity and steadiness of the results obtained, the Brazilian test is the most widely used laboratory test to estimate the tensile strength of rocks (Jaeger et al., 2009).

In the BTS test, a thin circular disc with a thickness-to-diameter ratio between 0.2 and 0.75 is diametrically compressed up to failure. The compression induces tensile stresses normal to the loading direction, which

are essentially constant over a region around the center. The indirect tensile strength is typically calculated based on the assumption that failure occurs at the point of maximum tensile stress, i.e., at the center of the disc. The tensile strength (σ_t) is a function of the applied axial load (F), the rock disc diameter (D) and the thickness (t) and can be determined by the following equation:

$$\sigma_t = \frac{2F}{\pi Dt} \quad [\text{Eq.6.1}]$$

Testing procedure for measuring the tensile strength of rocks is given as suggested methods by the ISRM (1978) and standards by the ASTM (D3967) which outlines both direct and indirect Brazilian test methods. It should be noted that the Brazilian test specimen should split along the compressive diametral line (see Figure 6.4), or else the test is regarded as exhibiting an invalid failure mode.

A comprehensive review and analysis between DTS and BTS have been conducted by Perras and Diederichs (2014). The authors showed that BTS obtained in standard testing is generally greater than the equivalent DTS and that this relationship is rock type dependent. The factor f , in $\text{DTS} = f \cdot \text{BTS}$, was found to be approximately 0.9 for metamorphic, 0.8 for igneous and 0.7 for sedimentary rocks.

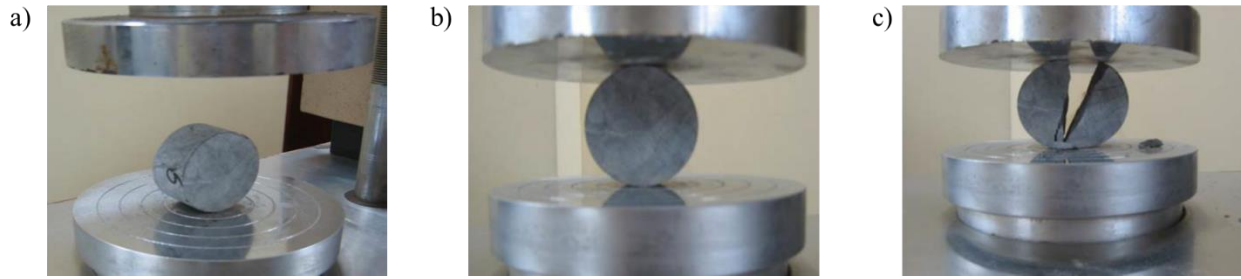


Figure 6.4 Brazilian tensile testing for rock samples a) before, b) during and c) after

6.2.2 Uncertainty in Intact Rock Strength Parameters

The Hoek-Brown model is one of the most widely used strength criteria in rock engineering practice (Bozorgzadeh et al., 2018). Although originally developed on an empirical basis through the research on brittle failure by Hoek (1965) and Brown (1970), the model's theoretical proof has recently been established (Zuo et al., 2015). The strength of intact rock material can be modelled with the simplest form of the Hoek-Brown Criterion, which may be written as (Hoek and Brown, 1980):

$$\sigma_1 = \sigma_3 + \sigma_c \left(m_i \frac{\sigma_3}{\sigma_c} + 1 \right)^{0.5} \quad [\text{Eq.6.2}]$$

Where the axial stress at failure (σ_1) is the dependent variable, the confining pressure (σ_3) is the independent variable, ' m_i ' and σ_c are the H-B model parameters to be estimated by non-linear regression analysis. The σ_c represents the value at which the best fit curve intersects the principal stress axis (σ_1). The m_i is an intact material constant that depends on the rock type.

Estimates of the H-B regression parameters (m_i and σ_c) should be obtained by combining tensile, uniaxial and triaxial test data (Langford & Diederichs, 2015; Bozorgzadeh et al., 2018; Contreras et al., 2018). Figure 6.5.a shows UCS, DTS and TX tests plotted on a σ_1 vs. σ_3 graph. It should be noted that the Brazilian test is not considered as an acceptable DTS value for inclusion in the analysis (Hoek & Brown, 2019). Therefore, adjustment factors should be applied to the BTS values. However, these must be viewed as estimates only and must be used with care and engineering judgment.

A best fit (mean) curve based on minimizing the squared residual or error is also shown in Figure 6.5.b as a continuous black line. Although simple and straightforward, this non-linear fitting approach is primarily used deterministically i.e. only the mean or average intact rock shear strength envelope is estimated. This type of analysis fails to account for the variability and uncertainty of the input rock testing data. To overcome this, a more comprehensive approach using statistical techniques is needed.

After calculating a suitable mean fit, the uncertainty in the data set can be quantified using Prediction Intervals (PI). A PI provides an estimate of the interval within which future data points will fall. For example, the interpretation of a 95% PI is that there is 95% probability that a new collected testing value will fall within the PI. These intervals are useful in providing upper and lower bounds for the testing data. Figure 6.5.b also includes the corresponding 68% and 95% PI for the data set which is given by the mean \pm one and two standard deviations.

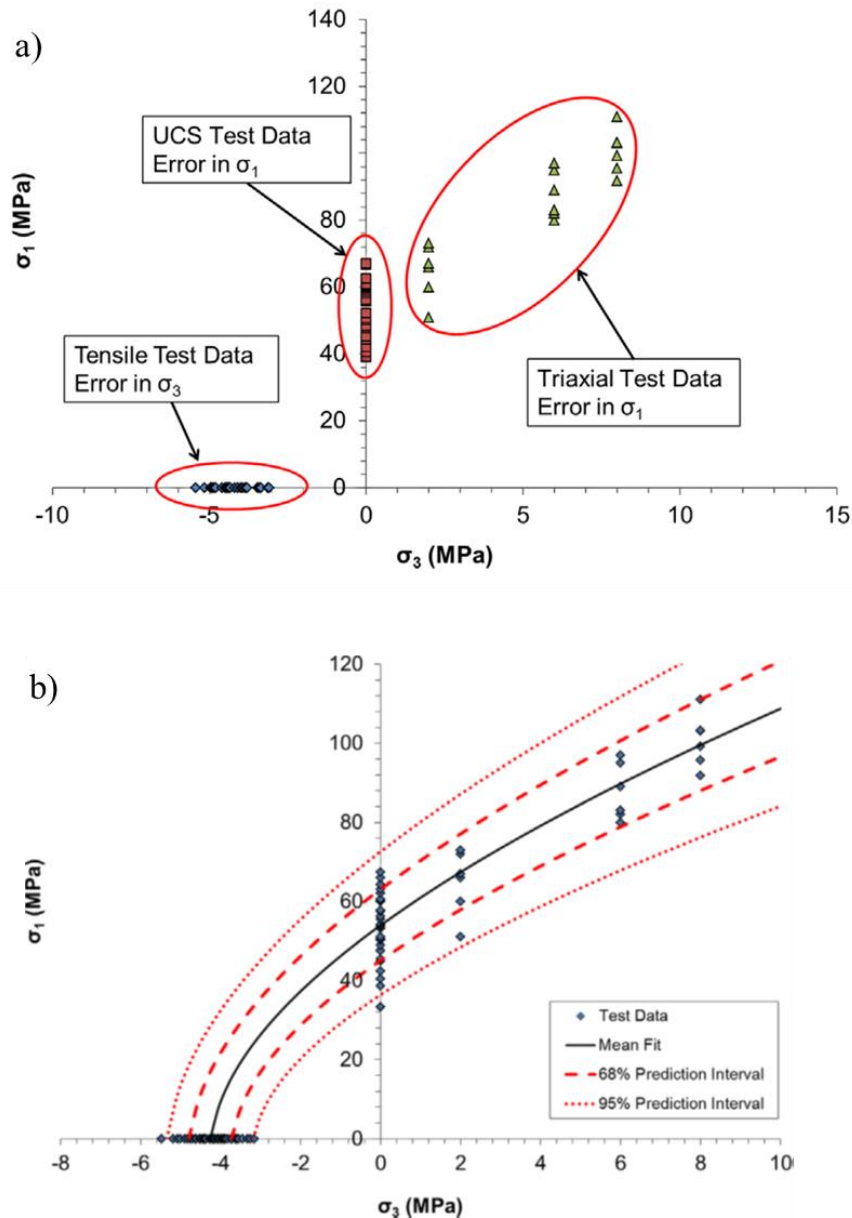


Figure 6.5 Intact rock strength envelopes. a) Combining DTS, UCS & TX tests and b) Intact rock strength variability (Langford & Diederichs, 2015)

6.3 Rock Mass Strength

The assessment of the rock mass strength is a key step for any type of stability analysis dealing with engineering structures, both open pit and underground. The general problem of rock mass strength estimation remains as one major challenge in rock mechanics. This is because laboratory tests, on the one hand, are not representative of a rock mass of significantly larger volume and in-situ large-scale rock mass testing, on the other hand, is seldom practically or economically feasible. Thus, the strength of a rock mass

is typically derived from an empirical failure criterion that combines input parameters based upon the intact rock strength, obtained through laboratory testing, and the characteristics of the rock mass, gathered from field mapping. In this respect, rock mass classification systems represent convenient tools to combine both intact rock and discontinuity properties (Sturzenegger, 2010). Rock Mass Classification Systems are briefly summarized below and their relationship with rock mass shear strength models is also addressed.

6.3.1 Rock Mass Classification Schemes

Rock mass classifications form the backbone of the empirical design approach which is widely used in rock engineering practice (Singh & Goel, 1999). Rock mass classification systems provide a framework for standardizing the data collection process related to the field site investigation (Hume, 2011). The quantitative output provided by a rock mass classification scheme is then used as input for further engineering design methods or numerical modelling software.

There are many rock mass classification systems developed for different purposes and/or applications. Since not all these classification schemes can be covered fully here, only those commonly used for rock slope engineering are addressed. The two most widely used rock mass classification systems for rock slope stability analysis and modelling are the Rock Mass Rating System (RMR) and Geological Strength Index (GSI).

Rock Mass Rating System (RMR)

The Geomechanics Classification, also known as the Rock Mass Rating (RMR) system, was initially developed by Bieniawski (1973) at the South African Council of Scientific and Industrial Research (CSIR) based upon his experience in shallow tunnels in sedimentary rocks (Singh & Goel, 1999). Since then, the RMR system has undergone subsequent refinements dealing with class boundaries and parameter ratings. Two major revisions as a result of newly added case histories were presented in 1976 and 1989 (Bieniawski, 1976; Bieniawski, 1989), also referred to as RMR₇₆ and RMR₈₉, respectively. Because of the different RMR versions, it is important to state which one is being used when RMR values are reported.

The RMR classification uses the following parameters whose ratings are added to obtain an RMR value.

- 1) Unconfined compressive strength of intact rock (UCS)
- 2) Rock Quality Designation (RQD)
- 3) Joint or discontinuity spacing
- 4) Condition of discontinuities
- 5) Groundwater conditions
- 6) Orientation of discontinuities

A. CLASSIFICATION – PARAMETERS AND THEIR RATINGS									
Parameter			Range of values						
1	Strength of intact rock material	Point-load strength index	>10 MPa	4 - 10 MPa	2 - 4 MPa	1 - 2 MPa	For this low range - uniaxial compressive test is preferred		
		Uniaxial comp. strength	>250 MPa	100 - 250 MPa	50 - 100 MPa	25 - 50 MPa	5 - 25 MPa	1 - 5 MPa	< 1 MPa
	Rating		15	12	7	4	2	1	0
2	Drill core Quality <i>RQD</i>		90% - 100%	75% - 90%	50% - 75%	25% - 50%	< 25%		
	Rating		20	17	13	8	3		
3	Spacing of discontinuities		> 2 m	0.6 - 2 . m	200 - 600 mm	60 - 200 mm	< 60 mm		
	Rating		20	15	10	8	5		
4	Condition of –discontinuities (See E)		Very rough –surfaces Not continuous No separation Unweathered rock	Slightly rough sur-faces Separation < 1 mm Slightly weathered walls	Slightly rough sur-faces Separation < 1 mm Highly weathered walls	Slickensided surfaces or Gouge < 5 mm thick or Separation 1-5 mm Continuous	Soft gouge >5 mm thick or Separation → > 5 mm Continuous		
	Rating		30	25	20	10	0		
5	Ground water	Inflow per 10 m tunnel length (l/m)	None	< 10	10 - 25	25 - 125	> 125		
		(Joint water press)/ (Major principal σ)	0	< 0.1	0.1, - 0.2	0.2 - 0.5	> 0.5		
		General conditions	Completely dry	Damp	Wet	Dripping	Flowing		
	Rating		15	10	7	4	0		
B. RATING ADJUSTMENT FOR DISCONTINUITY ORIENTATIONS (See F)									
Strike –and dip orientations			Very favourable	Favourable	Fair	Unfavourable	Very Unfavourable		
Ratings	Tunnels & mines		0	-2	-5	-10	-12		
	Foundations		0	-2	-7	-15	-25		
	Slopes		0	-5	-25	-50			
C. ROCK MASS CLASSES DETERMINED FROM TOTAL RATINGS									
Rating			100 ← 81	80 ← 61	60 ← 41	40 ← 21	< 21		
Class number			I	II	III	IV	V		
Description			Very good rock	Good rock	Fair rock	Poor rock	Very poor rock		
D. MEANING OF ROCK CLASSES									
Class number			I	II	III	IV	V		
Average stand-up time			20 yrs for 15 m span	1 year for 10 m span	1 week for 5 m span	10 hrs for 2.5 m span	30 min for 1 m span		
Cohesion of rock mass (kPa)			> 400	300 - 400	200 - 300	100 - 200	< 100		
Friction angle of rock mass (deg)			> 45	35 - 45	25 - 35	15 - 25	< 15		
E. GUIDELINES FOR CLASSIFICATION OF DISCONTINUITY conditions									
Discontinuity length (persistence)			< 1 m	1 - 3 m	3 - 10 m	10 - 20 m	> 20 m		
Rating			6	4	2	1	0		
Separation (aperture)			None	< 0.1 mm	0.1 - 1.0 mm	1 - 5 mm	> 5 mm		
Rating			6	5	4	1	0		
Roughness			Very rough	Rough	Slightly rough	Smooth	Slickensided		
Rating			6	5	3	1	0		
Infilling (gouge)			None	Hard filling < 5 mm	Hard filling > 5 mm	Soft filling < 5 mm	Soft filling > 5 mm		
Rating			6	4	2	2	0		
Weathering			Unweathered	Slightly weathered	Moderately weathered	Highly weathered	Decomposed		
Ratings			6	5	3	1	0		
F. EFFECT OF DISCONTINUITY STRIKE AND DIP ORIENTATION IN TUNNELLING**									
Strike perpendicular to tunnel axis					Strike parallel to tunnel axis				
Drive with dip - Dip 45 - 90°			Drive with dip - Dip 20 - 45°		Dip 45 - 90°		Dip 20 - 45°		
Very favourable			Favourable		Very favourable		Fair		
Drive against –dip - Dip 45-90°			Drive against –dip - –Dip 20-45°		–Dip 0-20 - Irrespective of strike°				
Fair			Unfavourable		Fair				

* Some conditions are mutually exclusive . –For example, if infilling is present, the roughness of the surface will be overshadowed by the influence of the gouge. –In such cases use A.4 directly.

** Modified after Wickham et al (1972).

Figure 6.6 Rock Mass Rating (RMR₈₉) System after Bieniawski (1989)

Information on these six parameters can be collected from either surface mapping or core logging. It should be noted, however, that joint persistence is the only parameter that cannot be measured through core logging as explained in Chapters 3 and 4. Once field data is gathered, they are assigned a relative weighting or rating value according to the system. As shown in Figure 6.6, the input RMR parameters are not equally important since they all have different ratings. The first five parameters are given non-negative weighting values whereas the sixth parameter can take up negative values. This sixth parameter is an adjustment factor accounting for the favorable or unfavorable orientation of discontinuities with respect to the engineering excavation. It is seldom used when evaluating the rock mass for rock slope engineering purposes. When adding the ratings of the first five parameters, one would obtain the so-called basic RMR (RMR_b) that symbolizes the rock mass quality. The RMR values are grouped into five classes as shown in Table 6.1.

Table 6.1 Rock mass classes based on the RMR system (Bieniawski, 1989)

Rock Mass Parameter	Rock Mass Rating						
Ratings	100 – 81	80 - 61	60 - 51	50 - 41	40 - 31	30 - 21	20 - 0
Class No.	I	II	III-A	III-B	IV-A	IV-B	V
Classification of Rock Mass	Very Good	Good	Fair		Poor		Very Poor
Rock Mass Cohesion	>400 kPa	300-400 kPa	200-300 kPa		100-200 kPa		<100 kPa
Rock Mass Friction Angle	>45°	35°-45°	25°-35°		15°-25°		<15°

Readers who wish to pursue further details on the Rock Mass Rating (RMR) System are advised to consult the work by Singh & Goel (1999, 2011), Bieniawski (1988, 1989, 1993).

Geological Strength Index (GSI)

The Geological Strength Index (GSI) system was introduced by Hoek and coworkers (Hoek, 1994; Hoek et al., 1995) and was developed to overcome some of the deficiencies that had been identified in using the RMR scheme for very poor quality rock masses (Brady & Brown, 1993; Eberhardt, 2010). The GSI value together with the properties of the intact rock have been widely used to estimate rock mass strength and deformation properties for different geological conditions. (Shu, 2014).

GEOLOGICAL STRENGTH INDEX FOR JOINTED ROCKS (Hoek and Marinos, 2000)

From the lithology, structure and surface conditions of the discontinuities, estimate the average value of GSI. Do not try to be too precise. Quoting a range from 33 to 37 is more realistic than stating that GSI=35. Note that the table does not apply to structurally controlled failures. Where weak planar structural planes are present in an unfavorable orientation with respect to the excavation face, these will dominate the rock mass behavior. The shear strength of surfaces in rocks that are prone to deterioration as a result of changes in moisture content will be reduced if water is present. When working with rocks in the fair to very poor categories, a shift to the right may be made for wet conditions. Water pressure is dealt with by effective stress analysis.

SURFACE CONDITIONS

VERY GOOD

Very rough, fresh unweathered surfaces

GOOD

Rough, slightly weathered, iron stained surfaces

FAIR

Smooth, moderately weathered and altered surfaces

POOR


Slacksided, highly weathered surfaces with compact coatings or fillings or angular fragments


VERY POOR


Slacksided, highly weathered surfaces with soft clay coatings or fillings


STRUCTURE


DECREASING SURFACE QUALITY →


 INTACT OR MASSIVE—intact rock specimens or massive *in situ* rock with few widely spaced discontinuities

 BLOCKY—well interlocked undisturbed rock mass consisting of cubical blocks formed by three intersecting discontinuity sets

 VERY BLOCKY—interlocked, partially disturbed mass with multi-faceted angular blocks formed by 4 or more joint sets

 BLOCKY/DISTURBED/SEAMY—folded with angular blocks formed by many intersecting discontinuity sets. Persistence of bedding planes or schistosity

 DISINTEGRATED—poorly interlocked, heavily broken rock mass with mixture of angular and rounded rock pieces

 LAMINATED/SHEARED—lack of blockiness due to close spacing of weak schistosity or shear planes

DECREASING INTERLOCKING OF ROCK PIECES ↓

90

80

70

60

50

40

30

20

10

N/A

N/A

N/A

N/A

Figure 6.7 Geological Strength Index (GSI) lookup chart for rock masses (Marinos & Hoek 2000).

The GSI number varies theoretically in the nominal range of 0 and 100, which is essentially the same range of rock mass quality covered by the RMR system. The GSI is based on a qualitative visual inspection of the rock mass by describing field conditions such as the interlocking of intact rock pieces and the joint surface quality. Marinos and Hoek (2000) proposed a GSI chart to classify rock mass quality by visual inspection alone. This is shown in Figure 6.7. GSI should ideally be assigned from field observation of the rock mass by suitably experienced engineering geological personnel. GSI values can sufficiently be determined from outcrop mapping, however, it cannot be directly assigned from drill core data. In the latter case, it is suggested to evaluate the core in terms of the 1989 version of Bieniawski's RMR classification and then use the expression: $GSI = RMR_{89} - 5$, where RMR_{89} has the groundwater rating set to 15 and the adjustment for joint orientation set to zero (Bieniawski, 1989). Thus, in the absence of GSI values, it can be obtained from RMR_{89} values as this is still of common practice in rock slope engineering.

Readers who wish to pursue further details on the Geological Strength Index (GSI) System are advised to consult the work by Sonmez & Ulusay (1999), Marinos & Hoek (2000), Marinos et al (2005, 2007), Hoek et al. (2013).

6.3.2 Rock Mass Shear Strength Models

The overall strength of a jointed rock mass depends on the mechanical properties of the intact rock pieces as well as the condition of the discontinuity surfaces separating those pieces. This section briefly describes current methods for estimating rock mass shear strength, as this is needed to perform slope stability analyses, based on the Generalized Hoek-Brown (G-H-B) and Equivalent Mohr-Coulomb (E-M-C) criteria.

It should be noted that the above-mentioned criteria should only be used when there is a large number of closely spaced discontinuities so that an isotropic rock mass behavior can be an adequate assumption. Such situation for rock slopes is mainly encountered at the global or overall scale of an open pit mine.

Generalized Hoek-Brown Model

The Generalized Hoek-Brown failure criterion for jointed rock masses is defined by Equation 6.3 (Hoek et al., 2002):

$$\sigma_1' = \sigma_3' + \sigma_c \left(m_b \frac{\sigma_3'}{\sigma_c} + s \right)^a \quad [\text{Eq.6.3}]$$

where σ_1' and σ_3' are the maximum and minimum effective stresses at failure respectively, m_b , s and a are constants which depend upon the characteristics of the rock mass, and σ_c is the uniaxial compressive strength of the intact rock. The material constants are determined for the rock mass using GSI as per Hoek et al. (2002) as follows.

$$m_b = m_i \exp\left(\frac{GSI-100}{28-14D}\right) \quad [\text{Eq.6.4}]$$

$$s = \exp\left(\frac{GSI-100}{9-3D}\right) \quad [\text{Eq.6.5}]$$

$$a = \frac{1}{2} + \frac{1}{6} \left(e^{-GSI/15} - e^{-20/3} \right) \quad [\text{Eq.6.6}]$$

In the above, m_i is a curve fitting parameter derived by combining tensile, uniaxial compressive and triaxial testing of intact rock as shown previously in section 6.2.3. The parameter m_b is therefore a reduced value of the intact rock value m_i , which accounts for the strength reducing effects of the rock mass conditions defined by GSI. GSI is estimated in the field from the chart shown in section 6.3.1. Strength reduction of the parameters s and a is done accordingly. D is a disturbance factor that can account for blast damage and stress relaxation, with values ranging from 0 for undisturbed conditions to 1 for very disturbed rock masses. Figure 6.8 shows the suggested D values for slopes and underground excavations.

excavations.



Small-scale blasting in civil engineering slopes results in modest rock mass damage when controlled blasting is used, as shown on the left-hand side of the photograph. Uncontrolled production blasting can result in significant damage to the rock face.

$D = 0.5$ for controlled presplit or smooth wall blasting with
 $D = 1.0$ for production blasting



In some weak rock masses, excavation can be carried out by ripping and dozing. Damage to the slopes is due primarily to stress relief.

Very large open pit mine slopes suffer significant disturbance due to heavy production blasting and stress relief from overburden removal.

$D = 0.7$ for mechanical excavation effects of stress reduction damage

$D = 1.0$ for production blasting

A transitional D relationship incorporating the effects of stress relaxation can be derived from the disturbance rating*

Figure 6.8 Guidelines for estimating disturbance factor D due to stress relaxation and blasting damage (Hoek & Brown, 2019)

The non-linear generalized Hoek – Brown criterion arrives at the strength envelope to the rock mass through the GSI index. This method allows us to estimate the rock mass strength envelope based on that of the intact rock which in turn is obtained through laboratory testing (e.g. BTS, UCS, TX). Thus, the generalized Hoek – Brown criterion basically weakens and scale the intact rock properties to that of the rock mass by means of the GSI value (Figure 6.9).

(Figure 6.9).

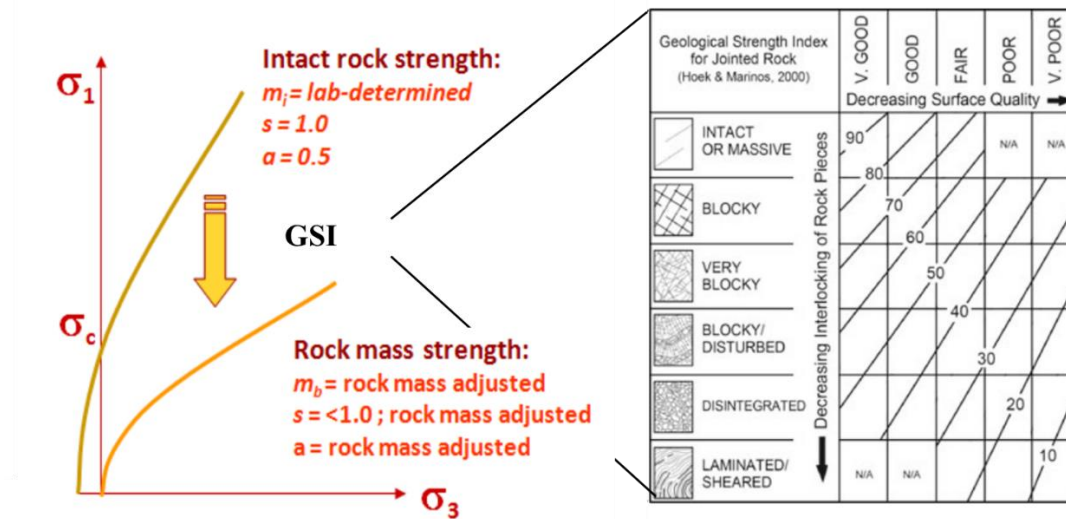


Figure 6.9 Transition of the Hoek-Brown envelope for intact rock to that for rock mass (Eberhardt, 2012)

The generalized Hoek–Brown criterion has been updated several times in response to experience gained with its use and the availability of more case studies. The most up-to-date version is given in Hoek & Brown (2019). This represents a detailed re-examination of the Hoek–Brown criterion during the past 38 years of its use to practical rock engineering problems.

Equivalent Mohr-Coulomb Model

Mohr-Coulomb's strength criterion for a rock mass is expressed as:

$$\tau = c + \sigma_n \tan \phi \quad [\text{Eq.6.7}]$$

Where τ is the shear strength along a plane of failure, σ_n is the normal stress acting on that same plane, c is cohesion and ϕ is the angle of friction. The Mohr-Coulomb's criterion is applied in rock mechanics for shear failure of rock joints and rock masses. As opposed to the Generalized Hoek-Brown criterium which is plotted on the principal stress plot (σ_1 vs σ_3), the Mohr-Coulomb's model is plotted on the normal(σ_n) vs shear (τ) plot (Figure 6.10). However, it can also be re-written in the following form:

$$\sigma_1 = \sigma_c + k\sigma_3 \quad [\text{Eq.6.8}]$$

Where k is the slope of the line relating σ_1 and σ_3 and, is σ_c the uniaxial compressive strength. The values of the friction angle (ϕ) and cohesion (c) can then be calculated using:

$$\sin\phi = \frac{k-1}{k+1} \quad [\text{Eq.6.9}]$$

$$c = \frac{\sigma_c(1-\sin\phi)}{2\cos\phi} \quad [\text{Eq.6.10}]$$

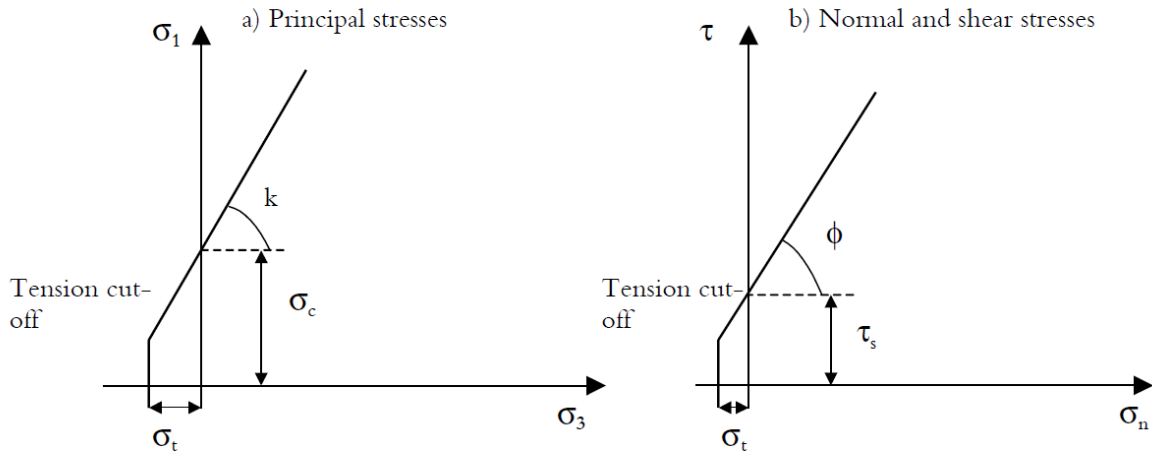


Figure 6.10 Mohr-Coulomb criterion in terms of a) Principal stresses and b) Normal and Shear stresses (Edelbro, 2003)

The use of the M-C criterion for representing the shear strength of the rock mass is done by fitting an average linear relationship to the non-linear H-B strength criterion for a range of stress confinement (σ_3). Thus, equivalent rock mass friction angles and cohesive strengths can be calculated from the Hoek-Brown parameters (Figure 6.11). The following equations can be used to assess the equivalent friction (ϕ) angle and cohesion (c) of the rock mass.

$$\phi' = \sin^{-1} \left[\frac{6am_b(s+m_b\sigma'_{3n})^{a-1}}{2(1+a)(2+a)+6am_b(s+m_b\sigma'_{3n})^{a-1}} \right] \quad [\text{Eq.6.11}]$$

$$c' = \frac{\sigma_{ci}[(1+2a)s+(1-a)m_b\sigma'_{3n}](s+m_b\sigma'_{3n})^{a-1}}{(1+a)(2+a)\sqrt{1+(6am_b(s+m_b\sigma'_{3n})^{a-1})/((1+a)(2+a))}} \quad [\text{Eq.6.12}]$$

Where $\sigma'_{3n} = \sigma'_{3max} / \sigma_{ci}$. Note that the value of σ'_{3max} represents the upper limit of confining stress over the relationship between the Hoek-Brown and Mohr-Coulomb failure envelopes is considered. The results of the studies using the circular failure analysis of Bishop for a wide range of slopes geometries and properties of rock masses have given the following empirical relationship (Hoek et al. 2002).

$$\frac{\sigma'_{3max}}{\sigma'_{cm}} = 0.72 \left(\frac{\sigma'_{cm}}{\gamma H} \right)^{-0.91} \quad [\text{Eq.6.13}]$$

where σ'_{cm} is the strength of the rock mass, defined as $(2c' \cos \phi') / (1 - \sin \phi')$, γ is the unit weight of the rock mass, H is the height of the slope.

The procedure for determining the Hoek-Brown and equivalent Mohr-Coulomb parameters can be carried out by using the Rocscience software package RocData. These relationships can also be easily implemented through an Excel spreadsheet.

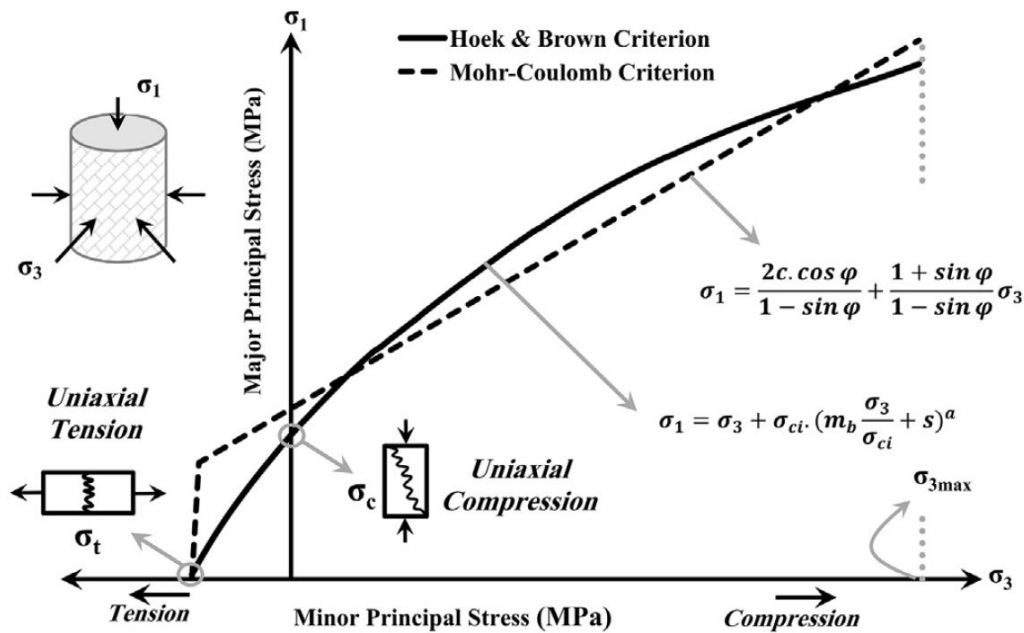


Figure 6.11 Relationship between maximum/minimum principal stresses of Hoek-Brown criterion and equivalent values obtained using Mohr-Coulomb criterion (Panji et al., 2016)

The conversion from H-B to M-C parameters is sometimes necessary given that most geotechnical software is written in terms of the Mohr-Coulomb parameters c and ϕ . Where geotechnical design software accepts Hoek-Brown input directly, it is preferable to use this input rather than estimates of the Mohr Coulomb parameters c and ϕ extrapolated from the non-linear Hoek-Brown failure envelope.

One of the reasons that the M-C criterium is often used in rock mechanics is that it is described by a simple mathematical expression, easily understood and simple to use. Also, there is more experience in its used, and this gives an intuitive feeling for the physical meanings of cohesion and friction, which is not the case for m_b , s and a . In terms of equivalencies, the parameter m_b is related to the frictional strength of the rock mass, and s , which is a measure of how fractured the rock mass is, is related to the rock mass cohesion. However, these are only descriptive relationships.

6.3.3 Uncertainty in Rock Mass Strength Parameters

Traditionally, the rock mass strength can be evaluated using a deterministic approach resulting in a single or mean rock mass strength envelope. As rock masses have a complex and uncertain nature, to deal with such complexity, the use of probabilistic approaches seems to be more appropriate in order to make more reliable characterizations in rock mass strength parameters (Basarir et al., 2016).

Figure 6.12 shows the procedure for estimating the variability in the rock mass strength envelopes through a Monte Carlo simulation method. First, RMR and/or GSI values are determined in the field based on the geological description of rock mass structure and block surface conditions. The five input parameters for the RMR (i.e. UCS, RQD, Spacing, Joint Condition and Water Condition) are considered as random input variables. This defines the range of each variable, given by its probability density function (PDF). A Monte Carlo simulation is then run to sample from these five distributions in order to arrive at the PDF of the RMR values. By using suitable conversion relationships, the PDF of GSI values can be obtained from the RMR distribution. Using the simulated probability density distributions of GSI with the uncertainty in intact rock parameters quantified from laboratory testing (UCS and m_i) the Hoek-Brown rock mass parameters can be estimated, i.e. ' m_b ', ' s ' and ' a '. It should be noted that a PDF for the Disturbance Factor (D) should also be assigned for Monte Carlo simulation. This D factor is typically obtained from previous experience or expert judgment.

The main benefit of the presented approach is the possibility of obtaining not only the expected value but also the variability in rock mass strength. Therefore, a much more complete understanding of rock mass behaviour is obtained. The different strength envelopes written in terms of the principal stresses (σ_1 vs σ_3) are also shown in Figure 6.12 as the final output of the Monte Carlo simulation approach. After characterization of the rock mass strength variability, a probabilistic stability analysis can be performed to calculate the probability of failure of a given rock slope.

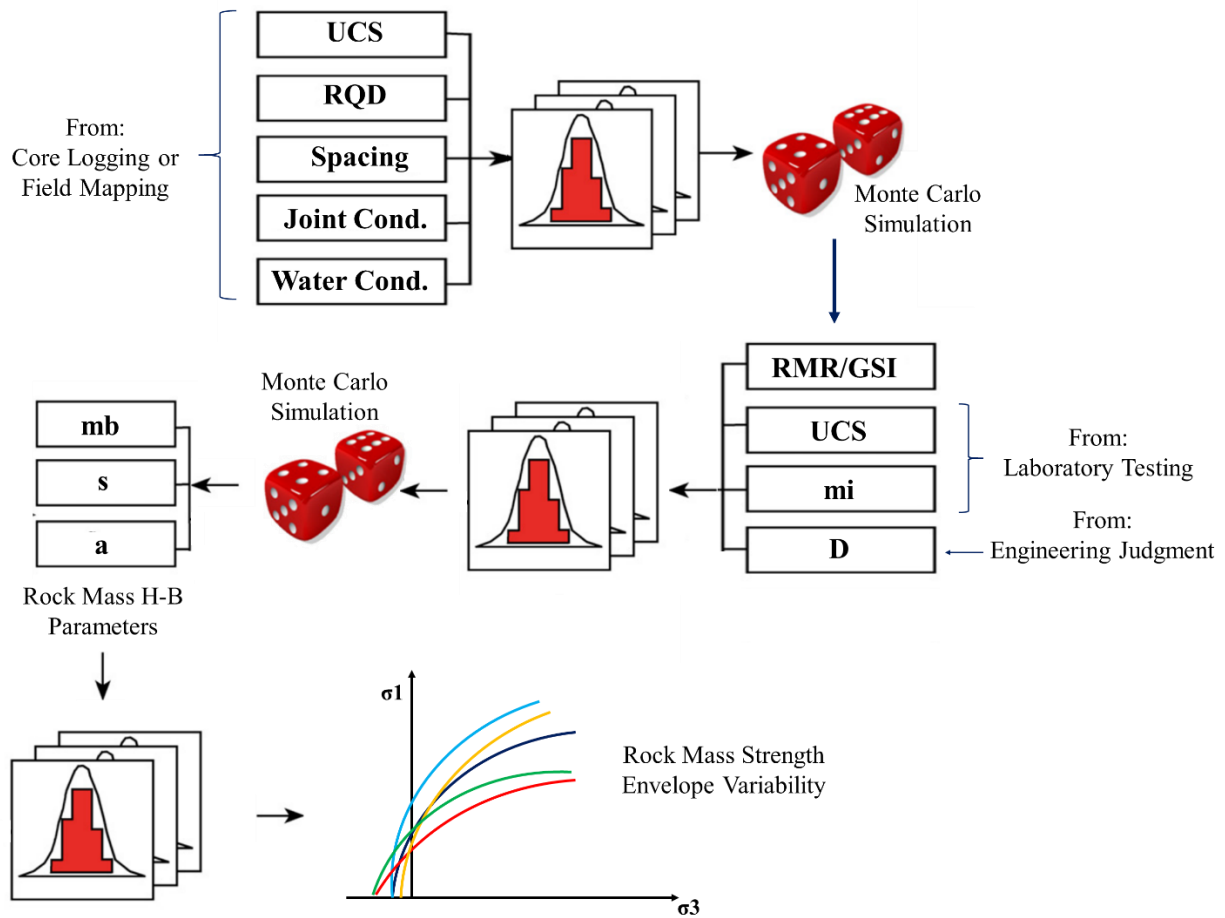


Figure 6.12 Monte Carlo simulation approach for estimation of Hoek-Brown rock mass parameters

6.4 Case Studies

In the following sections, three case studies, previously presented in chapters 4 and 5, will be assessed at the global scale slope. Both deterministic and probabilistic slope stability analyses are carried out by conventional limit equilibrium analyses using the Slide2D software from Rocscience Inc.

6.4.1 Case Study #1

Rock Mass Characterization

Field data collection was carried out for rock mass characterization purposes to support the development of a geotechnical model suitable for the open pit slope stability evaluation. Rock mass structural characteristics were measured directly by surface mapping on the existing bench slope faces. Field data collection consisted of geotechnical mapping and largely subjective observations of existing pit wall conditions for zone 05 of the open pit mine. Rock mass characterization was made using the Bieniawski (1989) RMR rock

mass classification system at each of the 36 mapping sites. The empirical relationship given as (Bieniawski, 1989)

$$\text{GSI} = \text{RMR}_{89} - 5 \quad [\text{Eq.6.13}]$$

was used to derive GSI values from RMR_{89} field measurements. A statistical analysis of the RMR data collected for zone 05 of the open pit mine showed that it follows a normal distribution with a mean and standard deviation of 40 and 15, respectively (Figure 6.13.a). Likewise, GSI calculated values were found to follow a normal distribution with a mean and standard deviation of 35 and 15, respectively (Figure 6.13.b). This indicates that the rock mass in the pit area is generally fair to poor quality as the RMR ranges from 20 to 60 and it classifies as a disturbed to very blocky rock mass based on the range of GSI values. Observations of no ‘significant’ seepage from pit walls during field mapping was reported and therefore the rock mass hydrogeological conditions are expected to be dry.

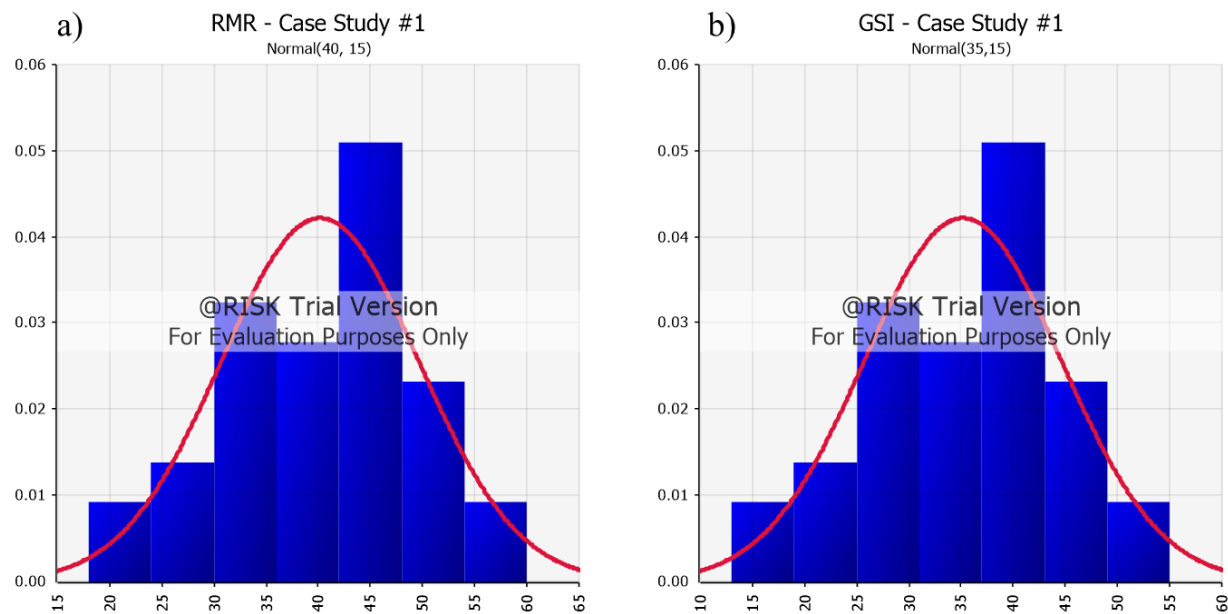


Figure 6.13 Histogram of rock mass characterization parameters a) RMR and b) GSI – Case study #1

Intact Rock Strength

Previous laboratory information comprised uniaxial compressive strength (UCS) testing conducted on 30 rock samples taken from zone 07 of the open pit mine. A distinction of the results was made based on the rock alteration type. Results for the UCS testing are summarized as box plots in Figure 6.14. From this, high UCS values can be thought to have resulted from silicification whereas an important decrease in the

rock is observed for the argillic alteration type. From a geomechanical standpoint silicification would be desirable as it would strengthen the host rock. On the contrary, argillic alteration would weaken the rock preventing us from cutting steeper slopes. Upon post-testing examination of the samples, it was noted that one belonging to a silicification alteration type had a very high value (293.3 MPa). This can presumably be due to the varying degree of silicification which increases with depth. It should be noted that zone 07 of the open pit mine is not the case study we are dealing with. However, the UCS test results from this neighbour zone gives us some reference of the UCS range value to be expected.

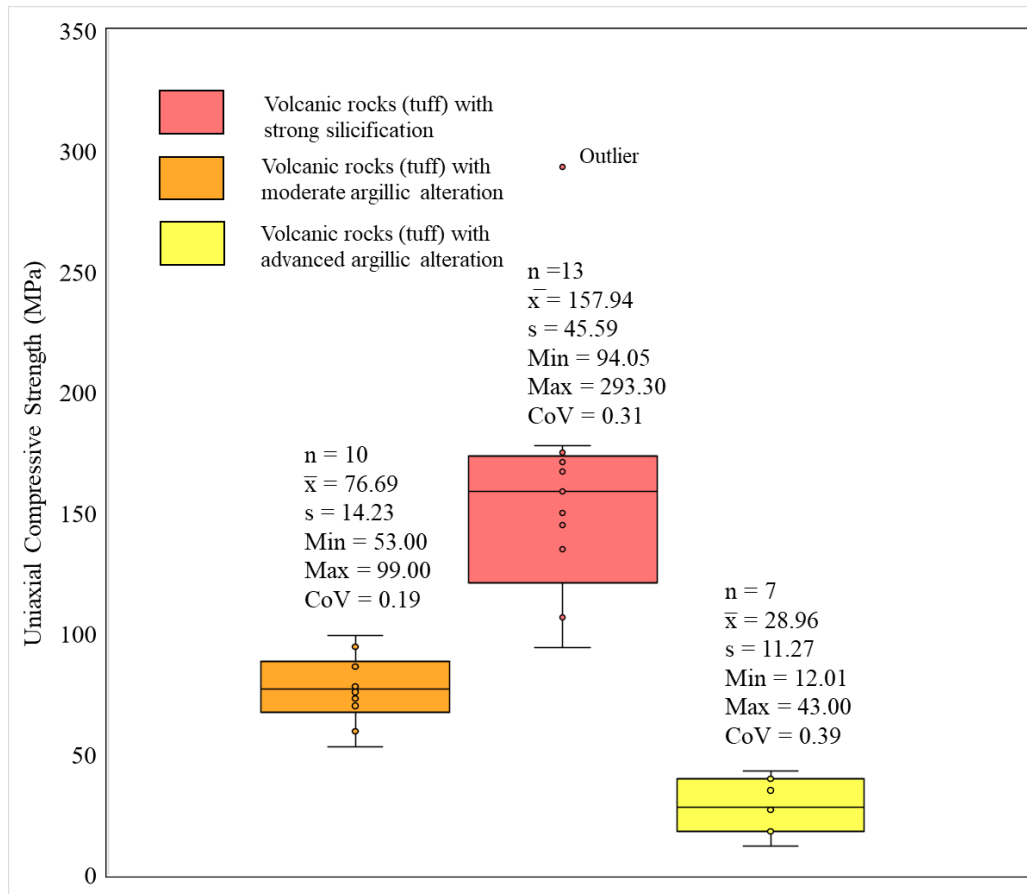


Figure 6.14 Box plots showing the Uniaxial Compressive Strength (UCS) of rock samples – case study #1

The case study presented in this section corresponds to zone 05. Rock types present within this zone show two main hydrothermal alteration types i.e. moderate and advanced argillic. Field estimates of intact rock strength for rock samples collected in zone 05 were obtained through PLT testing performed at each mapping site. PLT values were then converted to UCS estimates using the empirical equation:

$$UCS = 24 * I_{s50} \quad [Eq.6.13]$$

Where Is_{50} is the point load strength index corrected to a standard equivalent diameter (De) of 50 mm (Broch & Franklin, 1972).

Figure 6.15.a shows the distribution of UCS estimated values from PLT tests. It shows that UCS can be approximated as a lognormal distribution with mean 45 MPa and standard deviation of 15 MPa. The upper and lower expected bounds for the UCS values were defined as 25 and 85 MPa, respectively. This means that the rock is expected to have predominantly low to medium compressive strength (25-85 MPa). The m_i is an intact material constant that depends on the rock type. Hoek et al. (2002) suggest m_i value of 13 ± 5 for pyroclastic rocks such as tuff or ignimbrite. For this case study, a range of m_i between 5 and 12 with a most likely value of 7 was chosen based on the author's experience in dealing with similar materials. The distribution of m_i values was assumed to follow a triangular distribution as shown in Figure 6.15.b.

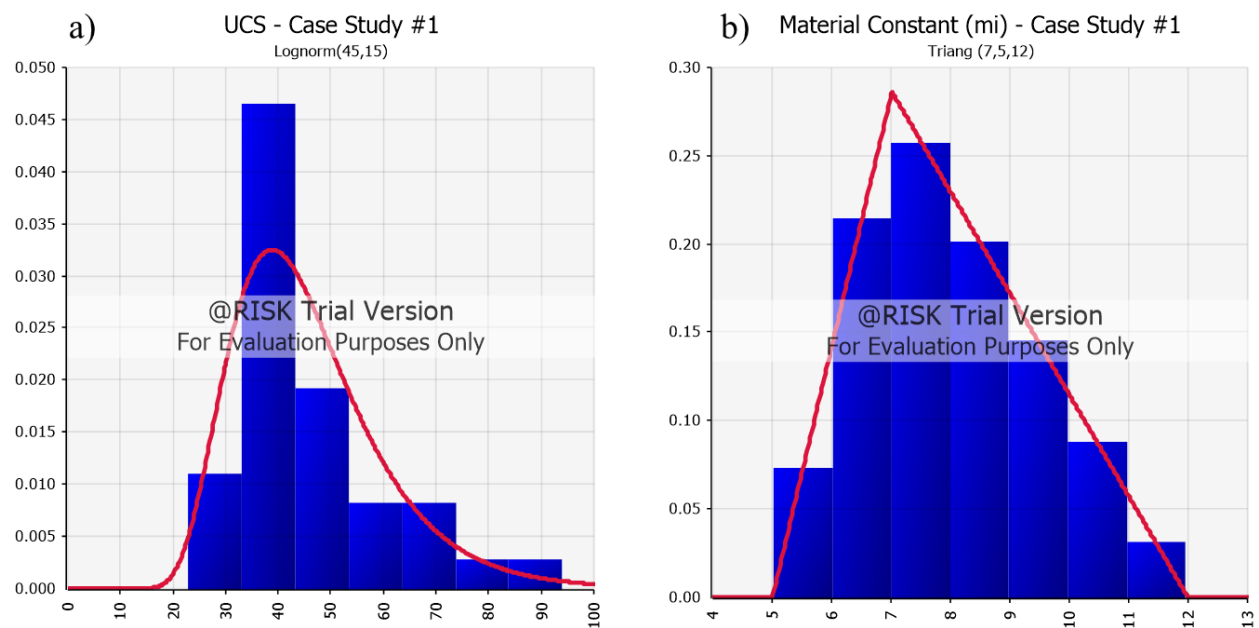


Figure 6.15 Intact rock properties a) UCS and b) m_i values – case study #1

The intact rock strength envelope for case study #1 is shown in Figure 6.16. Since neither triaxial nor Brazilian tensile testing was available at the time of this research, the envelopes were fitted to UCS tests data plus the assumption of m_i minimum and maximum expected values.

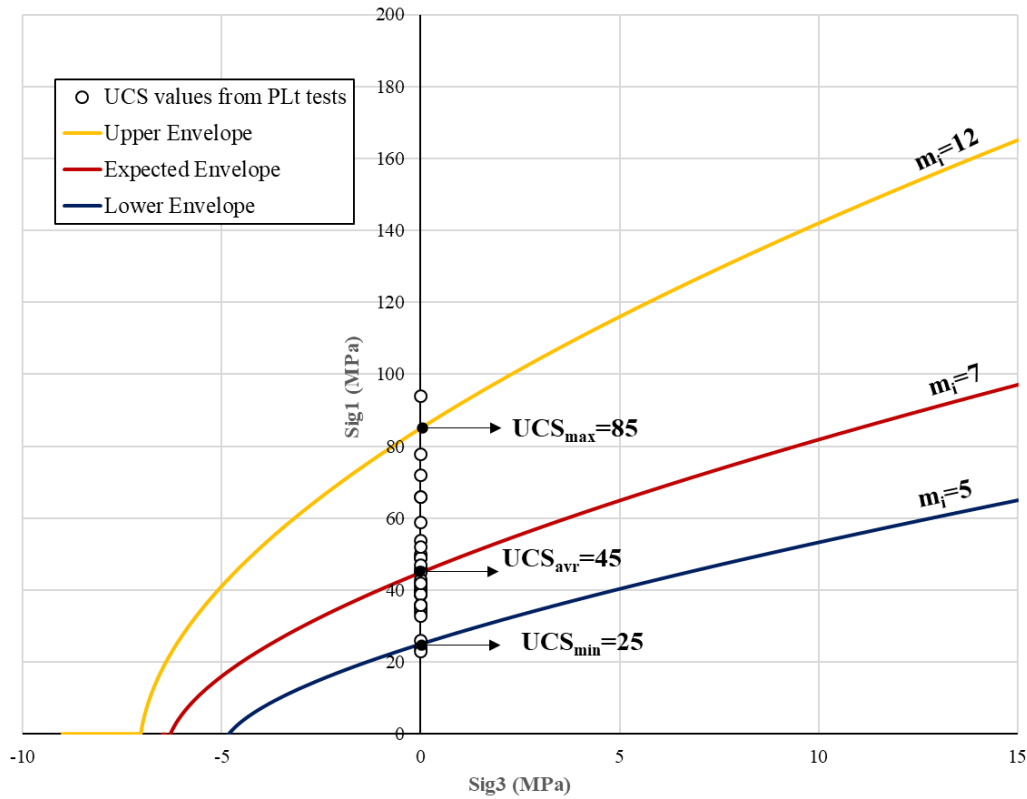


Figure 6.16 Intact rock strength envelope – case study #1

Figure XX shows the distribution of UCS values plotted in the σ_1 positive axis where $\sigma_3=0$. A closer look to these envelopes shows that the average curve has been fitted so that it intersects the σ_1 axis corresponding to the mean UCS value. Likewise, the upper and lower curves have been fitted so that they intersect the σ_1 axis corresponding to the maximum and minimum UCS value, respectively while complying with the assumption of min and max ' m_i ' assumed values.

Rock Mass Strength Envelope

The Generalized Hoek-Brown (G-H-B) criterion defines a curvilinear shear strength envelope that is considered a reasonable estimation of the behavior heavily jointed rock masses. This means that an important assumption of the G-H-B criterium is that the rock mass can be considered as an isotropic continuum medium. This is typically the case for blocky or very blocky rock masses such as the one we are dealing with in this case study #1. When following this approach, the intact rock envelope will be basically downgraded to represent the rock mass properties.

Primary input parameters for the Generalized Hoek-Brown criterion include: GSI, UCS, m_i and rock mass disturbance factor D, as defined by Hoek et al. (2002). D is typically caused by blast damage or due to unloading during mining. Experience shows that a value of D equal to 0.75 may be achievable for most open pit slopes with the application of good, controlled blasting practices. For this case study, a triangular

distribution for D was chosen with 0.75 as the most likely and 0.5 and 1.0 as the minimum and maximum values, respectively. Probability density functions (PDF) were selected to represent statistical distributions of each of the 4 primary parameters for the rock mass (Figure 6.17). The distributions selected were based upon the results of field and laboratory testing as explained before.

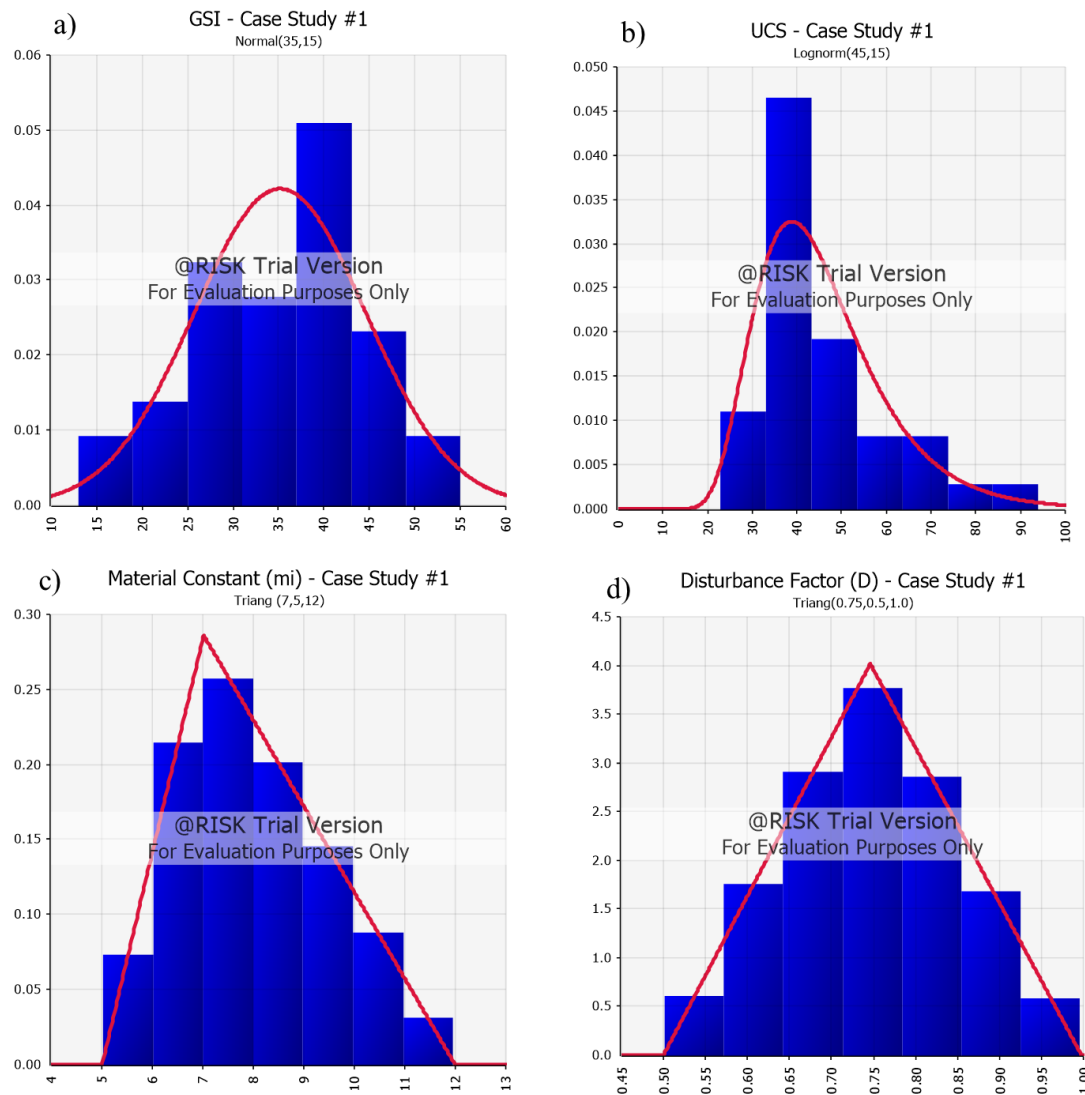


Figure 6.17 Input parameters for estimation of the rock strength envelope – case study #1

After the PDFs were selected to represent the four primary Generalized Hoek-Brown parameters (GSI, UCS, mi, and D), the commercial software @Risk 8.0 (Palisade), was used to perform a large number of stochastic simulations, sampling each of the four distributions during each simulation. Based on each set of primary parameters sampled, respective Hoek-Brown secondary parameters (mb, s and a) were calculated producing a PDF for each of these three secondary parameters (Figure 6.18).

From the repeated, randomized samplings of the secondary Hoek-Brown parameters, distributions of the shear strength vs normal stress relationships (Mohr-Coulomb) for the rock mass can be then calculated. However, further calculations will not be necessary to carry out since distributions of mb , s and a of the rock mass can be directly input into the LEM-based software Slide2D.

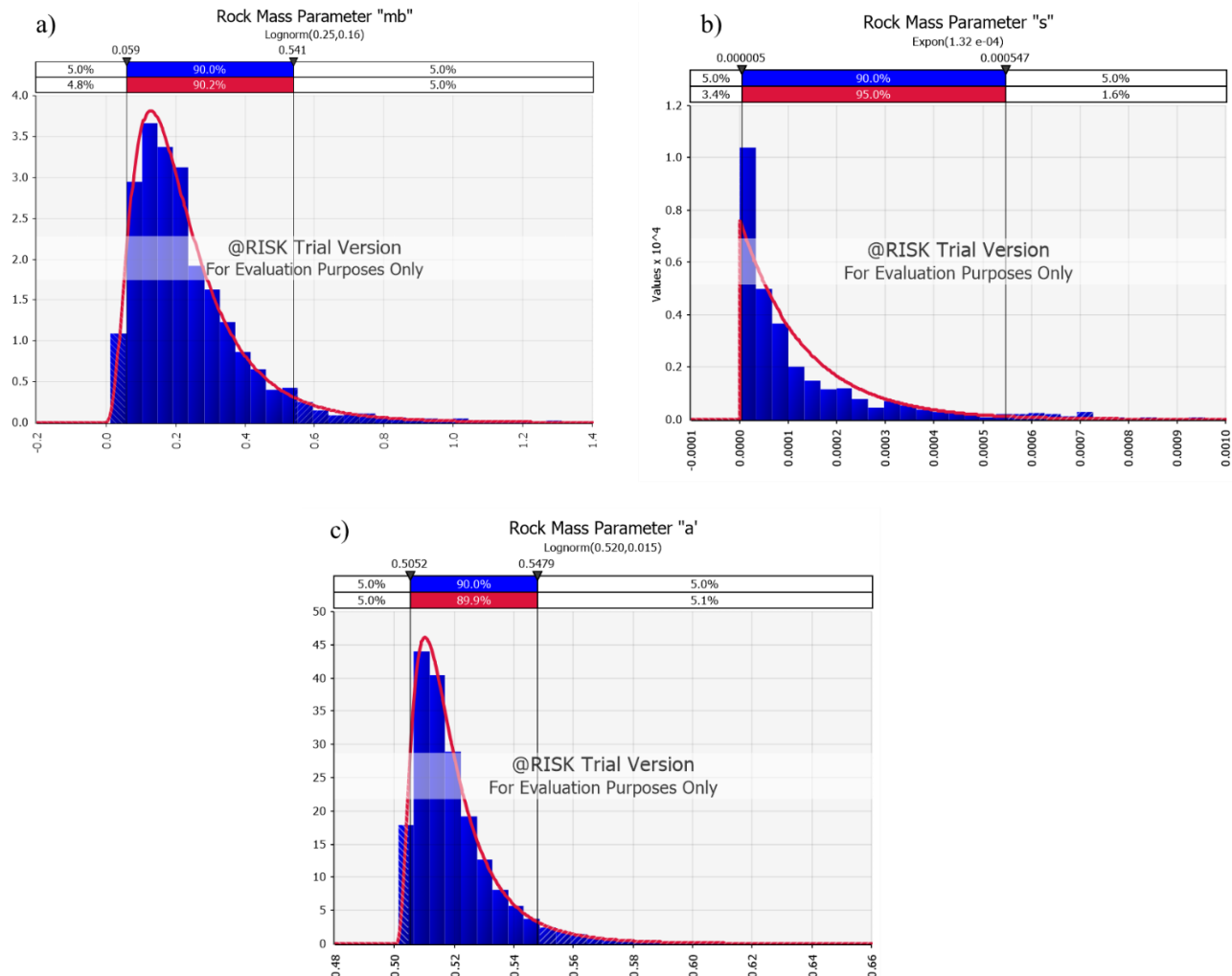


Figure 6.18 Distribution of estimated rock mass parameters a) ' mb ', b) ' s ' and c) ' a ' – case study #1

Global Slope Stability Analysis

Zone 05 of the open pit mine was divided into 6 sectors which contain a preferred slope orientation as explained in previous chapters (Figure 6.19.a). 2D sections were created for each of these sectors (Figure 6.19.b). The mathematical geotechnical model was then input into the commercially available geotechnical modeling software Slide2D developed by Rocscience Inc. Slide2D is a two-dimensional, limit equilibrium slope stability analysis program that assess the slope stability by various methods of slices. Spencer's

method (Spencer,1967) was selected for the limit equilibrium analyses of this evaluation due to its consideration of both force and moment equilibrium.

PDFs describing each of the secondary parameter distributions (m_b , s , and a) of the rock mass were directly input into Slide2D software. The Monte Carlo technique is used by the software during the analyses to randomly pick 10'000 samples from the secondary parameters m_b , s , and a , yielding a normal stress/shear strength envelope for each set of parameters. For each randomly generated strength envelope generated, a search of circular surfaces was conducted by the software deterministically evaluating the ratio of available resisting strength to driving force (i.e. safety factor) for each valid slip surface. The critical slip surface (surface with the lowest safety factor) for each of the stochastically generated strength conditions was stored and used for calculation of the overall probability of failure. In Slide2D software, the overall probability of failure for a slope is defined as the percentage of valid critical surfaces yielding a safety factor of less than 1.0 to the total number of valid slip surfaces.

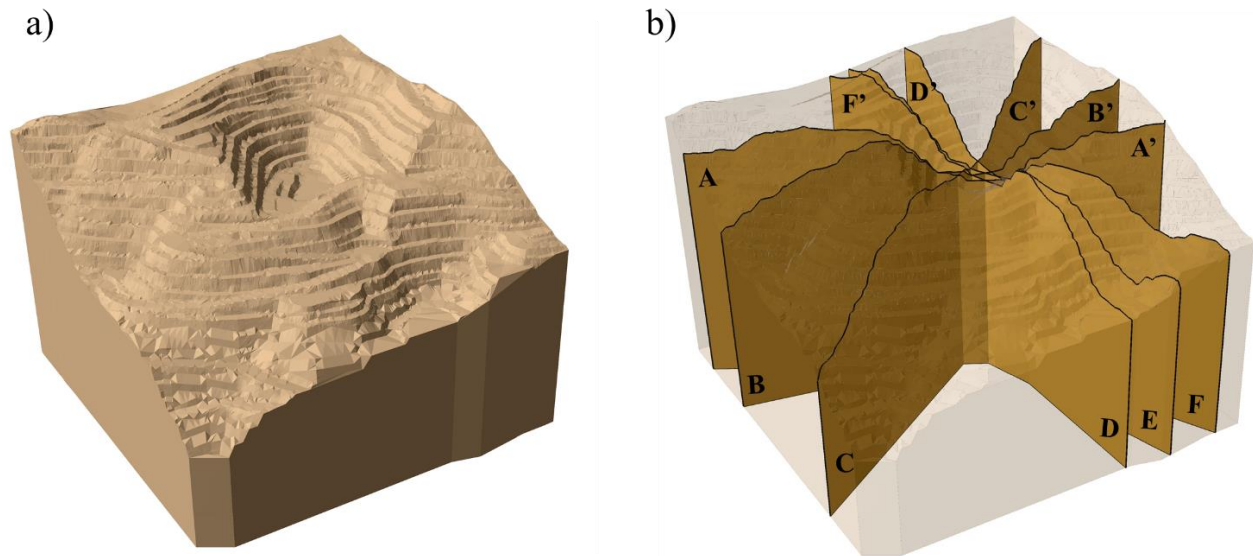
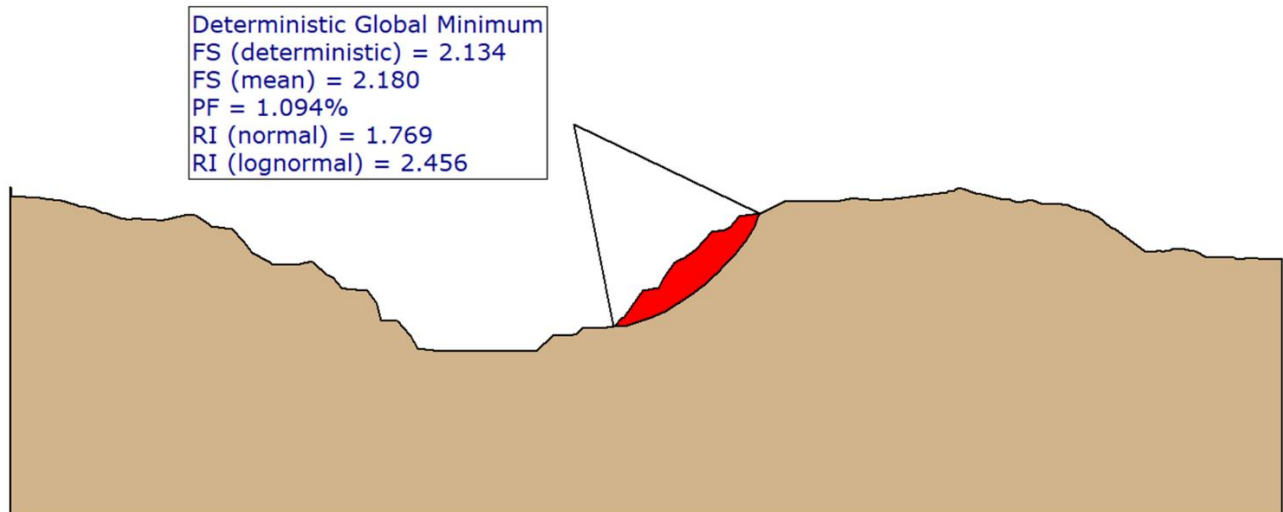
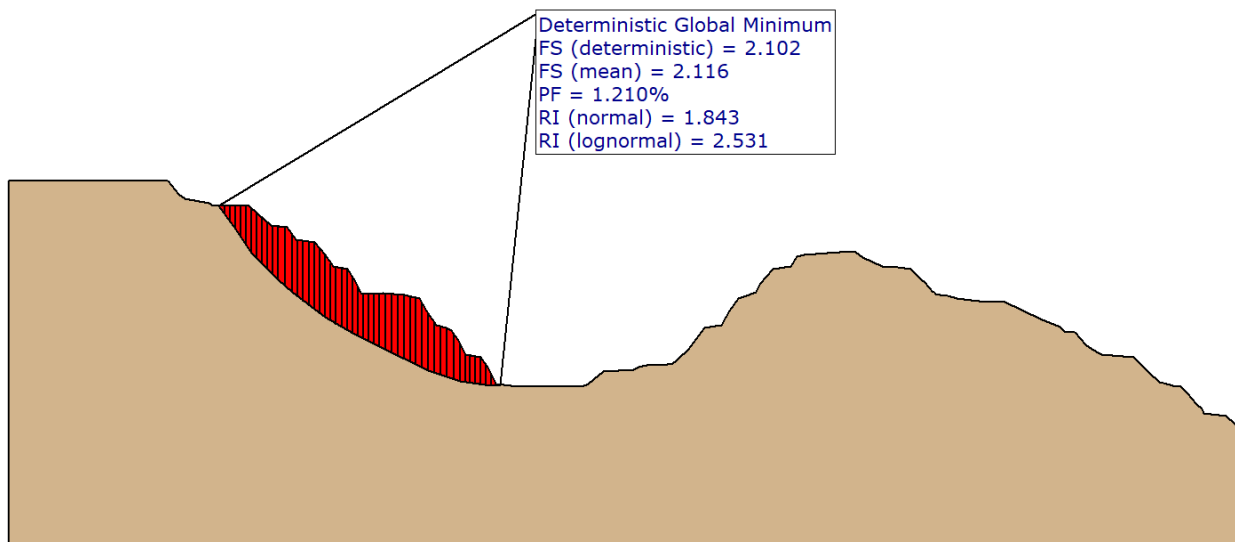
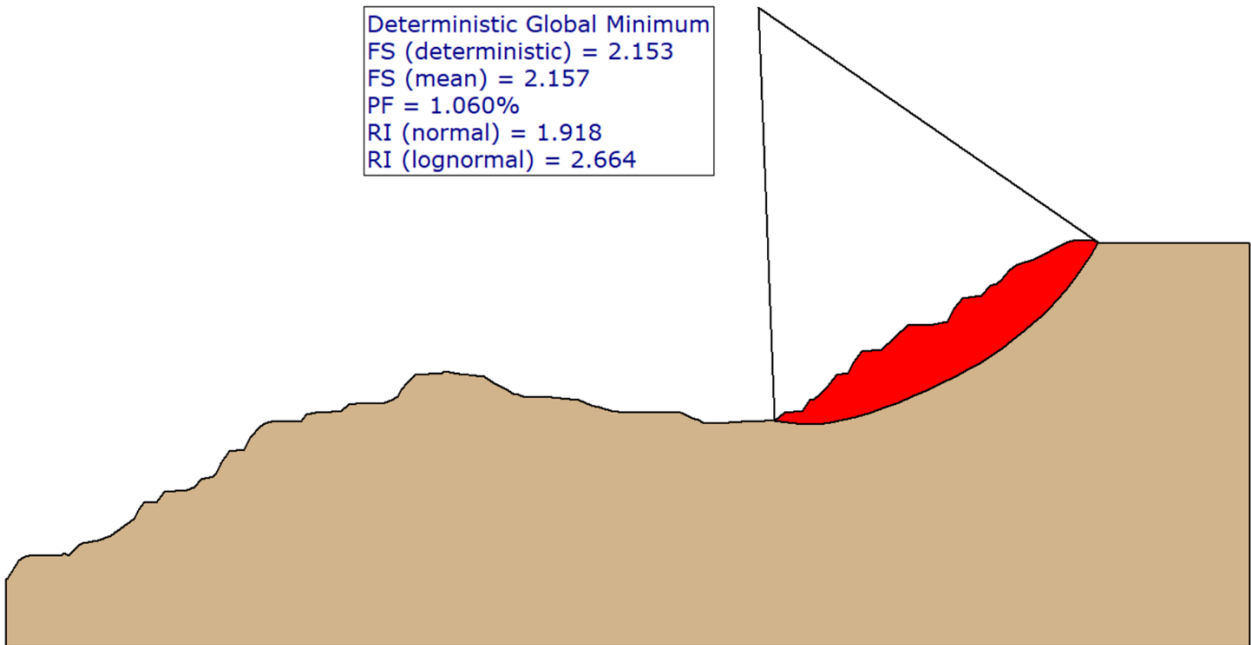
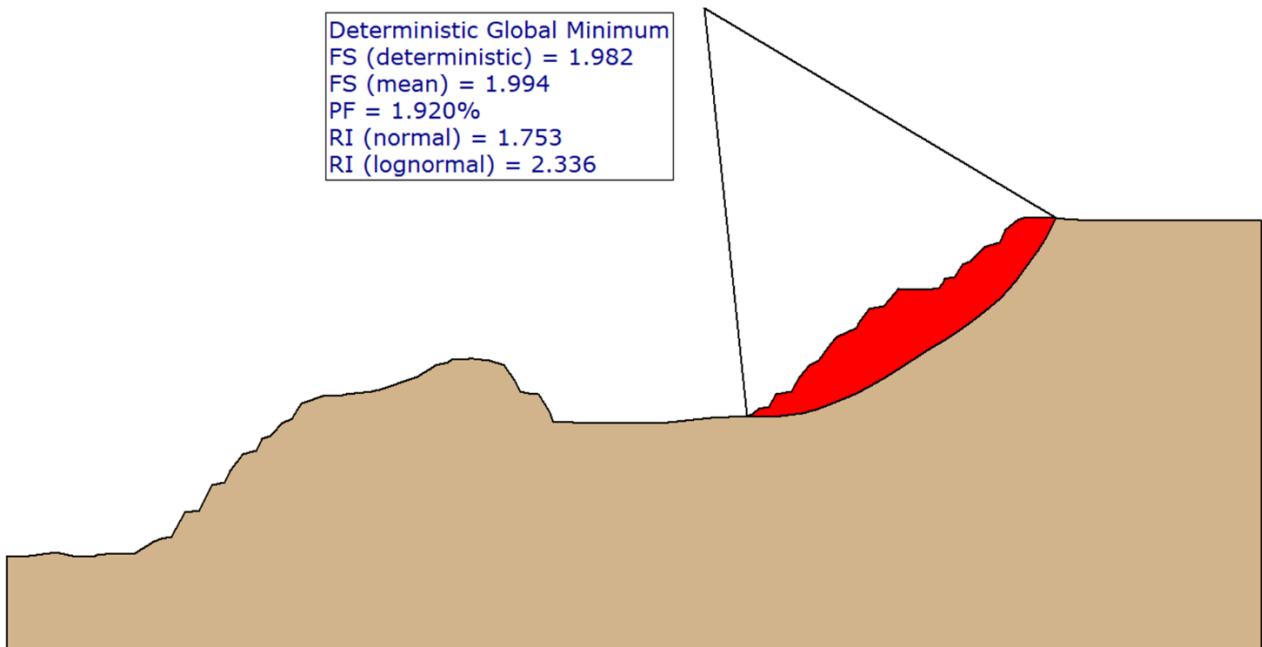


Figure 6.19 Case study #1 Open pit mine – zone 05 a) 3D perspective view and b) Cross sections

a) North Sector (Section A-A')**b) South Sector (Section B-B')**

c) South East Sector (Section C-C')**d) East Sector (Section D-D')**

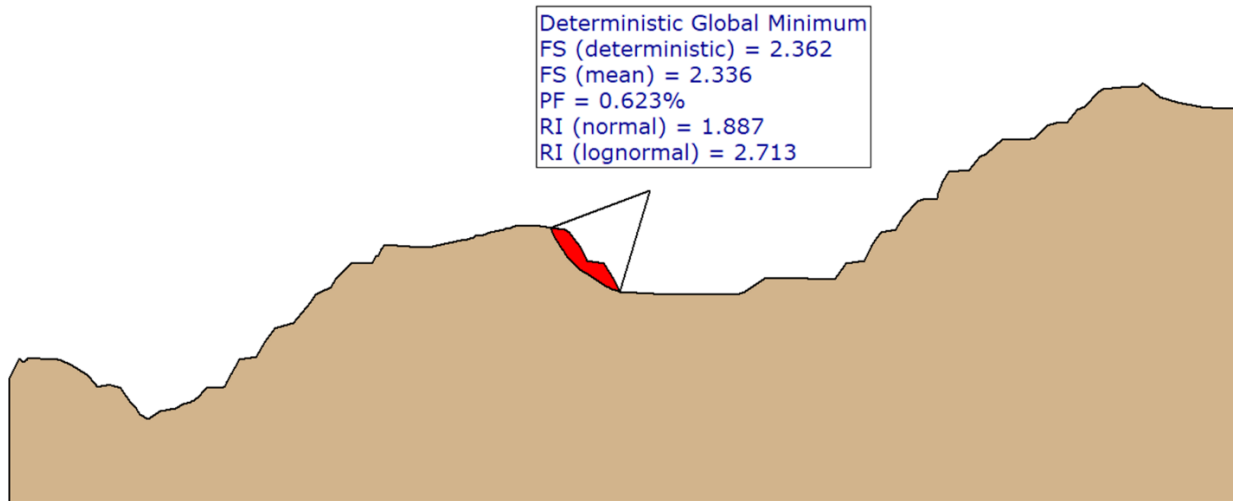
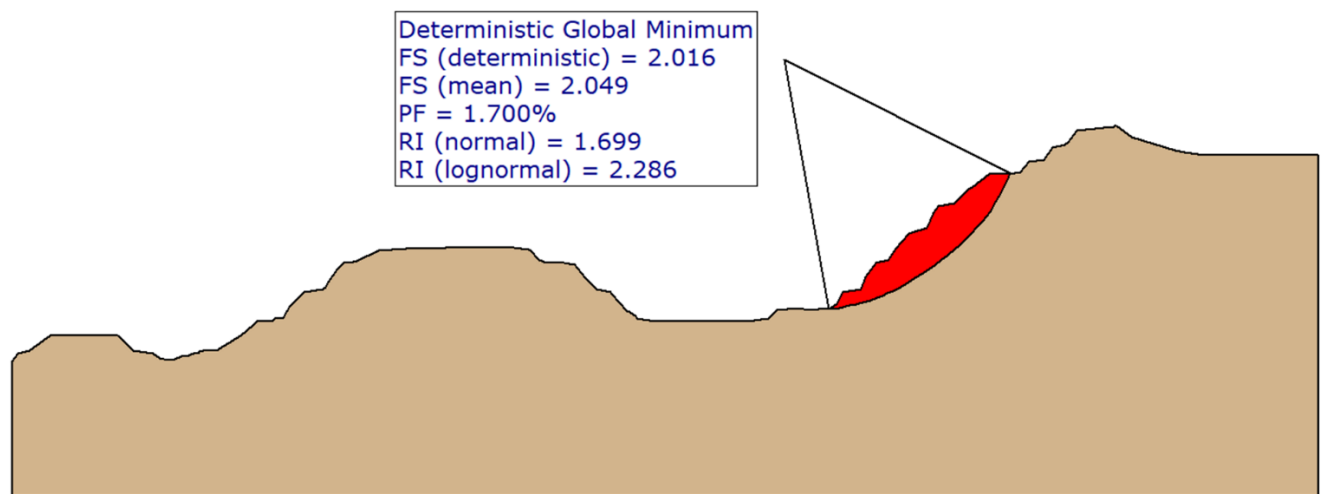
e) West Sector (Section E-E')**f) North East Sector (Section F-F')**

Figure 6.20 LEM Slope stability results – Case study #1

For the global slope stability analyses, a minimum FoS of 1.3 and a maximum PoF of 5% have been targeted for all the pit sectors. Table 6.2 summarizes the 2D LEM results for each pit wall sector. Figures 6.20-a to 6.20-f illustrate the geometry, geology, and the critical slip surface for each of the open pit sections. The modelling sections usually represent the highest slope in each sector. The overburden slope was negligible due to its insignificant thickness in the deposit area. Dry conditions were assumed for the open pit area as this was observed during the field mapping camping. The results of the limit equilibrium analyses indicate that a minimum FOS of 1.30 can be easily achieved for each of the design sectors. Also, all calculated PoF are below the maximum allowable of 5%, therefore the overall slope complies with the design criteria and it is deemed stable. These results also show that increased blasting disturbance and steeper slope angles can be considered provided that the FoS and PoF are not below and above the design criteria, respectively.

Table 6.2 Summary of the 2D LEM global slope stability analyses – Case study #1

Open Pit Sector	Cross Section	Strike (°)	Deterministic	Probabilistic
			FoS (Spencer)	PoF (FS<1.00)
North	A - A'	010°	2.13	1.09%
South	B - B'	075°	2.10	1.21%
South East	C - C'	030°	2.15	1.06%
East	D - D'	065°	1.98	1.92%
West	E - E'	090°	2.36	0.62%
North East	F - F'	145°	2.02	1.70%

6.4.2 Case Study #2

Rock Mass Characterization

Rock mass characterization was made using the Bieniawski (1989) RMR rock mass classification system. A total of 52 geotechnical oriented boreholes were performed, in two consecutive years: 22 in 2016 and 30 in 2017. The empirical relationship given as $GSI = RMR_{89} - 5$ (Bieniawski, 1989) was used to derive GSI values from RMR_{89} geotechnical core logging data.

A statistical analysis of the RMR data collected in drill holes showed that it follows a normal distribution for both the limestone and skarn. Figures 6.21.a and 6.21.b show the original logged RMR distribution for limestone and skarn, respectively. The RMR distribution for limestone has a mean and standard deviation of 60 and 10, whereas for the skarn it has a mean and standard deviation of 62 and 9. This indicates that the rock mass in the pit area is generally fair to good quality as the RMR ranges from 40 to 80. Distribution for GSI values are also shown as histograms in Figures 6.22.a and 6.22.b.

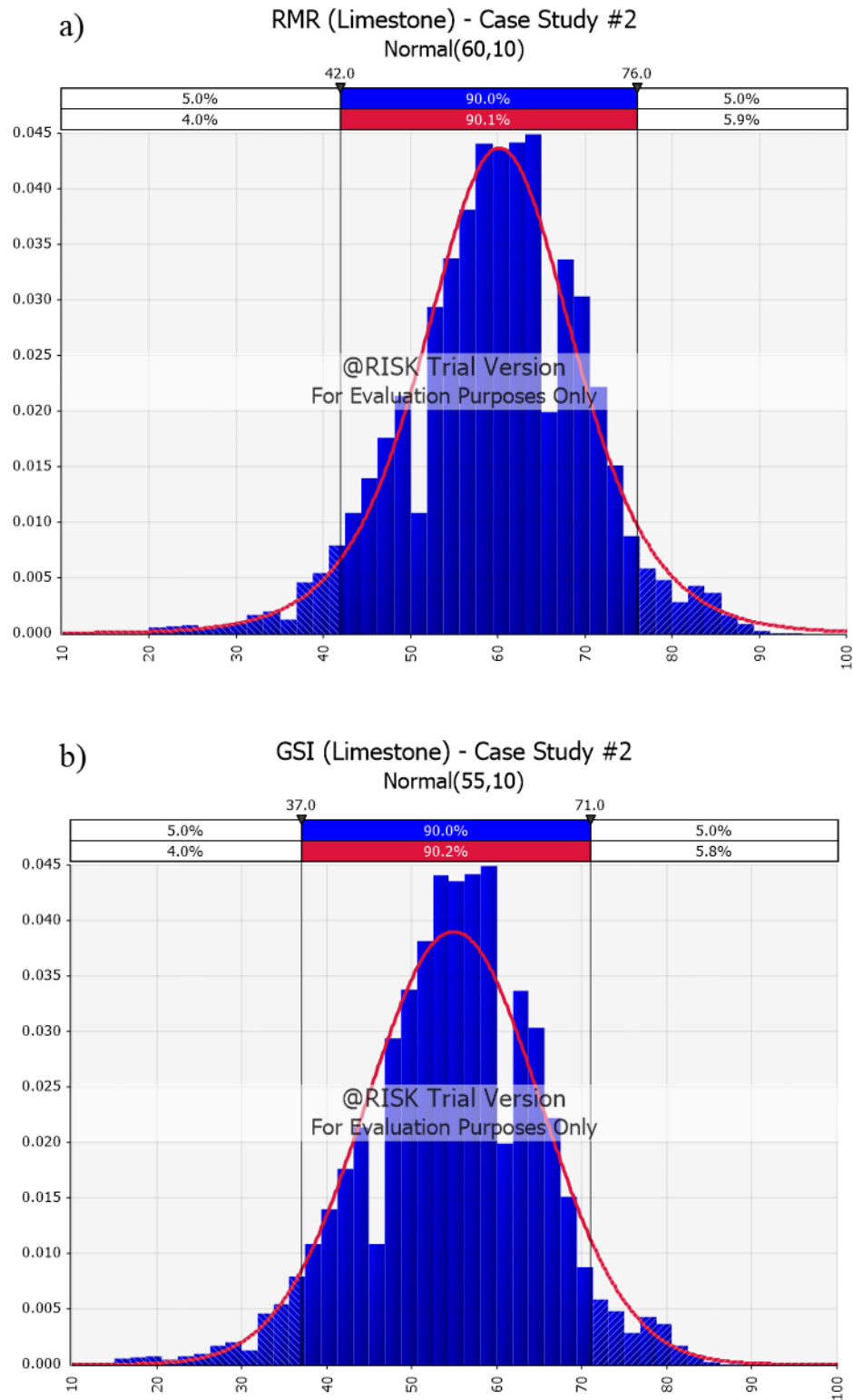


Figure 6.21 Histogram of a) RMR and b) GSI for the Limestone – case study #2

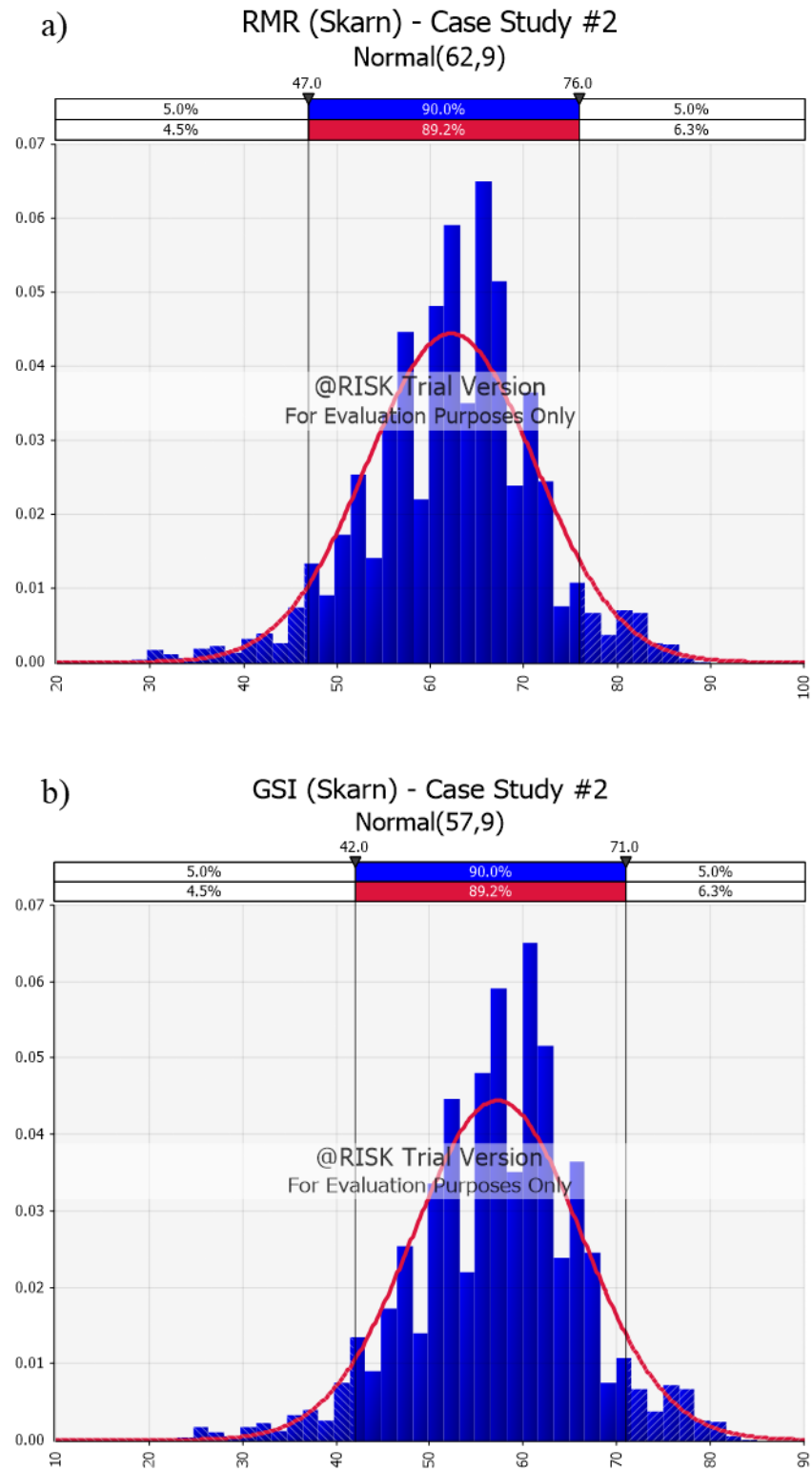


Figure 6.22 Histogram of a) RMR and b) GSI for the Skarn – case study #2

Intact Rock Strength Envelope

For this project a comprehensive laboratory testing data was available which comprised: Brazilian Tensile Strength (BTS), Unconfined Compressive Strength (UCS), and Triaxial (TX) tests. Since the pit walls are mainly cut in limestone and skarn, the intact rock strength envelopes for these two rock types are estimated based on the core samples collected during the drilling program. 48 UCS, 18 BTS and 45 TX tests were carried for characterizing the intact rock strength of limestone. Likewise, 27 UCS, 12 BTS and 27 TX tests were carried for describing the intact rock strength of skarn. This adds up to a total of 111 and 66 laboratory tests for limestone and skarn, respectively.

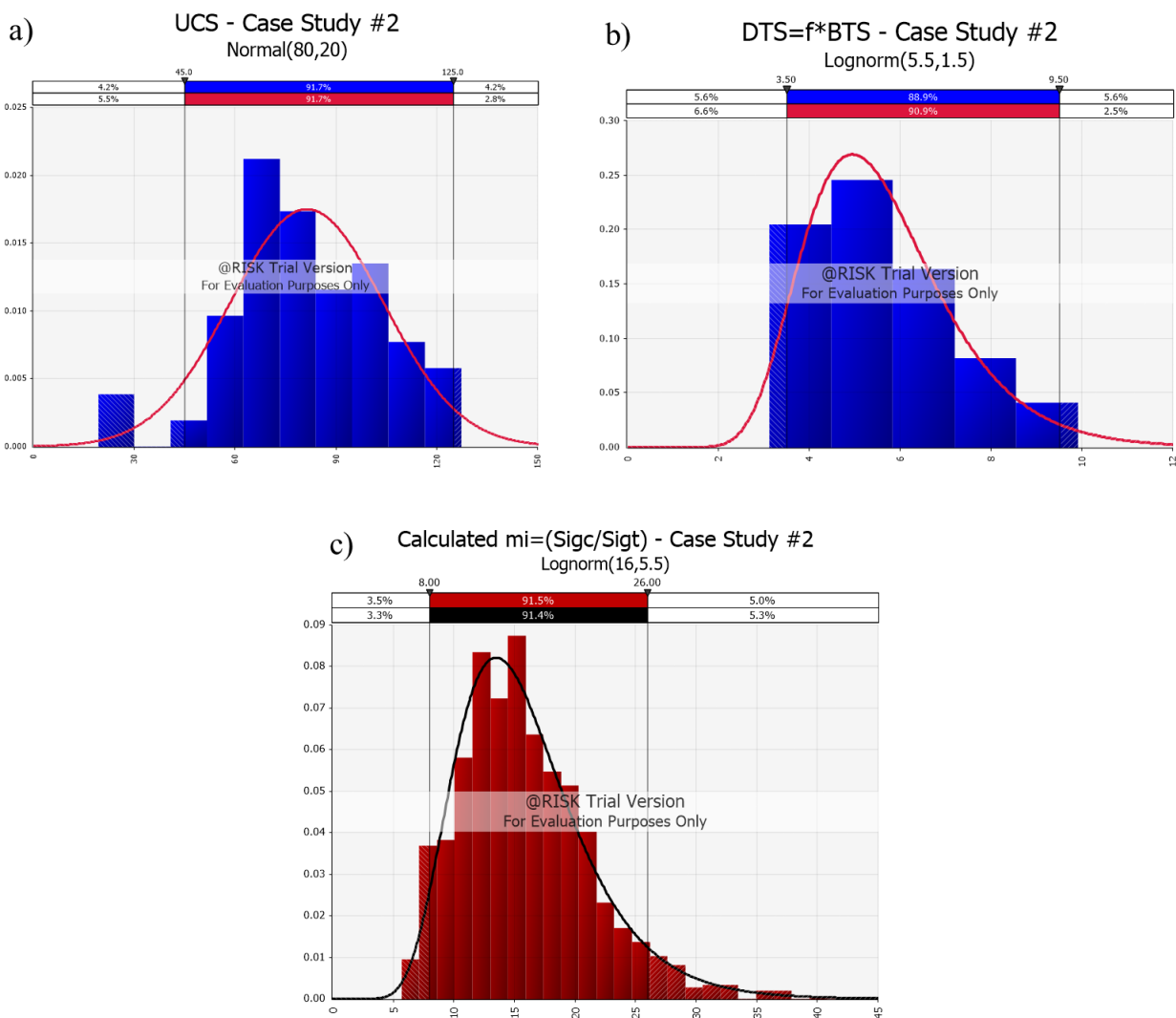


Figure 6.23 Intact rock properties for limestone a) UCS, b) DTS and c) m_i values – case study #2

The average UCS for limestone is 80 MPa, with approximately 90% of the data falling between 45 and 125 MPa. A normal distribution has been fitted to the limestone UCS values (Figure 6.23.a). The average UCS for the skarn is 85 MPa, with approximately 90% of the data falling between 55 and 110 MPa. A normal distribution has also been fitted to the UCS of the skarn (Figure 6.24.a). Indirect measurements of rock tensile strength were conducted by the Brazilian testing method. Direct Tensile Strength (DTS) was approximated by using a correction factor (f) such that $DTS=f*BTS$. A correction factor of 0.70 and 0.90 was used for the BTS of limestone and skarn, respectively, as suggested by Perras and Diederichs (2014). Calculated DTS values were fitted to lognormal distributions as shown in Figures Figure 6.23.b and 6.24.b.

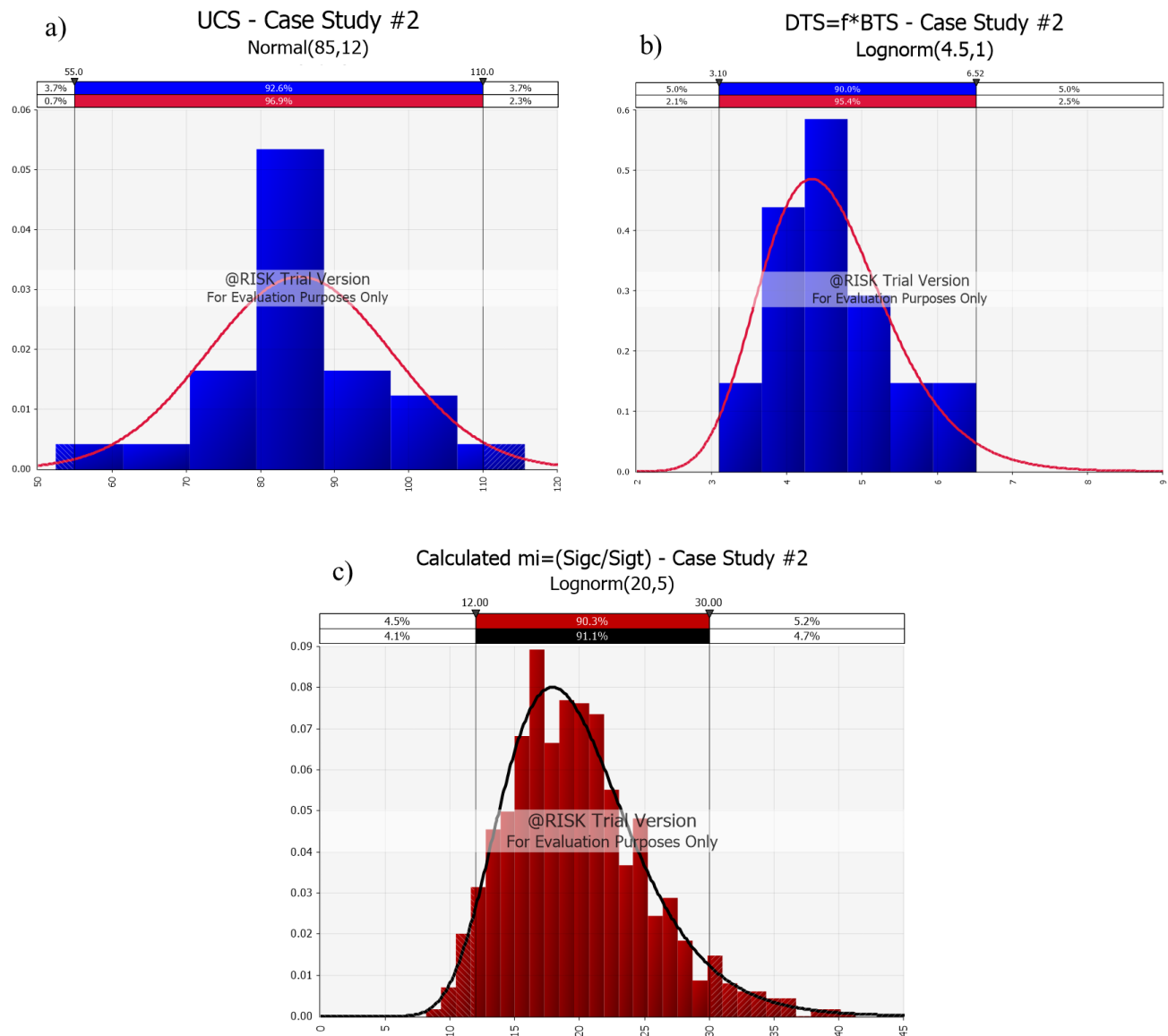


Figure 6.24 Intact rock properties for skarn a) UCS, b) DTS and c) m_i values – case study #2

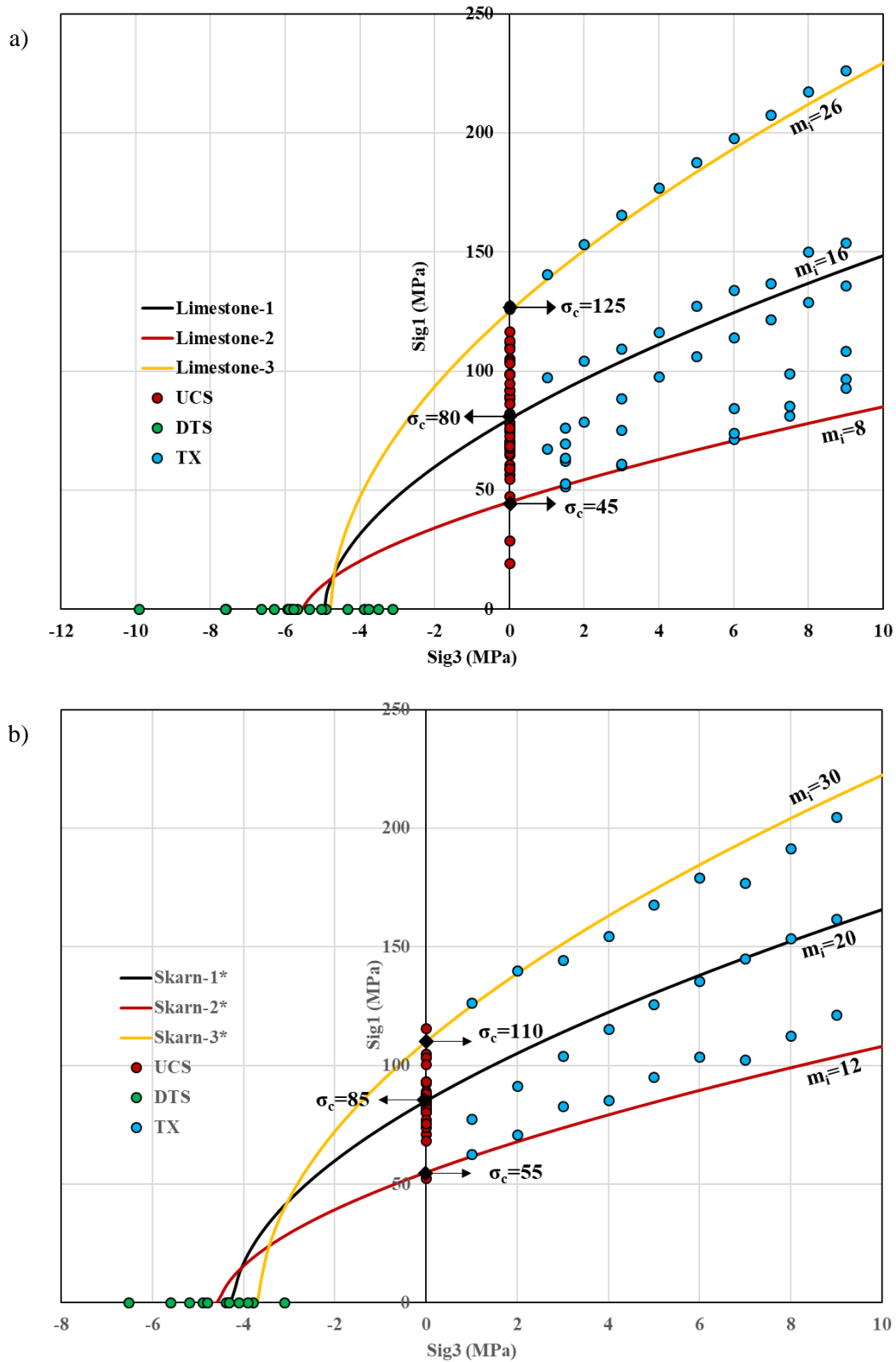


Figure 6.25 Intact rock strength envelope for a) limestone and b) skarn – Case study #2

The material or lithological constant ' m_i ' has been estimated following the relationship suggested by Hoek et al. (2002) which defines $m_i = (UCS/DTS)$. It should be noted that variability in the m_i parameter stems from variability in mineral content and/or grain size (Langford & Diederichs, 2013). In order to account for m_i variability a Monte Carlo simulation was carried out with the UCS and DTS PDF's as inputs. Figure 6.23-c and 6.24-c show the resulting PDF for the m_i values of the limestone and skarn, respectively. These were found to fit to a lognormal distribution. The average m_i value for limestone is 16, with approximately 90% of the data falling between 8 and 26. Also, the average m_i value for skarn is 20, with approximately 90% of the data falling between 12 and 30.

The intact rock strength envelope for limestone and skarn are shown in Figures 6.25-a and 6.25-b. In these plots UCS are plotted along the σ_1 positive axis, DTS following the σ_3 negative axis and TX tests on the first quadrant of the graph. It is worth noting that using the maximum and minimum m_i values for both rock types, obtained through the Monte Carlo analysis, shows a good match with observed triaxial testing data.

Rock Mass Strength Envelope

After the PDFs were selected to represent the four primary Generalized Hoek-Brown parameters (GSI, UCS, m_i , and D), the commercial software @Risk 8.0 (Palisade), was used to perform a large number of stochastic simulations, sampling each of the four parameter distributions during each simulation. Based on each set of primary parameters sampled, respective Hoek-Brown secondary parameters (m_b , s and a) were calculated producing PDFs for each of these three, secondary parameters (Figure 6.26 and 6.27).

Global Slope Stability Analysis

The open pit mine for case study #2 was divided into ten sectors from which five are within limestone, four in skarn and finally one that belongs to the overburden (soil-like) material. Since the final pit walls are cut in limestone and skarn, only these two rock types are dealt with in this section (Figure 6.28-a). Thus, the global stability analyses will focus on assessing the geotechnical stability of rock slopes. The slopes cut in overburden was part of another study that suggested using $BFA=45^\circ$ considering $c=10\text{kPa}$ and $\phi=35^\circ$ for this material. For each of the nine sectors cut in rock, 2D sections were created as shown in Figure 6.28-b.

Limit equilibrium analyses of the rock slopes were performed with Slide2D software. This program provides an estimate for the factor of safety against large-scale failures through the rock mass. In this analysis, a minimum factor of safety (FoS) of at least 1.50 was specified. Also, a maximum probability of failure (PoF) of 5% have been targeted for all pit sectors. The FoS and PoF are obtained by following a determinist and probabilistic calculation approach, respectively.

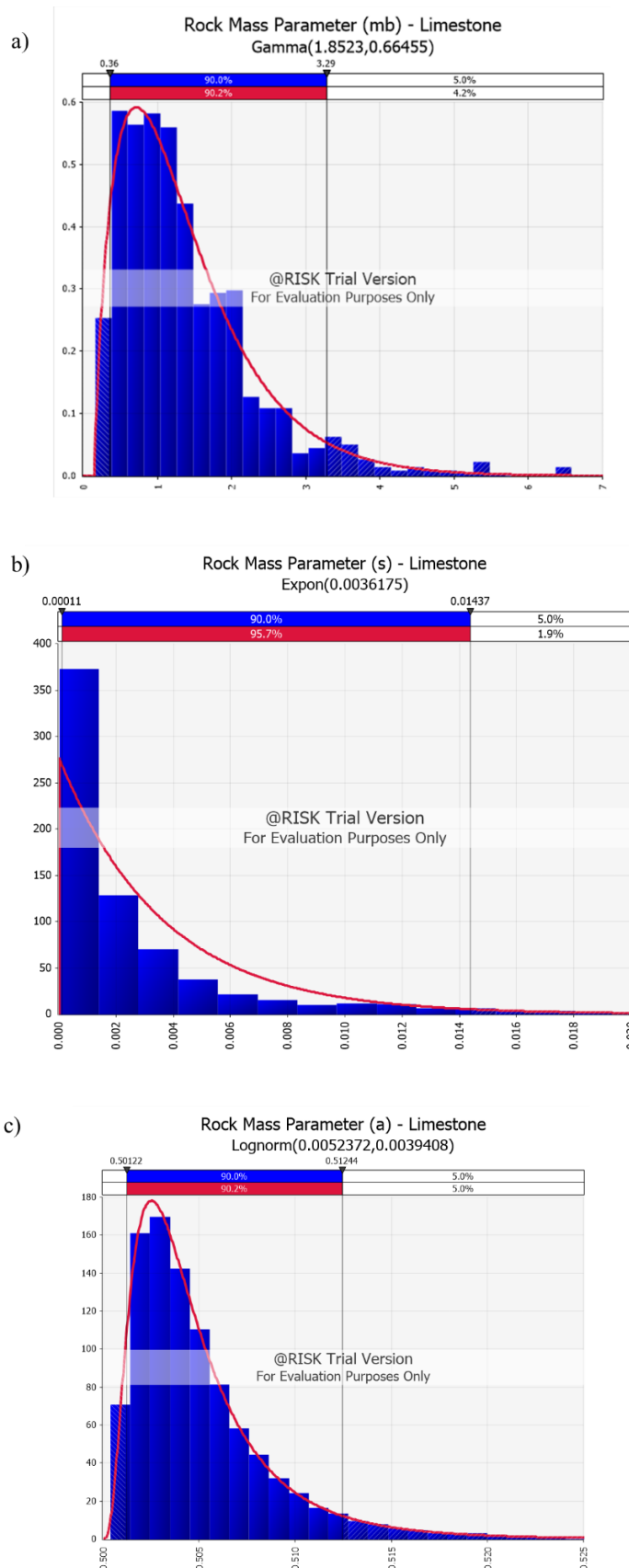
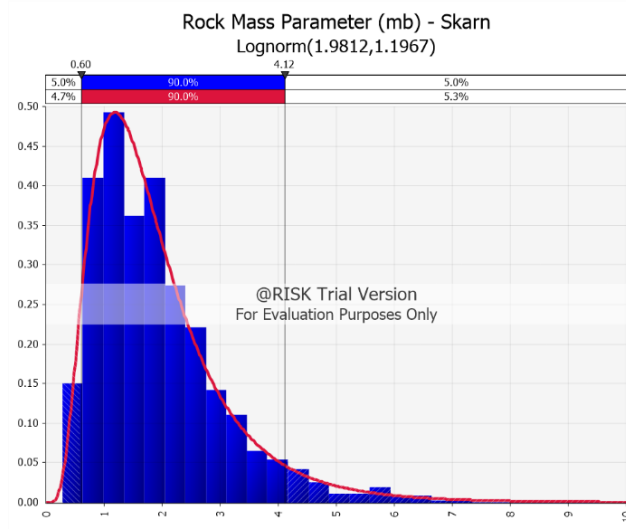
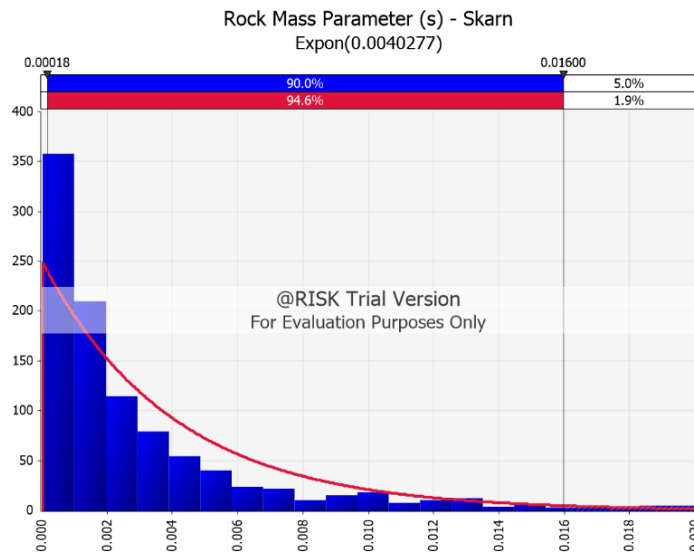


Figure 6.26 Distribution of estimated rock mass parameters for limestone a) 'mb', b) 's' and c) 'a' – Case study #2

a)



b)



c)

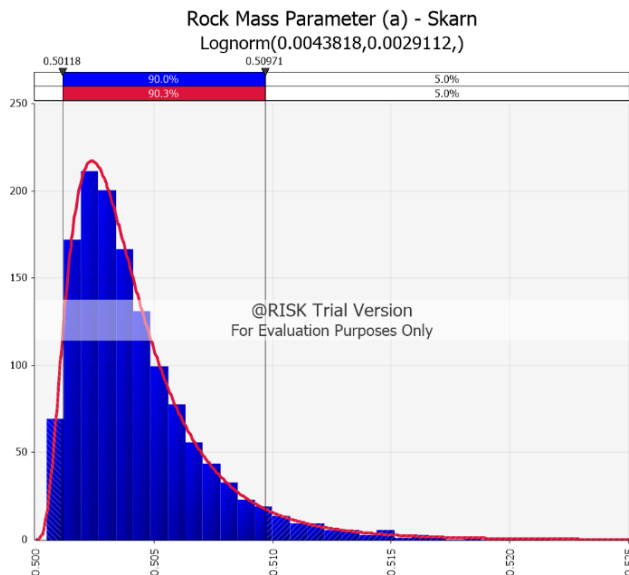


Figure 6.27 Distribution of estimated rock mass parameters for skarn a) 'mb',

b) 's' and c) 'a' – Case study #2

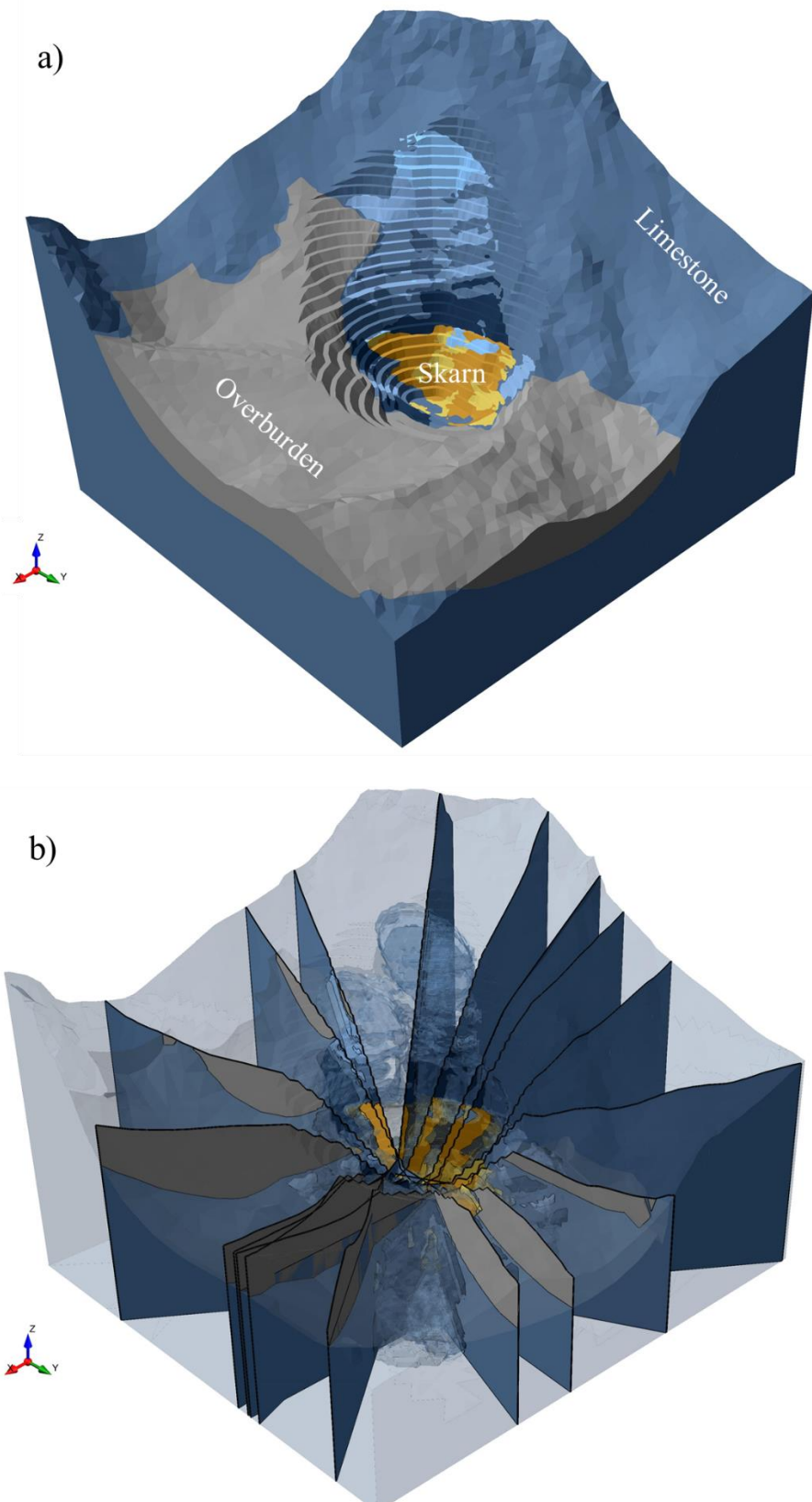


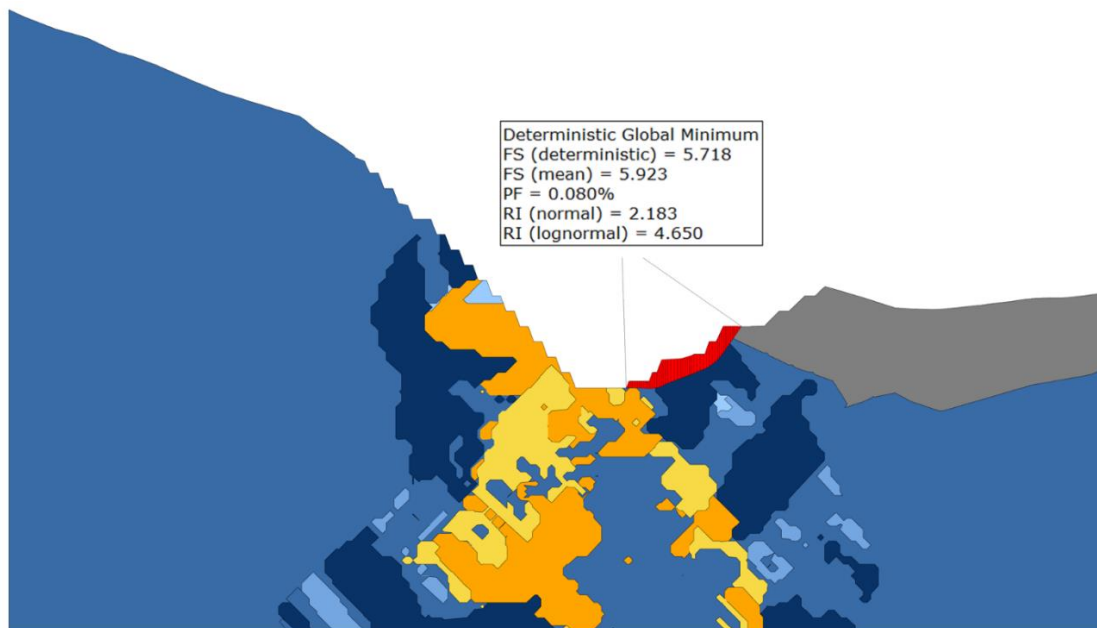
Figure 6.28 Case study #2 Open pit mine a) 3D perspective view and b) Cross sections

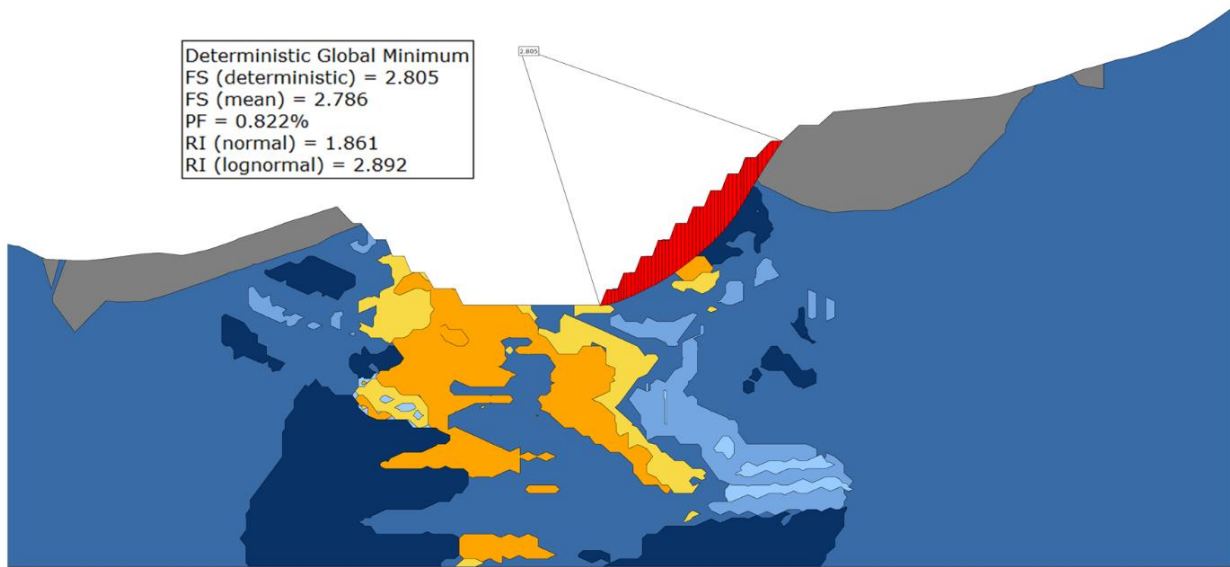
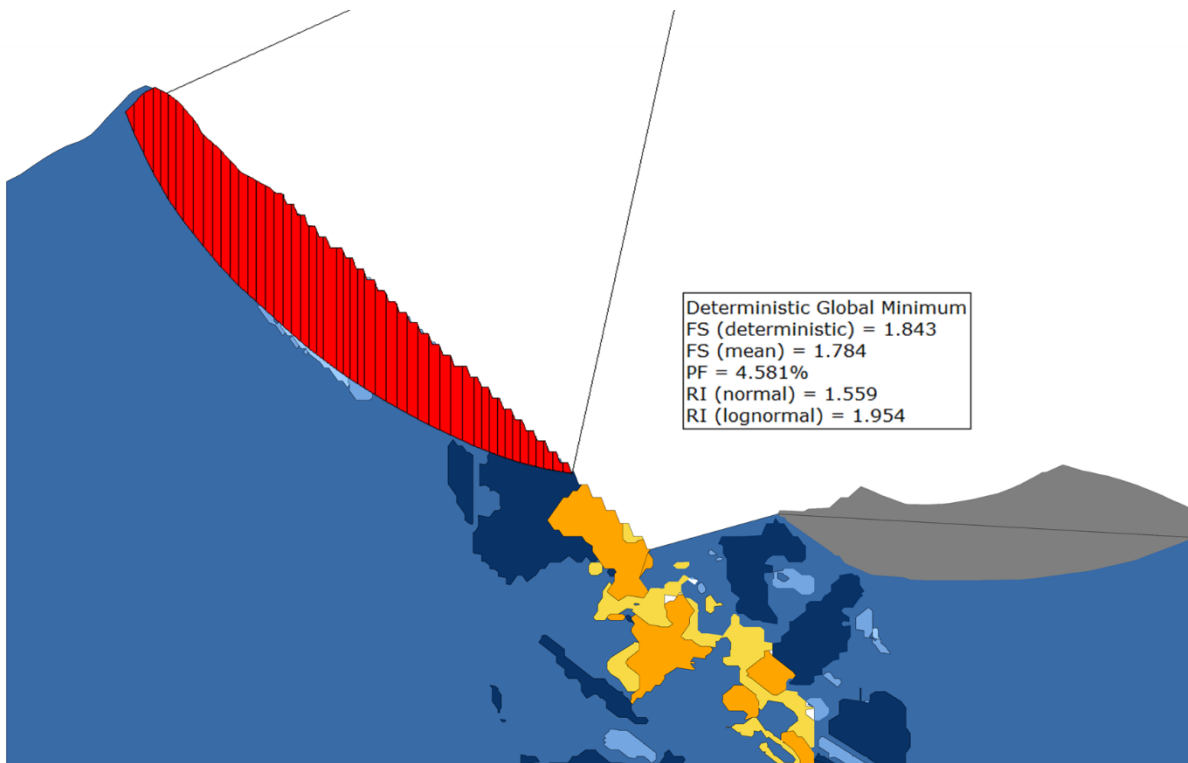
Table 6.3 summarizes the 2D LEM results for each pit wall sector. Figures 6.29-a to 6.29-i illustrate the geometry, geology, and the critical slip surface for each of the open pit sections. Slope stability calculations assumed that the pit wall will be depressurized (i.e. dry conditions) by implementing horizontal drains and/or pumping wells. The results of the limit equilibrium analyses indicate that the minimum FoS of 1.50 is achieved for each of the design sectors. Also, all calculated PoF are below the maximum allowable of 5%, therefore the overall pit slope design complies with the design criteria and it is deemed stable. These results also show that increased blasting disturbance and steeper slope angles can be considered provided that the FoS and PoF are not below and above the design criteria, respectively.

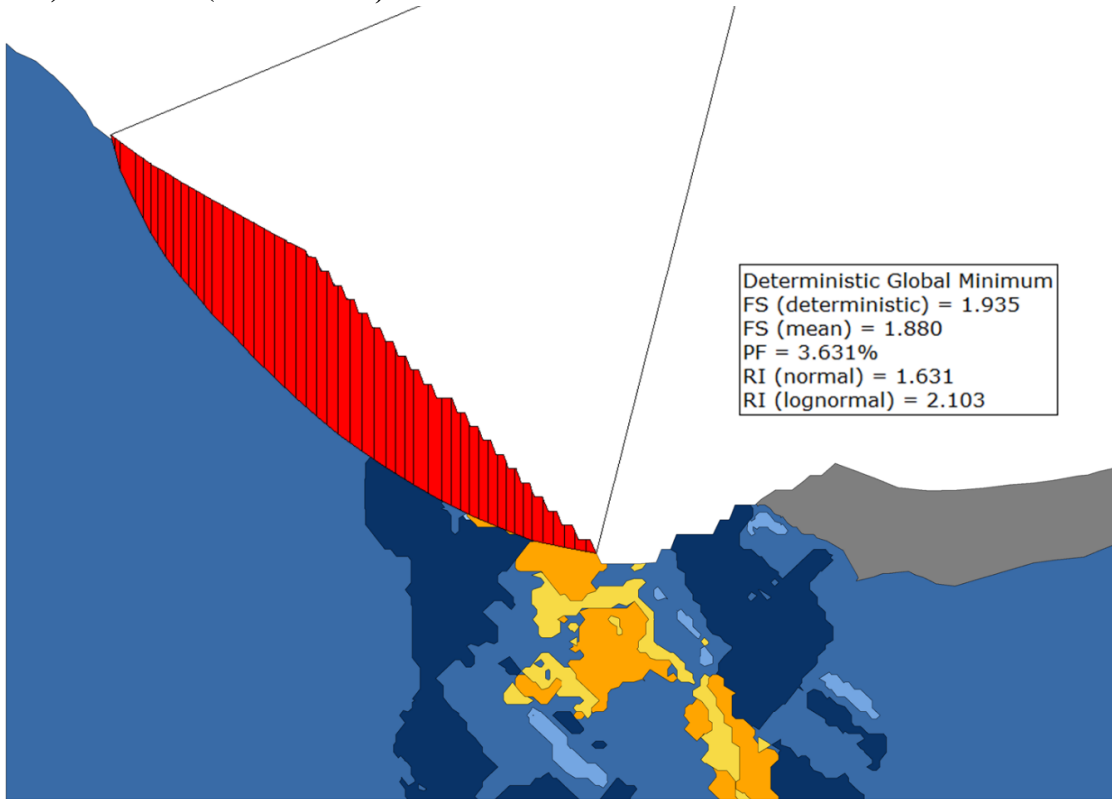
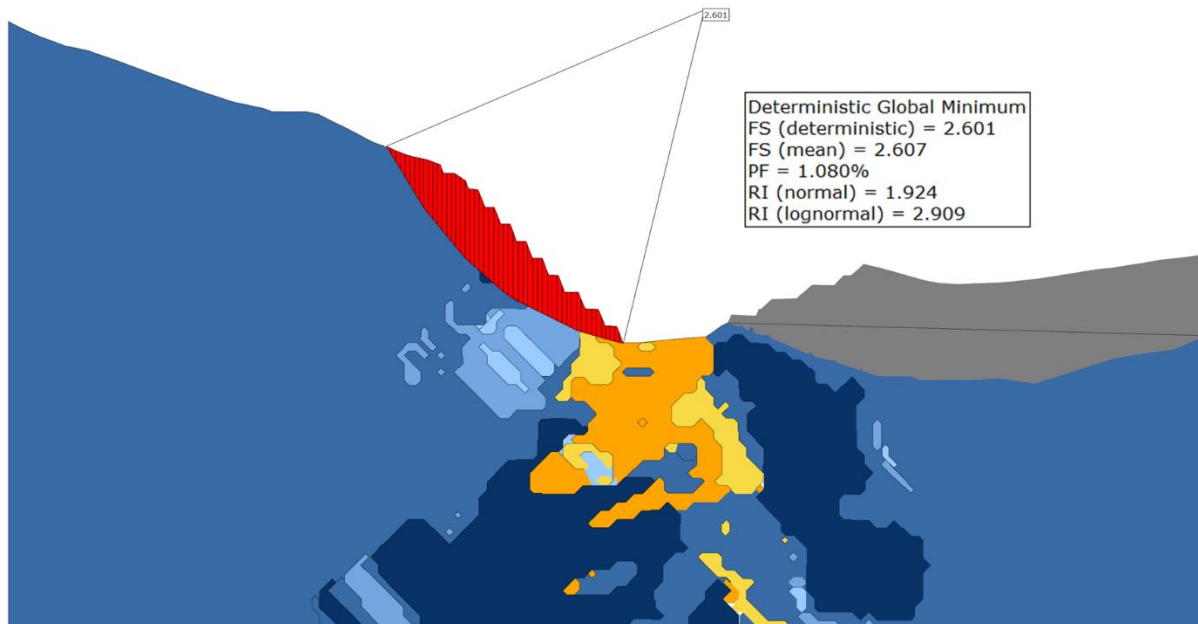
Table 6.3 Summary of the 2D LEM global slope stability analyses – Case study #2

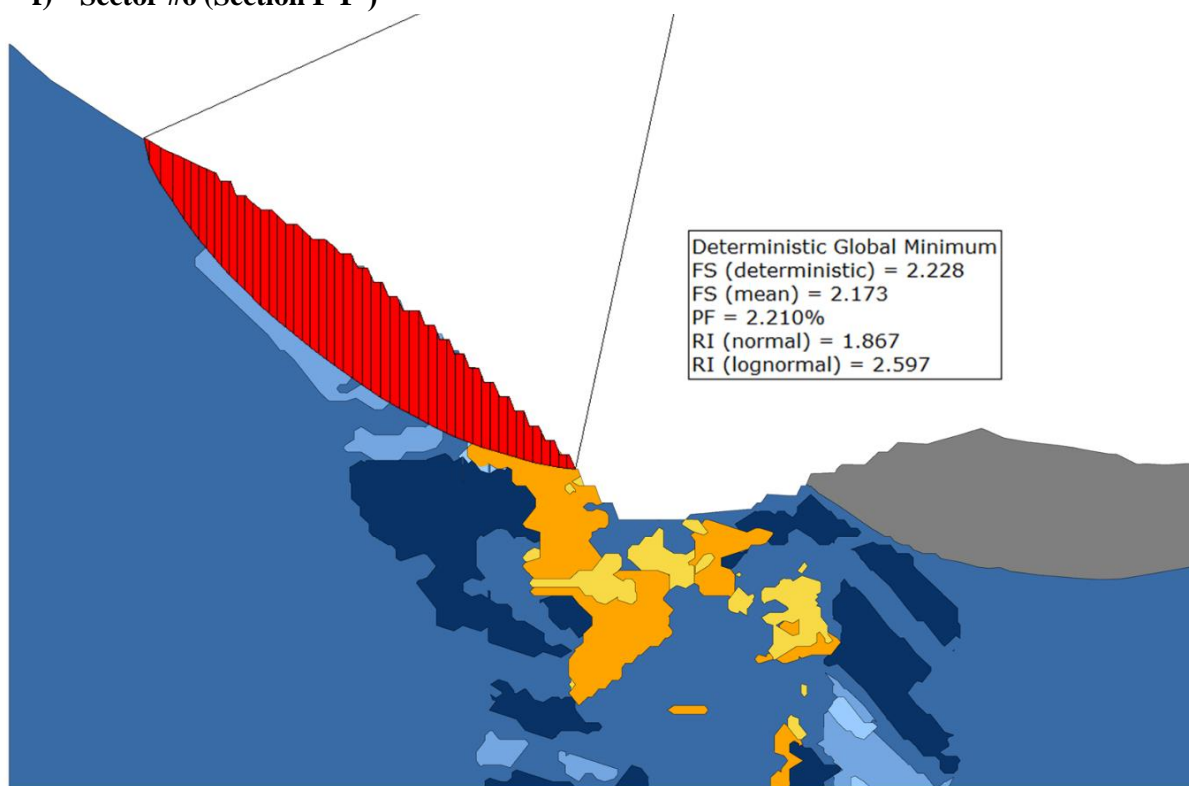
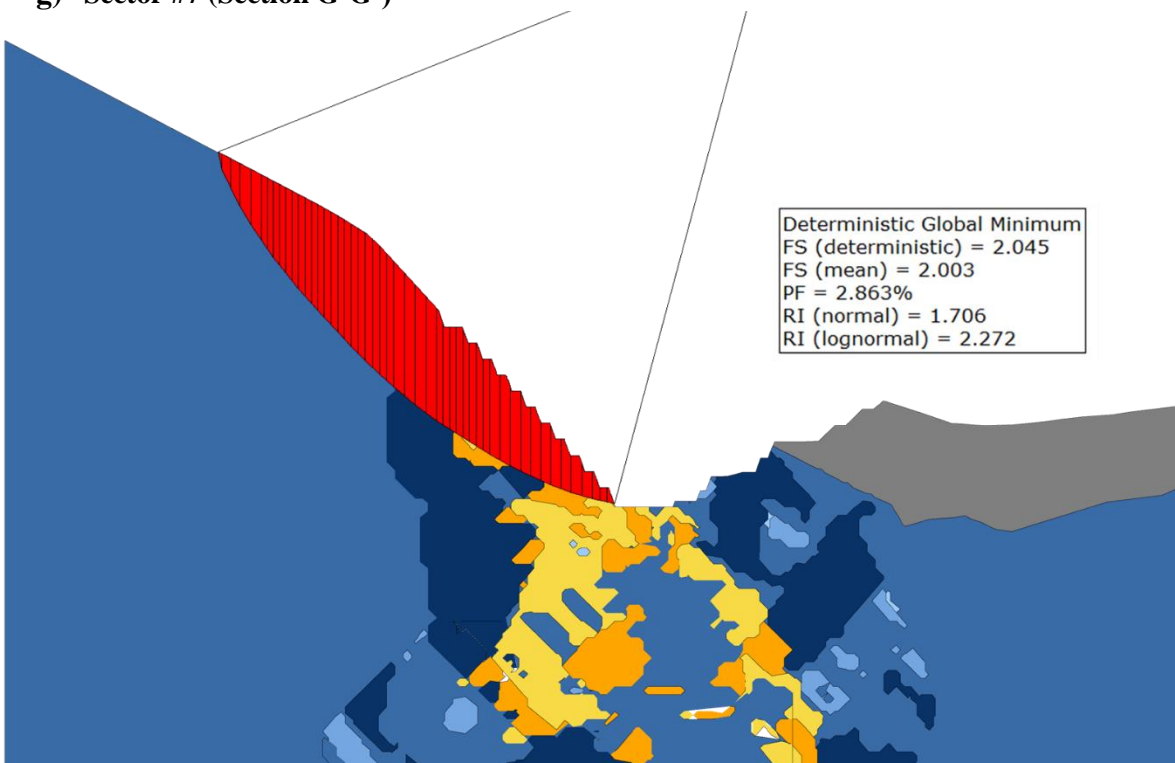
Rock Type	Open Pit Sector	Cross Section	Strike (°)	Deterministic	Probabilistic
				FoS (Spencer)	PoF (FS<1.0)
Limestone	1	A - A'	085°	5.7	0.08
	2	B - B'	155°	2.8	0.82
	3	C - C'	050°	1.8	4.58
	4	D - D'	070°	1.9	3.63
	5	E - E'	090°	2.6	1.08
Skarn	6	F - F'	020°	2.1	2.21
	7	G - G'	080°	2.0	2.86
	8	H - H'	125°	2.9	0.71
	9	I - I'	185°	5.3	0.14

a) Sector #1 (Section A-A')



b) Sector #2 (Section B-B')**c) Sector #3 (Section C-C')**

d) Sector #4 (Section D-D')**e) Sector #5 (Section E-E')**

f) Sector #6 (Section F-F')**g) Sector #7 (Section G-G')**

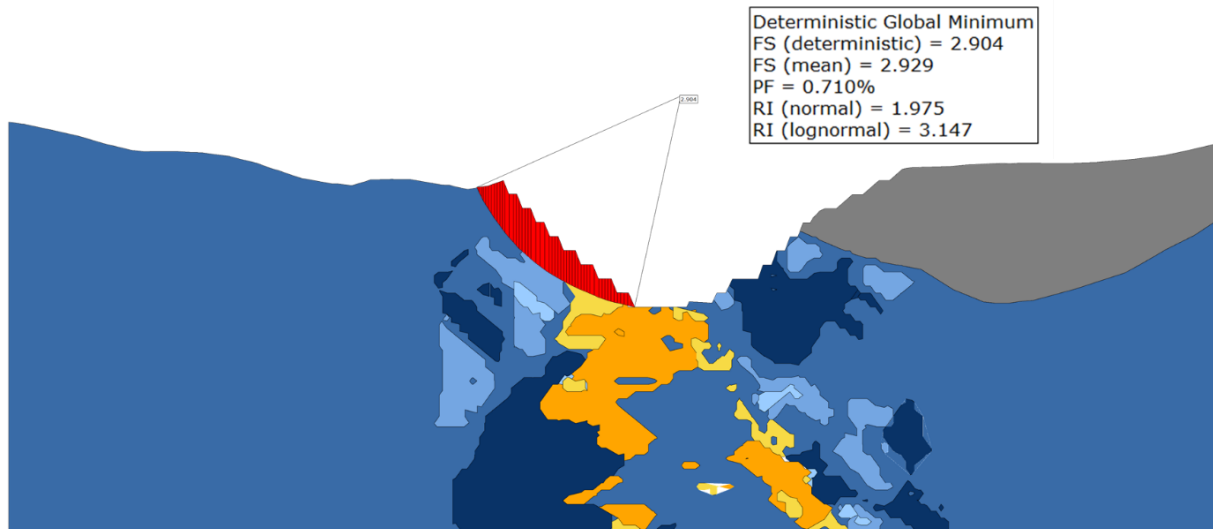
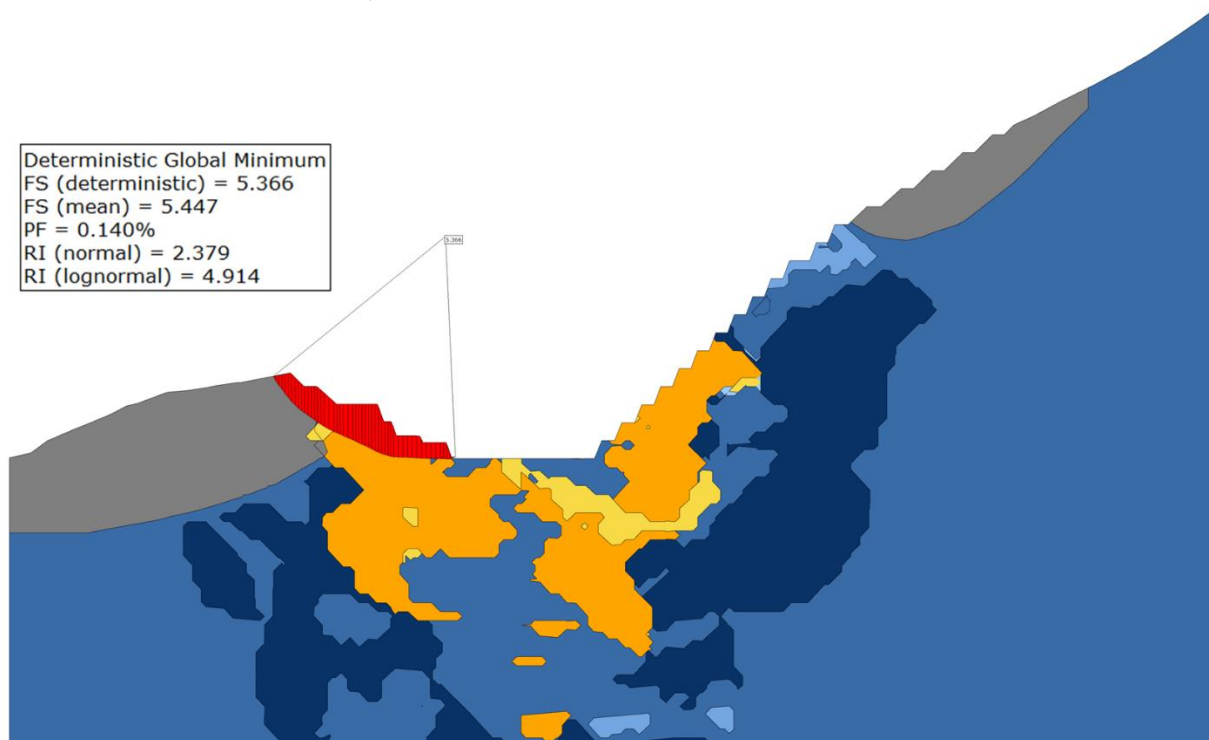
h) Sector #8 (Section H-H')**i) Sector #9 (Section I-I')**

Figure 6.29 2D LEM Slope stability results – Case study #2

6.4.3 Case Study #3

Rock Mass Characterization

The field data collection campaign consisted of extensive structural mapping of minor (i.e. rock joints) geological discontinuities. A total of 42 exposed bench faces cut in hornfels were mapped following the ISRM suggested procedures. A total of 575 rock joints were measured within the open pit mine. Rock mass characterization was made using the Bieniawski (1989) RMR rock mass classification system at each of the 42 mapping sites. The empirical relationship given as $GSI = RMR_{89} - 5$ (Bieniawski, 1989) was used to derive GSI values from RMR_{89} field measurements. A statistical analysis of the RMR data collected from the open pit mine showed that it fits well to a normal distribution with a mean and standard deviation of 60 and 5, respectively (Figure 6.30a). Likewise, GSI calculated values were found to follow a normal distribution with a mean and standard deviation of 55 and 5, respectively (Figure 6.30b). This indicates that the quality of the rock mass in the pit area ranges from fair to good and it classifies as a blocky to very blocky rock mass based on the range of GSI chart. Observations of no ‘significant’ seepage from pit walls during field mapping was reported and therefore the rock mass hydrogeological conditions are expected to be dry.

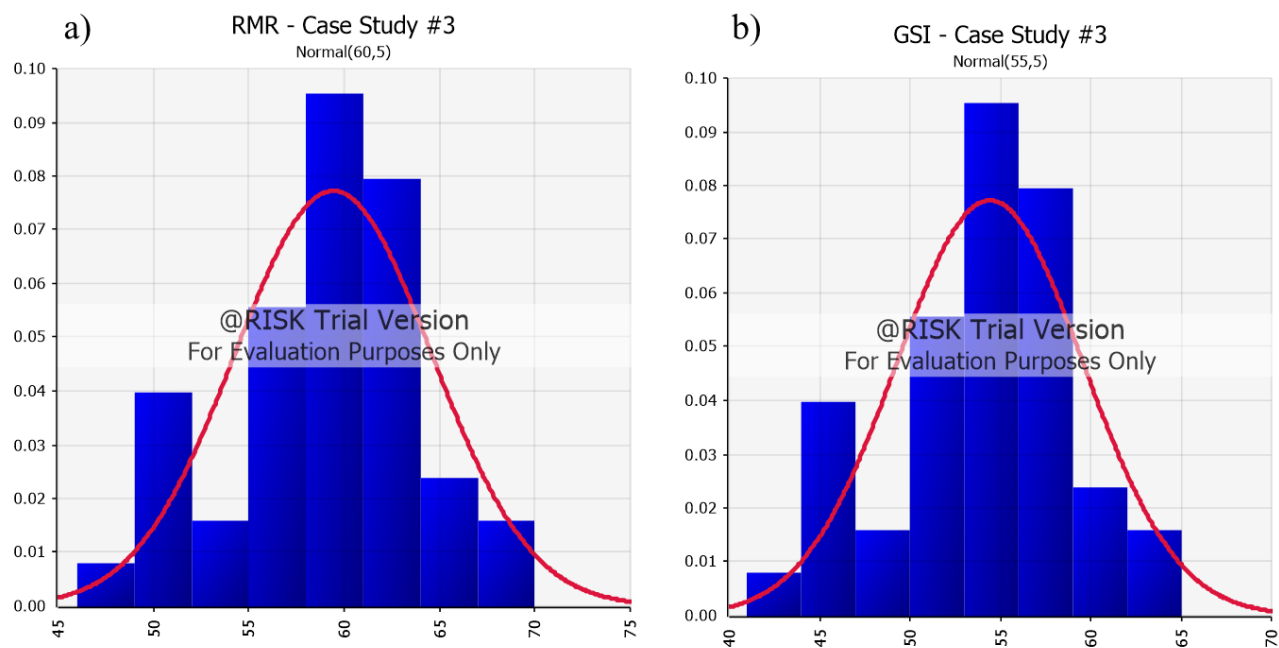


Figure 6.30 Histogram of rock mass characterization parameters a) RMR and b) GSI – case study #3

Intact Rock Strength Envelope

Field estimates of intact rock strength for rock samples collected at each mapping site were obtained through PLT testing. PLT values were then converted to UCS estimates using the empirical equation: $UCS = 24 \cdot Is_{50}$, where Is_{50} is point load strength index corrected to the standard equivalent diameter (De) of 50 mm (Broch & Franklin, 1972). Figure 6.31 shows the distribution of UCS estimated values from PLT tests. It shows that UCS can be fit to a normal distribution with mean 72 MPa and standard deviation of 23 MPa. The upper and lower expected bound for the UCS values were defined as 30 and 110 MPa, respectively. This means that the rock is expected to have predominantly low to medium compressive strength.

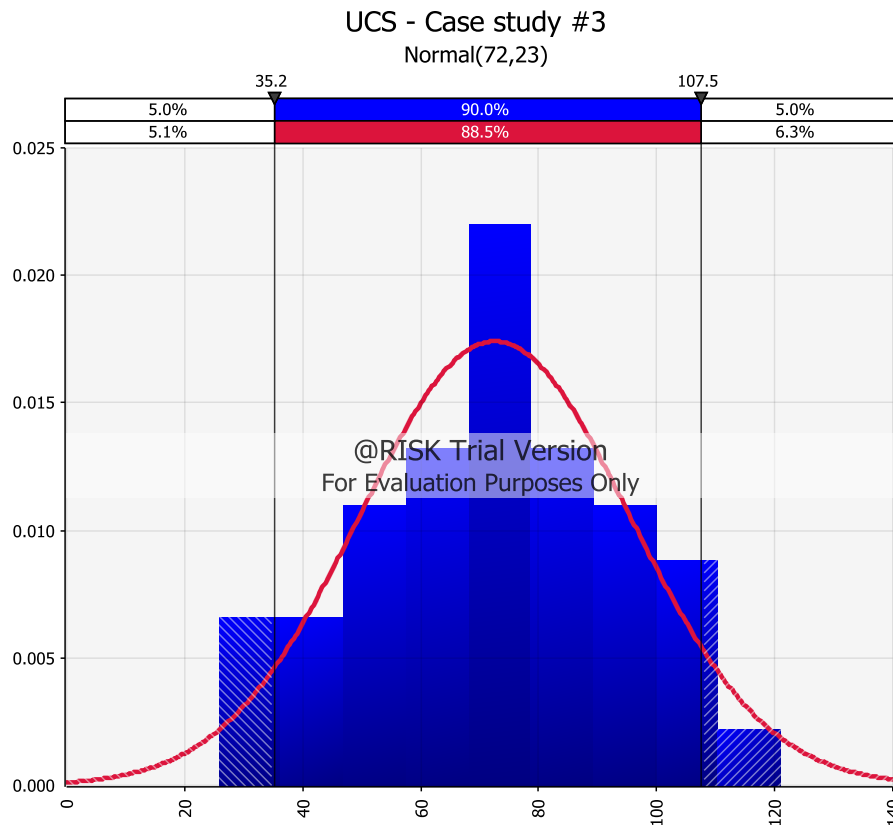


Figure 6.31 Figure Intact rock properties - UCS values

For this project, limited triaxial (TX) tests were available (12). The material or lithological constant ' mi ' has been estimated by combining estimate UCS values with measured TX tests. References given by Hoek et al. (2002) suggests a mi value of 19 ± 4 for pyroclastic rocks such as hornfels. For this case study, mi ranges between 14 and 22 with a most likely value of 18 was chosen based on the author's experience in dealing with similar materials. The distribution of mi values was assumed to follow a triangular distribution.

The intact rock strength envelope for the hornfels is shown in Figure 6.32. In this plot UCS tests are plotted along the σ_1 positive axis, and TX tests on the first quadrant of the graph. It is worth noting that using the assumed maximum and minimum m_i values for this rock type, shows a good match with observed triaxial testing data.

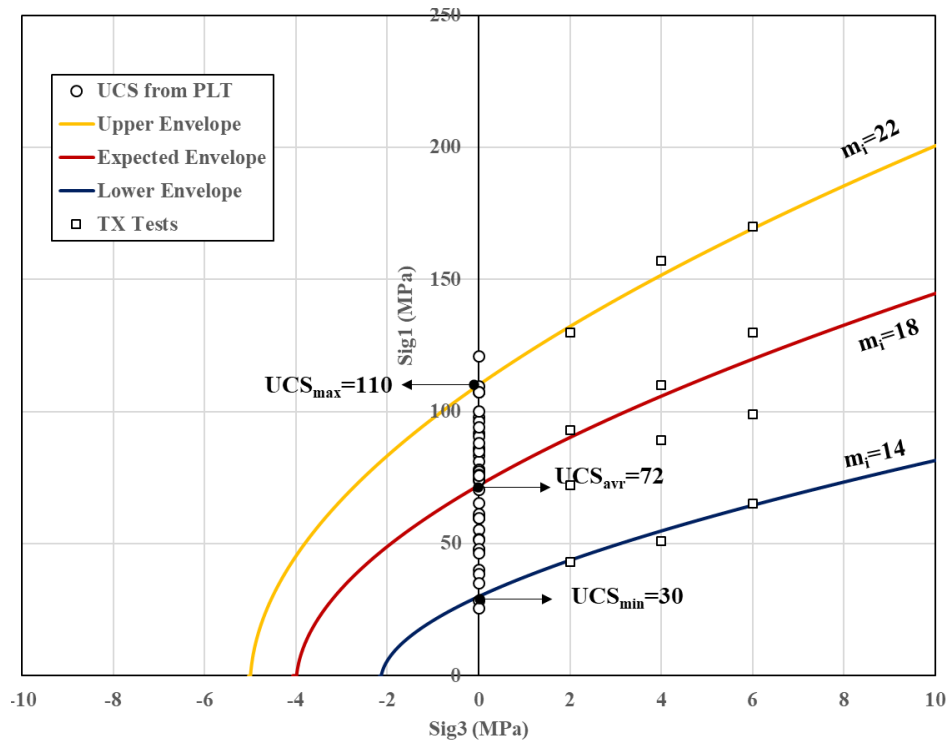


Figure 6.32 Intact rock strength envelope for hornfels – Case study #3

Anisotropic Rock Mass Strength Envelope

Overall scale rock mass failure in pit slopes, excluding a rock mass with very low RMR, typically occur as a combination of sliding along discontinuities and failures through the intact rock pieces. Rock mass strength derived using Generalized Hoek-Brown (G-H-B) criterion represents an isotropic type of strength. One of the underlying assumptions inherent in the G-H-B model is that there is no explicit structural control on the failure mechanism. As seen in Chapter 4, there is one dominant structure (Dip/Dip Direction: $70^\circ/074^\circ$) within the hornfels rock mass, possible as a result of the metamorphisms of the original rock type (i.e. sedimentary). As such, for case study #3 anisotropic rock mass strength parameters will be considered.

The approach to define an anisotropic strength model followed two steps: The first step uses the G-H-B model whose input parameters are UCS, GSI, m_i and D to define the overall rock mass strength. Second, a discontinuity set (S0: stratification) is defined as the main plane of anisotropy and its the shear strength

represented using the Barton Bandis failure criterion (B-B). Finally, a combination of the two failure criteria i.e. G-H-B and B-B is applied for the slope stability analysis. In this approach, different failure surface trials are analyzed by the LEM. If a given failure plane lies outside the dip range of the dominant joint, the rock mass strength is applied. Otherwise, if a failure plane lies between the maximum and minimum dip angle range, the joint shear strength is applied.

The dominant joint orientation was defined as a Fisher distribution with mean orientation of Dip/Dip Direction: $70^{\circ}/074^{\circ}$, and a K Fisher value of 19.2. For the B-b input parameters, the basic friction angle (ϕ_b) was set as a normal random variable with mean 29 and standard deviation of 1.4. The joint roughness coefficient (JRC) was defined as a triangular distribution with max, mean and min values of 1.5, 3.5 and 4.5. The joint compressive strength (JCS) used a Weibull distribution with two parameters: $\alpha = 1.4$ (scale parameter) and $\beta = 35.9$ (shape parameter). These three joint properties were also described in Chapter 4.

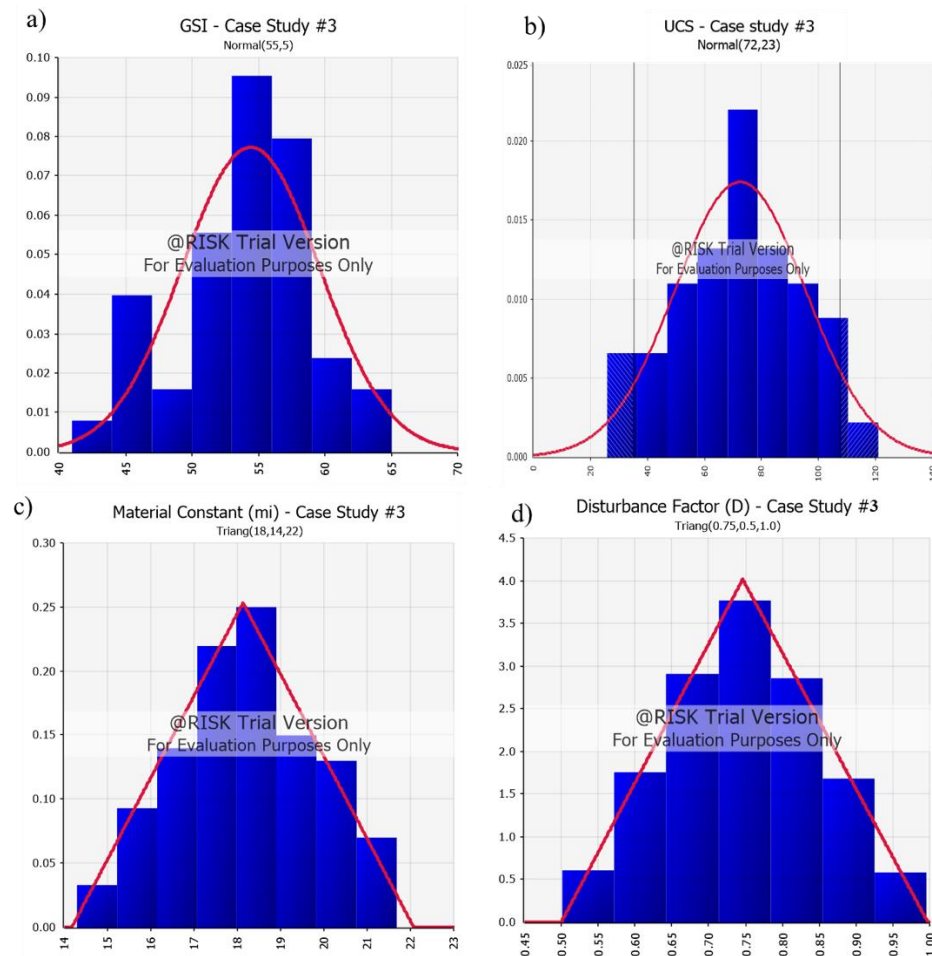


Figure 6.33 Input parameters for estimation of the rock strength envelope – case study #3

Probability density functions (PDF) of the (4) primary parameters for the rock mass (GSI, UCS, m_i and D) were input as statistical distributions (Figure 6.33) to define the overall rock mass strength. These distributions were selected upon the results of field and laboratory testing as explained before. After the PDFs were selected to represent the four primary Generalized Hoek-Brown parameters (GSI, UCS, m_i , and D), the commercial software @Risk 8.0 (Palisade), was used to perform a large number of stochastic simulations, sampling each of the four parameter distributions during each simulation. Based on each set of primary parameters sampled, respective Hoek-Brown secondary parameters (m_b , s and a) were calculated producing PDFs for each of these three, secondary parameters (Figure 6.34).

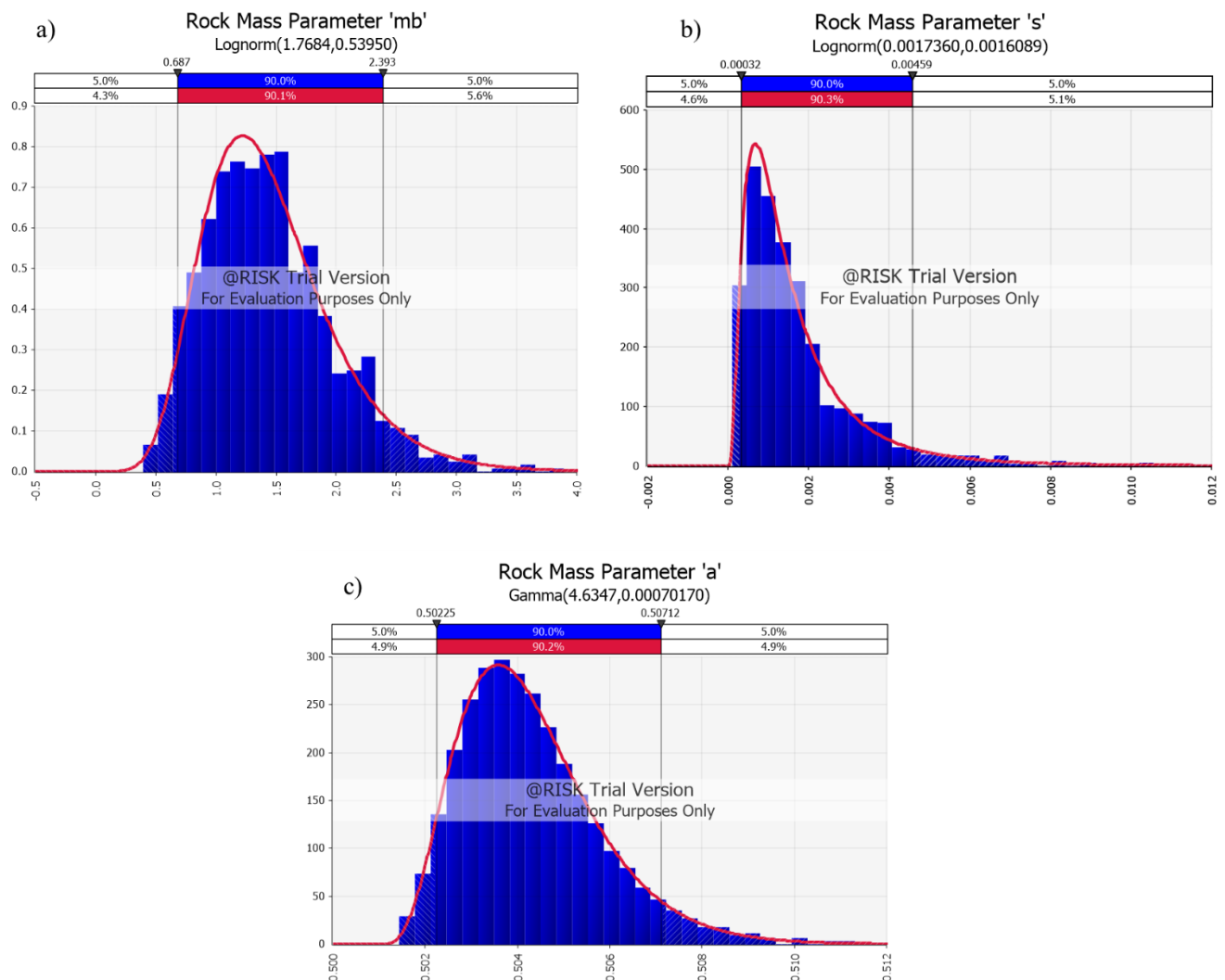


Figure 6.34 Distribution of estimated rock mass parameters a) 'mb', b) 's' and c) 'a' – case study #3

Global Slope Stability Analysis

The design sectors for case study #3 are named North (N), South (S), North East (NE) and South West (SW). 2D cross sections were created for each of these sectors (Figure 6.35).

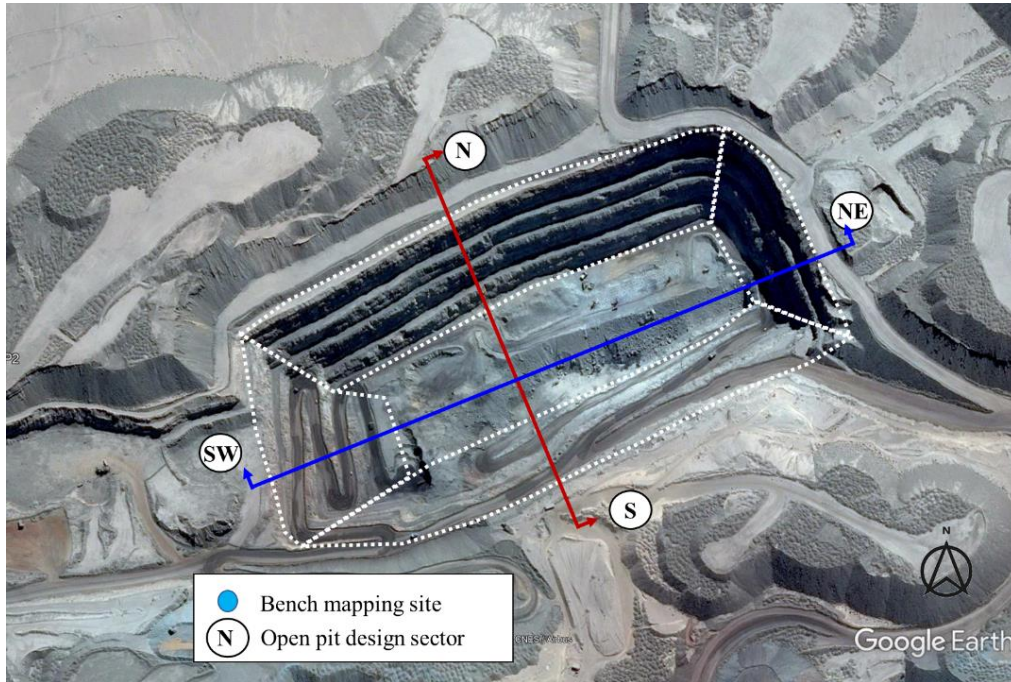


Figure 6.35 Case study #3 open pit mine cross sections.

Rock mass stability analysis was performed using the Slide2D limit equilibrium computer program (Rocscience). The limit equilibrium analyses were conducted to evaluate the overall slope stability of the anisotropic jointed rock mass. An anisotropic analysis was conducted due to the dominant north-eastward dipping structure within the rock mass, comprised of low strength discontinuity planes. A minimum Factor of Safety (FOS) of 1.5 and a maximum Probability of Failure (PoF) of 5% have been targeted. The FoS and PoF are obtained by following a determinist and probabilistic calculation approach, respectively. Spencer's method was selected for the limit equilibrium analyses of this evaluation due to its consideration of both force and moment equilibrium.

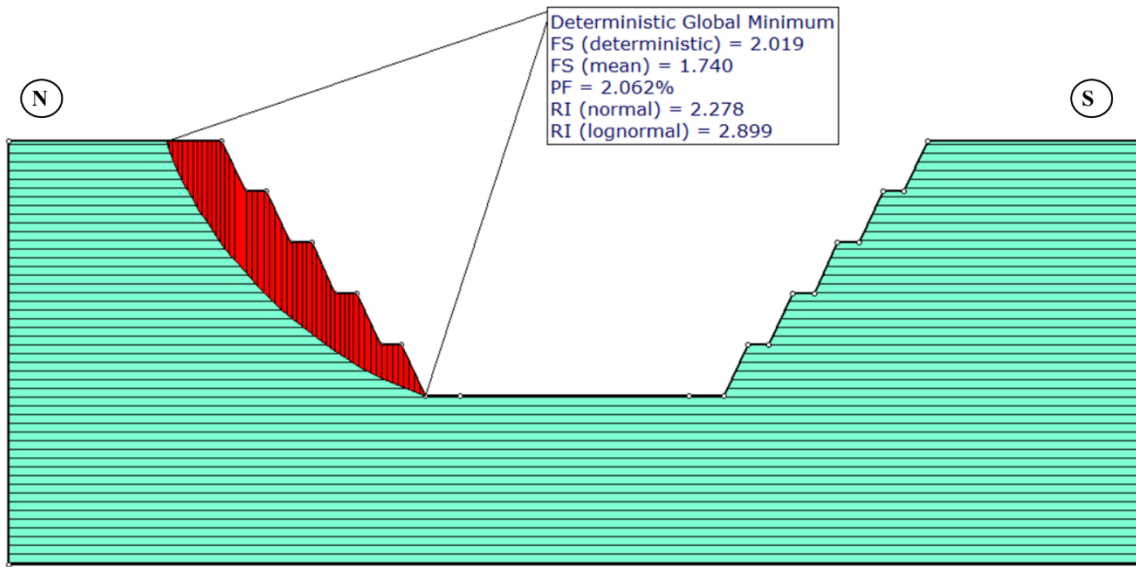
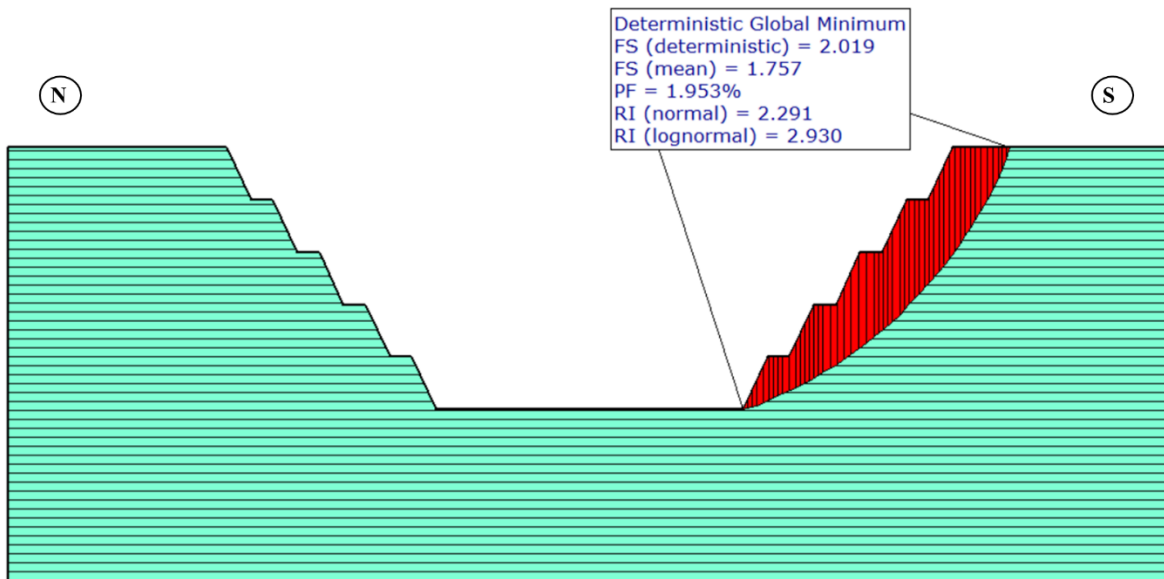
Table 6.4 summarizes the 2D LEM results for each pit wall sector. Figures 6.36a to 6.36d illustrate the geometry, geology, and the critical slip surface for each of the open pit sections. Also, the principal discontinuity set is represented with its apparent orientation relative to the slope direction of analysis. It should be noted that the slopes in sectors North and South cut perpendicular to the strike of the dominant joint structure and therefore it is expected that the dominant joint structure has no major influence on the

failure mechanism. The slope direction in the two remaining sectors South West and North East strike parallel to the dominant joint structure and it dips out of the slope for the SW wall, and towards the slope for the NW wall. Thus, the discontinuity set is likely to play a major role in the stability as an anisotropic surface. This is specially the case for the SW wall where the discontinuity set daylights into the slope. The modelling sections shown in Figures 6.36a to 6.36d represent the current slope geometry in each sector. Slope stability calculations were carried out under dry conditions given the pit mine is in a dry coastal region.

The results of the limit equilibrium analyses indicate that the minimum FoS of 1.50 is achieved for all design sectors. Also, all calculated PoF are below the maximum allowable of 5%, therefore the first conclusion that can be drawn is that the overall pit slope design complies with the design criteria and it can be deemed stable. A closer look to the FoS reveals that for all except for the SW slope wall, the resulting FoS are equal. This is because for sectors North and South the main discontinuity set strikes perpendicular to the slope direction and therefore it does not control the slope stability. The slope stability is controlled by the overall rock mass strength in this case. Although the NW slope wall cuts parallel to the discontinuity set strike, this set dips towards the slope and results in no major influence on stability. Thus, the resulting FoS is equal as for the cases in which stability is controlled by the overall rock mass strength. The pit slope in the SW sector shows the lowest FoS as a result of failure through the discontinuity set which dips out of the slope and has lower shear strength. The results for PoF vary for all four slopes with a maximum corresponding to the SW wall and minimum for the South and North East pit walls.

Table 6.4 Summary of the 2D LEM global slope stability analyses – Case study #3

Rock Type	Cross Section	Slope Side	Deterministic	Probabilistic	Obs.
			FoS (Spencer)	PoF (FS<1.0)	
Hornfels	N - S	North	2.02	2.06	Discontinuity set perpendicular to slope strike.
		South	2.02	1.95	
	SW - NE	South West	1.62	3.08	Discontinuity set dips out of the slope
		North East	2.02	1.95	Discontinuity set dips towards the slope

a) North Slope**b) South Slope**

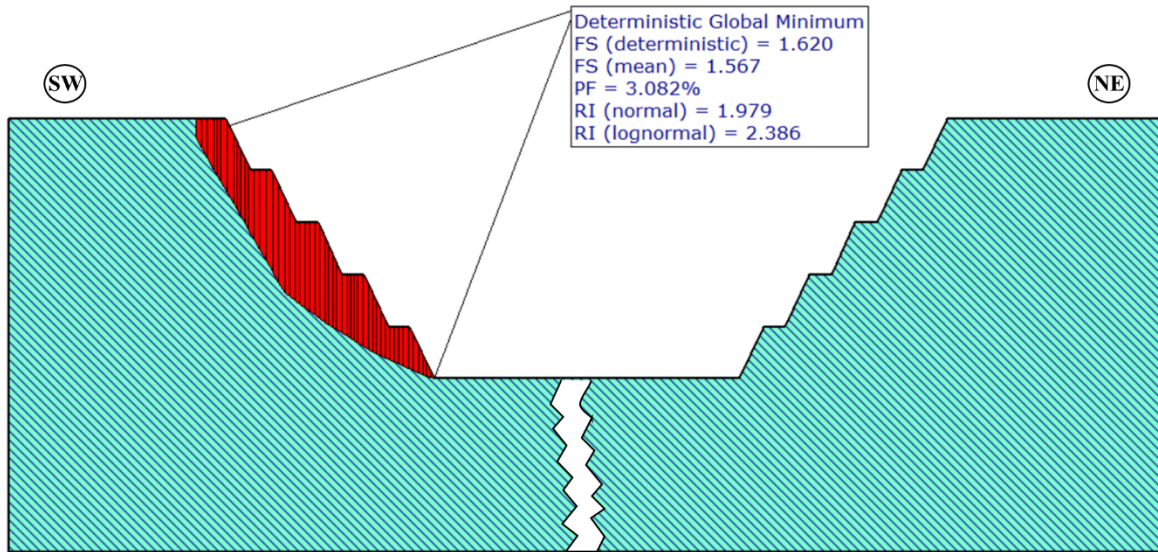
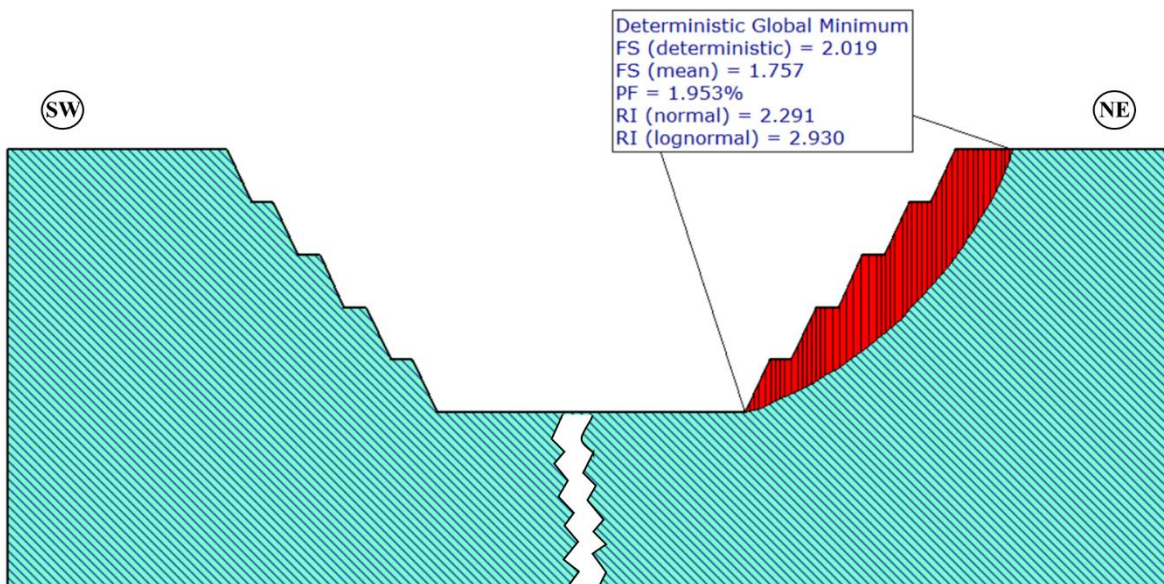
c) South West Slope**d) North East Slope**

Figure 6.36 2D LEM Slope stability results – Case study #3

6.5 Chapter Summary

Chapter 6 covers the main rock laboratory tests and rock mass classification schemes. Emphasis is given to the assessment of uncertainty in intact rock and rock mass Hoek-Brown strength envelopes. Finally, global pit slope stability analysis was carried out for three case studies and FoS as well as PoF were calculated.

- Case study #1: Zone 05 of the open pit mine was divided into 6 sectors. 2D sections were created for each of these sectors and LE analyses performed using the Slide2D software. Hoek-Brown rock mass parameters (mb, s and a) were derived from the PDFs corresponding to the UCS, GSI, mi and D parameters. The critical slip surface for each of the stochastically generated strength conditions were used for the PoF and the mean rock mass strength values for the deterministic FoS calculation. Dry conditions were assumed for the open pit area as this was observed during field mapping. The results of the LE analyses indicate that a minimum FOS of 1.30 can be easily achieved for each of the design sectors. Also, all calculated PoF are below the maximum allowable of 5%, therefore the overall slope complies with the design criteria and it is deemed stable.
- Case Study #2: A comprehensive laboratory testing data was available which comprised: Brazilian Tensile Strength (BTS), Unconfined Compressive Strength (UCS), and Triaxial (TX) tests. The overall rock mass strength parameters were derived using the Generalized Hoek-Brown (G-H-B) criterion and by combining rock testing and core logging data. The open pit mine was divided into ten sectors from which five are within limestone, four in skarn and finally one that belongs to the overburden (soil-like) material. Limit equilibrium analyses of the rock slopes were performed with Slide2D software. The LE results yielded a lowest FoS of 1.8 and highest PoF of 4.58%. Since both the FoS and PoF are above and below the target values of $FoS > 1.5$ and $PoF < 5\%$: respectively, the overall pit slope design complies with the design criteria and it is therefore considered stable under the static and dry conditions analyzed.
- Case study #3: For this project, limited triaxial (TX) tests were available (12). However, intact rock strength for rock samples collected at each mapping site were obtained through PLT testing. PLT values were then converted to UCS estimates. For this case study, a material constant 'mi' range between 14 and 22 with a most likely value of 18 was chosen based on the author's experience in dealing with similar materials. Rock mass stability analysis was performed using the Slide2D limit equilibrium software of Rocscience. Limit equilibrium analyses were conducted to evaluate the overall slope stability of the anisotropic jointed rock mass. An anisotropic analysis was conducted due to the dominant north-eastward dipping structure within the rock mass, comprised of low

strength discontinuity planes. A minimum Factor of Safety (FOS) of 1.5 and a maximum Probability of Failure (PoF) of 5% have been targeted. The results of the limit equilibrium analyses indicate that the minimum FoS of 1.50 is achieved for all design sectors. Also, all calculated PoF are below the maximum allowable of 5%, therefore it can be concluded that the overall pit slope design complies with the acceptability criteria and it can be deemed stable.

Chapter 7

Three-Dimensional Slope Stability Analysis

For slope stability assessment purposes, classical two-dimensional (2D) analysis have widely been used due to its relatively simple formulation. It is current industry practice to perform 2D slope stability analysis for open pit mining. However, 2D analyses rely on several assumptions that are seldom encountered in real open pit mines. Open pit geology and geometry is complex and inherently 3D in character which cannot be adequately captured into a 2D plane strain representation. Therefore, a 3D slope stability analyses is needed for a more accurate representation of the failure mechanisms. In this chapter, 3D slope stability analysis is introduced, and a comparison made between 2D and 3D slope stability results. The advantage of performing 3D Limit Equilibrium Analysis (LEA) and 3D Finite Element Analysis (FEA) to arrive at the direction and location of the critical failure surface for a given open pit slope is shown through different case studies.

7.1 Geometrical Complexities in Open Pit Mines

The importance of three-dimensional geometry in slope stability problems has long been recognized. However, given the complexity of extrapolating 2D analytical solutions into 3D and the computing power required to perform 3D analysis, it has resulted in 2D analysis being favored by both the industry and academia (Brideau, 2010). No until recently, 3D analysis and modeling techniques have started to be used for slope stability problems mainly because of the enhancements in computing capabilities and the availability of commercial 3D software packages.

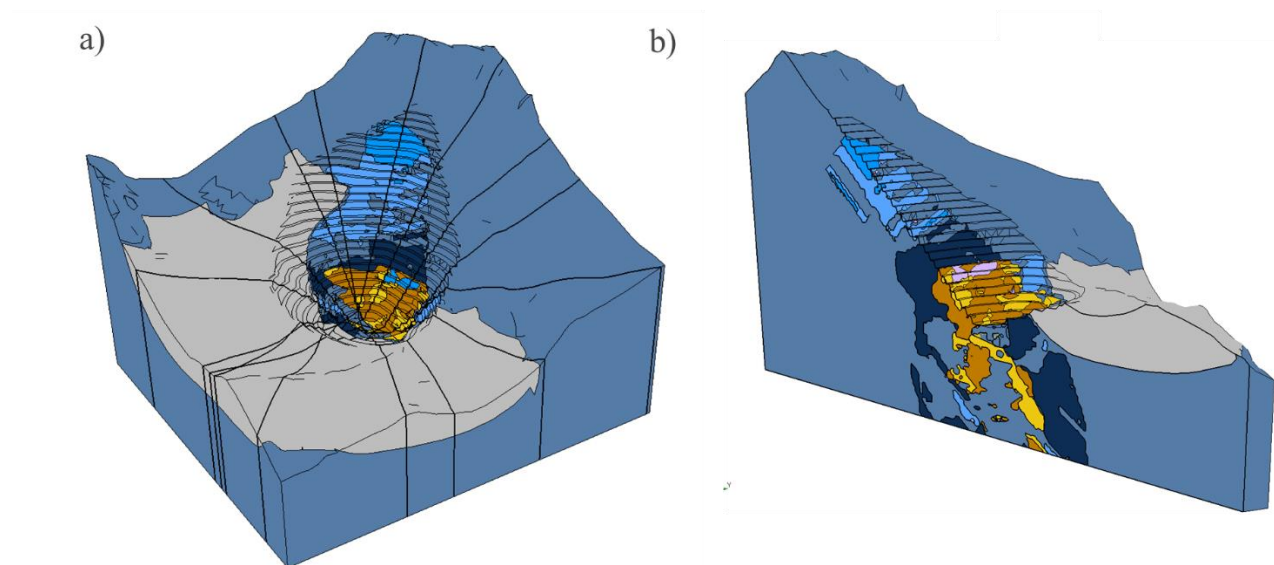


Figure 7.1 3D model of an open pit mine of complex geology and geometry. a) Different cross sections and b) 2D section cutting through the tallest pit wall.

For any 2D analysis, it is assumed that: 1) The slope profile is infinite in the transverse direction (i.e. plane strain conditions apply); 2) The sliding direction is predefined (i.e. the failure direction is parallel to the selected 2D cross section). Usually open pit mine geometries are typically 3D in character and cannot be simplified onto a 2D plane strain model. In addition, the sliding direction cannot be predefined a priori (Lu et al., 2013). Figure 7.1.a shows an open pit mine with complex geology and varying geometry and Figure 7.1.b shows a 2D cross section that has been chosen. It is intuitive to think that a 2D analysis for this case would not be able to capture the 3D effects of varying geology and geometry of the open pit mine. In this respect, the advantage of a 3D over a 2D slope stability analysis is that 1) The actual geology and geometry variability is accounted for, 2) The direction, location and shape of the critical failure is no longer assumed but an output of the 3D analysis (i.e. they become part of the solution).

7.2 Comparison of 2D vs. 3D Analyses Results

Extensive research has demonstrated that the factor of safety (FoS) obtained from 2D analysis is always smaller than the FoS resulting from a 3D approach (Zhang & Ding, 2005; Jiang & Yamagami, 2004; Griffiths & Marquez, 2007; Fredlund et al., 2012; Chakraborty, & Goswami, 2016). This is intuitively reasonable if one thinks that 2D (plane strain) condition neglects the resisting forces acting on the ending sides of the sliding mass. As a result, it has become common to assumed that 2D FoS always correspond to the most pessimistic slip surface section that can be analyzed. It is for this reason the most practicing engineers would prefer a 2D analysis in order to err on the side of safety. However, 2D analysis only yield conservative results if the most critical 2D cross section has been properly selected. For complex models the selection of a representative and critical 2D cross section is not an easy task and many 2D sections need to be analyzed in order to find the critical 2D section crossing the 3D model. This point is highlighted in the 3D example shown in Figure 7.2 taken from Griffiths & Marquez (2007).

The example shown in Figure 7.2 represents a 2:1 slope model of 10 m. height, with an out-of-plane length of 120 m. An oblique zone of weak material (painted in red) with undrained strength $C_u = 20$ kPa has been introduced into the slope with a surrounding material four times stronger with $C_u = 80$ kPa. Using the RS3 Finite Element software from Rocscience Inc., the 3D factor of safety is found to be approximately 1.52 and the mechanism clearly follows the weak layer as shown in Figure 7.2. When 2D stability analyses are then performed on successive cross sections moving along the slope's strike, the results of FoS vs. cross section distance shown in Figure 7.2 are obtained. It is seen that for cross sections taken on the side of the 3D slope model, where most of the slope material is strong, the 2D FoS results led to higher and therefore unconservative estimates of the factor of safety. On the other hand, for sections taken close to the middle of the slope, where there is a greater volume of the weak material, the 2D results led to lower, and therefore conservative, estimates of the factors of safety. The 2D factor of safety closely approached unity at the

middle cross section. An even more critical 2D plane, however, is the one that runs right down the middle of the weak soil. This 2D plane gives a 2.5:1 slope which is flatter than 2D cross sections running perpendicular to the slope's strike; it is, however, homogeneous and consists entirely of the weaker soil. A 2D slope stability analysis on this plane gives an even lower factor of safety of about 0.7. This result, also shown in Figure 7.2, is less than half of the factor of safety given by the 3D analysis and would be considered excessively conservative by geotechnical design standards. Even in the rather simple problem considered here, the results have shown a quite complex relationship between 2D and 3D factors of safety. The results confirm that 2D analysis will deliver conservative results only if a pessimistic 2D cross section for the 3D problem is selected; this may, however, lie well below the 'true' 3D factor of safety. It is also shown, however, that the selection of the 'wrong' 2D plane could lead to an unconservative result.

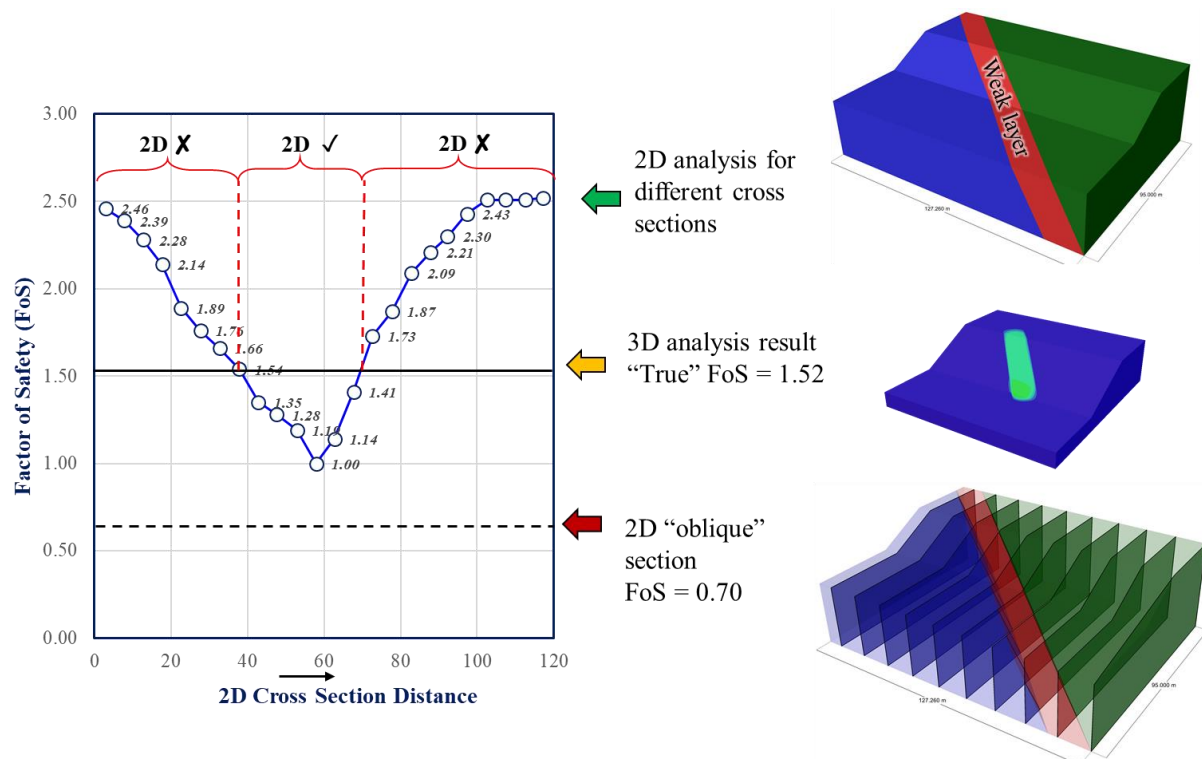


Figure 7.2 Factors of safety from 3D analysis and various 2D sections

7.2.1 3D Effect of Length of Extrusion

In slope stability analysis, two-dimensional (2D) method is usually employed under the assumption of plane strain condition, which is applied to the case of a slope of infinite length. However, the length of a rock slope is finite in engineering practice owing to the complex geometry or boundary conditions imposed. In this section, the impact of varying slope lengths will be investigated and a comparison between 2D and 3D analyses will be carried out.

The following example is taken from Zhang et al (2011). This is a homogeneous slope with a slope height of $H=5\text{m}$, and a slope angle $\alpha=26^\circ$. The 2D cross-section of which is shown in the upper right corner of Figure 7.3. The Mohr-Coulomb criterion is used as the shear strength model for the slope with the following parameters: unit weight $\gamma=17.64\text{ kN/m}^3$, cohesion $c=9.8\text{ kPa}$, friction angle $\phi=10^\circ$.

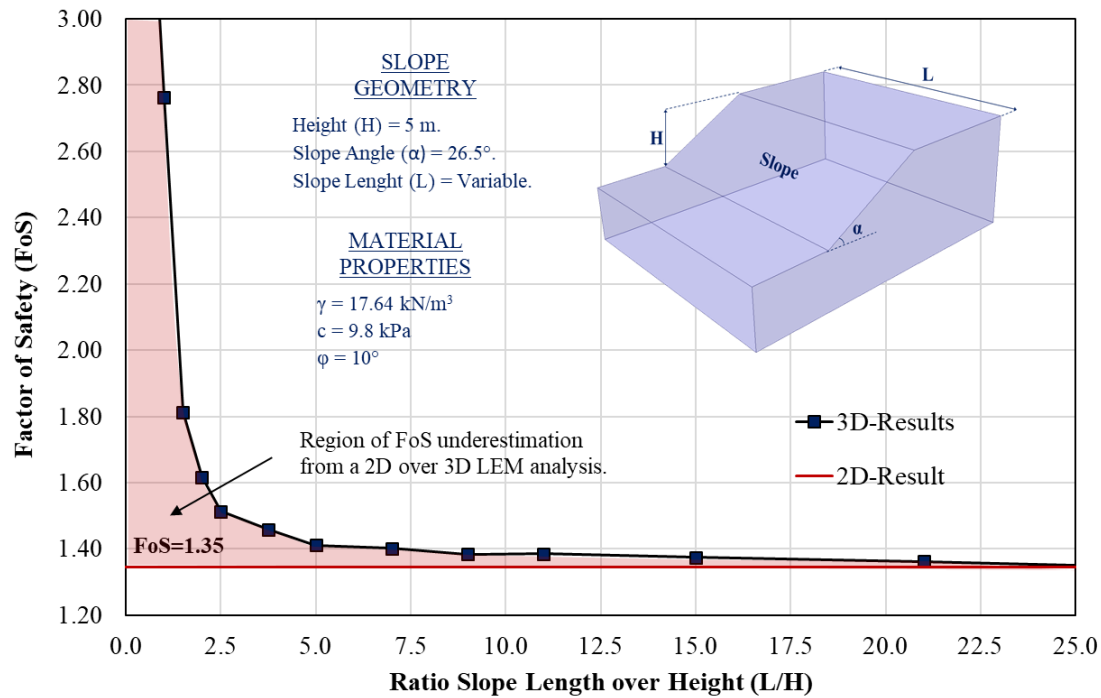


Figure 7.3 Comparison of 2D and 3D FoS for varying length of extrusion of a homogenous slope

The initial 2D cross section is gradually extruded at varying lengths in a direction perpendicular to the cross section to obtain the 3D straight slope model. Then, for each of the resulting 3D extruded models, a Factor of Safety (FoS) is solved by means of a 3D Limit Equilibrium Analysis (LEA). The software Slide3D from Rocscience Inc. was used to compute 3D FoS of the critical failure surface. The results for the 2D LEA are plotted in Figure 7.3 as an horizontal red line at a value of 1.35 which is the 2D FoS. The y-axis of this plot represents the varying extrusion length given as the ratio of the slope length over slope height (L/H). The 3D LEA yielded different values of FoS which are plotted in Figure 7.3 as a black continuous curve. The highlighted red area represents the relative difference between the FoS obtained by 3D and 2D analysis. As can be seen from Figure 7.3, a 2D analyses tend to be conservative and smaller than the 3D FoS. With the increase in the length of extrusion of the slope, the 3D effect gets less remarkable and the 3D FoS approaches that of a 2D analysis (i.e. plane strain solution) when the ratio $L/H > 10$. Thus, a 2D analysis can be thought to be representative of a 3D model when both the geology and geometry of the slope under study

is uniform for a length of up to 10 times the slope's height. This is seldom the case for open pit mines in which complex geology (heterogenous slope) and varying geometry (turning corners) are common.

7.2.2 3D Effect of Turning Corners

Slopes forming concave or convex corners are often constructed during the different stages and phases of open pit mining. The 3D curvature of a rock slope may have a significant influence on its stability (Kelesoglu, 2016). The usual assumption in two-dimensional analyses is that a slope is very long and straight in its lateral direction. This assumption is not justified in the case of open pit mining excavations where the effects of slope curvature may be important (Chowdhury et al., 2009).

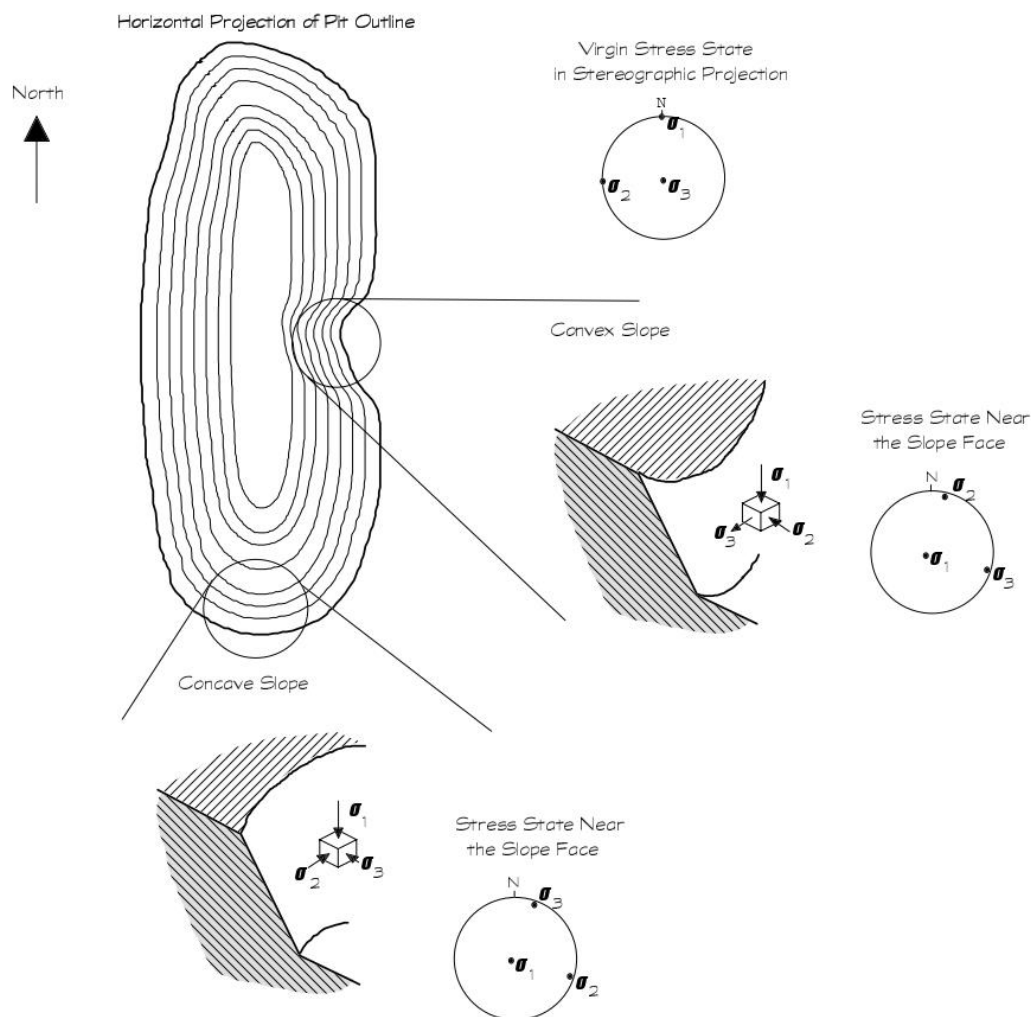


Figure 7.4 Stress conditions acting on an open pit mine with concave and convex slope curvatures (Sjöberg, 1999)

The influence of slope curvature (i.e. convex and concave) on the stability of excavated open pit mines was first discussed by Hoek (1970). He pointed out that there was a tendency for convex slopes to suffer instability in comparison to concave slopes. This difference in behavior was attributed to different stress conditions acting on the slope. Sjöberg (1999) showed the beneficial effects of concave shapes on slope stability since this tend to introduce compressive stresses which in turn increases stability by an arching action effect. In these concave regions, added confinement by the intermediate principal stress results in less destressing of pit walls (Figure 7.4). Convex curvature, on the other hand, tend to assist relaxation of normal stresses with consequent decrease of shear strength and opening of joints and fissures in some cases. Thus, for convex slopes the stress state will be much more unfavorable with the possibility that the minor principal stress become tensile and oriented tangential to the slope face (Figure 7.4). The influence of smooth to sharp curves on the stability of a slope has been further investigated among others by Cala (2007); Farzaneh (2008); Liu et al (2014); Kelesoglu (2016); Sun et al (2017) and Zhang et al (2018).

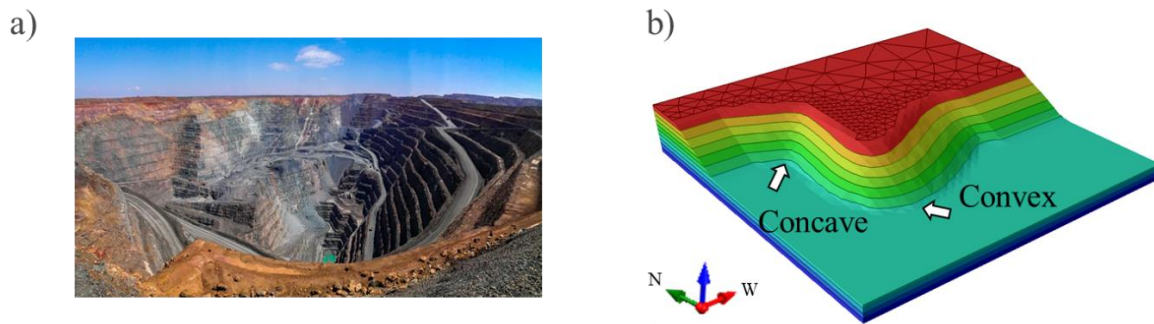


Figure 7.5 3D Effect of turning corners in pit slope stability: a) example of a real open pit mine and b) concave and convex slope curvatures

Figure 7.5.a shows an example of a real open pit mine exhibiting complex and varying geometry. Figure 7.5.b is an example taken from Jiang et al (2003) to investigate the 3D effects of concave and convex regions on slope stability computations. Figure 7.5b illustrates a general 3D asymmetrical slope model with a height of 9 m and with the following M-C shear strength parameters: unit weight $\gamma=17.66 \text{ kN/m}^3$, cohesion $c=11.7 \text{ kPa}$, friction angle $\phi=24.7^\circ$. The elastic properties of this material are also available and are reported as $E=50,000 \text{ kPa}$ and $\nu=0.4$.

The sliding direction for such model is unknown because of the complicated geometry of the slope surface. For such a problem, it is necessary to perform a full 3D slope stability analysis in order to obtain the failure direction and failure location within the 3D slope model. First, a 3D Limit Equilibrium Analysis (LEA) was carried out to search for the 3D critical slip surface direction by means of a dynamic programming and

random number algorithm implemented in the Slide3D software (Rocscience Inc.) The results of the LEA are shown in Figure 7.6.a. These indicate that the sliding occurs in a direction close to the steepest slope surface (i.e. N276°). Second, a 3D Finite Element Analysis (LEA) following the shear strength reduction method was also conducted with the aid of the RS3 software (Rocscience Inc). The slope was modelled as an elastic perfectly plastic material and the resulting Strength Reduction Factor (SRF) from the 3D modelling is shown in Figure 7.6.b. This figure also shows the location of the critical failure which can be interpreted from the total displacement plot. In this case, the critical failure occurs in the east slope wall of the model.

For this example, the 3D FEA results (FoS=1.39) are very similar to the solutions from 3D LEM (SRF=1.46). In the same fashion, when comparing the results from 2D FEA and 2D LEM, the difference is almost negligible i.e. FoS(2D) = 1.28 and SRF(2D) = 1.26. This proves that both LEA and FEA yield almost the same results when used for slope stability assessments. It is also worth noting the 2D results are lower than 3D results and this difference is found to be about 8.6% and 15.8% for LEA and FEA, respectively.

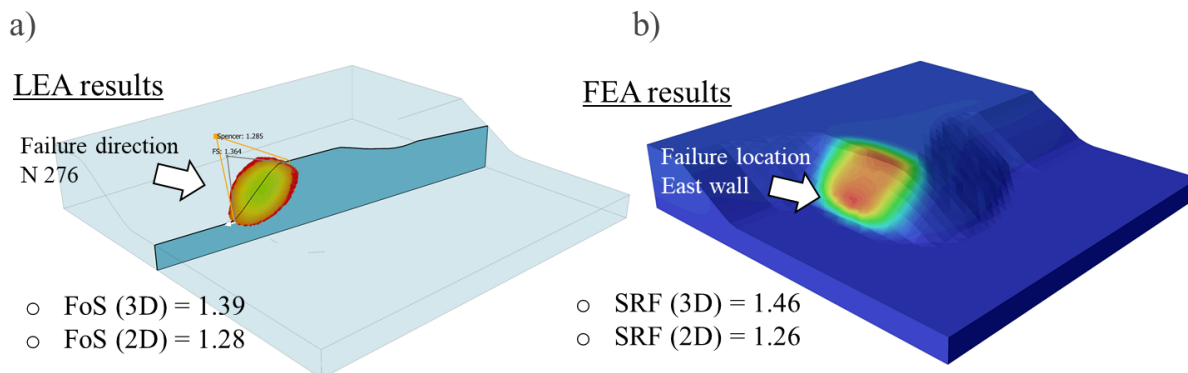


Figure 7.6 3D slope stability analysis using a) LEA and b) FEA

The above-mentioned values of 8.6% and 15.8% for LEA and FEA for the shown example, represent a sort of underestimation meaning that the ‘true’ 3D FoS or 3D SRF is being penalized by using a 2D analysis approach. At stake are questions related to possible increase of open pit depth and pit slope angles. If the ‘true’ 3D FoS or 3D SRF is aimed at this opens opportunities for optimization of the geotechnical design. Since small changes in overall pit slope angle can have a significant effect on the amount of waste rock that need to be moved and the overall economics of the open pit mine operation, it is worth carrying out a fully 3D slope stability analysis to gain more realism in the analysis and results.

7.3 3D Slope Stability Analysis

In the following sections a 3D slope stability assessment for each of the three case studies, previously presented in chapters 4, 5 and 6, is carried out. Both deterministic and probabilistic analyses were conducted by conventional limit equilibrium analyses using the Slide3D and by a finite element approach using the RS3 software; both from Rocscience Inc. In these analyses, a minimum factor of safety (FoS) of 1.50 was specified and a maximum probability of failure (PoF) of 5% have been targeted as an acceptability criterion for the pit slope design at the global scale. All input material properties for the three case studies shown below are the same as defined earlier in Chapter 6. Thus, the items below are mainly focused on the 3D slope stability analysis procedure and results. pit wall.

7.3.1 Case Study #1

A three-dimensional deterministic (i.e. using mean shear strength values) slope stability analysis was performed for the proposed open pit design.

Three-dimensional limit equilibrium slope stability analysis is simple in concept, and directly analogous to two-dimensional methods. While, in 2D a sliding mass is discretized into vertical slices, in 3D it is discretized into vertical columns. Extension of the classical 2D method of slices to 3D method of columns for slope stability purposes can be found in Huang et al (2002) and Cheng & Yip (2007). The 3D LEA used the same input parameters for the rock mass as reported in chapter 6.

A full 3D elastoplastic FE analysis model of case study#1 was constructed. The first step consisted of building a representative 3D geometry of the problem. The plan view dimensions of the domain are 450 m by 450 m. The domain dimensions are enough to eliminate the influence of the boundaries on the model. On the vertical boundary of the model, horizontal restraints (in both the X and Y directions) are applied. Fixed boundary conditions in X, Y and Z are applied at the bottom of the model. In a second step, the behavior of the rock mass was assumed to be governed by an elastoplastic constitutive relation based on the G-H-B strength criterion in which the residual strength parameters are equal to the peak parameters, thus defining an ideally elastoplastic material. Third, a hydrostatic in-situ stress field was assumed for which the gravitational (vertical) and tectonic (horizontal) components were equal i.e. K factor of 1.0. Finally, a finite element mesh using ten-node tetrahedron elements were used to discretize the analysis domain and the RS3 software used to run the developed FE model. Figures 7.7 and 7.8 show the results from 3D LEA and 3D FEA, respectively.

As it can be observed, the resulting critical failure surface are similar from both approaches. The FoS and SRF are 2.52 and 2.60 for the 3D LEA and 3D FEA, respectively. It should be noted that although both approaches yield almost the same results, there is an advantage of using LEA over FEA in terms of computing time. The 3D LEA took around 2 hours to analyze 850 slip surfaces for the entire pit model whereas the 3D FEA took 24 hours for a model with more than 800 000 elements. Therefore, it is not a matter of modelling approach (i.e. LEA or FEA) since both types of analyses provide similar results, it is in fact a matter of whether to use 2D vs 3D tool that makes the difference in the computed FoS or SRF.

From the 2D LEA results provided in Chapter 6, the critical sector for Case Study #1 was identified in sections D-D' and F-F' corresponding to the East and North East pit walls, respectively. These two cross sections showed the lowest FoS and highest PoF in 2D analysis. It is interesting to note that from the 3D LEA and 3D FEA results, the critical failure surface occurs indeed between the North and North sector of the pit mine. This shows that there is good agreement between 2D and 3D slope stability analyses as long as the critical cross section has been considered. However, it should be highlighted that the resulting FoS_{3D} is much greater than the FoS_{2D} as shown in Table 7.1. This also agrees with vast number of publications that claim that a 3D FoS is almost always higher than 2D FoS as the resisting forces acting on the ending sides of the sliding mass is considered.

Table 7.1 summarizes the results for the deterministic 3D LEA and 3D FEA, respectively. It highlights among other things, 3D to 2D FoS increment and compares the computing times for each method of analysis.

Table 7.1 3D LEA and 3D FEA deterministic stability analysis results – case study #1

Method of Analysis	Critical Open Pit Sector	FoS_{2D} / SRF_{2D}	FoS_{3D} / SRF_{3D}	2D-3D FoS or SRF Increment	Computing Time
LEM	N-NE	1.98	2.52	27%	2 Hrs
FEM	N-NE	2.10	2.60	23%	24 Hrs

Since it has been shown that LEA and FEA yield almost the same results, a three-dimensional probabilistic limit equilibrium analysis is now performed for the proposed open pit design. For the probabilistic analyses, the LEA over the FEA approach was chosen due to its relatively low computing time demands. It is the opinion of the author that 3D FEA used for slope stability assessment purposes although powerful is not

currently amenable to be used within an iterative Monte-Carlo simulation approach mainly because of its large computing times.

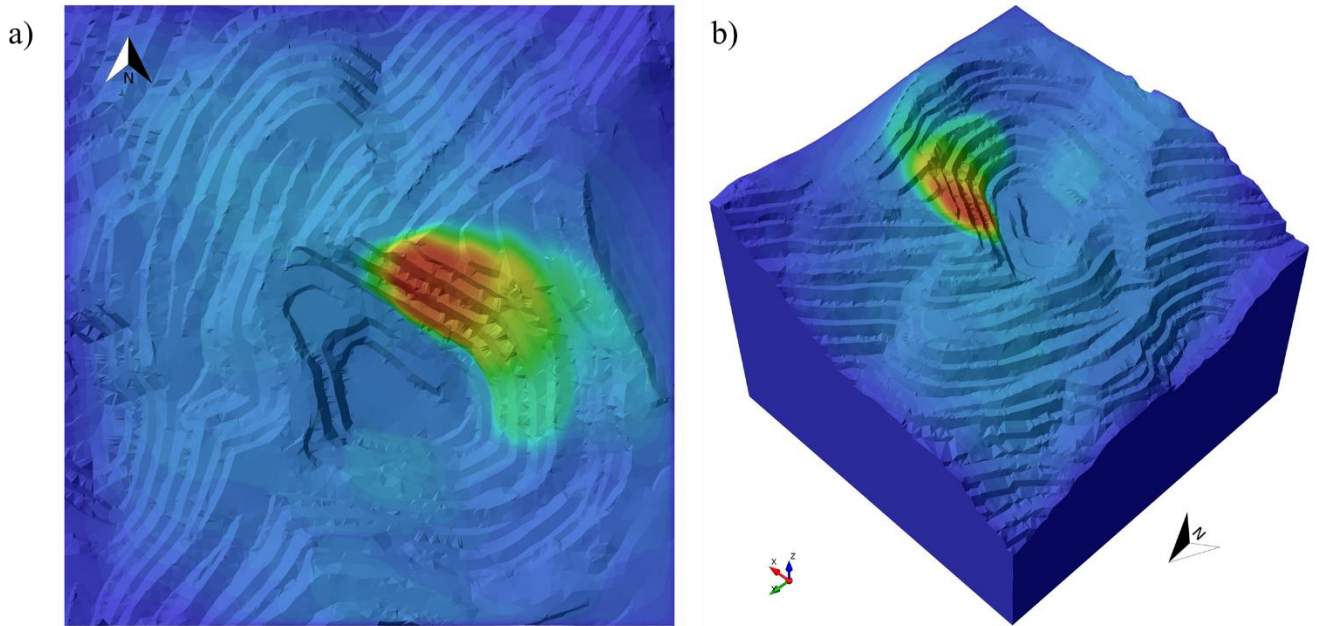


Figure 7.7 3D FEA results for the global open pit mine – case study #: a) Plan and b) Perspective view

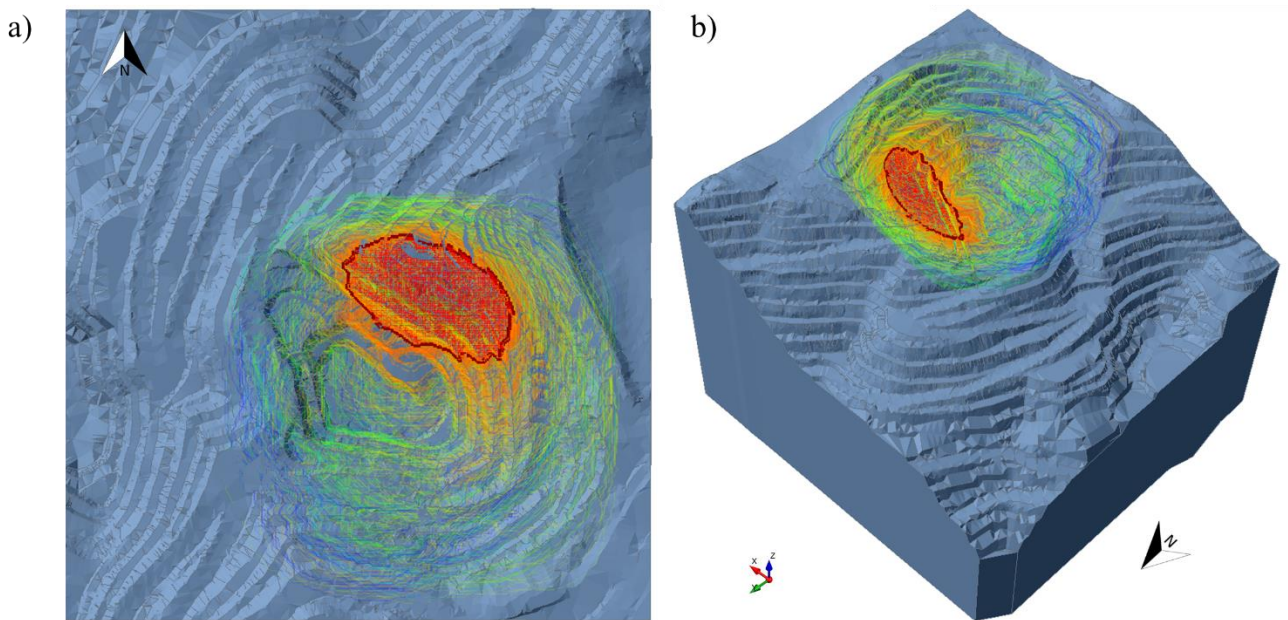


Figure 7.8 3D LEA results for the global open pit mine – case study #: a) Plan and b) Perspective view

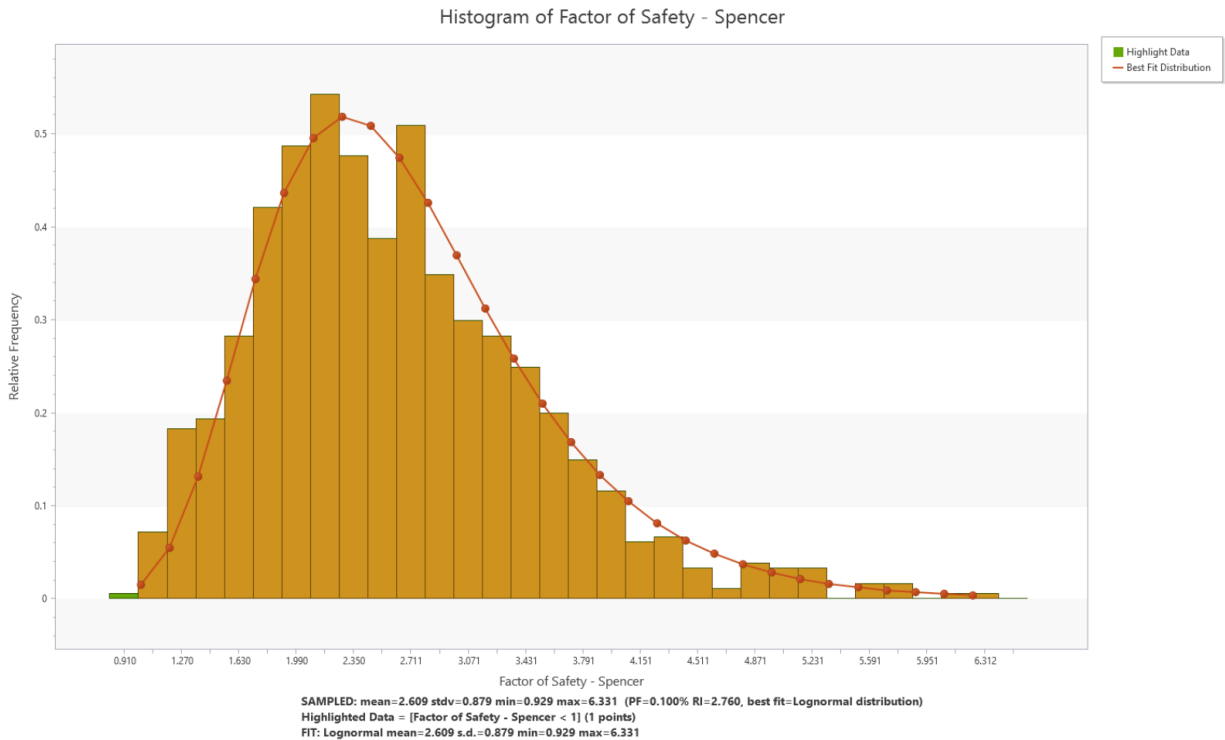


Figure 7.9 Histogram of the FoS from the 3D probabilistic LEA – case study #1

Figure 7.9 shows the histogram of the FoS distribution for 1000 Monte Carlo simulations within a 3D LEA. From this, the probability of pit slope failure $P[\text{FoS} < 1.0]$ is 0.1 %. The results of the three-dimensional limit equilibrium analyses indicate that the minimum FoS of 1.50 is achieved for the proposed open pit design. Also, the calculated Probability of Pit Slope Failure (PoF) is below the maximum allowable of 5%, therefore the proposed pit slope design complies with the design criteria and it is deemed stable.

7.3.2 Case Study #2

Figure 7.10.a shows the geology of the open pit mine project. Figure 7.10.b illustrates the proposed pit design whose stability is going to be assessed. This design comprises singles benches of 10 m height, a 6.5 m bench width and a bench face angle of 70° . When added a ramp of 25 m width, the overall slope angle for the pit resulted in 45° . The 3D LEA followed three steps.

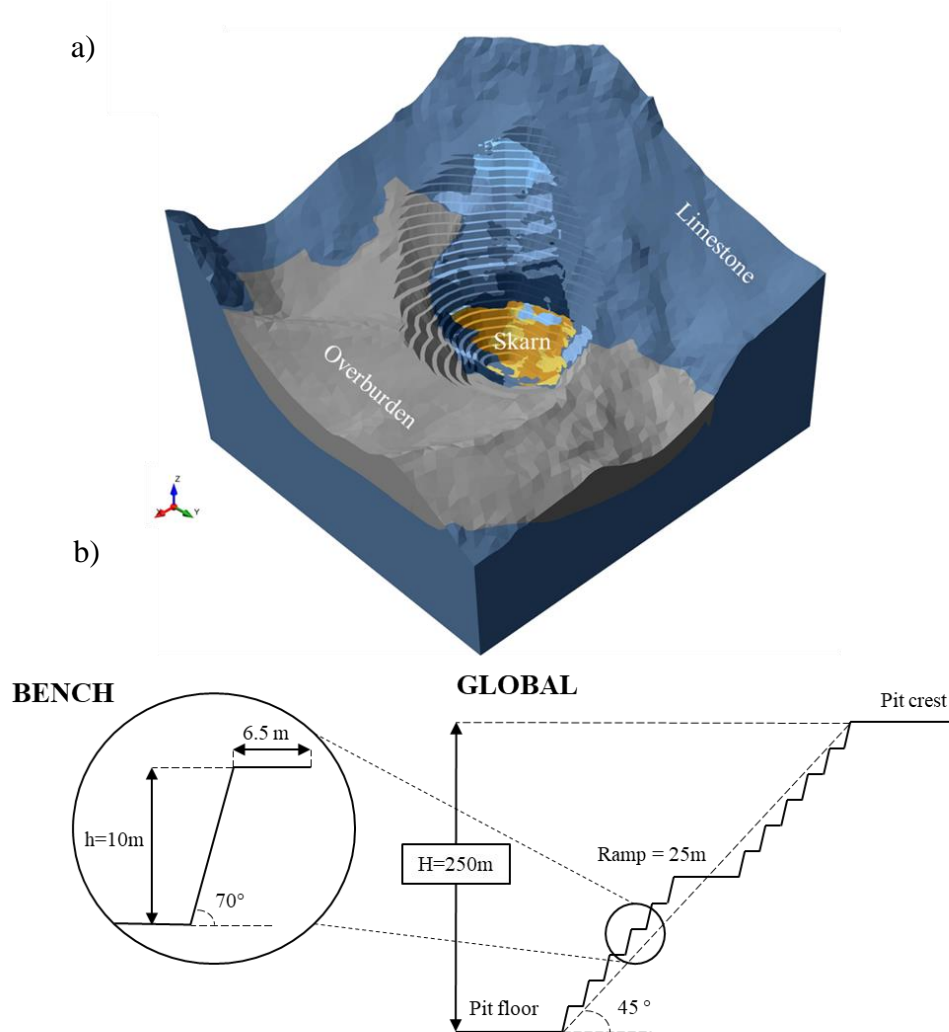


Figure 7.10 3D open pit model: a) Pit geology and b) Proposed open pit design

First, a deterministic analysis was run using the mean shear strength of the rock mass. In this 1250 slip surfaces (Figure 7.11.a) were analyzed and the one with the lowest FoS retained for the next step. For comparison purposes an 3D elastoplastic FEA was carried out for the same model and using the mean strength values of the rock mass.

The 3D elastoplastic FE analysis model of case study#2 was run in RS3 software. The dimensions of the model are 700 m by 700 m and a maximum depth of 500 m. The boundary restraints on the model sides were defined in both the X and Y directions and totally fixed in X, Y and Z at the bottom of the model. The behavior of the rock mass was assumed as an ideally elastoplastic material governed by the G-H-B strength criterion with residual equal to the peak strength values. A hydrostatic in-situ stress field was assumed for which the gravitational (vertical) and tectonic (horizontal) components were equal i.e. K factor of 1.0.

Figure 7.12 shows the results from 3D LEA and 3D FEA with a FoS and SRF of 2.80 and 2.75. The 3D LEA took around 4 hours to analyzed 1250 slip surface whereas the 3D FEA took 18 hours for a model with 650 000 elements. Table 7.2 summarizes the results for the deterministic 3D LEA and 3D FEA, respectively. It should be noted that there is an important increment from 2D FoS to 3D FoS in more than 50%. This can be attributed to the convexity of the tallest pit wall which is considered in the 3D analysis.

Table 7.2 3D LEA and 3D FEA deterministic stability analysis results – case study #2

Method of Analysis	Critical Open Pit Sector	FoS _{2D} / SRF _{2D}	FoS _{3D} / SRF _{3D}	2D-3D FoS or SRF Increment	Computing Time
LEM	SW	1.78	2.80	57%	4 Hrs
FEM	SW	1.80	2.75	53%	18 Hrs

In the second step, FoS's using the minimum and maximum shear strength values of the rock mass were computed. As can be seen in Figures 7.11.b, FoS's for the average and maximum shear strength envelopes comply with the target FoS which is 1.5. However, when using the minimum shear strength values the resulting FoS is a lot lower than 1.5. The question then arises as to how likely is this Fos is=0.7 to occur. A third step is needed, in which the whole distribution of FoS is calculated by means of a Monte Carlo iterative approach.

Figure 7.13 shows the histogram of the FoS distribution. It should be noted that the minimum (0.7) and maximum (7.8) FoS initially computed using the lowest and highest rock mas strength parameters, lie near the left and right-hand side on the distribution. The fact that theses FoS's lie on the tail of the distribution tells us that the probability of occurrence of such events are very low. Now we can report two types of probability for the overall pit slope:

- Probability of Slope Failure

$$P[\text{FoS} < \mathbf{1.0}] = 1.5 \%$$

- Probability of Unacceptable Performance

$$P[\text{FoS} < \mathbf{1.5}] = 3.5 \%$$

It should be noted that all slope stability calculations assumed that the pit wall will be depressurized (i.e. dry conditions) by implementing horizontal drains and/or pumping wells. The results of the three-dimensional limit equilibrium analyses indicate that the minimum FoS of 1.50 is achieved for the proposed

open pit design under static and dry conditions. Also, all calculated PoF are below the maximum allowable of 5%, therefore the overall pit slope design complies with the design criteria and it is deemed stable.

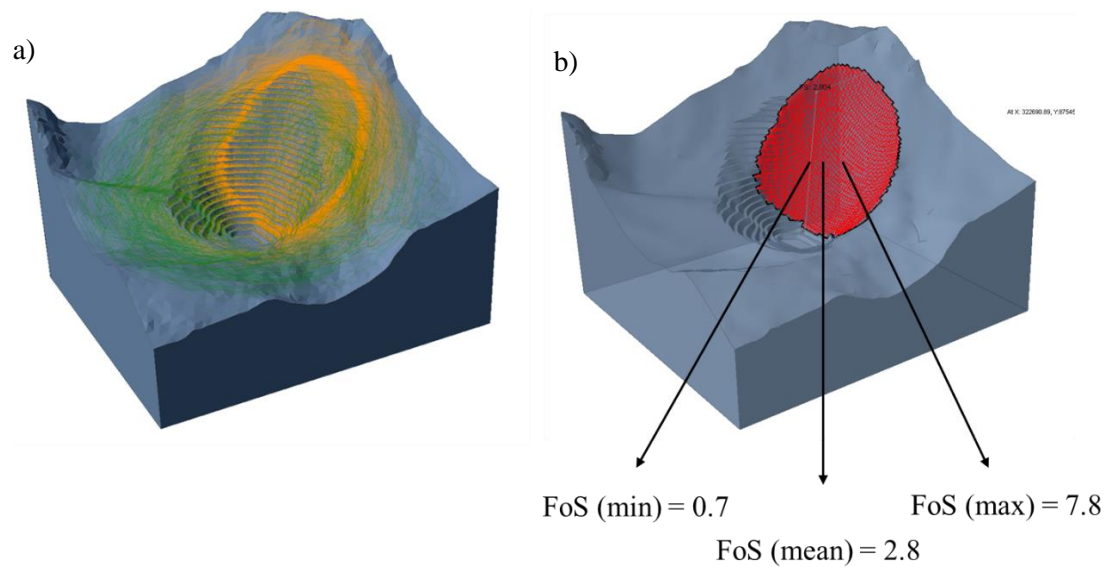


Figure 7.11 3D LEA for the pit mine – case study #2: a) Search of the critical failure surface and b) Calculation of the min, max and average FoS

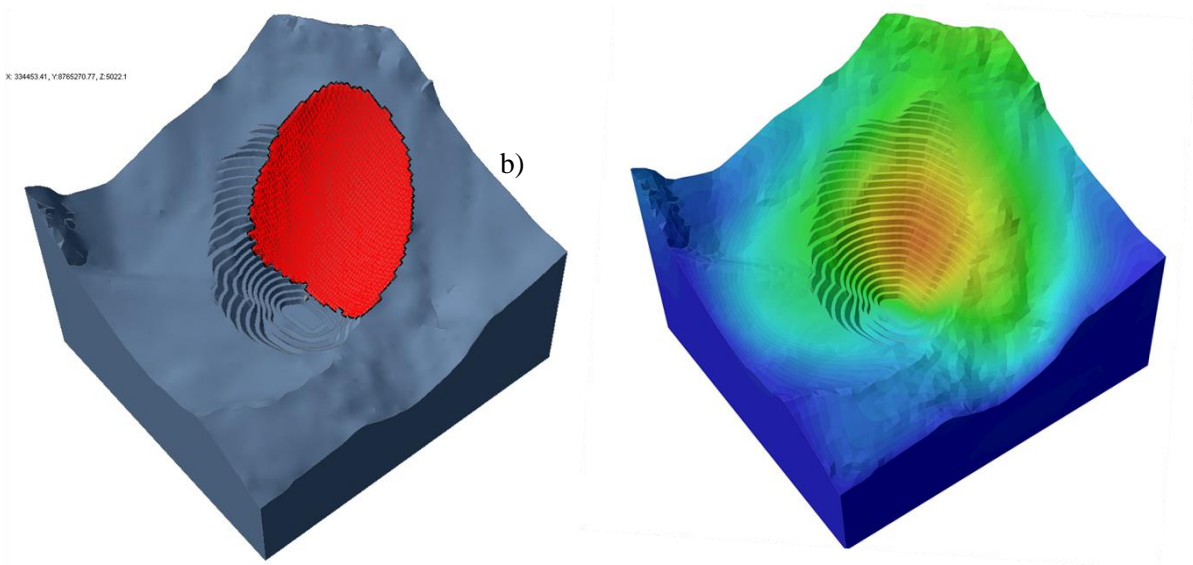


Figure 7.12 Comparison of analysis methods: a) 3D LEA b) 3D FEA – case study #2

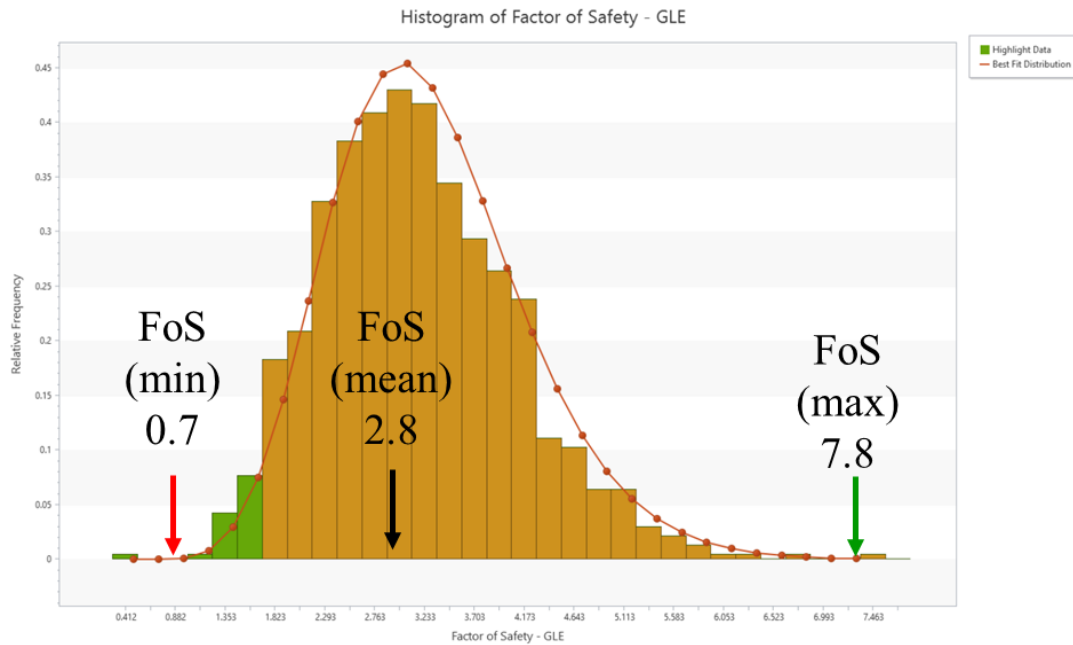


Figure 7.13 Histogram of the FoS from the 3D probabilistic LEA – case study #2

7.3.3 Case Study #3

3D LEA was conducted with Slide3D program (Rocscience) to evaluate the overall slope stability considering isotropic and anisotropic jointed rock mass conditions (Figures 7.14 and 7.16). An anisotropic analysis was conducted for the SW sector due to an adversely oriented discontinuity set. All other sectors i.e. N, S and NE were analyzed considering an isotropic rock mass behavior. Given the symmetry of the open pit (rectangular shape) each sector was analyzed as a 3D model obtained by an extruded length of 300 m for the North and South sectors and 550 m for the South West and North East sectors.

Table 7.2 3D LEA deterministic stability analysis results – case study #3

Method of Analysis	Rock Mass Behaviour	FoS _{2D}	FoS _{3D}	2D-3D FoS Increment
LEM	Isotropic	2.02	2.14	5.9%
	Anisotropic	1.62	1.78	9.8%

Table 7.3 summarizes the results for the deterministic 3D LEA. There is a small increment from 2D FoS to 3D FoS of 5.9% and 9.8% for the isotropic and anisotropic analysis, respectively. This can be attributed to the straight orientation of each pit wall sector i.e. absence of turning corner which makes the 2D plane strain assumptions valid and therefore the FoS_{2D} relatively closed to FoS_{3D} values.

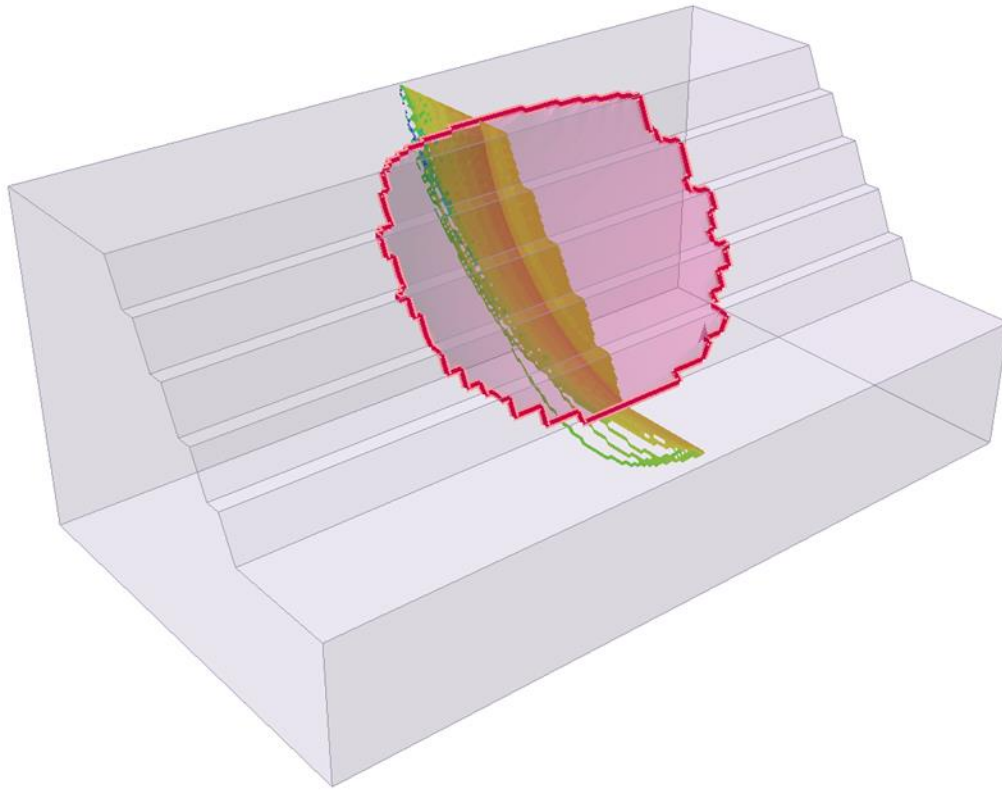


Figure 7.14 3D deterministic LEA isotropic rock mass – case study #3

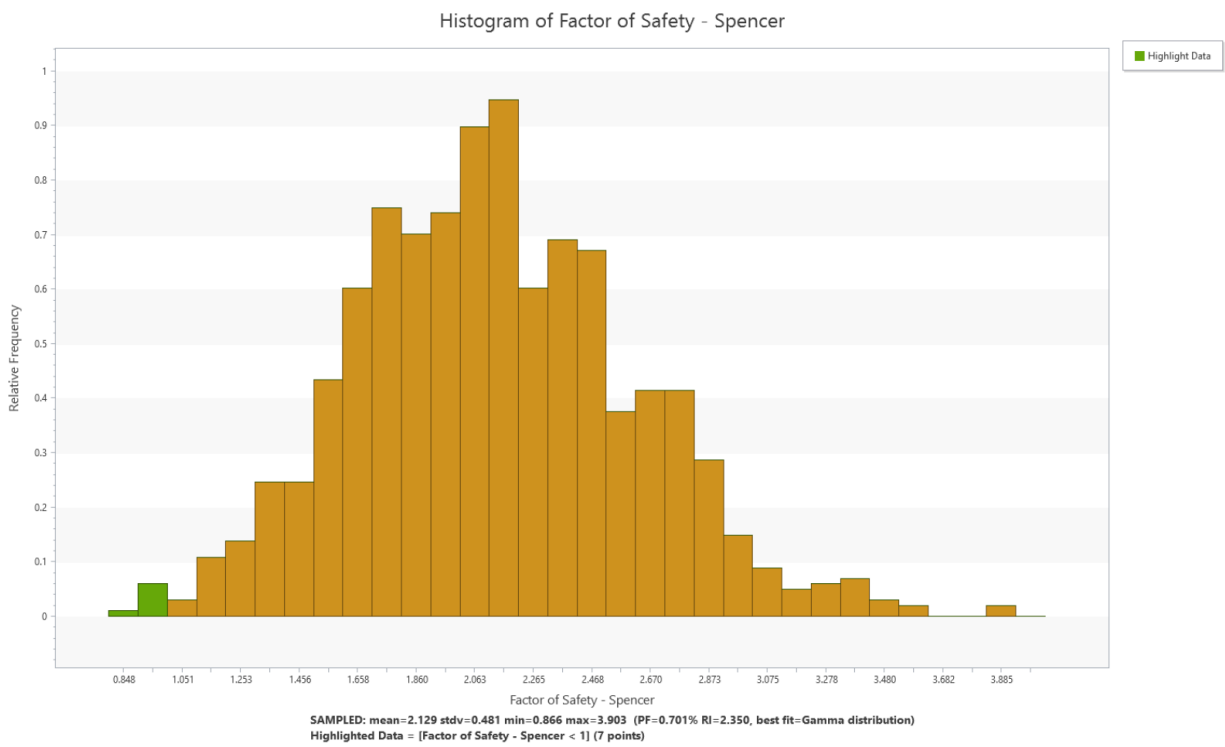


Figure 7.15 Histogram of the FoS from the 3D probabilistic LEA isotropic – case study #3

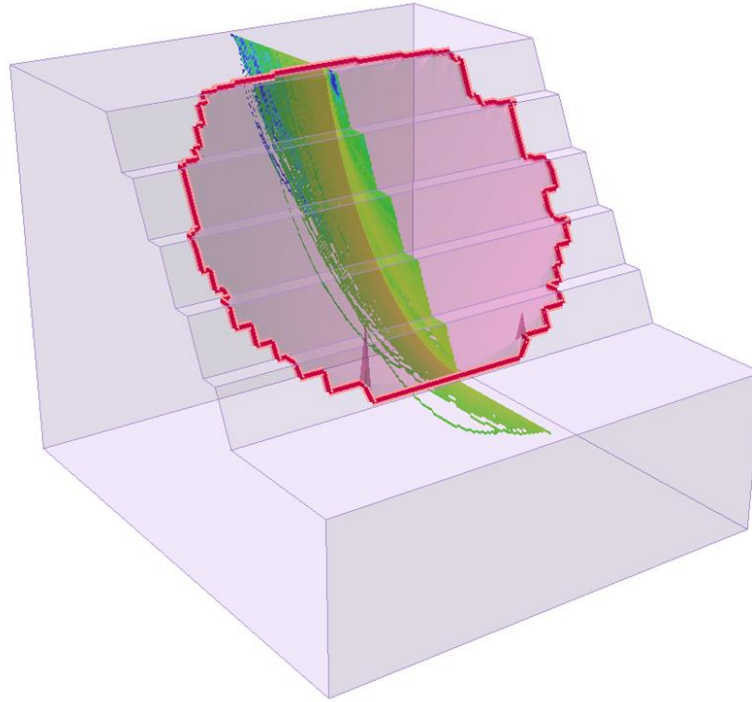


Figure 7.16 3D deterministic LEA anisotropic rock mass – case study #3

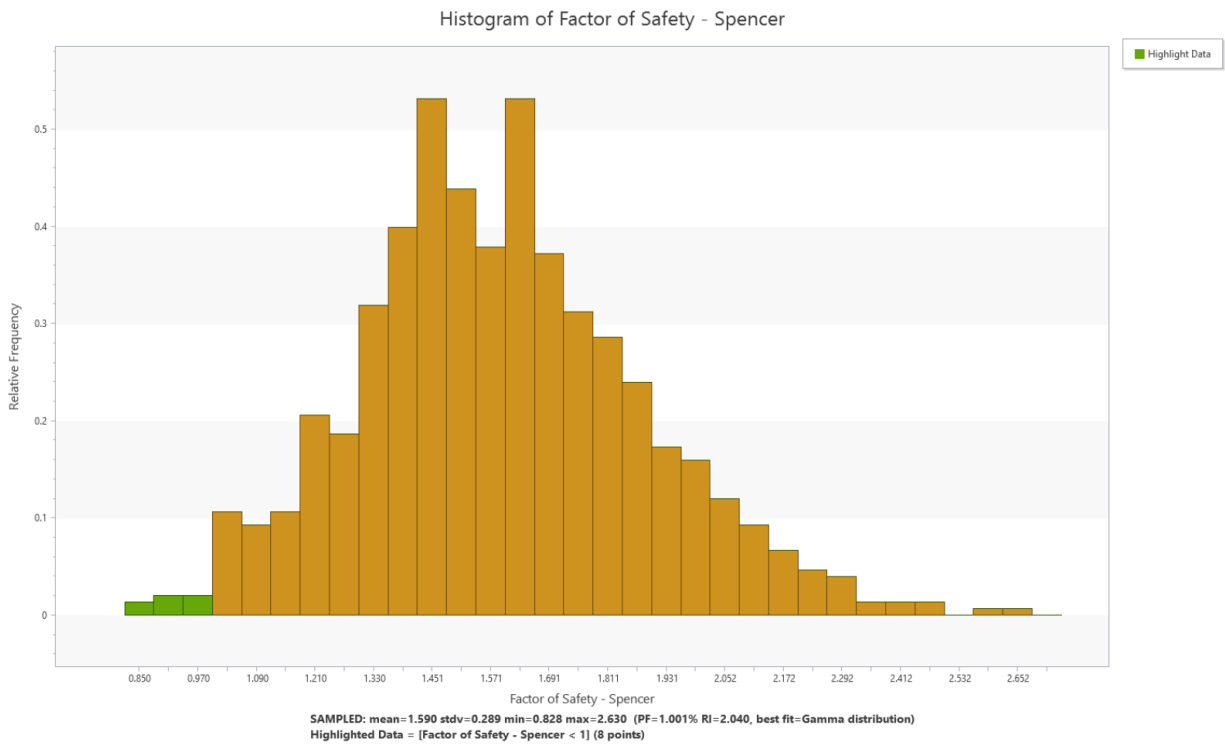


Figure 7.17 Histogram of the FoS from the 3D probabilistic LEA anisotropic – case study #3

Figure 7.15 and 7.17 show the histograms of the FoS distribution for 1000 Monte Carlo simulations within a 3D LEA for the isotropic and anisotropic analysis, respectively. From this, the probability of pit slope failure $P[\text{FoS} < 1.0]$ is 0.7 % and 1.0%. The results of the deterministic three-dimensional limit equilibrium analyses indicate that the minimum FoS of 1.50 is achieved for the proposed open pit design. Also, the calculated Probability of Pit Slope Failures (PoF) are below the maximum allowable of 5%, therefore the proposed pit slope design complies with the design criteria and it is deemed stable.

7.4 Chapter Summary

Chapter 7 explains the main limitations of two-dimensional slope stability analysis in open pit mining such as the difficulties in choosing the most critical 2D cross section, the effect of length of extrusion and the effect of turning corners. It also addressed the benefits gained from using three-dimensional tools via the LEA and FEA, highlighting the convenience of 3D LEA over 3D FEA due to computing time demands. Finally, 3D global pit slope stability analysis was carried out for three case studies and FoS as well as PoF were calculated. The results agree with the vast number of publications that claim that a 3D FoS is almost always higher than 2D FoS as the resisting forces acting on the ending sides of the sliding mass is considered.

- Case study #1: A three-dimensional deterministic LEA and FEA for the proposed open pit design was performed with similar results obtained from these two methods: $\text{FoS}=2.52$ and $\text{SRF}= 2.60$. From the 3D LEA and 3D FEA results, the critical failure surface occurs between the North and North sector of the pit mine. An increment of 3D FoS/SRF with respect to 2D FoS/SRF was found of 27% and 23% for the LEA and FEA. This is in good agreement with the general acceptance that 3D FoS/SRF are always higher than 2D FoS/SRF. A limit equilibrium approach was chosen for the three-dimensional probabilistic analysis due to its relatively fast computing times. From this, the probability of pit slope failure $P[\text{FoS} < 1.0]$ was found to be 0.1 %. Finally, the results show that the minimum FoS of 1.50 is achieved and the calculated PoF is below the maximum allowable of 5%, therefore the proposed pit slope design complies with the design criteria and it is deemed stable.
- Case Study #2: The geotechnical design for this open pit mine project comprises single benches of 10 m height, a 6.5 m bench width and a bench face angle of 70° . When added a ramp of 25 m width, the overall slope angle for the pit resulted in 45° . From the deterministic 3D LEA and 3D FEA results, a FoS and SRF of 2.80 and 2.75 was obtained with the critical failure surface occurring in the South West sector of the pit. The 3D LEA took around 4 hours to analyze 850 slip surfaces for the entire pit model whereas the 3D FEA took 18 hours for a model with more than 650 000 elements in the 3D mesh. From the probabilistic 3D LEA analysis, the Probability of Slope Failure

$P[FoS < 1.0]$ and Probability of Unacceptable Performance $P[FoS < 1.5]$ was calculated as 1.5 % and 3.5 %, respectively. Both FoS and PoF met the design requirements.

- Case study #3: Isotropic and anisotropic jointed rock mass conditions were distinguished due to an adversely oriented discontinuity set occurring in the South West sector. A small increment from 2D FoS to 3D FoS of 5.9% and 9.8% for the isotropic and anisotropic analysis was found, respectively. This can be arguably attributed to the straight orientation of each pit wall sector which makes the 2D plane strain assumptions valid and therefore the FoS2D relatively closed to FoS3D values. The results for the deterministic 3D LEA gave a FoS of 2.02 and 1.62 for the isotropic and anisotropic analysis, respectively. Likewise, the probability of pit slope failure $P[FoS < 1.0]$ was found to be 0.7 % and 1.0%. Also, the calculated Probability of Pit Slope Failure (PoF) is below the maximum allowable of 5%, therefore the proposed pit slope design complies with the design criteria and it is deemed stable.

Chapter 8

Summary and Conclusions

The research completed and presented in this thesis covers a comprehensive review on slope stability analysis in open pit mining by comparing the LEA vs FEA, the Deterministic vs Probabilistic approach and 2D vs 3D modelling tools. Three case studies have been thoroughly examined independently at the bench, inter-ramp and overall slope scale. The primary conclusions resulting from this thesis as well as some recommendations for future work are given in the following subsections.

8.1 Conclusions

Bench Slope:

- Rock slope instabilities for jointed rock masses at the bench scale mostly occur as the result of failure along structural discontinuities. As such, the bench slope design requires a sound understanding of the rock mass fabric which can be collected from surface mapping and/or core logging and which should preferably be complemented with photogrammetry mapping and/or televiewer logging data.
- A probabilistic bench slope stability analysis should focus on assessing three main input parameters: i) joint orientation (e.g. dip and dip direction), ii) joint shear strength (e.g. cohesion and friction), and iii) joint size (e.g. joint trace length).
- Discrete Fracture Network (DFN) modelling represents a powerful tool in assessing structurally controlled and gravity-driven instability types in jointed rock masses, not only for surface (e.g. slopes) but also for underground (e.g. stopes) mining environments.
- The case studies presented in chapter 4 followed a kinematic and kinetic approach whereby a FoS and PoF was calculated considering planar, wedge and toppling failure mechanisms for each sector.

Inter-Ramp Slope:

- Multi-bench or inter-ramp instabilities include failures that involve more than one bench. Inter-ramp slope design is typically performed through a deterministic analysis of major large-scale discontinuities or highly persistent minor rock joints.
- Both deterministic stereographic and limit equilibrium-based analyses for three case studies in chapter 5 were presented with the purpose to establish the optimum inter-ramp angle (IRA) which undercuts as few daylighting planes, wedges or blocks as possible.

Global Slope:

- Global scale failure mechanisms in open pit slopes are mainly controlled by the overall strength of the rock mass. As such, the engineering characteristics of both intact rock and discontinuities must be considered to arrive at good estimates of the rock mass strength properties.
- The uncertainty in intact rock strength parameters can be assessed using the non-linear Hoek and Brown equation by fitting a composite of tensile, uniaxial and triaxial testing data. The use of a Prediction Interval (PI) provides an estimate of upper and lower bounds for a given confidence level.
- As rock masses have a complex and uncertain nature, to deal with such complexity, the use of probabilistic approaches seems to be more appropriate in order to make more reliable characterizations in rock mass strength parameters shows the procedure for estimating the variability in the rock mass strength envelopes through a Monte Carlo simulation method
- A Monte Carlo simulation is run to arrive at the PDF of the RMR values by fitting a theoretical distribution to the five RMR input parameters. By using suitable conversion relationships, the PDF of GSI values can be obtained from the RMR distribution. Using the simulated probability density distributions of GSI with the uncertainty in intact rock parameters quantified from the above step, the Hoek-Brown rock mass parameters can be estimated, i.e. ' mb ', ' s ' and ' a '.
- Finally, in chapter 6 global pit slope stability analysis was carried out for three case studies and FoS as well as PoF were calculated. The results of the all LE analyses indicate that the minimum FOS of 1.50 and maximum allowable of 5% PoF is achieved for each of the design sectors. Therefore, the overall slope complies with the design criteria and it is deemed stable.

Deterministic vs Probabilistic Analysis

- Traditionally, slope stability assessment is carried out by means of a deterministic analysis whereby the input is a set of parameters that are fixed quantities, usually taken as the mean values of the data obtained from site investigation or laboratory testing.
- Although, simple and straightforward, the deterministic analysis fails to account for the different degrees of variability and uncertainty often encountered in rock properties.
- The application of probability theory provides rational means to treat the underlying uncertainties in a systematic manner. In recent years, the probabilistic approach along with the calculation of probability of failure (PoF) instead of a Factor of Safety (FoS) has become more common as a design criterium.

- There is a common misconception that a probabilistic-based analysis requires significantly more data, time and effort. Although the more data available at hand would translate into a more comprehensive rock mass characterization and this in turn into more representative results, statistical distribution can be assumed to fit certain input variables in order to gain an understanding of the probable behavior of the rock slope design.

Limit Equilibrium vs Finite Element Analysis

- The LE method has been widely used in slope stability assessments. Its main limitations arise because a prior assumption made in terms of the failure surface shape and location within the 2D cross section or 3D pit model. LE requires an iterative process to run different trial failure surfaces until the critical i.e. the one with the lowest FoS is found.
- The FE method applied to slope stability assessments makes no assumption of failure surface shape and location. The shear strength reduction technique is used whereby the rock mass strength is gradually reduced until failure is induced. In this type of analysis, the mathematical non convergence of the elastoplastic analysis is interpreted as a physical instability.
- It has been shown that both LE and FE yield the same results being the main advantage of the LEA its rapid calculation and for the FEA its ability to handle complex failure mechanisms.

Two- vs Three-Dimensional Analysis

- It is current industry practice to perform 2D stability analysis for pit slopes. However, 2D analyses rely on several assumptions that are seldom encountered in real open pit mines. Open pit geology and geometry is complex and inherently 3D in character which cannot be adequately captured into a 2D plane strain representation.
- 3D slope stability analyses are still not routinely performed for open pit slope design. However, the enhancements in computing capabilities and the availability of commercial 3D software packages have now enabled engineers to address slope stability problems using 3D tools. The advantages are i) actual representation of the complex and varying geology and geometry, ii) failure location becomes part of the solution and no a prior assumption.
- Extensive research has demonstrated that the factor of safety (FoS) obtained from 2D analysis is always smaller than the FoS resulting from a 3D approach. This means on the one hand that 2D analyses are too conservative and on the other hand that there is room for the optimization of the geotechnical design i.e. steeper slopes can be allowed.

- Given that 3D FEA is highly time consuming, it is currently not amenable for a probabilistic slope stability analysis. 3D LEM is proved to yield reliable results within acceptable computing time lengths.

8.2 Future Work

Several future research areas can be considered based upon the study conducted during this thesis:

- Construction of a DFN model at the inter-ramp pit slope scale for which probabilistic (e.g. joints) and deterministic (e.g. faults) types of geological discontinues are combined.
- Examination of the applicability of the Response Surface Method (RSM) for 3D probabilistic FEA as a mean to overcome the limitation of considerable running times of both numerical modelling and Monte Carlo simulation.
- Evaluation of the transition from open pit to underground for case study #3 from a geotechnical viewpoint with special emphasis on the crown pillar design and the in-situ stress field.
- Additional work on the validity of the linear elastic and perfectly plastic assumption to represent the rock mass post-peak behavior should be attempted.
- Further study on the assessment of disturbance factor 'D' of the Hoek-Brown criterium and its impact on the stability of pit slope for different rock mass quality classes should be carried out.

References

- Abdulai, M., & Sharifzadeh, M. (2019). Uncertainty and reliability analysis of open pit rock slopes: a critical review of methods of analysis. *Geotechnical and Geological Engineering*, 37(3), 1223-1247.
- Admassu, Y., & Shakoor, A. (2013). DIPANALYST: A computer program for quantitative kinematic analysis of rock slope failures. *Computers & geosciences*, 54, 196-202.
- Adoko, A. C., & Wu, L. (2011). Fuzzy inference systems-based approaches in geotechnical engineering: a review. *Electronic Journal of Geotechnical Engineering*, 16(1), 543-1.
- Agharazi, A. (2013). Development of a 3D equivalent continuum model for deformation analysis of systematically jointed rock masses. PhD Thesis. University of Alberta.
- Andreev, G. E. (1995). Brittle failure of rock materials. CRC press.
- Annavarapu, S., Kemeny, J., & Dessureault, S. (2012). Joint spacing distributions from oriented core data. *International Journal of Rock Mechanics and Mining Sciences*, 52, 40-45.
- Azadmehr, A., Jalali, S. M. E., & Pourrahimian, Y. (2019). An Application of Rock Engineering System for Assessment of the Rock Mass Fragmentation: A Hybrid Approach and Case Study. *Rock Mechanics and Rock Engineering*, 52(11), 4403-4419.
- Bae, D. S., Kim, K. S., Koh, Y. K., & Kim, J. Y. (2011). Characterization of joint roughness in granite by applying the scan circle technique to images from a borehole televiewer. *Rock mechanics and rock engineering*, 44(4), 497-504.
- Baecher, G. B. (1980). Progressively censored sampling of rock joint traces. *Journal of the International Association for Mathematical Geology*, 12(1), 33-40.
- Baecher, G. B., & Christian, J. T. (2005). Reliability and statistics in geotechnical engineering. John Wiley & Sons.
- Baecher, G. B., & Lanney, N. A. (1978). Trace length biases in joint surveys. In 19th US Symposium on Rock Mechanics (USRMS). American Rock Mechanics Association.
- Baecher, G. B., Lanney, N. A., & Einstein, H. H. (1977). Statistical description of rock properties and sampling. In The 18th US Symposium on Rock Mechanics (USRMS). American Rock Mechanics Association.
- Bai, T., Pollard, D. D., & Gao, H. (2000). Explanation for fracture spacing in layered materials. *Nature*, 403(6771), 753-756.
- Bandis S, Lumsden AC, Barton NR (1981). Experimental studies of scale effects on the shear behavior of rock joints. *International Journal of Rock Mechanics & Mining Sciences*;18:1-21.
- Bandis S (1980). Experimental Studies of Scale Effects on Shear Strength and Deformation of Rock Joints. London, United Kingdom: University of Leeds:141-154, 287-95.

- Bandis, S., A.C. Lumsden and N. Barton (1981). Experimental Studies of Scale Effects on the Shear Behaviour of Rock Joints. *Intl. J. Rock Mech. Sei. and Geom. Abstr.*, Vol. 18, pp. 1-21.
- Bar, N., & Barton, N. (2017). The Q-slope method for rock slope engineering. *Rock Mechanics and Rock Engineering*, 50(12), 3307-3322.
- Barton N (1982) Modelling rock joint behavior from in situ block tests: implications for nuclear waste repository design. Office of Nuclear Waste Isolation, Columbus, OH, 96 p, ONWI-308, September 1982
- Barton N, Bandis S, Bakhtar K (1985). Strength, deformation and conductivity coupling of rock joints. *Int J Rock Mech Min Sci*; 22:121-40.
- Barton N (2016). Non-linear shear strength descriptions are still needed in petroleum geomechanics, despite 50 years of linearity. In: *Proceedings of the 50th U.S. Rock Mechanics/Geomechanics Symposium*, Houston: American Rock Mechanics Association, ARMA 16-252, 12p.
- Barton, N and V. Choubey (1977). The Shear Strength of Joints in Theory and Practice. *Rock Mechanics*, Vol. 10, pp. 1-54.
- Barton, N. (1976). The shear strength of rock and rock joints. In *International Journal of rock mechanics and mining sciences & Geomechanics abstracts* (Vol. 13, No. 9, pp. 255-279). Pergamon.
- Barton, N. (1978). Suggested methods for the quantitative description of discontinuities in rock masses. *ISRM, International Journal of Rock Mechanics and Mining Sciences & Geomechanics Abstracts*, 15(6), 319-368.
- Barton, N (1973). Review on a new shear-strength criterion for rock joints. *Eng Geol*; 7:287-332.
- Barton, N., & Choubey, V. (1977). The shear strength of rock joints in theory and practice. *Rock mechanics*, 10(1-2), 1-54.
- Basahel, H., & Mitri, H. (2019). Probabilistic assessment of rock slopes stability using the response surface approach—a case study. *International Journal of Mining Science and Technology*, 29(3), 357-370.
- Basarir, H., Akdag, S., Karrech, A., & Ozyurt, M. (2016). The estimation of rock mass strength properties using probabilistic approaches and quantified GSI chart. In *ISRM International Symposium-EUROCK 2016*. International Society for Rock Mechanics and Rock Engineering.
- Bedi, A. & Harrison, J.P. (2013a) Characterization and propagation of epistemic uncertainty in rock engineering: a slope stability example. In: *Proc. International Symposium of the ISRM, Eurock 2013*, 21–26 September, Wroclaw, Poland.
- Bedi, A. & Harrison, J.P. (2013b) A comparison of Bayesian techniques and non-probabilistic models in rock engineering design. In: *Proc. 47th U.S. Rock Mechanics/ Geomechanics Symposium*, ARMA 2013, 23–26 June , California, USA.

- Bedi, A. (2014). A proposed framework for characterising uncertainty and variability in rock mechanics and rock engineering (Doctoral dissertation, Imperial College London).
- Bewick, R. P., Amann, F., Kaiser, P. K., & Martin, C. D. (2015). Interpretation of UCS test results for engineering design. In 13th ISRM International Congress of Rock Mechanics. International Society for Rock Mechanics and Rock Engineering.
- Bewick, R. P., Kaiser, P. K., & Valley, B. (2011). Interpretation of triaxial testing data for estimation of the Hoek-Brown strength parameter m_i . In 45th US rock mechanics/geomechanics symposium. American Rock Mechanics Association.
- Bieniawski, Z. (1973). Engineering Classification of Jointed Rock Masses. *The Civil Engineer in South Africa*, pp. 335-343.
- Bieniawski, Z. (1976). Rock mass classifications in rock engineering. In Z. Bieniawski (Ed.), *Exploration for rock engineering, proc. of the symp. 1*, pp. 97-106. Cape Town: A.A. Balkema.
- Bieniawski, Z. T. (1984). The design process in rock engineering. *Rock Mechanics and rock engineering*, 17(3), 183-190.
- Bieniawski, Z. (1988). The rock mass rating (RMR) system (geomechanics classification) in engineering practice. In *Rock Classification Systems for Engineering Purposes*. ASTM International.
- Bieniawski, Z. T. (1989). Engineering rock mass classifications: a complete manual for engineers and geologists in mining, civil, and petroleum engineering. John Wiley & Sons.
- Bieniawski, Z. T. (1993). Classification of rock masses for engineering: the RMR system and future trends. In *Rock Testing and Site Characterization* (pp. 553-573). Pergamon.
- Bleakly, D. C., Van Alstine, D. R., & Packer, D. R. (1985). How to Evaluate Orientation Data Quality Control. *Oil and Gas Journal*, 46-52.
- Bonilla-Sierra, V., Scholtès, L., Donzé, F. V., & Elmouttie, M. (2015). DEM analysis of rock bridges and the contribution to rock slope stability in the case of translational sliding failures. *International Journal of Rock Mechanics and Mining Sciences*, 80, 67-78.
- Bonilla-Sierra, V., Scholtes, L., Donzé, F. V., & Elmouttie, M. K. (2015). Rock slope stability analysis using photogrammetric data and DFN–DEM modelling. *Acta Geotechnica*, 10(4), 497-511.
- Bozorgzadeh, N. (2018). Contributions in uncertainty quantification towards reliability-based rock engineering design (Doctoral dissertation).
- Bozorgzadeh, N., Escobar, M. D., & Harrison, J. P. (2018). Comprehensive statistical analysis of intact rock strength for reliability-based design. *International Journal of Rock Mechanics and Mining Sciences*, 106, 374-387.
- Brady, B. H., & Brown, E. T. (1993). *Rock mechanics: for underground mining*. Springer science & business media.

- Brideau, M. A. (2010). Three-dimensional kinematic controls on rock slope stability conditions (Doctoral dissertation, Department of Earth Sciences-Simon Fraser University).
- Broch, E., & Franklin, J. A. (1972). The point-load strength test. In *International Journal of Rock Mechanics and Mining Sciences & Geomechanics Abstracts* (Vol. 9, No. 6, pp. 669-676). Pergamon.
- Brown, E. T. (1970). Strength of models of rock with intermittent joints. *Journal of Soil Mechanics & Foundations Div*, 96(SM6).
- Cabalar, A. F., Cevik, A., & Gokceoglu, C. (2012). Some applications of adaptive neuro-fuzzy inference system (ANFIS) in geotechnical engineering. *Computers and Geotechnics*, 40, 14-33.
- Cai, M., Kaiser, P. K., Tasaka, Y., Maejima, T., Morioka, H., & Minami, M. (2004). Generalized crack initiation and crack damage stress thresholds of brittle rock masses near underground excavations. *International Journal of Rock Mechanics and Mining Sciences*, 41(5), 833-847.
- Cała, M. (2007). Convex and concave slope stability analyses with numerical methods. *Archives of Mining Sciences*, 52(1), 75-89.
- Call, R. D. (1972). Analysis of geologic structure for open pit slope design. Thesis (PhD) University of Arizona, Tucson.
- Call, R.D., Savely, J.P and Nicholas, D.E (1976). Estimation of joint set characteristics from surface mapping data. In *Monograph on Rock Mech. Appl. in Mining*, W.A. Hustrulid (Ed.). AIME, New York. pp.65-73.
- Ceryan, N., Kesimal, A., & Ceryan, S. (2018). Probabilistic Analysis Applied to Rock Slope Stability: A Case Study From Northeast Turkey. In *Integrating Disaster Science and Management* (pp. 221-261). Elsevier.
- Chakraborty, A., & Goswami, D. (2016). State of the art: Three dimensional (3D) slope-stability analysis. *International Journal of Geotechnical Engineering*, 10(5), 493-498.
- Chaminé, H. I., Afonso, M. J., Ramos, L., & Pinheiro, R. (2015). Scanline sampling techniques for rock engineering surveys: insights from intrinsic geologic variability and uncertainty. In *Engineering Geology for Society and Territory-Volume 6* (pp. 357-361). Springer, Cham.
- Chang, L., & Konietzky, H. (2018). Application of the Mohr-Coulomb Yield Criterion for Rocks with Multiple Joint Sets Using Fast Lagrangian Analysis of Continua 2D (FLAC2D) Software. *Energies*, 11(3), 614.
- Cheng, Y. M., & Yip, C. J. (2007). Three-dimensional asymmetrical slope stability analysis extension of Bishop's, Janbu's, and Morgenstern-Price's techniques. *Journal of geotechnical and geoenvironmental engineering*, 133(12), 1544-1555.
- Chowdhury, R., Flentje, P., & Bhattacharya, G. (2009). *Geotechnical slope analysis*. CRC Press.

- Christian J.T., (2004) Geotechnical Engineering Reliability: How Well Do We Know What We Are Doing, Thirty-Ninth Karl Terzaghi Lecturer, 2003, Nashville, Tenn., Journal of Geotechnical and Geoenvironmental Engineering © ASCE / October 2004
- Coates, D F. (1977). Pit Slope Manual: Chapter 5: Design. CANMET (Canada Centre for Mineral and Energy Technology), CANMET REPORT 77-5, 126 p.
- Contreras, L. F., & Ruest, M. (2016). Unconventional methods to treat geotechnical uncertainty in slope design. In Proceedings of the First Asia Pacific Slope Stability in Mining Conference (pp. 315-330). Australian Centre for Geomechanics.
- Contreras, L. F., Brown, E. T., & Ruest, M. (2018). Bayesian data analysis to quantify the uncertainty of intact rock strength. Journal of Rock Mechanics and Geotechnical Engineering, 10(1), 11-31.
- Crouse, Ron (2008). Basic Slope Stability Analysis. Vector Peru S.A.C.
- Cylwik, S., Ryan, T., & Cicchini, P. (2011). Error Quantification in Oriented-Core Data and its Influence on Rock Slope Design. In Slope Stability 2011: International Symposium on Rock Slope Stability in Open Pit Mining and Civil Engineering.
- Davis, B. K., & Cowan, E. J. (2012). Oriented core—what the...?. In Proceedings of the Structural Geology and Resources. International Symposium Abstract Volume, Australian Institute of Geoscientists, Perth (pp. 61-63).
- Davis, J. C., & Sampson, R. J. (1986). Statistics and data analysis in geology (Vol. 646). New York et al.: Wiley.
- Deere, D. U., & Miller, R. P. (1966). Engineering classification and index properties for intact rock. Illinois Univ At Urbana Dept Of Civil Engineering.
- DeGraff, J. M., Meurer, M. E., Landis, L. H., & Lyons, S. (2007). Fracture Network Modeling and Dual Permeability Simulation of Carbonate Reservoirs. In 3rd EAGE North African/Mediterranean Petroleum and Geosciences Conference and Exhibition (pp. cp-16). European Association of Geoscientists & Engineers.
- Denby, B., & Scoble, M. J. (1984). Quantification of power law indices for discontinuity shear strength prediction. In The 25th US Symposium on Rock Mechanics (USRMS). American Rock Mechanics Association.
- Der Kiureghian, A., & Ditlevsen, O. (2009). Aleatory or epistemic? Does it matter?. Structural safety, 31(2), 105-112.
- Dershowitz, W. S., & Einstein, H. H. (1988). Characterizing rock joint geometry with joint system models. Rock mechanics and rock engineering, 21(1), 21-51.
- Dershowitz, W. S., & Herda, H. H. (1992). Interpretation of fracture spacing and intensity. In The 33th us symposium on rock mechanics (USRMS). American Rock Mechanics Association.
- Desai, C. S., & Christian, J. T. (1977). Numerical methods in geotechnical engineering. McGraw-Hill.

- Dowd, P. A., Xu, C., Mardia, K. V., & Fowell, R. J. (2007). A comparison of methods for the stochastic simulation of rock fractures. *Mathematical Geology*, 39(7), 697-714.
- Duncan, J. M. (2000). Factors of safety and reliability in geotechnical engineering. *Journal of geotechnical and geoenvironmental engineering*, 126(4), 307-316.
- E Sousa, L. R., Vargas Jr, E., Fernandes, M. M., & Azevedo, R. (2012). *Innovative numerical modelling in geomechanics*. CRC Press.
- Eberhardt, E. (2010). Review: GSI and Hoek-Brown Procedure. ITBA Mining.
- Eberhardt, E. (2012). The hoek–brown failure criterion. *Rock mechanics and rock engineering*, 45(6), 981-988.
- Edelbro, C. (2003). *Rock mass strength*. Luleå: Luleå University of Technology.
- Einstein, H. H., & Baecher, G. B. (1983). Probabilistic and statistical methods in engineering geology. *Rock mechanics and rock engineering*, 16(1), 39-72.
- Elliott, G. M. (1993). Triaxial testing for rock strength. In *Rock Testing and Site Characterization* (pp. 87-104). Pergamon.
- Elmo D., Stead D., Rogers S. (2015). Guidelines for the quantitative description of discontinuities for use in Discrete Fracture Network Engineering. In: *Proceedings of the 13th ISRM Congress*; Montreal. Paper 587.
- Elmo, D., & Stead, D. (2010). An integrated numerical modelling–discrete fracture network approach applied to the characterisation of rock mass strength of naturally fractured pillars. *Rock Mechanics and Rock Engineering*, 43(1), 3-19.
- Elmo, D., Yan, M., Stead, D., & Rogers, S. F. (2007). The importance of intact rock bridges in the stability of high rock slopes-towards a quantitative investigation using an integrated numerical modelling; discrete fracture network approach. In *Proceedings of the 2007 International Symposium on Rock Slope Stability in Open Pit Mining and Civil Engineering* (pp. 253-266). Australian Centre for Geomechanics.
- El-Ramly, H, Morgenstern, NR & Cruden, DM (2002). 'Probabilistic slope stability analysis for practice', *Canadian Geotechnical Journal*, vol 39, no. 3, pp. 665-683.
- Faramarzi, F., Farsangi, M. E., & Mansouri, H. (2013). An RES-based model for risk assessment and prediction of backbreak in bench blasting. *Rock mechanics and rock engineering*, 46(4), 877-887.
- Farzaneh, O., Askari, F., & Ganjian, N. (2008). Three-dimensional stability analysis of convex slopes in plan view. *Journal of Geotechnical and Geoenvironmental Engineering*, 134(8), 1192-1200.
- Fowler, M. J. (2013). Structural data bias in the digital age. In *Proceedings of the 2013 International Symposium on Slope Stability in Open Pit Mining and Civil Engineering* (pp. 219-225). Australian Centre for Geomechanics.

- Fredlund, M. D., Lu, H., & Fredlund, D. G. (2012). Benchmarking of a three-dimensional limit equilibrium slope stability software. Proceedings of GeoManitoba, Winnipeg, MN, Canada.
- Gaillot, P., Brewer, T., Pezard, P., & Yeh, E. C. (2007). Borehole imaging tools—principles and applications. *Scientific Drilling*, 5, 1-4.
- Giani, G. P. (1992). *Rock slope stability analysis*. CRC Press.
- Glastonbury, J., & Fell, R. (2000). Report on the analysis of "rapid" natural rock slope failures. University of New South Wales, School of Civil and Environmental Engineering.
- Gochioco, L. M., Magill, C., & Marks, F. (2002). The borehole camera: An investigative geophysical tool applied to engineering, environmental, and mining challenges. *The Leading Edge*, 21(5), 474-477.
- Goodman, R. E. (1989). *Introduction to rock mechanics* (Vol. 2). New York: Wiley.
- Goodman, R.E. (1976). *Methods of Geological Engineering in Discontinuous Rocks*. West Publishing, San Francisco.
- Goodman, Richard E. (1976). "Toppling of rock slopes." Proc. Speciality Conference on Rock Engineering for Foundation and Slopes. ASCE.
- Gravanis, E., Pantelidis, L., & Griffiths, D. V. (2014). An analytical solution in probabilistic rock slope stability assessment based on random fields. *International Journal of Rock Mechanics and Mining Sciences*, 71, 19-24.
- Grenon, M., & Hadjigeorgiou, J. (2010). Integrated structural stability analysis for preliminary open pit design. *International Journal of Rock Mechanics and Mining Sciences*, 47(3), 450-460.
- Griffiths, D. V., & Marquez, R. M. (2007). Three-dimensional slope stability analysis by elasto-plastic finite elements. *Geotechnique*, 57(6), 537-546.
- Grobler, H. P., Poropat, G., & Guest, A. R. (2003). Photogrammetry for structural mapping in mining. In 10th ISRM Congress. International Society for Rock Mechanics and Rock Engineering.
- Gudmundsson, A. (2011). *Rock fractures in geological processes*. Cambridge University Press.
- Guest, A. and Read, J., (2009). Geotechnical Model. In *Guidelines for Open Pit Slope Design*, Read J. and Stacey P., editors. CSIRO Publishing, Collingwood: pp. 201-212.
- Hadjigeorgiou, J. (1992). A study of frictional properties of rock masses. MEng thesis. McGill University.
- Haimson, B., & Chang, C. (2000). A new true triaxial cell for testing mechanical properties of rock, and its use to determine rock strength and deformability of Westerly granite. *International Journal of Rock Mechanics and Mining Sciences*, 37(1-2), 285-296.
- Harr, M. E. (1987). *Reliability-based design in civil engineering*. McGraw-Hill.

- Harrison, J. P., Hudson, J. A., & Popescu, M. E. (2002). Engineering rock mechanics: Part 2. Illustrative worked examples. *Appl. Mech. Rev.*, 55(2), B30-B31.
- Hassani, F P. 1980. A Study of the Physical and Mechanical Properties of Rocks and their Discontinuities Associated with Opencast Coal :Mining Operations. Ph.D. Thesis. University of Nottingham. p. 750.
- Herget, G. Pit Slope Manual (1977). Chapter 2 – Structural Geology; CANMET (Canada Centre for Mineral Technology, formerly Mines Branch, Energy, Mines and Resources Canada), CANMET REPORT77-41; 123 p; October 1977.
- Hocking, G., (1976). A method for distinguishing between single and double plane sliding of tetrahedral wedges. *Int. J. Rock Mech. Min. Sci. Geomech. Abstr.* 13, 225–226.
- Hoek E, Bray J. Rock slope engineering (1981). Revised 3rd ed. London: The Institution of Mining and Metallurgy.
- Hoek, E. (1965). Rock fracture under static stress conditions. CSIR.
- Hoek, E. (1970). Estimating the stability of excavated slopes in opencast mines. *Institution of Mining and Metallurgy A*, 105, A132.
- Hoek, E. (1971). Influence of rock structure on the stability of rock slopes. In *Proceedings of the 1st Conference on the stability in open pit mining*. The American Inst of Mining, Metallurgical and Petroleum Engineers. Inc. New York.
- Hoek, E. (1994). Strength of rock and rock mass. *ISRM News Journal*.
- Hoek, E., & Bray, J. D. (1981). *Rock slope engineering*. CRC Press.
- Hoek, E., & Brown, E. T. (2019). The Hoek–Brown failure criterion and GSI–2018 edition. *Journal of Rock Mechanics and Geotechnical Engineering*, 11(3), 445-463.
- Hoek, E., & Franklin, J. A. (1967). A simple triaxial cell for field or laboratory testing of rock. Imperial College of Science and Technology, University of London.
- Hoek, E., Carranza-Torres, C., & Corkum, B. (2002). Hoek-Brown failure criterion-2002 edition. *Proceedings of NARMS-Tac*, 1(1), 267-273.
- Hoek, E., Carter, T. G., & Diederichs, M. S. (2013). Quantification of the geological strength index chart. In *47th US rock mechanics/geomechanics symposium*. American Rock Mechanics Association.
- Hoek, E., Kaiser, P. K., & Bawden, W. F. (2000). *Support of underground excavations in hard rock*. CRC Press.
- Hoek, E., Read, J., Karzulovic, A., & Chen, Z. Y. (2000). Rock slopes in civil and mining engineering. In *ISRM International Symposium*. International Society for Rock Mechanics and Rock Engineering.

- Hoek, E., Kaiser, P.K. & Bawden, W.F. (1995). Support of Underground Excavations in Hard Rock. Rotterdam: Balkema, 215pp.
- Holcombe, R., Coughlin, T., & Oliver, N. (2013). Oriented Drillcore: Measurement, Conversion and QA/QC Procedures for Structural and Exploration Geologists. Oriented core manual. HCO consultants.
- Huang, C. C., Tsai, C. C., & Chen, Y. H. (2002). Generalized method for three-dimensional slope stability analysis. *Journal of geotechnical and geoenvironmental engineering*, 128(10), 836-848.
- Hudson, J. A., & Harrison, J. P. (2000). *Engineering rock mechanics: an introduction to the principles*. Elsevier.
- Hudson, J. (1992). *Rock engineering systems. Theory and practice*. New York : Ellis Horwood, 1992.
- Hudson, J. A. (1989). *Rock mechanics principles in engineering practice*. London: CIRIA, Construction Industry Research and Information Association..
- Hudson, J. A. (2013). A review of Rock Engineering Systems (RES) applications over the last 20 years. In *Rock Characterisation, Modelling and Engineering Design Methods* (pp. 419-424). Taylor & Francis.
- Hume, C. D. (2011). Numerical validation and refinement of empirical rock mass modulus estimation. Masters Thesis. Queen's University.
- Hunsche, U., & Albrecht, H. (1990). Results of true triaxial strength tests on rock salt. *Engineering Fracture Mechanics*, 35(4-5), 867-877.
- Irigaray, C., El Hamdouni, R., Jiménez-Perálvarez, J. D., Fernández, P., & Chacón, J. (2012). Spatial stability of slope cuts in rock massifs using GIS technology and probabilistic analysis. *Bulletin of Engineering Geology and the Environment*, 71(3), 569-578.
- Jaeger, J. C. (1971). Friction of rocks and stability of rock slopes. *Geotechnique* 2, No. 2, 97-134.
- Jaeger, J. C., Cook, N. G., & Zimmerman, R. (2009). *Fundamentals of rock mechanics*. John Wiley & Sons.
- Jiang, J. C., & Yamagami, T. (2004). Three-dimensional slope stability analysis using an extended Spencer method. *Soils and Foundations*, 44(4), 127-135.
- Jiang, J. C., Baker, R., & Yamagami, T. (2003). The effect of strength envelope nonlinearity on slope stability computations. *Canadian Geotechnical Journal*, 40(2), 308-325.
- Jianhua, W. (2008). DFN model: A new modelling technology for fracture. *Fault-Block Oil & Gas Field Journal*, vol.6.
- Jimenez-Rodriguez, R., Sitar, N. & Chacon, J. (2006) System reliability approach to rock slope stability. *Int J Rock Mech Min*, 43 (6), 847–859.

- Jing, L., & Hudson, J. A. (2002). Numerical methods in rock mechanics. *International Journal of Rock Mechanics and Mining Sciences*, 39(4), 409-427.
- Joughin, W. C. (2018). Dealing with uncertainty and risk in rock engineering design. In 1st International Conference on Advances in Rock Mechanics-TuniRock 2018. International Society for Rock Mechanics and Rock Engineering.
- Kahraman, S. (2001). Evaluation of simple methods for assessing the uniaxial compressive strength of rock. *International Journal of Rock Mechanics and Mining Sciences*, 38(7), 981-994.
- Kelesoglu, M. K. (2016). The evaluation of three-dimensional effects on slope stability by the strength reduction method. *KSCE Journal of Civil Engineering*, 20(1), 229-242.
- Kennedy, Bruce A., and Bruce A. Kennedy (1990). *Surface Mining*. SME.
- Kirsten Had (1983). Significance of the probability of failure in slope engineering. *The Civil Engineer in South Africa* 25(1).
- Kiureghian, A. D. & Ditlevsen, O. (2009) Aleatory or epistemic? Does it matter? *Struct Saf*, 31 (2), 105–112.
- Klar, A., Aharonov, E., Kalderon-Asael, B., & Katz, O. (2011). Analytical and observational relations between landslide volume and surface area. *Journal of Geophysical Research: Earth Surface*, 116(F2).
- Kliche, C. A. (1999). *Rock slope stability*. SME.
- Krahn, John (2003). "The 2001 RM Hardy Lecture: The limits of limit equilibrium analyses." *Canadian Geotechnical Journal* 40.3 (2003): 643-660.
- Kwasniewski, M., Li, X., & Takahashi, M. (Eds.). (2012). *True triaxial testing of rocks (Vol. 4)*. CRC Press.
- La Pointe, P. R., & Hudson, J. A. (1985). *Characterization and interpretation of rock mass joint patterns (Vol. 199)*. Geological Society of America.
- Langford, J. C. (2013). *Application of Reliability Methods to the Design of Underground Structures [Ph. D. thesis]*. Canada: Queen's University.
- Langford, J. C., & Diederichs, M. S. (2013). Reliability based approach to tunnel lining design using a modified point estimate method. *International Journal of Rock Mechanics and Mining Sciences*, 60, 263-276.
- Langford, J. C., & Diederichs, M. S. (2015). Quantifying uncertainty in Hoek–Brown intact strength envelopes. *International Journal of Rock Mechanics and Mining Sciences*, 74, 91-102.
- Leung, C. F., & Quek, S. T. (1995). Probabilistic stability analysis of excavations in jointed rock. *Canadian geotechnical journal*, 32(3), 397-407.

- Leyshon, P. R., & Lisle, R. J. (1996). *Stereographic projection methods in structural geology* (Vol. 1). Butterworth-Heinemann.
- Li, D., & Wong, L. N. Y. (2013). The Brazilian disc test for rock mechanics applications: review and new insights. *Rock mechanics and rock engineering*, 46(2), 269-287.
- Li, S. J., Feng, X. T., Wang, C. Y., & Hudson, J. A. (2013). ISRM suggested method for rock fractures observations using a borehole digital optical televiewer. *Rock mechanics and rock engineering*, 46(3), 635-644.
- Li, X., Du, K., & Li, D. (2015). True triaxial strength and failure modes of cubic rock specimens with unloading the minor principal stress. *Rock Mechanics and Rock Engineering*, 48(6), 2185-2196.
- Lisle, R. J., & Leyshon, P. R. (2004). *Stereographic projection techniques for geologists and civil engineers*. Cambridge University Press.
- Liu, H. A. N., Jisen, S. H. U., & Wei, Z. H. O. U. (2014). Research on mechanical and geometric characteristics of concave end-slope in open-pit mine with mining by areas. *Journal of Huazhong University of Science and Technology*, 42(3), 82-86.
- Liu, Q., Kieffer, D. S., & Bitenc, M. (2019). Three-dimensional UAV-based photogrammetric structural models for rock slope engineering. In *IAEG/AEG Annual Meeting Proceedings, San Francisco, California, 2018-Volume 1* (pp. 283-287). Springer, Cham.
- Lorig, L. J., Darcel, C., Damjanac, B., Pierce, M., & Billaux, D. (2015). Application of discrete fracture networks in mining and civil geomechanics. *Mining Technology*, 124(4), 239-254.
- Lorig, L. J., et al. (2015) "Application of discrete fracture networks in mining and civil geomechanics." *Mining Technology* 124.4 (2015): 239-254.
- Lu, H. H., Fredlund, M. D., & Fredlund, D. G. (2013). Three-dimensional limit equilibrium analysis of open pits. In *Proceedings of the 2013 International Symposium on Slope Stability in Open Pit Mining and Civil Engineering* (pp. 541-554). Australian Centre for Geomechanics.
- Macciotta, R., Martin, C. D., Morgenstern, N. R., & Cruden, D. M. (2016). Development and application of a quantitative risk assessment to a very slow-moving rock slope and potential sudden acceleration. *Landslides*, 13(4), 765-785.
- Marinos, P., & Hoek, E. (2000). GSI: a geologically friendly tool for rock mass strength estimation. In *ISRM international symposium*. International Society for Rock Mechanics and Rock Engineering.
- Marinos, P., Marinos, V., & Hoek, E. (2007). The Geological Strength Index (GSI): a characterization tool for assessing engineering properties for rock masses. In *Proceedings International Workshop on Rock Mass Classification for Underground Mining*, Mark, Pakalnis and Tuchman (editors), Information Circular (Vol. 9498, pp. 87-94).
- Marinos, V. I. I. I., Marinos, P., & Hoek, E. (2005). The geological strength index: applications and limitations. *Bulletin of Engineering Geology and the Environment*, 64(1), 55-65.

- Marjoribanks, R. W. (2002). Structural logging of drill core. Australian Institute of Geoscientists.
- Markland, J.T., (1972). A useful technique for estimating the stability of rock slopes when the rigid wedge sliding type of failure is expected. *Imp. Coll. Rock Mech. Res. Rep.* 19, 10.
- Mathis, J. I. (1988). Development and verification of a three dimensional rock joint model (Doctoral dissertation, Luleå tekniska universitet).
- Mazzoccola, D. F., & Hudson, J. A. (1996). A comprehensive method of rock mass characterization for indicating natural slope instability. *Quarterly Journal of Engineering Geology and Hydrogeology*, 29(1), 37-56.
- Miller, S. M., & Borgman, L. E. (1984). Probabilistic characterization of shear strength using results of direct shear tests. *Geotechnique*, 34(2), 273-276.
- Miyoshi, T. (2018). Influence of data characterization process on the kinematic stability analysis of engineered rock slopes using discrete fracture network models and its implications for rock mass classification system (Doctoral dissertation, University of British Columbia).
- Mullarkey, P. W., & Fenvesf, S. J. (1986). Fuzzy logic in a geotechnical knowledge-based system: CONE. *Civil Engineering Systems*, 3(2), 58-81.
- Muralha, J., Grasselli, G., Tatone, B., Blümel, M., Chryssanthakis, P., & Yujing, J. (2014). ISRM suggested method for laboratory determination of the shear strength of rock joints: revised version. *Rock mechanics and rock engineering*, 47(1), 291-302.
- Nadim, F. (2007) Tools and strategies for dealing with uncertainty in geotechnics. In: Griffiths, D. V. & Fenton, G. A. (eds.) *Probabilistic Methods in Geotechnical Engineering*. New York, Springer. pp. 71-95.
- Narendranathan, S., McBeath, S., Ayemin, K., & Lee, E. C. (2016). 'An alternate approach for deriving rock slope shear strength parameters within weak jointed rock masses', in PM Dight (ed.), *Proceedings of the First Asia Pacific Slope Stability in Mining Conference*, Australian Centre for Geomechanics, Perth, pp. 721-730
- Nelson, R. A., Lenox, L. C., & Ward Jr, B. J. (1987). Oriented core: its use, error, and uncertainty. *AAPG Bulletin*, 71(4), 357-367.
- Nicholas, D. E., & Sims, D. B. (2001). Collecting and using geologic structure data for slope design. *Slope Stability in Surface Mining*. SME Littleton, Co, 11-26.
- Nikolić, M., Roje-Bonacci, T., & Ibrahimbegović, A. (2016). Overview of the numerical methods for the modelling of rock mechanics problems. *Tehnički vjesnik*, 23(2), 627-637.
- Nilsen, B., (2000). New trends in rock slope stability analyses. *Bull. Eng. Geol. Environ.* 58, 173-178.
- Norrish, N. I., & Wyllie, D. C. (1996). Rock slope stability analysis. *Landslides: Investigation and Mitigation: Transportation Research Board Special Report*, 247, 391-425.

- Oberkampff, W. L., Helton, J. C., Joslyn, C. A., Wojtkiewicz, S. F. & Ferson, S. (2004) Challenge problems: uncertainty in system response given uncertain parameters. *Reliab Eng Syst Safe*, 85 (1-3), 11–19.
- Obregon, C., & Mitri, H. (2019). Probabilistic approach for open pit bench slope stability analysis—A mine case study. *International Journal of Mining Science and Technology*, 29(4), 629-640.
- Ortiz, R., Silva, G., & Michalak, N. (2015). Application of the Response Surface Methodology to 3DEC Analysis of Open Pit Slopes. In *ISRM Regional Symposium-8th South American Congress on Rock Mechanics*. International Society for Rock Mechanics and Rock Engineering.
- Panda, B. B., & Kulatilake, P. H. S. W. (1995). Study of the effect of joint geometry parameters on the permeability of jointed rock. In *Proceedings of 35th US Symposium on Rock Mechanics*, Reno, University of Nevada (pp. 273-8).
- Pande, G., Beer, G., & Williams, J. (1990). *Numerical methods in rock mechanics*. United States: N. p., 1990. Web.
- Panji, M., Koohsari, H., Adampira, M., Alielahi, H., & Marnani, J. A. (2016). Stability analysis of shallow tunnels subjected to eccentric loads by a boundary element method. *Journal of Rock Mechanics and Geotechnical Engineering*, 8(4), 480-488.
- Park, H. J., Lee, J. H., Kim, K. M., & Um, J. G. (2016). Assessment of rock slope stability using GIS-based probabilistic kinematic analysis. *Engineering geology*, 203, 56-69.
- Park, H. J., Um, J. G., Woo, I. & Kim, J. W. (2012) Application of fuzzy set theory to evaluate the probability of failure in rock slopes. *Eng Geol*, 125, 92–101.
- Park, H. J., West, T. R., & Woo, I. (2005). Probabilistic analysis of rock slope stability and random properties of discontinuity parameters, Interstate Highway 40, Western North Carolina, USA. *Engineering Geology*, 79(3-4), 230-250.
- Park, H., & West, T. R. (2001). Development of a probabilistic approach for rock wedge failure. *Engineering Geology*, 59(3-4), 233-251.
- Peacock, D. C. P., Harris, S. D., & Mauldon, M. (2003). Use of curved scanlines and boreholes to predict fracture frequencies. *Journal of Structural Geology*, 25(1), 109-119.
- Pease, K. A., Howard, A. L., & Refer, M. C. (1995). The Observational Approach Applied To Open Pit Mine Slopes'. *Proceedings America Society of Mining and Reclamation*, 617-624.
- Perras, M. A., & Diederichs, M. S. (2014). A review of the tensile strength of rock: concepts and testing. *Geotechnical and geological engineering*, 32(2), 525-546.
- Phillips, F. C. (1955). The use of stereographic projection in structural geology (Vol. 79, No. 3, p. 236). LWW.
- Piteau, D. R., & Martin, D. C. (1982). Mechanics of rock slope failure. In *Proc. 3rd International Conference on Stability in Surface Mining* (Vancouver, June 1-3, 1981) (pp. 113-169).

- Prasetyo, S. H., Gutierrez, M., & Barton, N. (2017). Nonlinear shear behavior of rock joints using a linearized implementation of the Barton–Bandis model. *Journal of Rock Mechanics and Geotechnical Engineering*, 9(4), 671-682.
- Priest SD & Brown ET (1983). Probabilistic stability analysis of variable rock slopes. *Transactions of Institution of Mining and Metallurgy, Section A: Mining Industry* 92, A1–12.
- Priest, S. D. (1985). *Hemispherical projection methods in rock mechanics*. Allen & Unwin.
- Priest, S. D. (1998). *Discontinuity analysis for rock engineering*. Springer Science & Business Media.
- Priest, S. D., & Hudson, J. A. (1976, May). Discontinuity spacings in rock. In *International Journal of Rock Mechanics and Mining Sciences & Geomechanics Abstracts* (Vol. 13, No. 5, pp. 135-148). Pergamon.
- Priest, S. D., & Hudson, J. A. (1981). Estimation of discontinuity spacing and trace length using scanline surveys. In *International Journal of Rock Mechanics and Mining Sciences & Geomechanics Abstracts* (Vol. 18, No. 3, pp. 183-197). Pergamon.
- Priest, S.D. (1993). “Discontinuity Analysis for Rock Engineering”. Chapman and Hall, London.
- Qi-hu, Q. I. A. N. (2012). Challenges faced by underground projects construction safety and countermeasures. *Chinese Journal of Rock Mechanics and Engineering*, 31(10), 1945-1956.
- Read, J., & Stacey, P. (2009). *Guidelines for open pit slope design*. CSIRO.
- Read, S., & Richards, L. (2014). Correlation of direct and indirect tensile tests for use in the Hoek–Brown constant mi. Masses-Alejano, Peruchó, Olalla and Jiménez (eds) *Rock engineering and rock mechanics: structures in and on rock*. Taylor and Francis, London, 161-166.
- Reflex Instruments (2013). ACT I & II TM Core Orientation Process. Minerals Division of Imdex Limited. Perth, West Australia.
- Rogers, S. F., Kennard, D. K., Dershowitz, W. S., & Van As, A. (2007). Characterizing the in situ fragmentation of a fractured rock mass using a discrete fracture network approach. In *Rock Mechanics: Meeting Society’s Challenges and Demands, Proceedings of the 1st Canada-US Rock Mechanics Symposium*. Vancouver, Canada: Taylor & Francis (pp. 137-143).
- Romana, Manuel (1991). "SMR classification." 7th ISRM Congress. International Society for Rock Mechanics and Rock Engineering.
- Rozos, Dimitrios & Pyrgiotis, L. & Skias, S. & Tsangaratos, Paraskevas. (2008). An implementation of rock engineering system for ranking the instability potential of natural slopes in Greek territory. An application in Karditsa County. *Landslides*.
- Ruf, J. C., Rust, K. A., & Engelder, T. (1998). Investigating the effect of mechanical discontinuities on joint spacing. *Tectonophysics*, 295(1-2), 245-257.

- Salmi, Ebrahim Fathi, and Saeed Hosseinzadeh. (2015). "Slope stability assessment using both empirical and numerical methods: a case study." *Bulletin of Engineering Geology and the Environment* 74.1 (2015): 13-25.
- Savely, J. P. (1972). Orientation and engineering properties of jointing in Sierrita Pit. Arizona. Thesis (MS) University of Arizona, Tucson.
- Savely, J. P. (1987). Probabilistic Analysis of Fractured Rock Masses.
- Shu, B. (2014). Rock slope stability investigations in three dimensions for a part of an open pit mine in USA.
- Singh, B., & Goel, R. K. (1999). Rock mass classification: a practical approach in civil engineering (Vol. 46). Elsevier.
- Singh, B., & Goel, R. K. (2011). Engineering rock mass classification: tunneling, foundations, and landslides. Waltham, MA: Butterworth-Heinemann,.
- Singhal BBS, Gupta RP. Applied Hydrogeology of Fractured Rocks. Dordrecht: Kluwer Academic Publisher, 2010:13-33.
- Sivakugan, N., Shukla, S. K., & Das, B. M. (2013). Rock mechanics: an introduction. Crc Press.
- Sjöberg, J. (1999). Analysis of large scale rock slopes (Doctoral dissertation, Luleå tekniska universitet).
- Sonmez, H., & Ulusay, R. (1999). Modifications to the geological strength index (GSI) and their applicability to stability of slopes. *International Journal of Rock Mechanics and Mining Sciences*, 36(6), 743-760.
- Spencer, E. (1967). A method of analysis of the stability of embankments assuming parallel inter-slice forces. *Geotechnique*, 17(1), 11-26.
- Spross, J., Johansson, F., Stille, H., & Larsson, S. (2014). Towards an improved observational method. In *ISRM Regional Symposium-EUROCK 2014*. International Society for Rock Mechanics and Rock Engineering.
- Spross, J., Stille, H., Johansson, F., & Palmstrøm, A. (2019). Principles of risk-based rock engineering design. *Rock Mechanics and Rock Engineering*, 1-15.
- Stead, D., & Wolter, A. (2015). A critical review of rock slope failure mechanisms: The importance of structural geology. *Journal of Structural Geology*, 74, 1-23.
- Stead, D., Eberhardt, E., Coggan, J., & Benko, B. (2001). Advanced numerical techniques in rock slope stability analysis-Applications and limitations. In *International conference on landslides-causes, impacts and countermeasures* (pp. 615-624).

- Steffen, O. K. H., Contreras, L. F., Terbrugge, P. J., & Venter, J. (2008). A risk evaluation approach for pit slope design. In The 42nd US Rock Mechanics Symposium (USRMS). American Rock Mechanics Association.
- Stille, H., & Virely, D. (2014). How to refine the observational method as described in EC7 in applied rock mechanics. In ISRM Regional Symposium-EUROCK 2014. International Society for Rock Mechanics and Rock Engineering.
- Sturzenegger, M., & Stead, D. (2009). Close-range terrestrial digital photogrammetry and terrestrial laser scanning for discontinuity characterization on rock cuts. *Engineering Geology*, 106(3-4), 163-182.
- Styles, T., Coggan, J., & Pine, R. (2011). Stability analysis of a large fractured rock slope using a DFN-based mass strength approach. In *Proceedings of the International Symposium on Rock Slope Stability in Open Pit Mining and Civil Engineering*, Vancouver, Canada. September 18 (Vol. 21, p. 2011).
- Su, R., Zong, Z. H., & Wang, J. (2005). Acoustic borehole televiewer with high resolution and its application to deep formation for geological disposal of nuclear waste. *Yanshilixue Yu Gongcheng Xuebao/Chin. J. Rock Mech. Eng.*, 24(16), 2922-2928.
- Sullivan TD (2006). Pit slope design and risk – a view of the current state of the art. In *Proceedings of International Symposium on Stability of Rock Slopes in Open Pit Mining and Civil Engineering*, Cape Town. South African Institute of Mining and Metallurgy, Johannesburg.
- Sun, C., Chai, J., Xu, Z., & Qin, Y. (2017). 3D stability charts for convex and concave slopes in plan view with homogeneous soil based on the strength-reduction method. *International Journal of Geomechanics*, 17(5), 06016034.
- Swan G & Sepulveda R (2000). Slope stability at Collahausi. In *Slope Stability in Surface Mining* (eds WA Hustrulid, KM McCarter & DJA Van Zyl), pp. 163–170. SME, Colorado.
- Tannant, D. D. (2015). Review of photogrammetry-based techniques for characterization and hazard assessment of rock faces. *International Journal of Georesources and Environment-IJGE (formerly Int'l J of Geohazards and Environment)*, 1(2), 76-87.
- Tatone, B. S., & Grasselli, G. (2010). ROCKTOPPLE: A spreadsheet-based program for probabilistic block-toppling analysis. *Computers & geosciences*, 36(1), 98-114.
- Terzaghi, K. (1961). Past and future of applied soil mechanics. *J. Boston Soc. Civ Engr*, 68, 110-139.
- Peck, R. B. (1969). Ninth Rankine Lecture: Advantages and limitations of the observational method in applied soil mechanics. *Geotechnique*, 19(2), 171-187.
- Terzaghi, R.D. (1965) Sources of Error in Joint Surveys, *Geotechnique*, Vol. 15, pp. 287–304
- Thomas, R. D. H., Neilsen, J. M., Wilson, H. F., & Lamb, P. (2015). Structural interpretation from Televiewer surveys. In *Proceedings of the Ninth Symposium on Field Measurements in Geomechanics* (pp. 729-741). Australian Centre for Geomechanics.

- Tuckey, Z. S. (2012). An integrated field mapping-numerical modelling approach to characterising discontinuity persistence and intact rock bridges in large open pit slopes (Doctoral dissertation, Science: Department of Earth Sciences).
- Udd, J.E .. P. Leinberger and R. Kozarycz (1981). The Stability of Cut Slopes in Chazy Limestone in a Montreal-area Quarry. *CIM Bulletin* Vol. 74. No. 829. pp. 65-72.
- Ureel, S., Momayez, M., & Oberling, Z. (2013). Rock core orientation for mapping discontinuities and slope stability analysis. *IJRET: International*.
- Uzielli, M., Lacasse, S., Nadim, F., & Phoon, K. K. (2006). Soil variability analysis for geotechnical practice. Characterization and engineering properties of natural soils, 3, 1653-1752.
- Villaescusa, E. (1991). A three-dimensional model of rock jointing. Thesis PhD. University of Queensland, Brisbane.
- W. Hustrulid, M. Kuchta, R. Marin (2013). Open pit mine – planning & design. Fundamentals, vol. 1, CRC Press (2013)
- Wang, X., & Mauldon, M. (2006). Proportional error of the Terzaghi correction factors. In *Golden Rocks 2006, The 41st US Symposium on Rock Mechanics (USRMS)*. American Rock Mechanics Association.
- Wawersik, W. R., Carlson, L. W., Holcomb, D. J., & Williams, R. J. (1997). New method for true-triaxial rock testing. *International Journal of Rock Mechanics and Mining Sciences*, 34(3-4), 330-e1.
- Weir, F. M. (2015). The future of structural data from boreholes. *International Journal of Geotechnical Engineering*, 9(3), 223-228.
- Williams JH, Johnson CD (2004) Acoustic and optical borehole-wall imaging for fractured-rock aquifer studies. *J Appl Geophys* 55(1-2):151-159
- Wines, D. R., & Lilly, P. A. (2003). Estimates of rock joint shear strength in part of the Fimiston open pit operation in Western Australia. *International Journal of Rock Mechanics and Mining Sciences*, 40(6), 929-937.
- Wittke, W. (1990). *Rock mechanics: Theory and Applications with Case Histories*. Berlin: Springer.
- Wittke, W. (2014). *Rock mechanics based on an anisotropic jointed rock model (AJRM)*. John Wiley & Sons.
- Wong, L. N. (2013). Determination of normal joint spacing from apparent joint spacing measurements. *Global View of Engineering Geology and the Environment*, 615-622.
- Wyllie, D. C., & Mah, C. (2014). *Rock slope engineering*. CRC Press.
- Yong, R., Li, C. D., Ye, J., Huang, M., & Du, S. (2016). Modified limiting equilibrium method for stability analysis of stratified rock slopes. *Mathematical Problems in Engineering*, 2016.

- Yongyue, S., Yanjun, S., Yuanchun, S., & Chenghu, W. (2010). Applications of acoustic borehole televiewer in geotechnical investigation [J]. *Geotechnical Investigation & Surveying*, 8.
- Yow, J.L. (1987). "Blind zones in the acquisition of discontinuity orientation data". *International Journal of Rock Mechanics and Mining Sciences and Geomechanics Abstracts*. Technical Note. 24: 5, 317- 318.
- Zevgolis, I. E., Deliveris, A. V., & Koukoulas, N. C. (2018). Probabilistic design optimization and simplified geotechnical risk analysis for large open pit excavations. *Computers and Geotechnics*, 103, 153-164.
- Zhang, F., Leshchinsky, D., Gao, Y., & Yang, S. (2018). Three-dimensional slope stability analysis of convex turning corners. *Journal of Geotechnical and Geoenvironmental Engineering*, 144(6), 06018003.
- Zhang, J. F., & Ding, H. (2005). Generalized 3 d limit-equilibrium method for slope stability analysis and its application. *Yanshilixue Yu Gongcheng Xuebao/Chin. J. Rock Mech. Eng.*, 24(3), 365-370.
- Zhang, K., Ping, C. A. O., Liu, Z. Y., Hu, H. H., & Gong, D. P. (2011). Simulation analysis on three-dimensional slope failure under different conditions. *Transactions of Nonferrous Metals Society of China*, 21(11), 2490-2502.
- Zhang, L. (2016). *Engineering properties of rocks*. Butterworth-Heinemann.
- Zhang, L., & Einstein, H. H. (2000). Estimating the intensity of rock discontinuities. *International Journal of Rock Mechanics and Mining Sciences*, 37(5), 819-837.
- Zheng, J., Kulatilake, P. H. S. W., & Deng, J. (2015). Development of a probabilistic block theory analysis procedure and its application to a rock slope at a hydropower station in China. *Engineering Geology*, 188, 110-125.
- Zuo, J., Liu, H., & Li, H. (2015). A theoretical derivation of the Hoek–Brown failure criterion for rock materials. *Journal of Rock Mechanics and Geotechnical Engineering*, 7(4), 361-366.

Appendix
Structural Data of Case Studies

Case Study #1

Mapping Site	Dip (°)	DipDir (°)
1	60	55
1	60	70
1	65	185
1	70	180
1	53	188
1	65	145
1	70	150
1	75	155
1	78	192
1	83	198
1	56	95
1	40	15
1	35	10
1	83	45
1	80	248
1	80	54
1	60	165
2	80	115
2	88	285
2	72	200
2	55	205
2	47	215
2	65	5
2	64	355
2	40	220
2	46	155
2	75	230
2	70	280
2	80	0
2	84	15

Mapping Site	Dip (°)	DipDir (°)
2	24	70
2	27	55
2	55	320
2	80	25
2	87	265
2	60	165
2	24	357
3	72	140
3	83	150
3	88	160
3	87	160
3	90	155
3	85	208
3	70	30
3	88	187
3	65	140
3	68	145
3	60	135
3	83	225
3	85	190
3	84	192
3	82	310
4	84	54
4	69	52
4	81	41
4	83	40
4	88	126
4	89	280
4	88	285
4	30	329

Mapping Site	Dip (°)	DipDir (°)
4	35	324
4	37	280
4	75	190
4	74	170
4	81	120
4	87	55
4	76	155
4	74	86
4	80	80
5	75	265
5	86	280
5	85	108
5	80	105
5	76	5
5	80	330
5	88	0
5	73	20
5	68	205
5	53	290
5	55	325
5	28	325
5	30	265
5	78	275
5	87	250
5	73	185
5	65	182
5	40	335
5	42	340
6	54	325
6	43	295

Mapping Site	Dip (°)	DipDir (°)
6	73	170
6	60	340
6	75	285
6	55	195
6	70	175
6	80	185
6	85	175
6	42	305
6	30	315
6	80	115
6	84	65
6	75	330
6	75	110
6	53	320
6	78	5
6	48	225
7	72	213
7	73	208
7	74	208
7	84	325
7	80	320
7	78	140
7	88	120
7	84	18
7	48	220
7	80	15
7	10	135
7	8	25
7	80	288
7	70	123

Mapping Site	Dip (°)	DipDir (°)
7	66	182
7	64	184
8	78	350
8	62	5
8	82	325
8	75	55
8	74	50
8	70	282
8	80	260
8	83	275
8	56	253
8	88	165
8	85	350
8	68	40
8	85	20
8	63	135
8	82	75
8	78	342
8	85	340
8	75	155
8	76	245
8	68	115
9	86	153
9	72	165
9	80	172
9	79	166
9	64	154
9	67	30
9	82	26
9	88	248

Mapping Site	Dip (°)	DipDir (°)
9	71	252
9	58	275
9	83	335
9	34	309
9	57	335
9	70	210
9	86	16
9	53	323
9	62	331
10	72	5
10	87	24
10	77	350
10	76	348
10	26	8
10	42	330
10	80	258
10	77	70
10	35	375
10	83	98
10	68	120
10	43	305
10	28	315
10	42	320
10	50	3
10	66	258
10	70	183
11	80	15
11	70	8
11	76	187
11	73	185

Mapping Site	Dip (°)	DipDir (°)
11	80	196
11	75	200
11	23	145
11	35	175
11	62	180
11	78	265
11	77	105
11	80	263
11	33	18
11	30	350
11	40	340
12	75	165
12	72	185
12	88	180
12	75	220
12	76	232
12	78	88
12	64	65
12	75	163
12	81	180
12	28	20
12	23	30
12	33	18
12	87	3
12	82	358
12	40	312
12	38	318
12	87	68
12	73	40
13	65	210

Mapping Site	Dip (°)	DipDir (°)
13	85	95
13	78	70
13	83	75
13	87	325
13	60	140
13	75	330
13	60	200
13	57	205
13	20	263
13	82	150
13	65	145
13	73	325
14	50	178
14	72	125
14	78	105
14	80	108
14	87	312
14	70	200
14	66	185
14	73	170
14	75	105
14	30	332
14	33	325
14	30	338
14	54	15
14	80	145
14	48	195
14	47	220
14	76	240
14	86	230

Mapping Site	Dip (°)	DipDir (°)
14	87	38
14	73	95
14	72	25
15	58	212
15	72	218
15	70	140
15	64	155
15	70	310
15	72	325
15	50	190
15	55	185
15	80	85
15	78	95
15	80	78
15	88	265
15	88	82
15	83	85
15	68	110
16	50	52
16	72	64
16	81	331
16	66	291
16	76	311
16	71	120
16	87	45
16	76	349
16	67	350
16	48	15
16	55	144
16	83	2

Mapping Site	Dip (°)	DipDir (°)
16	80	5
16	85	344
16	78	230
16	80	2
17	78	180
17	77	32
17	78	183
17	76	215
17	77	240
17	38	335
17	50	340
17	57	352
17	76	147
17	58	176
17	54	178
17	80	272
17	86	278
18	63	220
18	64	195
18	87	278
18	68	100
18	70	105
18	75	220
18	74	232
18	68	278
18	52	272
18	32	274
18	78	235
18	87	130
18	86	312

Mapping Site	Dip (°)	DipDir (°)
18	88	97
18	77	155
18	86	320
18	27	287
18	21	275
19	85	345
19	88	340
19	74	174
19	83	330
19	74	350
19	62	350
19	70	230
19	76	255
19	68	140
19	63	122
19	60	90
19	70	176
19	74	150
19	80	195
19	72	245
19	65	234
19	85	230
19	66	158
19	88	276
19	82	255
20	87	2
20	90	355
20	85	178
20	80	15
20	78	280

Mapping Site	Dip (°)	DipDir (°)
20	82	87
20	85	92
20	73	30
20	68	8
20	85	280
20	78	5
20	62	342
20	25	310
20	78	315
20	45	130
20	34	140
20	65	132
20	40	125
20	88	40
20	85	245
21	70	335
21	75	340
21	88	135
21	78	18
21	80	15
21	83	20
21	60	285
21	75	295
21	68	300
21	74	285
21	74	345
21	87	8
21	60	25
21	42	5
21	48	2

Mapping Site	Dip (°)	DipDir (°)
21	28	20
21	32	295
21	57	65
21	90	45
22	73	18
22	80	10
22	85	350
22	33	358
22	31	2
22	43	350
22	38	355
22	77	55
22	88	88
22	77	250
22	88	265
22	84	20
22	78	12
22	74	262
23	47	15
23	53	357
23	80	85
23	78	260
23	73	45
23	82	50
23	45	350
23	25	4
23	65	320
23	70	352
23	83	290
23	77	278

Mapping Site	Dip (°)	DipDir (°)
23	80	280
23	85	30
23	73	220
24	85	4
24	75	50
24	90	35
24	80	94
24	85	100
24	50	98
24	38	300
24	30	310
24	33	325
24	32	322
24	82	170
24	74	165
24	85	240
24	70	175
24	65	190
24	42	320
24	35	330
24	83	125
24	80	320
24	65	325
25	72	178
25	70	185
25	86	174
25	63	115
25	74	105
25	79	258
25	84	262

Mapping Site	Dip (°)	DipDir (°)
25	65	82
25	85	193
25	80	210
25	45	285
25	54	278
25	60	240
25	43	275
25	40	290
25	70	195
25	80	172
25	58	285
25	85	358
25	80	7
26	70	298
26	73	320
26	84	10
26	88	223
26	73	45
26	88	220
26	80	243
26	77	50
26	86	262
26	25	45
26	40	15
26	68	180
26	66	160
26	57	178
26	45	46
26	30	50
26	72	120

Mapping Site	Dip (°)	DipDir (°)
27	78	275
27	88	95
27	85	250
27	87	225
27	76	210
27	60	200
27	65	205
27	55	20
27	68	88
27	77	85
27	20	345
27	15	285
27	78	150
27	70	160
27	57	170
27	50	230
27	77	150
27	52	15
27	67	265
27	85	145
28	78	110
28	83	107
28	86	115
28	88	128
28	80	210
28	80	220
28	78	205
28	23	330
28	10	345
28	25	300

Mapping Site	Dip (°)	DipDir (°)
28	63	175
28	83	130
28	83	200
28	80	212
28	32	290
28	20	348
28	85	105
28	87	300
28	85	198
28	87	170
28	22	275
28	20	315
29	86	335
29	82	330
29	80	350
29	87	30
29	87	15
29	78	188
29	75	195
29	74	88
29	88	120
29	70	110
29	76	30
29	84	95
29	86	305
29	73	10
29	88	115
29	84	285
29	77	320
29	25	240

Mapping Site	Dip (°)	DipDir (°)
30	80	135
30	85	145
30	60	45
30	60	160
30	50	150
30	82	255
31	78	80
31	86	88
31	80	103
31	43	345
31	48	332
31	38	338
31	82	210
31	88	120
31	58	103
31	75	105
31	76	192
31	72	185
31	58	172
31	88	210
31	32	335
31	40	350
31	37	348
32	86	310
32	85	322
32	43	175
32	15	300
32	15	260
32	84	280
32	80	30

Mapping Site	Dip (°)	DipDir (°)
32	73	40
32	87	46
32	74	80
32	85	180
32	78	10
32	88	358
32	86	5
32	79	2
32	88	270
32	85	65
32	66	340
32	10	30
33	70	110
33	75	105
33	66	130
33	78	295
33	85	270
33	65	120
33	38	195
33	25	205
33	36	195
33	65	315
33	48	290
33	88	55
33	48	128
33	67	55
33	63	18
33	68	205
34	90	285
34	84	305

Mapping Site	Dip (°)	DipDir (°)
34	74	98
34	78	120
34	82	198
34	87	179
34	84	165
34	74	210
34	85	20
34	88	295
34	78	95
34	18	40
34	20	285
34	25	310
34	67	185
34	85	160
34	70	280
34	78	145
35	76	272
35	80	265
35	76	268
35	86	305
35	80	247
35	33	330
35	42	350
35	40	15
35	83	350
35	85	4
35	84	352
35	85	340
35	80	2
35	78	92

Mapping Site	Dip (°)	DipDir (°)
35	80	258
35	58	180
35	86	20
35	82	358
36	70	83
36	25	230
36	88	235
36	88	66
36	28	82
36	82	165
36	82	3
36	90	140
36	4	54
36	48	330
36	38	22
36	60	145
36	72	178
36	37	345
36	82	72
36	50	195
36	78	35
36	88	333

Case Study #2

Mapping Site	Dip (°)	DipDir (°)	Discontinuity Type
Site-01	22	158	Joint
Site-01	24	159	Joint
Site-01	60	004	Joint
Site-01	64	008	Joint
Site-01	65	005	Joint
Site-01	78	170	Joint
Site-01	78	185	Joint
Site-01	78	182	Joint
Site-01	30	115	Joint
Site-01	32	112	Joint
Site-01	30	118	Joint
Site-01	65	242	Joint
Site-01	68	265	Joint
Site-01	73	253	Joint
Site-014	84	335	Joint
Site-014	85	330	Joint
Site-014	82	330	Joint
Site-014	85	335	Joint
Site-014	84	335	Joint
Site-014	60	325	Joint
Site-014	58	320	Joint
Site-014	62	325	Joint
Site-014	60	325	Joint
Site-014	70	100	Bedding
Site-014	68	100	Bedding
Site-014	85	180	Joint
Site-014	89	175	Joint
Site-015	87	335	Joint

Mapping Site	Dip (°)	DipDir (°)	Discontinuity Type
Site-015	85	330	Joint
Site-015	86	334	Joint
Site-015	85	334	Joint
Site-015	87	335	Joint
Site-015	85	335	Joint
Site-015	58	325	Joint
Site-015	55	325	Joint
Site-015	85	065	Joint
Site-015	82	065	Joint
Site-015	85	060	Joint
Site-016	83	178	Joint
Site-016	80	178	Joint
Site-016	85	175	Joint
Site-016	83	175	Joint
Site-016	82	178	Joint
Site-016	68	250	Joint
Site-02	77	342	Joint
Site-02	78	344	Joint
Site-02	70	352	Joint
Site-02	25	212	Joint
Site-02	28	208	Joint
Site-02	24	205	Joint
Site-02	88	072	Joint
Site-02	88	071	Joint
Site-02	75	068	Joint
Site-02	78	172	Joint
Site-02	81	178	Joint
Site-02	82	174	Joint

Mapping Site	Dip (°)	DipDir (°)	Discontinuity Type
Site-02	62	008	Joint
Site-02	62	020	Joint
Site-02	72	008	Joint
Site-023	40	280	Joint
Site-023	65	265	Bedding
Site-023	80	175	Joint
Site-024	87	218	Bedding
Site-024	15	160	Joint
Site-024	84	160	Joint
Site-025	84	343	Joint
Site-025	55	230	Bedding
Site-025	13	190	Joint
Site-026	88	160	Joint
Site-026	43	088	Joint
Site-026	64	250	Bedding
Site-027	48	005	Joint
Site-027	29	130	Joint
Site-027	74	255	Bedding
Site-028	84	330	Joint
Site-028	08	020	Joint
Site-028	55	260	Bedding
Site-029	82	335	Joint
Site-029	69	081	Joint
Site-029	09	170	Joint
Site-03	85	166	Joint
Site-03	76	164	Joint
Site-03	85	172	Joint
Site-03	72	344	Joint

Mapping Site	Dip (°)	DipDir (°)	Discontinuity Type
Site-03	76	348	Joint
Site-03	71	341	Joint
Site-03	15	238	Joint
Site-03	17	243	Joint
Site-03	12	241	Joint
Site-03	85	268	Joint
Site-03	82	265	Joint
Site-03	76	264	Joint
Site-030	86	345	Joint
Site-030	10	180	Joint
Site-030	80	245	Joint
Site-031	08	170	Joint
Site-031	76	240	Joint
Site-031	82	348	Joint
Site-032	20	190	Bedding
Site-032	70	325	Joint
Site-032	84	240	Joint
Site-033	73	347	Joint
Site-033	63	250	Joint
Site-033	24	208	Bedding
Site-034	63	322	Joint
Site-034	45	094	Joint
Site-034	87	102	Joint
Site-035	68	260	Bedding
Site-035	82	315	Joint
Site-035	28	140	Joint
Site-036	75	345	Joint
Site-036	08	250	Joint

Mapping Site	Dip (°)	DipDir (°)	Discontinuity Type
Site-036	68	255	Bedding
Site-037	55	270	Bedding
Site-037	85	340	Joint
Site-037	65	080	Joint
Site-038	70	256	Bedding
Site-038	86	330	Joint
Site-038	46	050	Joint
Site-039	87	342	Joint
Site-039	70	260	Bedding
Site-039	16	015	Joint
Site-04	82	346	Joint
Site-04	80	352	Joint
Site-04	78	352	Joint
Site-04	62	242	Joint
Site-04	68	244	Joint
Site-04	70	246	Joint
Site-04	82	172	Joint
Site-04	85	168	Joint
Site-04	84	167	Joint
Site-040	71	243	Bedding
Site-040	52	062	Joint
Site-040	11	170	Joint
Site-041	65	247	Bedding
Site-041	50	020	Joint
Site-041	08	180	Joint
Site-041	70	174	Joint
Site-042	67	260	Bedding
Site-042	62	004	Joint

Mapping Site	Dip (°)	DipDir (°)	Discontinuity Type
Site-042	07	170	Joint
Site-043	80	000	Joint
Site-043	65	250	Bedding
Site-043	31	085	Joint
Site-044	70	258	Bedding
Site-044	50	335	Joint
Site-044	11	150	Joint
Site-045	59	265	Bedding
Site-045	54	000	Joint
Site-045	05	210	Joint
Site-05	70	264	Bedding
Site-05	66	008	Joint
Site-05	65	005	Joint
Site-05	72	264	Joint
Site-05	75	262	Joint
Site-05	78	176	Joint
Site-05	80	172	Joint
Site-05	77	173	Joint
Site-06	78	086	Joint
Site-06	84	082	Joint
Site-06	85	081	Joint
Site-06	84	174	Joint
Site-06	78	172	Joint
Site-06	78	170	Joint
Site-06	75	004	Joint
Site-06	76	005	Joint
Site-06	82	006	Joint
Site-07	60	145	Joint

Mapping Site	Dip (°)	DipDir (°)	Discontinuity Type
Site-07	60	155	Joint
Site-07	65	160	Joint
Site-07	72	080	Joint
Site-07	68	081	Joint
Site-07	74	083	Joint
Site-07	03	090	Joint
Site-07	03	088	Joint
Site-07	05	087	Joint
Site-08	85	182	Joint
Site-08	84	186	Joint
Site-08	82	178	Joint
Site-08	80	087	Joint
Site-08	80	088	Joint
Site-08	80	088	Joint
Site-08	78	004	Joint
Site-08	75	004	Joint
Site-08	72	005	Joint
Site-08	30	150	Joint
Site-08	60	348	Joint
Site-09	78	346	Joint
Site-09	68	347	Joint
Site-09	70	345	Joint
Site-09	80	068	Joint
Site-09	78	066	Joint
Site-09	80	070	Joint
Site-10	85	345	Joint
Site-10	75	342	Joint
Site-10	83	346	Joint

Mapping Site	Dip (°)	DipDir (°)	Discontinuity Type
Site-10	47	243	Joint
Site-10	65	245	Joint
Site-10	53	243	Joint
Site-10	55	246	Joint
Site-10	35	325	Joint
Site-10	38	328	Joint
Site-10	35	340	Joint
Site-11	85	008	Joint
Site-11	82	006	Joint
Site-11	85	008	Joint
Site-11	60	092	Joint
Site-11	65	088	Joint
Site-11	60	090	Joint
Site-11	42	315	Joint
Site-11	60	315	Joint
Site-11	20	012	Joint
Site-11	22	015	Joint
Site-12	70	065	Joint
Site-12	65	068	Joint
Site-12	70	070	Joint
Site-12	70	348	Joint
Site-12	72	350	Joint
Site-12	70	350	Joint
Site-13	72	352	Joint
Site-13	70	348	Joint
Site-13	76	348	Joint
Site-13	38	205	Joint
Site-13	45	210	Joint

Mapping Site	Dip (°)	DipDir (°)	Discontinuity Type
Site-13	60	158	Joint
Site-13	55	155	Joint

Case Study #3

Dip (°)	DipDir (°)	Mapping Site	Persistence	Spacing	Aperture	Infilling	Roughness	Weathering
64	86	Site - 01	3	1	5	4	4	4
74	87	Site - 01	2	4	4	5	5	3
28	172	Site - 01	2	4	4	4	4	3
80	267	Site - 01	2	4	4	4	3	3
81	81	Site - 01	3	4	4	4	3	4
65	223	Site - 01	2	4	3	4	3	3
56	294	Site - 01	2	1	3	4	3	3
46	181	Site - 01	2	4	3	4	3	3
52	68	Site - 01	4	1	5	5	5	4
83	97	Site - 01	3	4	4	4	3	3
74	122	Site - 01	3	1	5	5	3	3
73	255	Site - 01	3	4	4	4	3	3
87	96	Site - 01	3	4	4	4	3	3
72	214	Site - 02	3	3	4	2	2	2
75	58	Site - 02	3	3	4	4	2	2
60	259	Site - 02	3	1	4	4	2	2
76	59	Site - 02	3	3	4	2	2	2
58	78	Site - 02	3	1	1	2	2	3
78	52	Site - 02	2	3	4	4	2	2
49	244	Site - 02	3	3	4	4	2	2
89	234	Site - 02	2	1	1	3	2	3
76	168	Site - 02	3	3	4	2	2	2
70	68	Site - 02	3	3	4	4	2	2
75	68	Site - 02	3	3	4	2	2	2
70	325	Site - 02	3	3	4	2	2	2
84	58	Site - 03	2	3	3	4	3	2
27	201	Site - 03	3	3	3	4	3	2
49	136	Site - 03	3	1	4	1	3	2
83	75	Site - 03	3	4	3	4	3	2

79	78	Site - 03	2	5	3	4	3	3
30	214	Site - 03	3	5	3	4	3	3
75	61	Site - 03	3	3	3	4	3	2
28	198	Site - 03	3	3	3	4	3	2
53	174	Site - 03	3	3	3	4	3	2
76	61	Site - 03	3	3	3	4	4	2
22	196	Site - 03	3	3	3	1	4	2
40	150	Site - 03	2	4	3	4	3	2
62	62	Site - 03	3	3	3	4	3	2
88	233	Site - 03	2	4	3	4	3	3
61	70	Site - 03	2	4	3	4	3	3
33	101	Site - 03	2	3	4	4	3	2
71	58	Site - 04	3	4	4	4	3	3
47	96	Site - 04	3	3	4	4	3	3
30	234	Site - 04	3	1	4	4	4	3
78	63	Site - 04	2	3	4	4	4	2
44	68	Site - 04	2	3	3	4	3	2
72	60	Site - 04	3	3	3	4	3	2
42	138	Site - 04	3	3	3	4	3	2
54	93	Site - 04	3	3	3	4	3	2
67	59	Site - 04	2	3	4	4	3	2
31	234	Site - 04	3	2	4	4	4	2
72	54	Site - 04	2	4	4	4	3	2
47	140	Site - 04	2	2	5	5	4	3
43	65	Site - 04	2	3	4	4	3	3
30	108	Site - 04	2	3	4	4	4	3
13	217	Site - 05	3	2	5	3	4	2
48	293	Site - 05	3	3	3	2	4	3
57	55	Site - 05	3	3	3	2	4	2
55	93	Site - 05	3	3	4	2	4	2
53	299	Site - 05	3	3	4	2	4	3
59	78	Site - 05	3	3	4	2	4	2
52	293	Site - 05	3	3	4	2	4	2
83	152	Site - 05	3	3	4	2	4	2

63	57	Site - 05	3	3	3	2	4	2
34	93	Site - 05	3	1	1	3	4	3
74	336	Site - 05	3	3	4	2	4	2
42	99	Site - 05	3	3	4	2	4	2
86	180	Site - 06	2	2	4	4	3	3
35	107	Site - 06	3	1	4	4	3	2
74	208	Site - 06	2	2	4	4	3	3
81	356	Site - 06	2	2	5	4	3	3
87	193	Site - 06	2	2	3	4	3	3
42	194	Site - 06	3	4	4	4	3	3
51	199	Site - 06	2	4	4	1	4	3
47	49	Site - 06	2	4	3	4	3	2
59	188	Site - 06	3	4	4	4	3	3
24	9	Site - 06	3	1	5	4	4	2
24	4	Site - 06	2	4	3	4	3	2
68	31	Site - 06	2	4	3	4	3	2
82	338	Site - 07	2	4	4	4	2	3
47	325	Site - 07	3	3	5	4	2	4
36	259	Site - 07	3	4	4	4	2	4
64	62	Site - 07	3	4	4	4	3	3
88	243	Site - 07	4	1	5	5	1	5
77	321	Site - 07	3	4	4	4	2	3
79	347	Site - 07	4	1	5	5	1	5
84	315	Site - 07	3	4	4	4	3	3
65	94	Site - 08	4	4	4	2	2	2
65	178	Site - 08	4	4	4	4	2	2
77	72	Site - 08	4	4	3	4	2	3
55	301	Site - 08	4	4	4	4	2	2
59	69	Site - 08	4	2	4	2	2	2
50	190	Site - 08	4	3	3	2	2	2
82	213	Site - 08	4	3	4	2	2	2
85	57	Site - 09	3	4	4	4	3	2
59	141	Site - 09	3	4	4	4	3	2
59	137	Site - 09	3	4	4	4	3	3

78	112	Site - 09	4	2	5	5	4	3
21	162	Site - 09	3	3	3	4	3	3
71	133	Site - 09	3	3	4	4	4	3
58	51	Site - 09	3	3	4	4	3	3
84	293	Site - 09	3	4	4	4	3	3
66	80	Site - 09	3	2	4	4	3	3
75	191	Site - 09	4	2	4	4	3	3
61	268	Site - 09	4	1	5	5	2	3
69	156	Site - 09	3	4	4	4	3	3
79	33	Site - 10	3	3	3	4	4	2
69	27	Site - 10	2	4	2	4	4	3
73	286	Site - 10	2	3	3	4	5	3
38	324	Site - 10	3	4	4	4	5	3
46	158	Site - 10	3	3	4	4	5	3
70	327	Site - 10	4	1	4	5	4	4
68	71	Site - 10	3	3	4	4	5	3
81	348	Site - 10	4	1	3	5	1	4
68	71	Site - 10	3	3	4	4	5	3
79	344	Site - 10	3	3	4	4	5	3
20	167	Site - 10	3	3	3	4	5	3
70	160	Site - 10	3	3	2	4	3	2
18	135	Site - 10	3	3	2	4	4	2
71	66	Site - 11	3	4	3	4	2	2
55	151	Site - 11	3	3	4	4	2	3
80	68	Site - 11	3	3	3	4	2	2
45	112	Site - 11	3	3	4	4	2	3
11	314	Site - 11	3	3	4	4	2	3
31	254	Site - 11	3	3	4	4	2	3
68	96	Site - 12	3	4	4	4	2	2
34	174	Site - 12	3	3	4	4	2	2
72	181	Site - 12	3	3	4	4	2	3
69	65	Site - 12	3	3	4	4	3	3
51	353	Site - 12	3	3	4	4	3	3
66	61	Site - 12	2	4	4	4	2	3

18	357	Site - 12	3	3	4	4	3	3	3
68	96	Site - 12	2	4	4	4	2	3	3
31	167	Site - 12	3	3	3	4	2	3	3
71	166	Site - 12	3	3	4	4	3	3	3
78	81	Site - 13	3	4	3	4	4	2	2
83	78	Site - 13	3	3	4	4	4	2	2
82	355	Site - 13	3	3	4	4	3	2	2
67	139	Site - 13	3	3	3	4	4	2	2
41	212	Site - 13	3	3	3	4	3	2	2
86	300	Site - 13	3	1	5	5	1	5	5
39	190	Site - 13	3	3	4	4	3	2	2
73	20	Site - 13	3	4	3	4	3	2	2
76	297	Site - 13	3	1	5	5	1	5	5
81	327	Site - 13	3	4	4	4	4	3	3
72	73	Site - 13	3	4	4	4	4	3	3
73	104	Site - 14	4	1	5	5	1	4	4
78	101	Site - 14	2	3	4	2	2	3	3
65	271	Site - 14	2	3	3	4	2	3	3
56	182	Site - 14	3	3	3	4	2	3	3
72	72	Site - 14	2	3	4	4	2	3	3
60	186	Site - 14	2	3	4	4	2	2	2
52	233	Site - 14	3	1	4	4	2	2	2
66	318	Site - 14	4	1	5	3	3	3	3
20	29	Site - 14	1	4	3	4	2	2	2
78	91	Site - 14	1	4	3	4	2	2	2
61	130	Site - 14	2	3	4	4	3	3	3
60	96	Site - 14	2	4	4	4	2	2	2
72	316	Site - 14	4	1	4	4	3	3	3
73	258	Site - 14	2	4	4	4	2	2	2
77	261	Site - 14	2	4	4	4	2	2	2
68	59	Site - 14	2	4	4	4	2	2	2
43	131	Site - 14	2	4	3	4	2	2	2
53	256	Site - 14	3	2	3	4	2	2	2
71	259	Site - 14	2	4	4	4	2	2	2

69	100	Site - 14	3	3	4	4	4	2	2
69	79	Site - 15	4	3	4	4	2	2	2
32	189	Site - 15	2	3	3	4	3	3	2
38	325	Site - 15	2	2	3	4	3	3	2
77	325	Site - 15	4	1	4	4	2	2	2
70	83	Site - 15	3	3	4	4	2	2	2
45	199	Site - 15	2	4	3	4	3	2	2
78	263	Site - 15	3	1	4	4	2	2	2
48	245	Site - 15	3	1	4	4	2	2	2
47	203	Site - 15	3	2	4	4	3	2	2
84	183	Site - 15	3	2	4	4	2	2	2
69	327	Site - 15	4	1	4	4	2	2	2
75	75	Site - 15	2	3	4	4	3	2	2
26	82	Site - 15	3	2	4	4	2	2	2
36	265	Site - 15	2	2	4	4	2	2	2
77	65	Site - 16	4	4	3	4	3	2	2
18	172	Site - 16	4	4	3	4	4	2	2
64	7	Site - 16	4	4	3	4	3	2	2
70	70	Site - 16	4	1	5	3	1	4	4
83	73	Site - 16	4	1	5	3	1	4	4
76	71	Site - 16	4	1	5	3	1	4	4
83	73	Site - 16	4	3	3	4	3	3	3
26	213	Site - 16	4	1	3	4	3	2	2
62	109	Site - 16	4	3	4	4	4	2	2
60	242	Site - 16	4	4	4	4	4	2	2
71	73	Site - 16	4	4	4	2	3	3	3
39	139	Site - 16	4	3	4	2	4	2	2
18	352	Site - 16	4	4	4	2	4	2	2
67	80	Site - 16	4	3	4	4	3	2	2
65	100	Site - 17	3	4	3	4	2	3	3
83	289	Site - 17	3	1	5	3	1	3	3
42	347	Site - 17	3	3	3	2	2	2	2
52	135	Site - 17	2	2	3	4	2	3	3
85	207	Site - 17	3	3	4	4	2	3	3

65	48	Site - 17	3	3	3	4	2	3
40	178	Site - 17	4	1	5	3	1	3
46	352	Site - 17	3	2	2	2	2	2
50	130	Site - 17	3	3	3	4	2	2
74	42	Site - 17	3	3	4	4	2	2
68	64	Site - 17	3	3	3	4	2	2
61	328	Site - 17	3	3	4	2	2	2
42	142	Site - 17	3	3	3	4	2	2
71	70	Site - 17	4	3	3	4	2	2
49	161	Site - 17	4	1	5	3	2	4
72	67	Site - 17	4	3	4	2	3	2
75	142	Site - 17	3	4	4	4	3	2
72	133	Site - 17	3	4	4	4	3	2
74	69	Site - 17	3	4	4	4	3	3
75	357	Site - 18	3	4	4	4	4	3
68	266	Site - 18	2	1	5	5	2	4
65	68	Site - 18	3	4	3	4	3	2
35	127	Site - 18	3	4	4	4	3	2
86	47	Site - 18	3	4	4	4	3	2
61	160	Site - 18	3	2	4	4	3	3
75	5	Site - 18	3	2	4	4	3	3
73	356	Site - 18	3	4	4	4	3	3
74	65	Site - 18	3	4	3	4	3	2
75	8	Site - 18	3	4	4	4	3	3
78	168	Site - 18	3	1	5	5	2	4
46	109	Site - 18	3	4	4	4	3	2
35	162	Site - 18	3	1	5	5	2	3
60	298	Site - 18	3	3	4	4	3	2
52	33	Site - 18	3	3	4	4	3	2
56	112	Site - 18	3	3	4	4	3	2
88	236	Site - 18	3	3	4	4	4	2
48	71	Site - 19	2	3	3	4	3	2
49	155	Site - 19	3	2	3	4	4	2
50	192	Site - 19	3	1	4	4	4	2

20	99	Site - 19	3	1	3	4	4	2
67	74	Site - 19	2	4	3	4	3	2
82	65	Site - 19	2	4	4	4	3	2
42	6	Site - 19	4	2	4	4	4	2
46	3	Site - 19	2	4	3	4	4	2
58	68	Site - 19	3	3	3	4	3	2
75	65	Site - 19	2	4	3	4	3	2
35	163	Site - 19	3	2	3	4	4	2
51	65	Site - 19	2	3	3	4	3	2
58	66	Site - 19	2	4	4	4	3	2
73	64	Site - 19	3	1	5	5	2	3
24	1	Site - 19	2	1	4	4	4	2
64	276	Site - 19	2	4	4	4	3	2
32	99	Site - 19	2	1	3	4	3	2
64	78	Site - 19	2	3	3	4	3	3
70	90	Site - 20	3	4	4	4	2	2
37	240	Site - 20	1	4	4	4	3	2
70	76	Site - 20	2	3	4	4	2	2
32	99	Site - 20	2	3	4	4	2	2
68	84	Site - 20	4	2	4	4	2	2
70	71	Site - 20	2	4	4	4	2	2
76	76	Site - 20	2	3	3	4	2	2
38	182	Site - 20	1	3	3	4	3	2
70	204	Site - 20	2	3	4	4	2	2
72	196	Site - 20	2	2	4	4	2	2
77	68	Site - 20	2	4	4	4	2	2
74	85	Site - 20	2	3	3	4	2	2
68	71	Site - 20	2	3	4	4	2	3
45	202	Site - 20	2	2	3	4	2	3
33	91	Site - 20	2	3	3	4	3	3
86	128	Site - 20	4	1	4	4	2	3
77	120	Site - 20	3	4	4	4	3	2
76	80	Site - 20	2	4	4	4	2	2
36	197	Site - 20	2	3	4	4	3	2

50	344	Site - 21	4	1	4	4	2	2	2
70	301	Site - 21	2	1	4	4	2	2	2
76	72	Site - 21	2	3	4	4	2	2	2
62	266	Site - 21	2	3	4	4	3	2	2
58	229	Site - 21	2	3	4	4	3	2	2
39	179	Site - 21	2	2	4	4	3	2	2
73	67	Site - 21	2	3	4	4	2	2	2
73	71	Site - 21	3	4	4	4	2	2	2
59	229	Site - 21	3	2	4	4	2	2	2
62	246	Site - 21	2	3	3	4	2	3	3
56	330	Site - 21	3	1	4	4	2	2	2
73	252	Site - 21	2	3	4	4	3	2	2
54	255	Site - 21	2	1	3	4	2	2	2
73	78	Site - 21	2	3	4	4	3	2	2
76	64	Site - 22	4	3	4	4	3	2	2
64	174	Site - 22	4	3	4	4	3	2	2
38	327	Site - 22	4	3	4	4	3	2	2
72	50	Site - 22	4	4	4	4	3	3	3
62	65	Site - 22	4	1	5	5	4	3	3
39	325	Site - 22	4	3	4	4	3	3	3
83	114	Site - 22	4	1	5	5	3	3	3
71	57	Site - 23	3	4	4	4	3	4	4
34	202	Site - 23	3	4	4	4	3	3	3
72	306	Site - 23	3	3	4	4	3	3	3
67	4	Site - 23	3	4	4	4	3	4	4
47	143	Site - 23	3	2	4	4	3	3	3
75	325	Site - 23	3	3	4	4	3	3	3
77	61	Site - 23	3	4	4	4	3	4	4
67	327	Site - 23	3	4	4	4	3	4	4
43	63	Site - 23	2	3	4	4	3	4	4
71	275	Site - 24	3	4	4	4	4	3	3
72	158	Site - 24	3	4	4	4	3	4	4
18	323	Site - 24	3	4	4	4	3	3	3
61	296	Site - 24	2	2	3	4	4	2	2

83	59	Site - 24	3	3	3	4	4	3	4	3
60	329	Site - 24	3	3	3	4	4	4	4	3
75	169	Site - 24	3	3	3	4	4	4	4	3
77	146	Site - 24	3	4	4	4	4	4	4	4
71	50	Site - 24	3	4	4	4	4	4	4	4
77	339	Site - 25	3	3	4	4	4	5	3	3
71	68	Site - 25	3	3	4	4	4	5	3	3
43	310	Site - 25	3	3	4	4	4	5	3	3
70	154	Site - 25	3	3	4	4	4	5	4	4
79	149	Site - 25	2	4	4	4	4	4	4	4
65	56	Site - 25	3	3	4	4	4	5	3	3
78	142	Site - 25	2	4	4	4	4	5	3	3
16	252	Site - 25	2	4	4	4	4	5	4	4
40	345	Site - 25	3	4	4	4	4	5	3	3
76	344	Site - 25	4	1	5	5	5	4	4	4
74	144	Site - 26	3	4	4	4	4	2	3	3
79	118	Site - 26	3	4	4	4	4	2	3	3
17	43	Site - 26	3	4	4	4	4	3	3	3
32	228	Site - 26	3	4	4	4	4	3	3	3
75	59	Site - 26	4	1	5	4	2	4	4	4
35	154	Site - 26	3	4	4	4	2	4	4	4
71	44	Site - 26	3	4	4	4	3	3	3	3
72	142	Site - 26	3	3	4	4	2	3	3	3
32	341	Site - 26	2	3	4	4	3	3	3	3
58	181	Site - 26	3	3	3	4	2	3	3	3
41	53	Site - 26	3	3	3	4	2	3	3	3
79	88	Site - 27	4	2	4	4	3	3	3	3
82	2	Site - 27	3	4	4	4	3	4	4	4
11	251	Site - 27	3	4	4	4	3	4	4	4
52	199	Site - 27	4	1	5	4	3	4	4	4
76	343	Site - 27	4	1	5	4	3	4	4	4
82	132	Site - 27	2	4	4	4	3	4	4	4
56	260	Site - 27	3	4	4	4	3	4	4	4
62	142	Site - 27	3	3	4	4	3	4	4	4

82	312	Site - 27	3	4	4	4	4	3	4
78	47	Site - 27	3	4	4	4	4	3	4
76	62	Site - 28	3	2	4	4	4	2	3
40	75	Site - 28	2	3	4	4	4	2	3
81	10	Site - 28	3	2	4	4	4	2	3
72	156	Site - 28	4	2	4	4	4	2	3
67	330	Site - 28	3	2	4	4	4	2	3
16	223	Site - 28	2	3	4	4	4	2	3
55	207	Site - 28	3	1	4	4	4	2	3
56	153	Site - 29	3	3	4	4	4	2	2
65	159	Site - 29	3	1	4	4	4	2	2
56	333	Site - 29	4	2	4	4	4	2	2
27	204	Site - 29	3	2	4	4	4	2	2
57	298	Site - 29	3	2	4	4	4	2	2
64	159	Site - 29	3	3	4	4	4	2	2
55	332	Site - 29	3	3	4	4	4	2	2
52	260	Site - 29	2	2	4	4	4	2	2
60	247	Site - 29	3	1	4	4	4	2	2
79	42	Site - 30	2	2	4	4	4	5	3
83	324	Site - 30	2	2	4	4	4	4	3
70	98	Site - 30	3	3	4	4	4	5	3
80	300	Site - 30	2	3	5	4	4	5	3
85	255	Site - 30	4	1	4	4	4	4	3
75	51	Site - 30	4	2	4	4	4	4	3
79	283	Site - 30	3	1	4	4	4	5	3
40	6	Site - 30	1	3	4	4	4	5	3
55	263	Site - 30	2	4	3	4	4	5	3
52	120	Site - 30	5	1	4	4	4	2	3
80	34	Site - 30	2	3	4	4	4	5	3
70	96	Site - 31	3	4	4	4	4	3	3
56	22	Site - 31	3	3	4	4	4	3	3
25	185	Site - 31	3	3	4	4	4	3	4
62	107	Site - 31	2	4	4	4	4	3	4
62	51	Site - 31	2	4	4	4	4	3	4

40	172	Site - 31	3	3	4	4	3	4
62	129	Site - 31	3	4	4	4	3	4
71	46	Site - 31	3	4	4	4	3	4
66	7	Site - 31	3	3	3	4	3	3
68	74	Site - 32	2	3	4	4	2	3
35	321	Site - 32	2	3	4	4	2	3
34	280	Site - 32	2	3	4	4	2	3
70	80	Site - 32	3	3	4	4	2	3
31	55	Site - 32	3	1	4	4	2	3
26	285	Site - 32	1	4	4	4	2	3
55	139	Site - 32	3	1	4	4	2	3
45	267	Site - 32	3	3	3	4	3	3
64	111	Site - 32	4	3	4	4	3	3
39	313	Site - 32	3	3	4	4	2	3
70	12	Site - 32	3	2	4	4	3	3
74	2	Site - 32	2	3	4	4	3	3
42	254	Site - 32	2	3	3	4	2	3
43	147	Site - 32	2	3	4	4	2	3
34	293	Site - 32	2	3	4	4	3	3
63	236	Site - 32	4	1	4	4	2	3
50	79	Site - 33	3	3	4	4	3	3
36	219	Site - 33	3	3	4	4	3	3
77	2	Site - 33	3	3	3	4	3	3
47	150	Site - 33	3	3	3	4	3	3
82	297	Site - 33	3	4	4	4	3	3
59	231	Site - 33	3	1	5	5	3	4
64	95	Site - 33	3	4	4	4	3	4
67	83	Site - 34	3	3	3	4	2	3
70	355	Site - 34	3	3	3	4	2	3
38	165	Site - 34	2	4	4	4	3	4
65	76	Site - 34	3	4	4	4	2	3
67	14	Site - 34	2	2	3	4	2	3
82	326	Site - 34	3	2	4	4	3	3
77	75	Site - 34	3	3	4	4	2	3

76	87	Site - 34	3	4	3	4	2	4
48	357	Site - 34	3	3	3	4	2	3
77	352	Site - 34	3	3	3	4	2	3
68	70	Site - 34	3	4	3	4	2	3
28	232	Site - 34	3	3	3	4	3	4
69	95	Site - 35	3	1	4	4	4	2
32	320	Site - 35	3	3	4	4	4	2
26	146	Site - 35	3	3	4	4	4	2
66	99	Site - 35	4	1	4	4	2	3
64	93	Site - 35	2	3	3	4	3	2
26	165	Site - 35	1	3	3	4	3	2
78	258	Site - 35	4	1	5	5	2	2
84	261	Site - 35	2	3	3	4	3	2
66	108	Site - 35	3	3	4	4	3	2
29	338	Site - 35	1	3	4	4	3	2
72	224	Site - 35	2	2	3	4	3	2
46	131	Site - 35	4	1	4	4	2	2
76	275	Site - 35	3	2	4	4	4	2
70	155	Site - 35	3	1	4	4	2	3
38	168	Site - 36	3	4	4	4	3	2
36	321	Site - 36	2	4	4	4	3	2
57	105	Site - 36	2	3	4	4	4	2
59	88	Site - 36	2	3	3	4	3	2
26	288	Site - 36	1	4	3	4	3	2
29	290	Site - 36	2	2	4	4	3	2
52	335	Site - 37	4	1	4	4	5	2
52	335	Site - 37	3	2	4	4	4	2
73	102	Site - 37	3	3	4	4	3	2
19	160	Site - 37	2	3	4	4	3	2
30	255	Site - 37	3	3	4	4	3	2
62	354	Site - 37	3	3	4	4	3	2
72	22	Site - 37	2	1	4	4	3	2
30	302	Site - 38	3	3	4	4	2	2
45	157	Site - 38	2	3	4	4	2	2

84	273	Site - 38	3	2	5	4	4	2	2
65	134	Site - 38	3	3	4	4	4	2	2
74	258	Site - 38	3	3	4	4	4	2	2
63	124	Site - 38	3	3	4	4	4	2	2
33	315	Site - 38	4	3	4	4	4	2	2
74	260	Site - 38	3	2	4	4	4	2	2
66	94	Site - 38	3	3	4	4	4	2	2
69	354	Site - 38	3	1	4	4	4	3	2
52	137	Site - 39	4	2	4	4	4	2	2
38	252	Site - 39	3	2	4	4	4	3	2
63	155	Site - 39	3	2	4	4	4	2	2
38	93	Site - 39	1	2	4	4	4	3	2
58	178	Site - 39	4	2	4	4	4	3	2
56	144	Site - 39	2	3	4	4	4	2	2
46	155	Site - 39	2	3	4	4	4	2	2
72	151	Site - 39	3	2	4	4	4	2	2
52	258	Site - 39	3	2	4	4	4	3	2
68	90	Site - 40	4	3	4	4	4	3	3
74	326	Site - 40	3	3	3	4	4	2	3
55	174	Site - 40	3	3	4	4	4	2	4
83	24	Site - 40	3	3	4	4	4	2	4
53	200	Site - 40	4	1	5	4	4	2	4
75	95	Site - 40	3	3	4	4	4	2	3
60	316	Site - 40	3	3	4	4	4	2	3
74	60	Site - 41	3	4	3	4	4	3	3
76	192	Site - 41	3	4	3	4	4	4	3
31	278	Site - 41	3	4	3	4	4	4	3
75	61	Site - 41	3	3	4	4	4	3	3
86	116	Site - 41	3	2	3	4	4	3	4
28	222	Site - 41	3	4	4	4	4	3	3
53	8	Site - 41	3	2	3	4	4	4	3
80	66	Site - 41	3	4	3	4	4	3	3
83	38	Site - 42	3	3	3	4	4	3	2
29	273	Site - 42	3	3	4	4	4	3	3

34	117	Site - 42	3	3	3	4	3	3
75	14	Site - 42	3	1	5	3	2	3

(*) Joint conditions i.e. persistence, spacing, infilling, roughness and degree of weathering are given as semi-quantitative values ranging from 1 to 5 according to the RMR classes given by Bienawski (1989).